



UNIVERSITÀ DEGLI STUDI DI MILANO

Dottorato di Ricerca in Scienze della Terra
Ciclo **XXXI**



Geomechanical characterization of rock masses for tunnel excavation with TBM

Ph.D. Thesis

Giacomo Armetti
Matricola R11266

Tutor
Prof.ssa Tiziana Apuani

Academic Year
2017 - 2018

Coordinator
Prof. ssa Elisabetta Erba

Co-Tutor
Prof. Maria Migliazza

ABSTRACT

The prediction of Tunnel Boring Machine (TBM) performances and the comprehension of the relationship between the geological, mechanical and structural features of a rock mass and the machine behaviour are fundamental in order to select the most effective tunnel construction methods and to estimate the condition of excavation in terms of time and economic costs of the infrastructure.

The general purpose of this work is to carry out predictive models utilisable during the early stage of tunnel planning and realisation; for this purpose, many approaches have been considered.

Simple and multiple, both linear and nonlinear, regression analyses have been performed in order to achieve an empirical equation able to estimate the principal TBM performance indices (ROP and FPI). In addition, Multiple Correspondence Analysis and clustering have been developed. A modified version of the Rock Engineering System has been performed and used to obtain a predictive model.

This study focuses on the exploratory tunnel named “La Maddalena”, located in Northern Italy, Western Alps, where geological surveys data have been continuously performed during tunnel construction; this allowed the collection of a large amount of geological, geotechnical and TBM performance data.

INDEX

1	INTRODUCTION	1
1.1	General purpose	1
1.2	Work organisation and thesis structure	2
2	MECHANISED TUNNELLING	5
2.1	Introduction	5
2.2	Types of Tunnel Boring Machines	6
	2.2.1 <i>Open type TBM</i>	7
	2.2.2 <i>Shield type TBM</i>	9
	2.2.3 <i>Closed mode TBM</i>	11
2.3	Rock breakage mechanism	12
	2.3.1 <i>Disc cutters</i>	12
	2.3.2 <i>Rock failure</i>	13
2.4	TBM performance indices	16
	2.4.1 <i>Rate of penetration</i>	16
	2.4.2 <i>Advance rate</i>	16
	2.4.3 <i>Coefficient of utilisation</i>	17
	2.4.4 <i>Penetration rate per revolution</i>	17
	2.4.5 <i>Field penetration index</i>	17
	2.4.6 <i>Specific penetration</i>	18
	2.4.7 <i>Specific excavation rate</i>	18
2.5	Factors influencing the TBM performances	19

2.5.1	<i>Geological and geotechnical factors</i>	19
2.5.2	<i>Mechanical factors</i>	20
2.5.3	<i>Operational factors</i>	21
3	LA MADDALENA EXPLORATORY TUNNEL PROJECT	23
3.1	Introduction	23
3.1.1	<i>Mont Cenis Base Tunnel</i>	25
3.2	La Maddalena exploratory tunnel	28
3.2.1	<i>General features and purpose</i>	28
3.2.2	<i>Geographical location</i>	28
3.2.3	<i>Tunnel route</i>	29
3.2.4	<i>Encountered rock mass lithologies</i>	30
3.2.5	<i>Rock supports and reinforcements</i>	31
3.2.6	<i>The Tunnel Boring Machine “Gea”</i>	34
4	GEOLOGICAL SETTING	39
4.1	Introduction	39
4.2	Penninic domain	40
4.2.1	<i>Grand Saint Bernard nappe</i>	40
4.3	Tectono-stratigraphic unit of Ambin	42
4.3.1	<i>Clarea complex</i>	44
4.3.2	<i>Ambin complex</i>	46
4.4	Structural evolution of Ambin	48
4.4.1	<i>Pre-Alpine evolution</i>	48
4.4.2	<i>Ductile Alpine evolution</i>	48

4.4.3	<i>Brittle Alpine evolution</i>	49
4.4.4	<i>Neotectonics</i>	50
5	ROCK MASS CHARACTERIZATION	55
5.1	Introduction	55
5.2	Intact rock property determination	57
5.2.1	<i>Lithological description</i>	57
5.2.2	<i>Micro-petrographic description</i>	58
5.2.3	<i>Uniaxial compressive strength</i>	61
5.2.4	<i>Determination of rock abrasivity</i>	69
5.2.5	<i>Determination of rock hardness</i>	73
5.3	Quantitative description of discontinuities	76
5.3.1	<i>Types of discontinuity</i>	80
5.3.2	<i>Orientation</i>	81
5.3.3	<i>Spacing between discontinuities</i>	89
5.3.4	<i>Volumetric joint count</i>	94
5.3.5	<i>Rock Quality Designation index, RQD</i>	96
5.3.6	<i>Rock block volume</i>	98
5.3.7	<i>Groundwater conditions</i>	100
5.3.8	<i>Joint conditions</i>	101
5.4	Rock mass classifications	110
5.4.1	<i>Rock Mass Rating (RMR) system</i>	110
5.4.2	<i>Geological Strength Index (GSI)</i>	117
5.5	Seismic wave propagation	121

5.5.1	<i>Tunnel Seismic Prediction System</i>	121
5.5.2	<i>Tunnel Seismic Prediction results</i>	123
5.6	Tunnel depth	126
5.7	Conclusive remarks	128
5.7.1	<i>Domain I</i>	129
5.7.2	<i>Domain II</i>	130
5.7.3	<i>Domain III</i>	131
6	TBM PERFORMANCE ANALYSIS	133
6.1	Field TBM performance database	134
6.1.1	<i>The first part of the database (DB1)</i>	134
6.1.2	<i>The second part of the database (DB2)</i>	136
6.2	Measured TBM performances	137
6.2.1	<i>Rate of Penetration distribution</i>	137
6.2.2	<i>Field Penetration Index</i>	139
6.3	Conclusion	142
7	COMPARISON BETWEEN DIRECT GEOSTRUCTURAL SURVEY AND SEISMIC METHODS FOR PREDICTING GEOLOGICAL FRAMEWORK AHEAD TUNNEL FACE	143
7.1	Introduction	143
7.2	Comparison of the results	144
7.2.1	<i>Prediction of significant lithological changes</i>	144
7.2.2	<i>Estimation of fracturing degree of rock masses and presence of shear or weakness zones prediction</i>	145
7.2.3	<i>Estimation of orientation of the principal elements of discontinuities</i>	147

7.3	Conclusion	152
8	LITERATURE MODELS FOR PREDICTING TBM PERFORMANCES AND THEIR APPLICATION TO “LA MADDALENA” EXPLORATORY TUNNEL	153
8.1	Approaches for predicting TBM performance	154
8.1.1	<i>Introduction</i>	154
8.1.2	<i>Theoretical models for predicting TBM performance</i>	155
8.1.3	<i>Empirical models for predicting TBM performance</i>	157
8.1.4	<i>Final observation about theoretical and empirical predictive models</i>	166
8.1.5	<i>Artificial intelligence techniques for predicting TBM performance</i>	168
8.1.6	<i>Final observation about artificial intelligence technique</i>	172
8.2	Evaluation of various TBM performance prediction models based on field data from “La Maddalena” tunnel	174
8.2.1	<i>Cassinelli et al. (1982) model</i>	175
8.2.2	<i>Innaurato et al. (1991) model</i>	177
8.2.3	<i>Khademi Hamidi et al. (2010) models</i>	179
8.2.4	<i>Hassanpour models</i>	182
8.2.5	<i>Delisio et al., models</i>	189
8.3	Conclusion	193
9	DEVELOPMENT OF TBM PERFORMANCE PREDICTIVE MODELS	199
9.1	Introduction	199
9.2	Theoretical concepts	200
9.2.1	<i>Correlation between variables</i>	200
9.2.2	<i>Simple linear regression analysis</i>	202
9.2.3	<i>Multiple linear regression analysis</i>	206

9.2.4	<i>Nonlinear regression analysis</i>	209
9.3	Effects of single rock/rock mass properties on TBM performances	210
9.3.1	<i>Uniaxial compressive strength</i>	210
9.3.2	<i>Quartz content</i>	212
9.3.3	<i>Alpha angle</i>	213
9.3.4	<i>Spacing between weakness planes</i>	214
9.3.5	<i>Joint volumetric count</i>	216
9.3.6	<i>Rock quality designation index</i>	217
9.3.7	<i>Joint conditions</i>	218
9.3.8	<i>Tunnel Depth</i>	220
9.3.9	<i>Rock Mass Rating</i>	221
9.3.10	<i>Geological Strength Index</i>	223
9.4	Combined effect of rock/rock mass properties on TBM performances	224
9.4.1	<i>Empirical models to predict the rate of penetration</i>	225
9.4.2	<i>Empirical models to predict the field penetration index</i>	230
9.5	Conclusion	236
10	CLUSTER ANALYSIS OF ROCK MASS PARAMETERS FOR TBM PERFORMANCE ESTIMATION	237
10.1	Multidimensional data analysis	238
10.1.1	<i>Introduction</i>	238
10.1.2	<i>Euclidean space</i>	239
10.1.3	<i>Principal component methods</i>	240
10.1.4	<i>Cluster analysis</i>	248
10.1.5	<i>Observations</i>	254

10.2	Application to “La Maddalena” case study	255
	<i>10.2.1 Introduction</i>	255
	<i>10.2.2 Relationship among geological and geomechanical variables</i>	256
	<i>10.2.3 Relationship among geological – geomechanical variables and TBM performance</i>	265
	<i>10.2.4 Regression analyses on clusters</i>	270
10.3	Conclusion	280
11	ROCK ENGINEERING SYSTEM: FROM THE INTERACTION MATRIX TO TBM PERFORMANCE ESTIMATION	281
11.1	Theoretical aspects	281
	<i>11.1.1 General concepts</i>	281
	<i>11.1.2 Matrix resolution</i>	282
	<i>11.1.3 Atlas of rock engineering system</i>	284
	<i>11.1.4 Matrix coding</i>	285
	<i>11.1.5 Cause-effect plot</i>	286
	<i>11.1.6 Theorems 1 and 2</i>	289
11.2	RES application to TBM performance estimation	290
	<i>11.2.1 Rock mass parameters involved in RES application</i>	290
	<i>11.2.2 Interaction matrix</i>	290
	<i>11.2.3 Predictive model development</i>	294
11.3	Conclusion	301
12	PREDICTIVE MODEL VALIDATION	303
12.1	Introduction	303
12.2	Validation of ROP models	306

12.2.1	<i>Validation of RL2 model</i>	306
12.2.2	<i>Validation of RNL model</i>	309
12.2.3	<i>Validation of ROP models carried out for each cluster</i>	311
12.3	Validation of FPI models	315
12.3.1	<i>Validation of FL4 model</i>	315
12.3.2	<i>Validation of FNL model</i>	317
12.3.3	<i>Validation of FPI models carried out for each cluster</i>	319
12.3.4	<i>Validation of FPI model obtained by means of RES approach</i>	323
12.4	Conclusion	324
13	CONCLUSION	327
14	REFERENCES	331

APPENDIX I: Schemes used during geological surveys

APPENDIX II: Histograms of frequency of the principal geological and geotechnical variables

APPENDIX III: Longitudinal geological section of “La Maddalena” tunnel

APPENDIX IV: The generic underground excavation matrix; Hudson, 1992

1 INTRODUCTION

1.1 General purpose

The general purpose of this thesis is to investigate the relationship between the geological, mechanical and structural features of rock masses and the performances of Tunnel Boring Machine used for the excavation in order to carry out empirical models able to predict the behaviour of a machine operating in a specific geomechanical context.

Understanding the influence of geological ground conditions on the TBM performances is fundamental both to select the most appropriate machine and to estimate the costs and the times of tunnel realisation to the purpose of making mechanised tunnelling cheaper, safer and more effective than the traditional method.

This research work focuses on “La Maddalena” exploratory tunnel, which is one of the infrastructures related to the planned Lion-Turin high speed railway. La Maddalena is located in Susa Valley, Western Alps, North Italy.

In order to achieve this objective an extensive field work has been performed. The entire tunnel length (about 7000 meters) has been continuously surveyed and a large amount of information about discontinuity properties has been collected; moreover, several rock matrix indices have been acquired. The principal operating parameters have been acquired during tunnelling and analysed to the purpose of carrying out the performance indices to be relate to rock mass features. A large database containing the rock mass and intact rock features and the TBM indices has been built and implemented. Data elaboration allowed for a detailed ground characterisation and TBM performance description.

The relationship between the geological parameters and the machines ones has been investigated by means of different approaches with the aim of developing TBM performance predictive models. In particular, regression analyses, multiple correspondence analyses and clustering, and the Rock Engineering System (Hudson, 1992) have been performed.

In a first stage, a detailed literature review allowed to select fourteen existing predictive models in order to evaluate their applicability to La Maddalena tunnel, by comparing the measured performance and the calculated ones.

1.2 Work organisation and thesis structure

Simple and multiple regression analyses, both linear and nonlinear, have been performed to quantify the correlation between the independent variables (geological and geotechnical properties) and the response ones (TBM performances).

Multiple correspondence analysis and cluster analysis have been performed in order to objectively divide the rock mass into homogeneous portions, considered as different classes of excavatability.

The Rock Engineering System (Hudson, 1992) has been applied by providing some modifications to the original version, in order to define a situ-specific cause-effect matrix able to define the geomechanical factors predisposing a certain machine response. The final purpose is to define an empirical TBM performance predictive equation on the basis of the cause-effect matrix.

The predictive capability of the regression models carried out during this work has been tested by comparing the performances measured during tunnelling and the ones estimated by means of the predictive model.

1.2 Work organisation and thesis structure

This thesis is divided into three parts:

The first part consisted of an extensive field work, with the purpose of collecting a large amount of geological, structural and mechanical information as well as TMB data collection. In the first part of this research work, rock mass and machine performance have been described in detail; this part took a long time.

The second phase was devoted to an accurate statistical analysis of the relationship between rock mass parameters and machine performances. As a result, empirical predictive modes have been obtained.

The third phase was dedicated to the validation of the obtained models. In this part, both their capability to explain the relationship between geological parameters and TBM performances, and to predict TBM indices have been evaluated.

The working procedure followed during the research is represented in Figure 1.1.

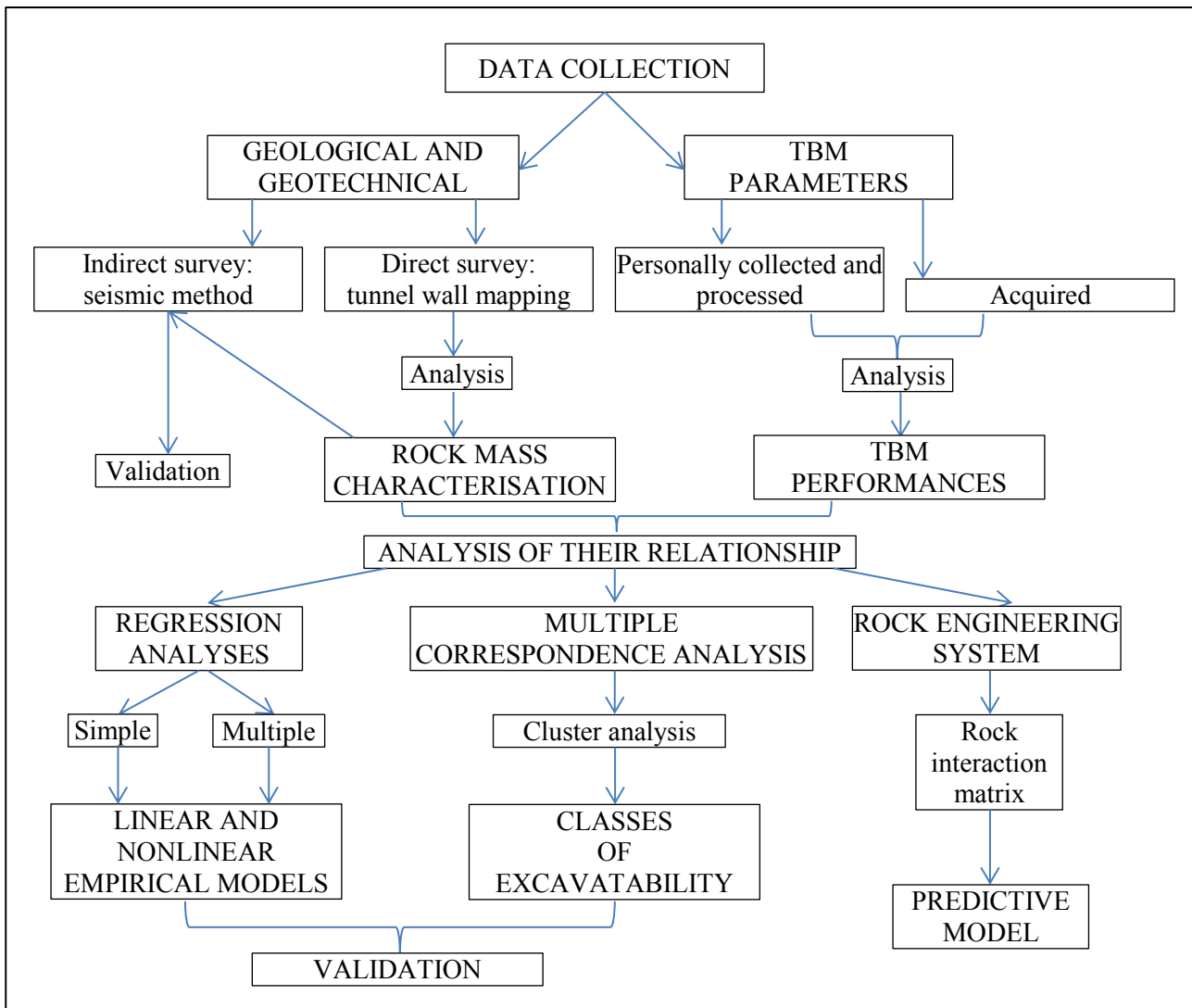


Figure 1.1 Working flow chart.

A brief summary of each chapter is provided:

Chapter 2: in this chapter a brief overview about mechanised tunnelling is provided. The main working principles of TBM, the different types of machines, the geological contexts in which they are involved and the most common TBM performance indices are discussed.

Chapter 3: this chapter describes the general aspects of “La Maddalena”, as the TBM used for the excavation, the types of supports required, the encountered geological formations, etcetera. The main features of Lyon-Turin rail and the Mont Cenis Base Tunnel are also described.

Chapter 4: the regional and local geological settings of the area hosting “La Maddalena” tunnel are described in this chapter. Particular attention was given to the lithological description of the formations encountered during tunnelling and to neotectonic framework.

1.2 Work organisation and thesis structure

Chapter 5: the description of geological and geomechanical features of the excavated rock mass has been provided in this chapter. Here, both the results of tunnel wall mapping, personally carried out, and the acquired results of laboratory tests on rock samples are presented. Global description of rock mass is provided.

Chapter 6: this chapter is about the TBM performance indices acquisition, elaboration and analysis. The statistical description of registered performances has been provided.

Chapter 7: it is devoted to describe the comparison between the information collected during direct geological surveys, described in Chapter 5, and the one obtained by means of an indirect survey method: the so called Tunnel Seismic Prediction System.

Chapter 8: this chapter provides an overview about the TBM performance predictive methods and the description of their advantages and disadvantages. Some of these models have been applied to this case study and the results have been commented here.

Chapter 9: an overview about the statistical regression methods has been supplied. The results of simple (single rock parameter correlated with TBM index) and multiple (more than one geological parameter vs. machine one), linear and nonlinear regression analyses have been described.

Chapter 10: a general description of the multiple correspondence analysis (MCA) and cluster analysis (CLA) is supplied. In this chapter the MCA and CLA performed on La Maddalena tunnel data has been set up, moreover, a detailed geological description of each obtained cluster has been provided.

Chapter 11: in this chapter the Rock Engineering System is introduced. Some modifications with respect to the classical approach have been proposed and its application to La Maddalena case study and the obtained results have been discussed.

Chapter 12: the validations of the obtained predictive models are described in this chapter and a critical discussion about their reliability and their findings is also provided.

Chapter 13: this chapter summarises the general conclusions of the thesis.

2 MECHANISED TUNNELLING

2.1 Introduction

Tunnel Boring Machines, TBMs, were introduced in 1950s in order to mechanise tunnelling operations, improve worker safety conditions and make mechanised tunnelling more convenient and quicker than the traditional “drill and blast”.

There are different types of TBMs (see Paragraph 2.2) but all of them are composed by a main body and by a back-up system and consist of four system groups (Maidl et al., 2008):

- *Boring system*: composed by the cutterhead, the cutters and the cutterhead drive;
- *Thrust system*: where the main tools are the thrust cylinders; it includes also the clamping structure and the rear and front support;
- *Rock cutting removal system*: it has the aim of removing the muck from the tunnel by means of cutterhead buckets and conveyor belts;
- *Lining and support system*: this system depends on the type of machine.

The basic operational principle of TBMs is that rotation and thrust are simultaneously applied to the cutterhead: the first one is guaranteed by the torque generated by TBM motors and the second one by means of thrusts cylinders. The cutters mounted on the cutterhead are responsible to the rock mass breakage; the resulting muck is collected by the specific buckets situated on the cutterhead and moved outside the tunnel by means of the conveyor system.

On the basis of the geological and geomechanical context in which the tunnel has to be realised different types of rock reinforcements and rock supports can be installed, such as bolts, steel wires, shotcrete, etc..

2.2 Types of Tunnel Boring Machines

2.2 Types of Tunnel Boring Machines

Construction companies produce various types of TBMs in order to face the different geological and geomechanical contexts and different systems are used to classify them. Firstly, it is possible to distinguish soil/soft ground TBMs and rocky ones.

Generally, the geological and structural setting in which TBM has to work determines its selection; Figure 2.1 provides a clear example of the suggested machine for each of the most common geological settings.

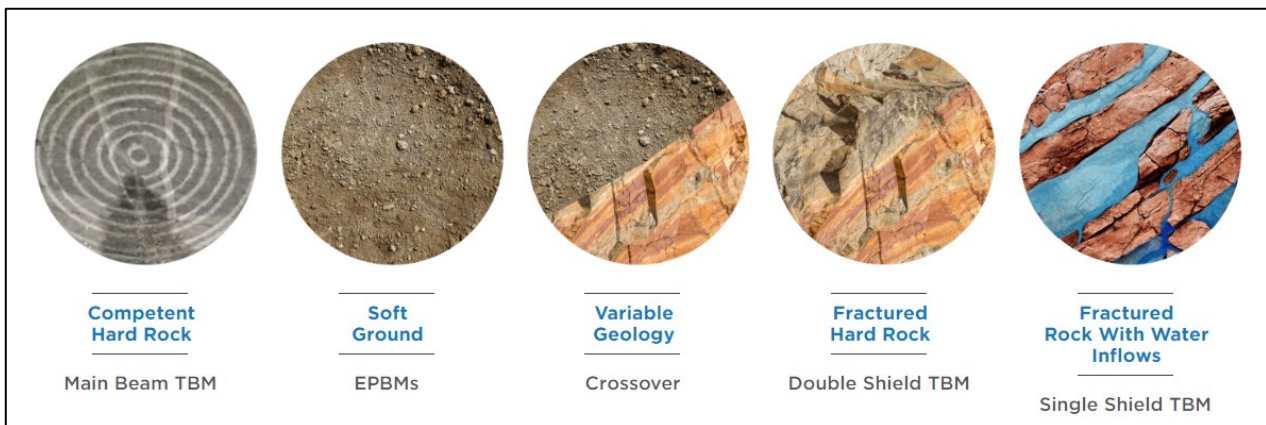


Figure 2.1 Geological contexts and suggested TBM (Robbins Company).

One of the most important distinctions in rock TBM classification is between the open (or gripper) and the shield TBM. In the diagram reported in Figure 2.2, a list of gripper and shield TBM subcategories has been provided.

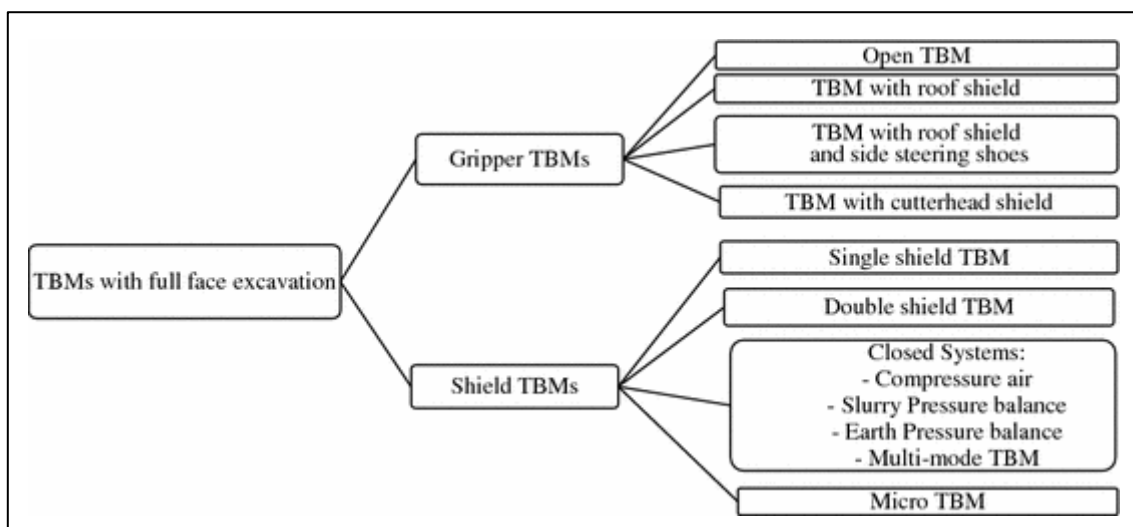


Figure 2.2 Types of TBMs (Zou, 2017).

2.2.1 Open type TBM

The open type TBM, also called gripper TBM, is widely used for tunnel excavation where rock masses are characterised by global good quality and stand-up time long enough to put in work the required supports in safety conditions, given that usually there are not any protection unit for the worker.

In some cases a partial shield behind the cutterhead can be installed, in particular, it is possible to install a roof shield (on the crown) or a side steering shoes (on the crown and the walls); moreover, some machines have a shield protecting the cutterhead.

In Figure 2.3 open TBM without any shields and the three partial shield application solution are shown.

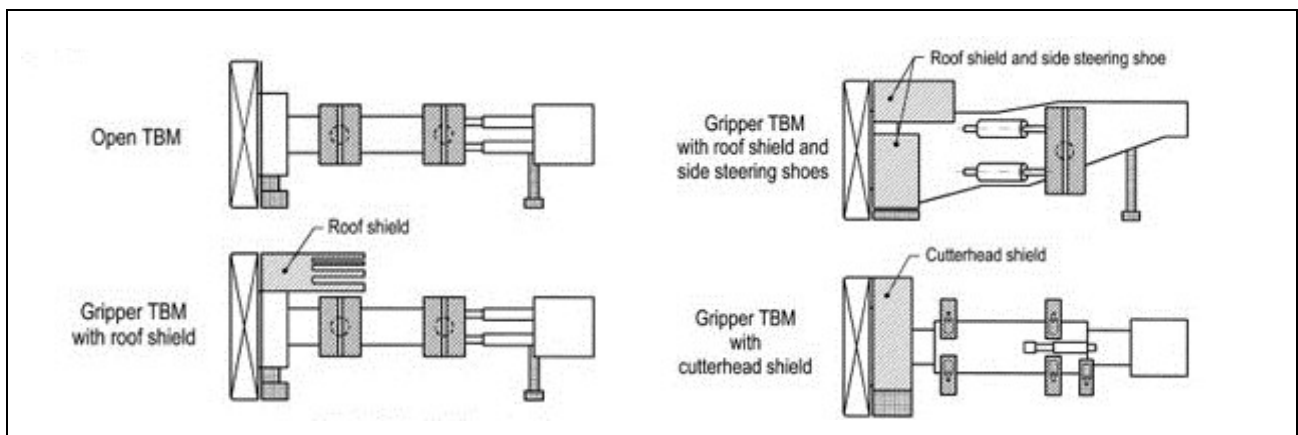


Figure 2.3 Schemes of open type TBM; a) without any shield, b) with roof shield, c) with roof shield and side steering shoe, c) with cutterhead shield (Maidl et al., 2008).

The clamping system is composed by the gripper group which includes the gripper plates. Hydraulic jacks move the grippers.

If a single gripper system is present, we have a main beam TBM (Robbins type); on the contrary if a double gripper system (named Kelly) is presents, we have a Kelly beam TBM (Jarva type).

Boring cycle of an open TBM is composed by four principal steps.

Firstly, the gripper shoes are pushed against tunnel walls previously excavated (by means of laterally extendible hydraulic cylinders) and rear legs are lifted, then thrust cylinders push the cutterhead against the tunnel face and, at the same time, the cutterhead is rotating. In this way cutters start to cut the rock, and single pieces called chips are broken out of the rock mass. The excavated material is taken up by buckets situated at the cutterhead and after some passages rock

2.2 Types of Tunnel Boring Machines

chips are removed from the tunnel. Cutterhead rotation is stopped when the bore stroke is completed; at this point rear legs are extended. The last stage is called regripping, in this phase gripper plates are retracted and the retraction of thrust cylinders makes the gripper unit slide forward.

In Figure 2.4 the most important elements characterising a gripper TBM are reported.

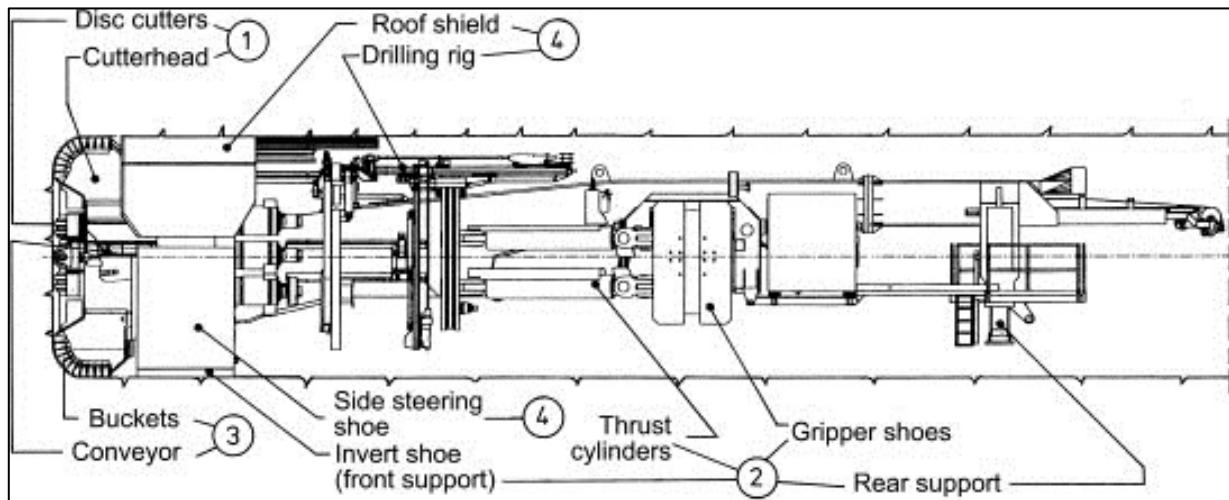


Figure 2.4 Elements characterising a gripper TBM (Maidl et al., 2008).

Open TBM grants free access to the tunnel walls, in this way, when the excavation is realised by means of one of the TBMs belonging to this group, geologists and engineers have the possibility to directly collect geological, structural and mechanical data about the encountered rock masses.

For this reason the open TBM is the most adopted in the construction of exploratory tunnels.

2.2.2 Shield type TBM

The shield TBM differs from the open ones for the presence of one or two shields. These cover the main body of the TBM, and not only a limited part of it behind the cutterhead. This group of machines is utilised in low quality rock masses, in jointed ones, in which stand-up time is limited or very limited and it is not long enough to allow the miners to put in operation supports and linings. The shield has the function of avoid tunnel collapse and of making operators work in safe conditions.

The group of shield TBMs is divided in single shield TBM and double shield TBM.

2.2.2.1 Single shield TBM

This group of TBMs is usually used to excavate jointed rock masses with low stand-up time; in these contexts single shield TBMs can guarantee high tunnelling performances thanks to the pre-cast segmental lining or pipe jacking tunnelling methods.

The substantial difference between open and shield TBM is that in the first group the contrast required by thrust cylinders to transfer the thrust to the cutterhead is provided by rock tunnel walls, whereas in the second group the contrast is provided by lining, given that rock mass strength in which single shield TBMs are used generally lower that the one characterising the rock mass in which open TBM are adopted.

The boring process is cyclic because when bore stroke is completed thrust cylinders have to be retracted and the ring erector has to install the pre-cast segmental lining.

In Figure 2.5 a typical diagram for a single shield TBM is provided.

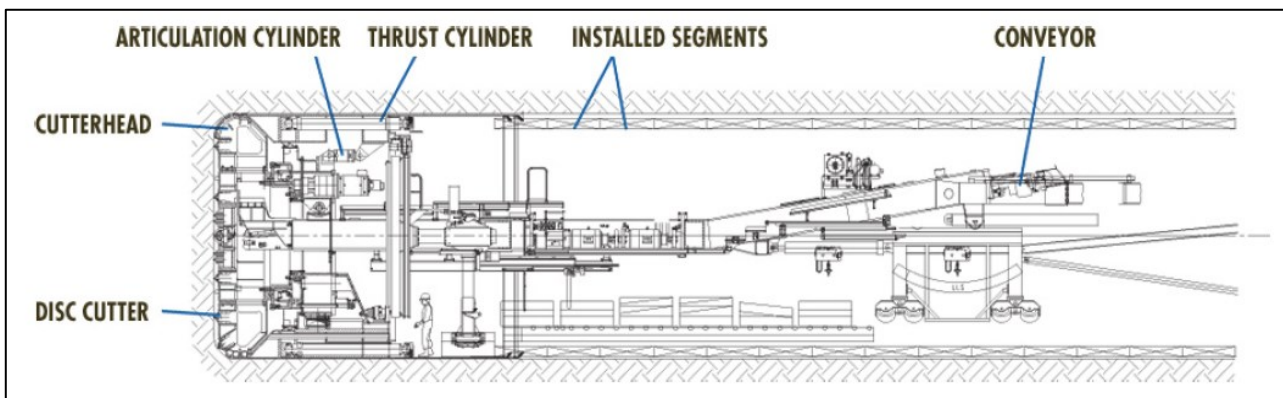


Figure 2.5 Diagram for a single shield TBM (Robbins Company).

2.2 Types of Tunnel Boring Machines

2.2.2.2 Double shield TBM

Double shield TBMs, also called telescopic shields, are frequently used in long tunnel excavation in hard rocks when high fractured or shear zones and faults may be present. They are suggested for stable and unstable geological conditions.

The double shield TBMs are considered the most sophisticated ones because they are a combination of gripper and single shield machines. They guarantee very high tunnelling performances by working in continuous tunnelling mode.

They consist of two principal elements: a front shield with cutterhead, drive and main bearing; and a gripper shield with gripping units, auxiliary thrust cylinders and tailskin (Herrenknecht AG). The two parts of the shield are connected by the main thrust cylinders and a telescopic shield protects them. When stable rock mass conditions occur the machine is braced against the tunnel walls by means of the gripper shoes, in this way the front shield can be advanced independently of the gripper shield thanks to the main thrust cylinders. The segments are installed in the tailskin section while the machine is tunnelling.

When a bore stroke is completed the gripper shoes are loosened and the auxiliary thrust cylinders make the gripper shield push behind the front shield.

In Figure 2.6 the principal components of a double shield TBM are shown.

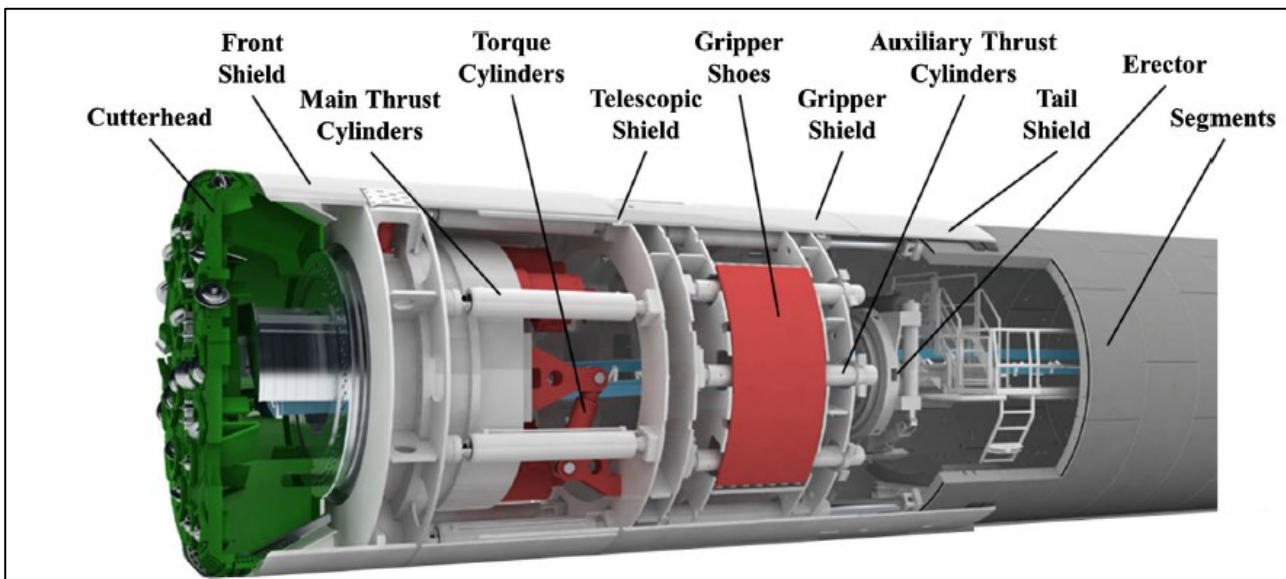


Figure 2.6 Principal components of a double shield TBM (Herrenknecht AG).

2.2.3 Closed mode TBM

This type of TBMs is generally used for the excavation of soils, very soft rocks or grounds under the water table and in general where tunnel face needs to be supported. On the basis of tunnel face balancing system it is possible to distinguish three main groups of close mode TBMs: the compressed air machines, the slurry shield machines and the earth pressure balance (EPB) ones:

- In the *compressed air machines* the element that balances the tunnel face pressure is the compressed air;
- *Slurry shield machines* balance the horizontal ground and water pressure by means of a mixture of bentonite and water; they are used for the excavation of sand and fine gravel (Figure 2.7);
- In the *EPB* the balancing material is the one excavated with the addition of liquid or foam conditioning agents. EPB machines are used to excavate clay, silt and fine sand (Figure 2.8).

There is another type of machines belonging to the closed mode TBM; it is represented by the crossover TBMs (also called multi-mode TBMs or hybrid machine). This group of machines is able to work both in open-mode and in closed-mode. In the first case they excavate as a single shield TBM, in the second one they work as slurry shield or EPB machine. Some cross over TBM are designed with the purpose of passing from EPB to slurry and vice versa when they are working in closed-mode. For these reasons the hybrid machine are particularly suggested for the excavation in highly variable geological contexts.

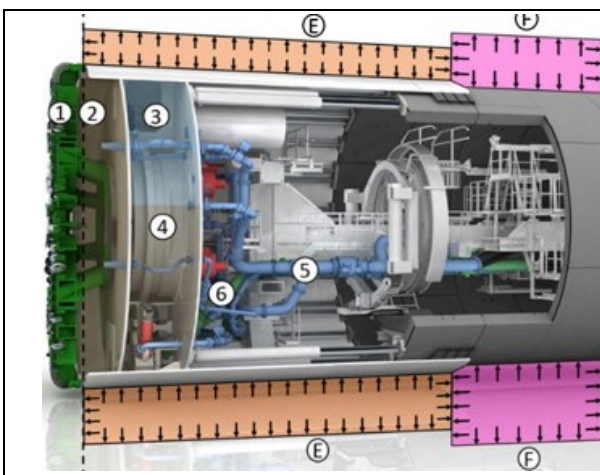


Figure 2.7 Slurry shield TBM. 1: cutterhead, 2: excavation chamber, 3: air bubble, 4: working chamber, 5: slurry feed line, 6: slurry return line, E: slurry radial shield pressure, F: grout pressure (Mooney et al., 2016).

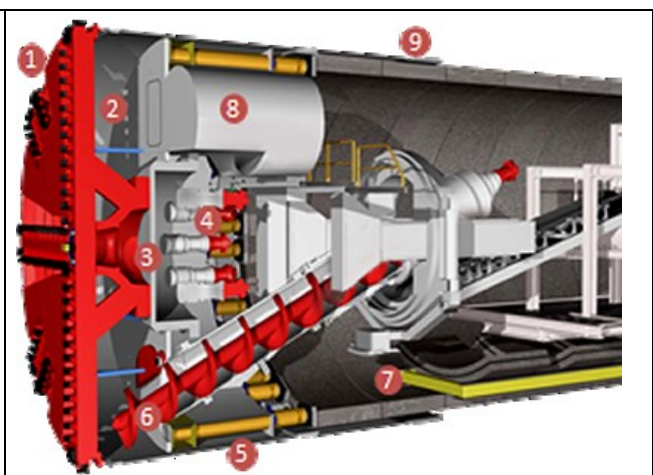


Figure 2.8 EPB TBM. 1: cutting wheel, 2: excavation chamber, 3: pressure bulkhead, 4: main drive, 5: thrust cylinders, 6: screw conveyor, 7: erector, 8: double chamber airlock, 9: tailskin with integrated grout lines (Institute of Geology of Malaysia).

2.3 Rock breakage mechanism

2.3 Rock breakage mechanism

TBMs excavate rock masses through crushing and rotating by applying high pressure on the rock face with high thrust forces while chipping and rotating by means of a number of tools (disc cutters) installed on the machine face, the cutterhead. Disc cutters cause the rock failure and the formation of slabs of rock, also called chips, guaranteeing tunnel advance.

2.3.1 Disc cutters

The cutters (Figure 2.9) installed on the cutterhead are responsible for the rock cutting. There is a large variety of cutters designed for different ground conditions; in hard rock contexts disc tools are typically used: single discs (the most employed), twin discs (generally mounted in the center of cutterhead) and double discs. The cutters are mounted on roller bearings and can be replaced in front of or behind the machine face.

In the Figure 2.10 a schematic representation of a disc cutter with its principal component is reported.



Figure 2.9 Single disc cutter.

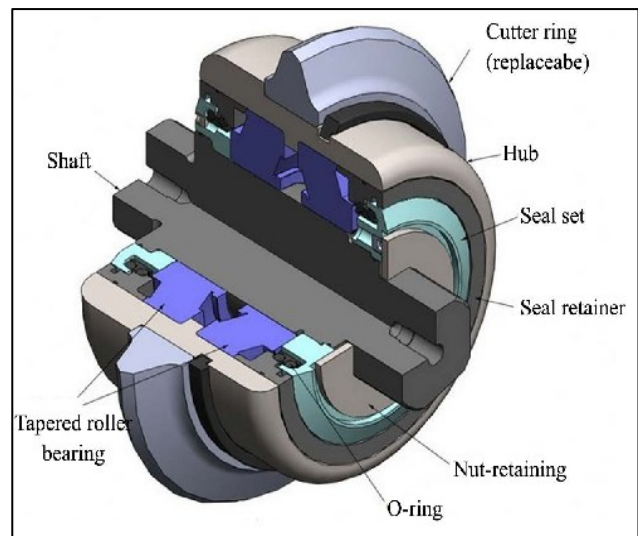


Figure 2.10 Disc cutter components (Xia et al 2015).

On the market there is a wide range of cutter diameters up to 6'' (150 mm) for microtunnels realisation, 12'' (305 mm), 20'' (508 mm), in hard rock tunnelling the most employed diameter are 17'' (432 mm) and 19'' (483 mm). Cutter geometry seriously affects tunnelling, for example the increase in the diameter implies an increase in both load limit and linear velocity.

The cutter steel alloy has to be selected on the basis of the rock properties; when soft ground conditions occur, standard steel should be chosen, in presence of hard and abrasive rocks the best

solution could be the heavy duty steel and in case of abrasive soft ground hard-faced version (Palmieri Company) is frequently adopted.

2.3.2 Rock failure

Before explaining the rock breakage process under TBM rolling cutters it is necessary to introduce the cutter movements performed during their action and the forces acting on them.

Each cutter performs two rotational movements during its work:

- It rotates around disc axis: this movement is due to the contact with the rock face;
- It rotates around the tunnel axis: this movement is due to the cutterhead rotation.

As for the forces acting on the cutters during their rotation, it is possible to distinguish three forces, as shown in Figure 2.11.

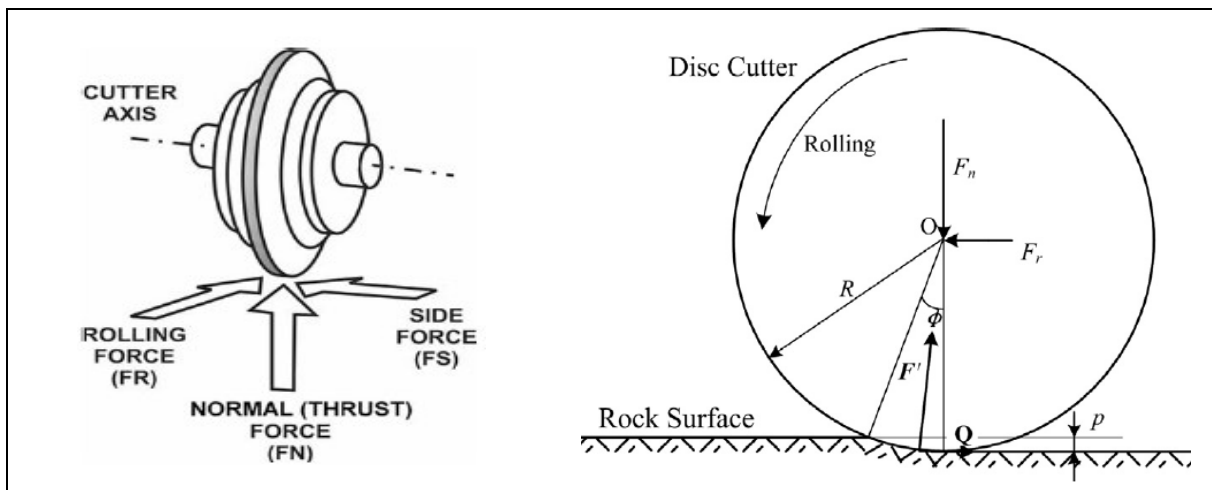


Figure 2.11 The forces acting on the cutter; R : cutter radius, p : penetration depth, ϕ angle between cutter and rock (on the left Balci et al., 2009; on the right Wang et al., 2015).

- The *normal force* (thrust force), F_n , is the force that the cutterhead applies to the cutter in the vertical direction. It is the force necessary to maintain the tool at the desired level of penetration (Balci et al 2009);
- The *rolling force*, F_r , is the force applied to the disc in the rolling direction by means of cutterhead torque (Wang et al., 2009). F_r is used to estimate the specific energy requirement, that is the amount of energy needed to excavate a unit volume of rock (Balci et al., 2009);
- The *side force*, F' , is represented by the perpendicular action force of the rock and acts on the contact surface between the cutter and the rock (Wang et al., 2015).

2.3 Rock breakage mechanism

The rock breakage mechanism by means of TBM rolling cutters can be divided into two continuous stages (Gong and Zhao, 2009). In the first one, named indentation, the disc intrudes into the rock mass, generating internal cracks, large and small fragments.

The second stage is characterized by the propagation of cracks between two adjacent cutters. They converge towards each other and coalesce, in this way rock chips are generated between two cutters.

More precisely Cook et al. (1984) described the following phases: the building up of a stress field followed by the formation of a damaged zone, the generation of surface chipping and finally a crater formation. As a consequence of the indentation process, three different sectors can be observed: the crushed zone, the crack and the elastic one (Cook et al., 1984; Chiaia, 2001; Gong et al., 2006). The penetration process composed of multiple indentation cycles, and each of them expands the crushed zone and crack propagation allowing the meeting of fractures generated by adjacent cutters.

Cutters have to be mounted on the cutterhead in order to allow the crack intersection and the minimum consumption of cutting energy. In order to guarantee an optimum cutting geometry a parameter given by the ratio between cutter spacing and penetration rate has been introduced and it should range between 10, for soft rocks and 20 for hard ones (Ozdemir, 1992; Rostami, 2008; Rostami et al, 2017).

This discussion is graphically represented by Figure 2.12.

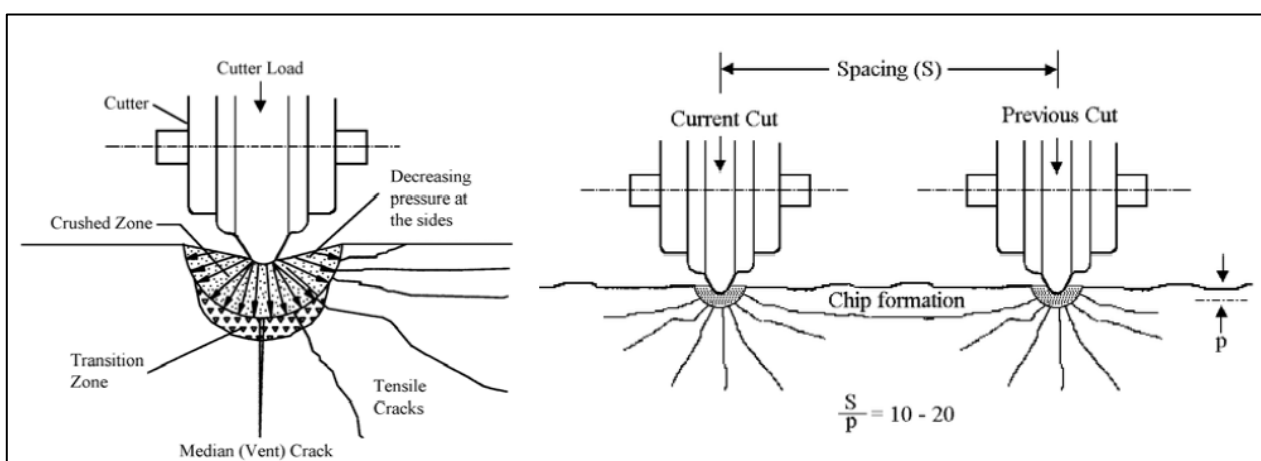


Figure 2.12 Rock chip formation under cutter action (Herrenknecht, 2003).

When the spacing between cutters is too small overcrushing occurs, this causes high consumption of specific energy; whereas when spacing is too large chips cannot be generated (Figure 2.13).

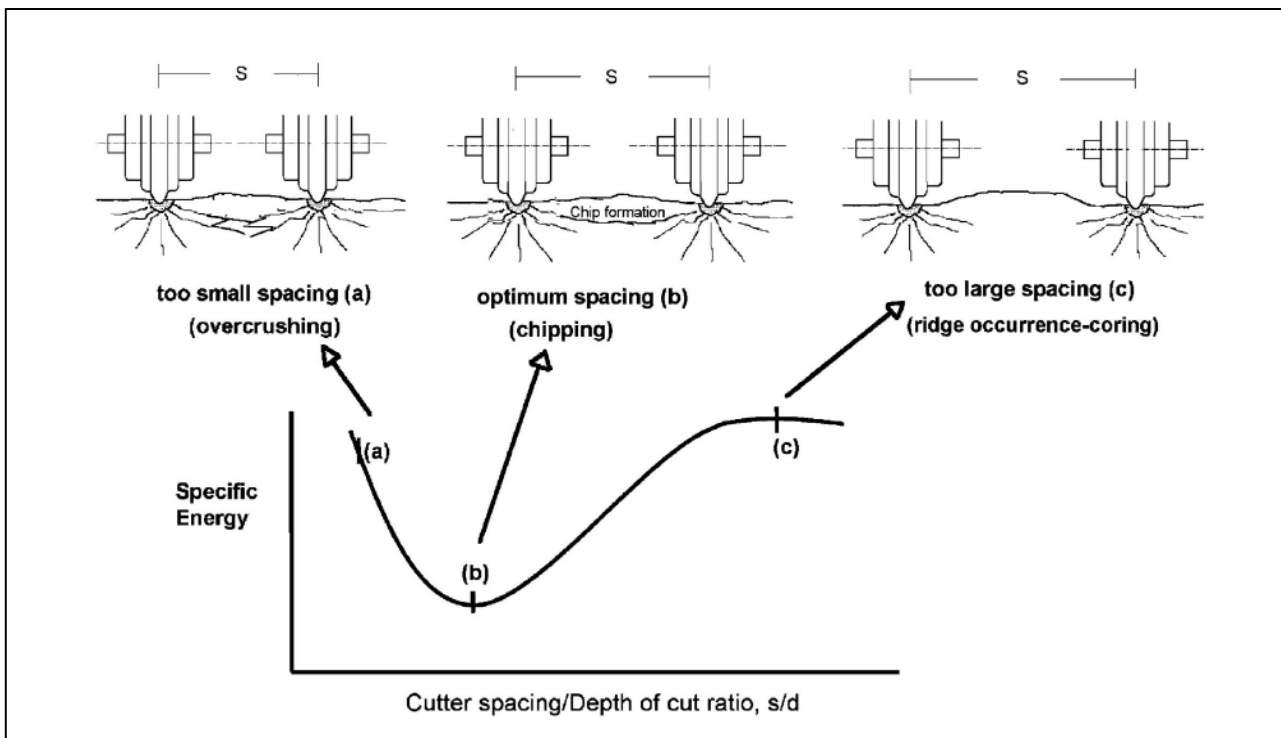


Figure 2.13 Cutter spacing and specific energy consumption (Tuncdemir et al., 2008).

The spacing between joints occurring in a rock mass has a great influence on the chip forming process. The role of joint spacing on rock fragmentation under cutter action has been studied by many researchers (e.g. Gong et al., 2006; Sun et al., 2011; Liao et al., 2013) by means of field tests, laboratory tests (e.g. indentation test) and numerical simulation methods.

In particular, Gong et al. (2006) demonstrated that when joints are low spaced (spacing range from 50 mm to 80 mm) the joints were favourable to rock fragmentation; on the contrary, joints had a little influence on rock breakage mechanism when spacing is higher than 500 mm. In this case, crack process is similar to the one observed for the single cutter action on the rock without fractures (Gong et al., 2006).

2.4 TBM performance indices

2.4 TBM performance indices

Over the years, many researchers have introduced various indices in order to assess the boreability of a rock mass. These indices are commonly known as TBM performance indices.

Here they have been listed and a brief description for each of them is provided.

2.4.1 Rate of penetration

The rate of penetration (ROP) or penetration rate (PR) is defined as the excavated length in a continuous phase during the effective boring time; it represents net penetration. This time does not consider machine breakdown, downtimes for TBM maintenance, excavation stop for reinforcement or support element or lining installation.

ROP can be calculated as:

$$ROP = \frac{L_e}{T_e} \quad (2.1)$$

where L_e is the excavated length and T_e is the effective boring time.

ROP is generally expressed in [m/h] or in [mm/min].

ROP does not consider any machine specification or operational parameter.

2.4.2 Advance rate

The advance rate, AR, contrariwise to ROP, is the ratio between excavated length and total time, which includes the time necessary to bore, to install supports and lining, the time needed for the TBM ordinary and extraordinary maintenance, etc..

AR is calculated in accordance to:

$$AR = \frac{L_e}{T_t} \quad (2.2)$$

where L_e is the excavated length and T_t is the total time necessary to do all the required tunnelling operations.

AR is generally expressed in [m/h] or in [mm/min].

AR, like ROP, does not consider any machine specification or operational parameter.

2.4.3 Coefficient of utilisation

The coefficient of utilisation is the ratio between AR and ROP:

$$U = \frac{AR}{ROP} \quad (2.3)$$

U is expressed in percent [%].

In stable rock masses the AR is considerably lower than ROP and U ranges between 30 – 50 % due to machine daily maintenance (Nielsen and Ozdemir, 1993; Boniface, 2000; Sapigni et al., 2002). In rock masses characterised by low quality ROP could be potentially high, but AR is generally low due to the reinforcement and support installation necessity, the gripper bearing failure, etcetera. For this reason, U results as low as 5 – 10 % or less (Barla and Pelizza, 2000; Sapigni et al., 2002).

2.4.4 Penetration rate per revolution

The penetration rate per revolution is the effective bored length for each complete revolutions of the cutterhead. It can be calculated in accordance to the equation 2.4:

$$PRev = \frac{ROP * 1000}{RPM * 60} \quad (2.4)$$

where ROP is the rate of penetration and RPM is the number of complete cutterhead revolution in one minute.

PRev is expressed in [mm/rev].

2.4.5 Field penetration index

The field penetration index, FPI, (Hamilton and Dollinger, 1979; Nelson et al., 1983; Tarkoy and Marconi, 1991; Klein et al., 1995) is the ratio between the total force acting on the cutterhead or acting on each cutter and the penetration rate per revolution. It represents the force necessary to obtain a determinate penetration during a single revolution.

FPI can be calculated according with:

$$FPI = \frac{Fn}{PRev} \quad (2.5)$$

where Fn is the force acting on each cutter or on the cutterhead.

2.4 TBM performance indices

FPI is measured in [kN/cutter/mm/rev] or in [kN/mm/rev] if the total force acting on the cutterhead is considered and not the force acting on each cutter.

FPI has been introduced in order to represent a normalised measure of ROP, specified in terms of applied thrust on the cutters for a specific penetration rate per revolution in various geological and geomechanical situations.

The use of FPI implies a linear relationship between penetration and thrust, however a nonlinear relationship occurs (Rostami, 1997; Laughton, 1998; Gong and Zhao, 2007). This limitation is overcome if the machine penetration is higher than the threshold penetration, suggested equal to 1 mm/rev by Gong and Zhao (2007), where ROP and thrust relationship is linear.

2.4.6 Specific penetration

The specific penetration, SP, (Alber, 2000) is the inverse of FPI. SP can be calculated according to the following formula:

$$SP = \frac{PRev}{Fn} \quad (2.4)$$

SP is measured in [mm/rev/kN/cutter] or in [mm/rev/kN] if the total force acting on the cutterhead is considered and not the force acting on each cutter.

SP has been introduced by Alber (2000) with the aim of combining the thrust and the cutterhead revolution rate with the penetration rate, this allow penetration rate to be normalised against rock mass strength variations (Farrokh et al., 2012).

Being SP the inverse of FPI, the discussion carried out for FPI limitation can be considered valid for SP.

2.4.7 Specific excavation rate

The specific excavation rate, SER, was developed by Stevenson (1999) in order to combine the specific penetration and the tunnel cross area, in fact it can be calculated as the ratio between the excavated volume per each cutterhead revolution and the thrust per cutter. Final formulation is:

$$SER = A * SP \quad (2.4)$$

where A is the tunnel cross section area. SER is measured in [(m³/rev)/(kN/cutter)].

2.5 Factors influencing the TBM performances

There are several factors able to influence mechanised tunnelling; they can be divided into three groups:

- *Geological and geotechnical* factors: related to the ground that has to be excavated, they can change considerably during tunnel length. They include both properties related to the intact rocks (as strength, texture, mineralogy, abrasivity) and to the rock masses (as fracturing degree, joint orientation, groundwater flow conditions);
- *Mechanical* factors: these are related to the machine and for this reason they are constant during the excavation. This group includes the TBM characteristics, like type of TBM, diameter, cutter specifications;
- *Operational* factors: as support installation or experience of workers. As the geological factors, they may be subject to significant changes during the excavation.

2.5.1 Geological and geotechnical factors

The geological, structural, geomechanical and hydrogeological context in which a tunnel construction takes place is the factor that most significantly influences the TBM performances; for this reason, the selection of a TBM to be used in a tunnel project should be made on the basis of the geological condition of the site.

It is necessary to consider that a TBM selection is irreversible, so, in order to guarantee an appreciable construction level and avoid machine stops, a detailed rock masses characterisation is fundamental since the project stages.

One of the most influencing parameter is the rock strength; generally when it increases the penetration decreases and the thrust required to guarantee a penetration is high (Yagiz, 2008; Gong and Zhao, 2009; Khademi Hamidi et al., 2010; Armetti et al., 2017).

Fracturing degree also affects TBM performance. Penetration is facilitated when the rock mass is jointed, so this situation could increase ROP, however the occurrence of high fractured ground requires the installation of supports and reinforcements determining low values of AR. Moreover, if the rock mass is strongly fractured and the spacing between discontinuities is smaller than disk spacing, there is no (or little) chip formation, but regrinding of rock blocks. This significantly reduces the penetration. Also the orientation of discontinuities with respect to the tunnel axis could influence the penetration, the most favourable angle is of 60° (Bruland et al., 1998; see Chapter 5).

2.5 Factors influencing the TBM performances

Generally it is possible to assert that high quality rock masses are more difficult to be penetrated by a TBM and as a result low values of ROP and high ones of FPI are measured. Supports are rarely requested so AR is generally high.

On the contrary, when tunnelling is performed in low quality rock masses net penetration is generally high and the associated requested thrust is low, however AR is low due to the long time needed to install supports.

2.5.2 Mechanical factors

The features of machines, cutterheads and cutters are the mechanical factors that influence the TBM performances. These characteristics are the result of design stages and they cannot be modified during excavation phases; sometimes modification can be operated on cutter alloy or profile.

The machine type influences tunnelling, for example double shield TBMs allow for continuous boring cycle (accelerating tunnel construction) in contrast to gripper type (see section 2.2). Generally machine size affects its performances. The highest performances can be registered with small TBMs: this is due to the cutterhead rotation speed; which is higher for small diameters than for large ones. Moreover large size machines require more maintenance time than the small ones.

Some measures as flat cutterhead profile and cutter protection allow the reduction of cutter and cutterhead wear and breakage, especially when jointed conditions occur (Delisio and Zhao, 2014).

Cutter features (type, profile, material and diameter) seriously affect the performances of a TBM. In particular, Roxborough and Phillips (1975) and Phillips and Bilgin (1977) assert that larger cutters require higher thrust in order to obtain the same penetration for a rock mass, being disc -rock contact area larger. The thrust capacity increases when cutter diameter increases and, as a consequence, the penetration. Cutters characterised by larger diameters have a longer life because they rotate slower for a given head rotation speed and they are able to collect more material to wear before to be replaced (Roby et al., 2008).

2.5.3 Operational factors

The operational factors that influence the TBM performance can be divided into two groups: the constant factors and the variable ones.

The constant ones cannot be modified during the excavation, for example the shape and the diameter of the tunnel. On the contrary the variable can be modified on the basis of the geotechnical conditions encountered. This group is represented by machine thrust, torque, power and all TBM driving choices that can adjusted on the basis of rock mass strength and fracturing degree. For example in very hard rock thrust is maintained low in order to avoid excessive cutter consumption and machine damages.

3 LA MADDALENA EXPLORATORY TUNNEL PROJECT

“La Maddalena” exploratory tunnel is one of the infrastructures related to the realization of the high speed/high capacity rail that aims to connect Lyon (France) to Turin (Italy). For this reason, a synthetic description Lyon-Turin section and of Mont Cenis Base Tunnel is provided prior to the description of La Maddalena project.

3.1 Introduction

The “Core Network Europe” was presented by the European Commission in October 2011; it will connect the regions, the capital, the hubs and the ports over the Alps and Pyrenees, allowing the modal shift in order to reduce the CO₂ emissions.

The objective is to achieve a 17,500 km network of high capacity/high speed rails and Lyon-Turin Lyne is the fundamental joint of the railway line designed with the purpose of linking Algeciras (Spain) to Budapest (Hungary); it is located in the central sector of the so called “Mediterranean Corridor number 3”, of the TEN-T Trans-European conventional rail network. It will connect the regions, the capital, the hubs and the ports over the Alps and Pyrenees.

The areas along the Mediterranean Corridor (in particular the Lombardy, the Rhone-Alpes region, Catalonia and Madrid) are considered one of the most important socio-economics regions within the European Union. For these reasons it is currently one of the most important European projects.

In particular Corridor number 3 will connect Algeciras, Madrid, Tarragona, Seville, Valencia, Tarragona, Barcelona, Perpignan, Lyon, Turin, Milan, Venice, Ljubljana and Budapest.

In Figure 3.1 the nine network corridors are presented with different colours, the green one in the Mediterranean Corridor, number 3.

3.1 Introduction

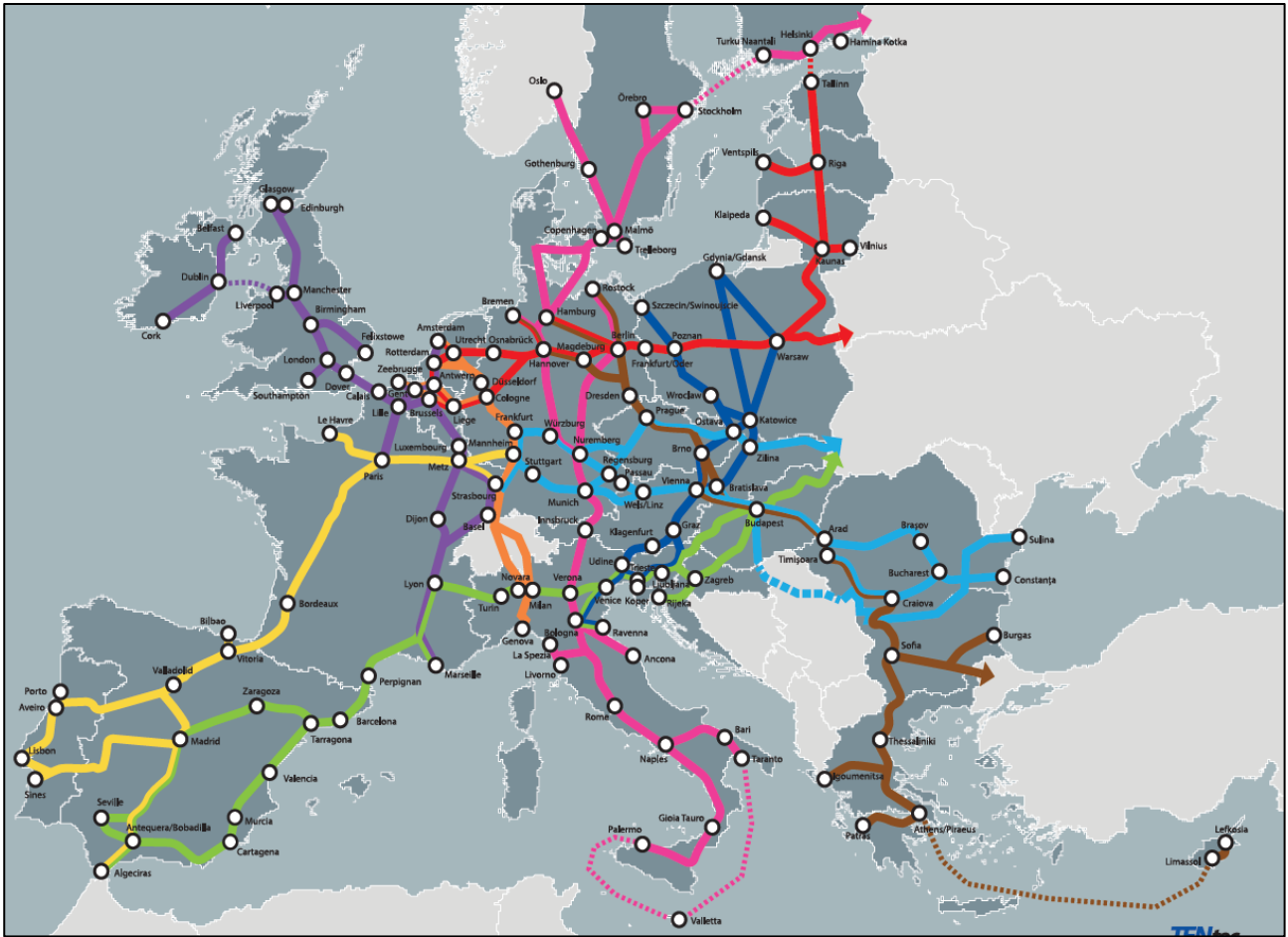


Figure 3.1 The Core Network Corridors. Green line: Mediterranean corridor, yellow: Atlantic, violet: North Sea-Mediterranean, orange: Rhine-Alpine, red: North Sea-Baltic, pink: Scandinavian-Mediterranean, dark blue: Baltic-Adriatic, light blue: Rhine-Danube, brown: Orient/East-Mediterranean. (European Commission).

The missing section is the rail link between Italy (Turin) and France (Lyon); nevertheless, it is highly strategic because it will connect South-West Countries of Europe with Central and Eastern European regions. Failing Lyon-Turin link means hampering transport relations and so trade between Spain, France and Italy and between these Countries and Central and Eastern Europe.

As it is possible to observe from Figure 3.1 Lyon-Turin railway line is located in the middle of two long communication axes that run North-South (North Sea-Mediterranean Corridor) and East-West (Mediterranean Corridor).

3.1.1 Mont Cenis Base Tunnel

The new Lyon-Turin line has a length of 235 km and its core element is represented by a 57.5 km length base tunnel named Mont Cenis Base Tunnel (MCBT); the promoter and owner company is TELT, Tunnel Euroalpin Lyon-Turin, previously (LTF, Lyon Turin Ferroviare).

Today the freight traffic between Italy and France is relevant and the rail mode is supported by the old Fréjus railway, which is not adequate to answer the need presented. As for Italy-France axis, it has been estimated that only a little part of goods traffic is guaranteed by rail mode, because of there are relevant constraints in terms of time and costs associated with the old Fréjus railway (compared with German axis 29% and Swiss axis 64%). For these reason, Mont Cenis Base Tunnel is the main project of the whole Corridor 3.

The tunnel has been designed with the purpose of connecting Susa (Turin Area, North Italy) to Saint Jean de Maurienne (France); it crosses two states, Italy and France, and it will have a total length of 57.5 km: 12.5 km of tunnel will be realised in Italy and the others 45 km in France. Given that it is designed as a twin tube tunnel its effective length will be equal to 115 km. Considering that 170 communication bypasses (located each 333 meters), 4 intermediates accesses, 5 ventilation systems and 3 underground security areas have been planned, the total tunnel length is nearly of 160 km, 80 km of them by means of TBM and 80 with traditional method. The designed tube diameter is approximately of 10 meters.

A schematic representation of tunnel structure is provided in Figure 3.2.

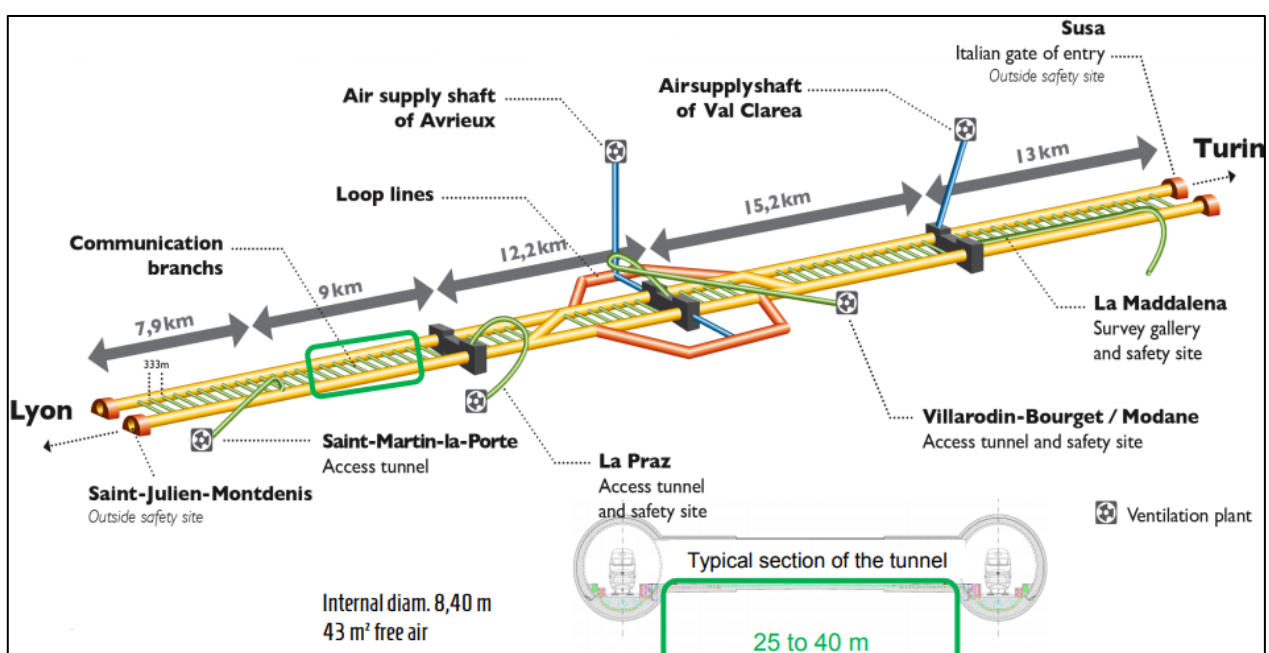


Figure 3.2 Structure of Mont Cenis Base Tunnel (TELT).

3.1 Introduction

3.1.1.1 Geological prevision

The new Mont Cenis tunnel will cross seven geological zones (Figure 3.3):

- *Ultradauphinoise Zone*: the principal rocks encountered by the tunnel are sandstones and schists;
- *Sub-Briançonnaise Zone*: in this zones tunnel crosses the Croix des Tête Massif, characterised by charbonatic rocks (limestones, marls and dolostones);
- *Houillère Briançonnaise Zone*: as for Houillère Briançonnaise Zone MCBT encounters the Bréquin-Orelle, La Praz and Fourneaux Units; it consists of schist, sandstones and charconatic levels;
- *Inner Briançonnaise Zone (Vanoise)*: the prevalent lithologies are gneiss and micaschist;
- *Gypsum Nappe Zone*: the former are evaporitic rocks (like gypsum and anhydrite), charbonatic rocks, dolostones and calc-schist;
- *Briançonnaise Zone of Ambin Massif*: characterised by gneiss and micaschist;
- *Piemontese Zone*: the former is prevalently calc-schist.

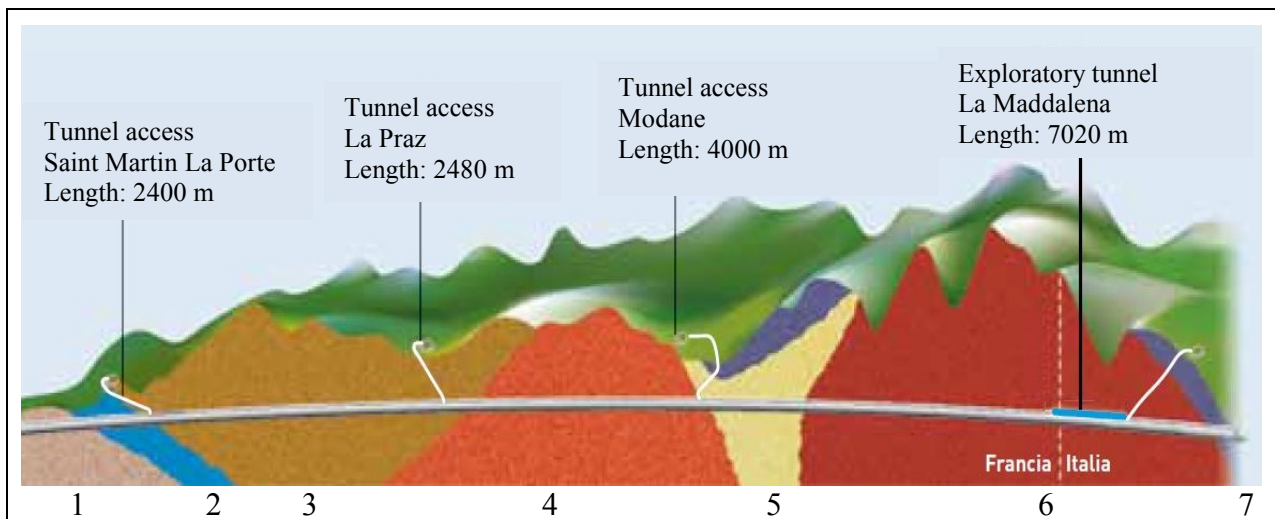


Figure 3.3 Geological section of Mont Cenis tunnel. 1: *Ultradauphinoise Zone*, 2: *Sub-Briançonnaise Zone*, 3: *Houillère Briançonnaise Zone*, 4: *Inner Briançonnaise Zone*, 5: *Gypsum Nappe Zone*, 6: *Briançonnaise Zone of Ambin Massif*, 7: *Piemontese Zone* (LTF, 2012).

3.1.1.2 Access and exploratory tunnel

Prior to the realisation of Mont Cenis, four access/exploratory tunnels had been constructed. Only one of them is located on the Italian side: “La Maddalena” exploratory tunnel. The other three are sited on the French side, they are: Saint Martin La Porte, La Praz and Modane tunnels (Figure 3.4).

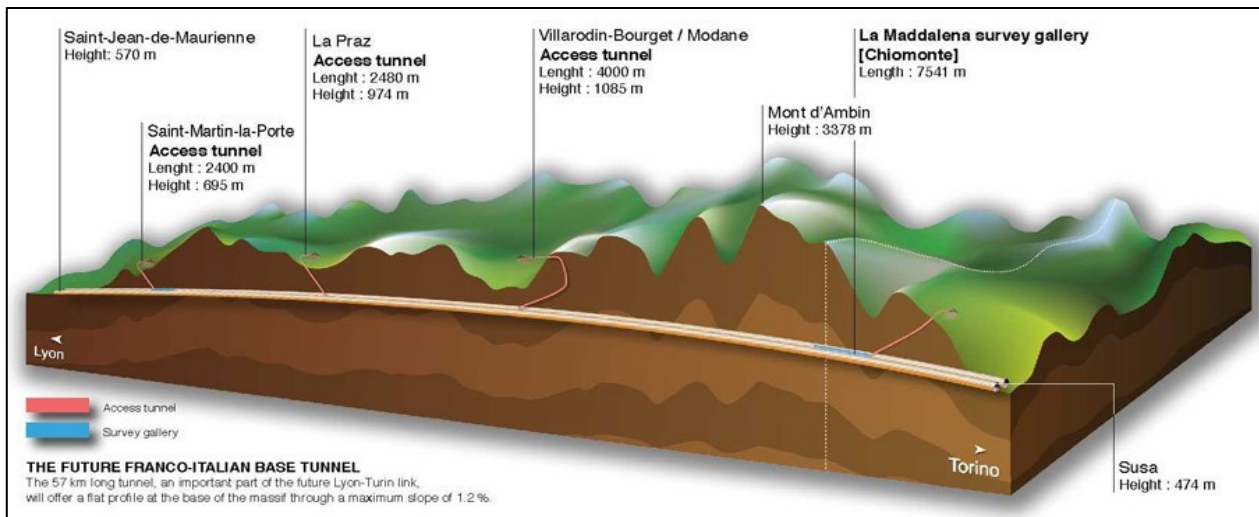


Figure 3.4 Accesses and exploratory tunnels of MCBT (Tunneltalk, 2013).

- *Saint Martin La Porte*: the tunnel of Saint Martin La Porte has been characterised by two working phases. During the first one, from 2003 to 2010, an access tunnel was realized. Since 2016 an exploratory tunnel has been built down Saint Martin La Porte access with the purpose to investigate the geological conditions of one of the most complex zones of Mont Cenis. The excavation has been realised by means of an 11.21 m diameter TBM named “Federica”. The encountered rock masses consist of schists and sandstones belonging to Houillère Briançonnaise Zone;
- *La Praz*: the tunnel access named “La Praz” is 2480 meters long and 11 meters in diameter, it was constructed between 2005 and 2005 adopting traditional drill and blast method. The access tunnel of La Praz was excavated into schist and sandstone belonging to Houillère Briançonnaise Zone;
- *Modane*: it is an access tunnel long 4000 meters and with a diameter of 10.40 m. it was constructed between 2005 and 2007 with drill and blast method. The encountered rock masses consist of quartzite, micaschist belonging to Inner Briançonnaise Zone (Vanoise) and limited levels of anhydrite. Relevant groundwater circulation has been observed at the contact between the evaporitic rocks and the quartzite;
- *La Maddalena*: the exploratory tunnel named “La Maddalena” is described in Paragraph 3.2.

3.2 La Maddalena exploratory tunnel

3.2 La Maddalena exploratory tunnel

3.2.1 General features and purpose

La Maddalena is one of the four preliminary infrastructures related to MCBT excavation. The excavation works started in 2012 and concluded in 2017, it is long 7020 meters and it has a diameter equal to 6.30 meters.

La Maddalena is an exploratory tunnel realised with the purpose to collect geological, geomechanical, structural and hydrogeological data and all that useful information necessary to plan the excavation of the Mont Cenis Base Tunnel. Before its planning it is fundamental to understand the rock mass behaviour as consequence of mechanized tunnelling.

In accordance with the global good quality of La Maddalena rock mass and with the necessity to directly map the tunnel walls and to install monitoring systems into rock mass, the excavation was carried out by means of open type Tunnel Boring Machine.

The description of the involved TBM is reported in the following paragraph.

La Maddalena has been planned considering both its primary aim (to gather geological information) and its future utilization; in fact, during MCBT construction La Maddalena will be used as access and ventilation tunnel and during working phase of MCBT it will become a security tunnel.

3.2.2 Geographical location

The exploratory tunnel of La Maddalena is located in North Italy, in Piedmont Region in Turin province.

The tunnel access and the yard are sited in Chiomonte Municipality, in the locality named “La Maddalena” that gives the name to the tunnel; it is at an altitude of 615.5 m on sea level and it is overhung by “Clarea” viaduct of A32 Torino-Bardonecchia motorway (Figure 3.5).



Figure 3.5 Geographical position of the access to La Maddalena tunnel in Chiomonte, Italy (Google Maps)

3.2.3 Tunnel route

The length of tunnel is 7020.0 meters, its orientation was decided during the planning phase and it ranges from 307° (from North) at the beginning of excavation to $N333^\circ$ until Pk. 3 + 090 m, at the end of excavation tunnel axis orientation is $N299^\circ$. The tunnel rises with a gradient of 0.34% until pk. 1 + 500.0 m, then it descends with a gradient of 3.32% for 1600 m at the altitude of 573.40 m on sea level; it is the deeper point of the whole project (Padovese et al, 2017). From this point the excavation rises with a maximum gradient of 1.20% in order to reach the level of the base tunnel.

A map with La Maddalena and MCBT routes has been reported in Figure 3.6.

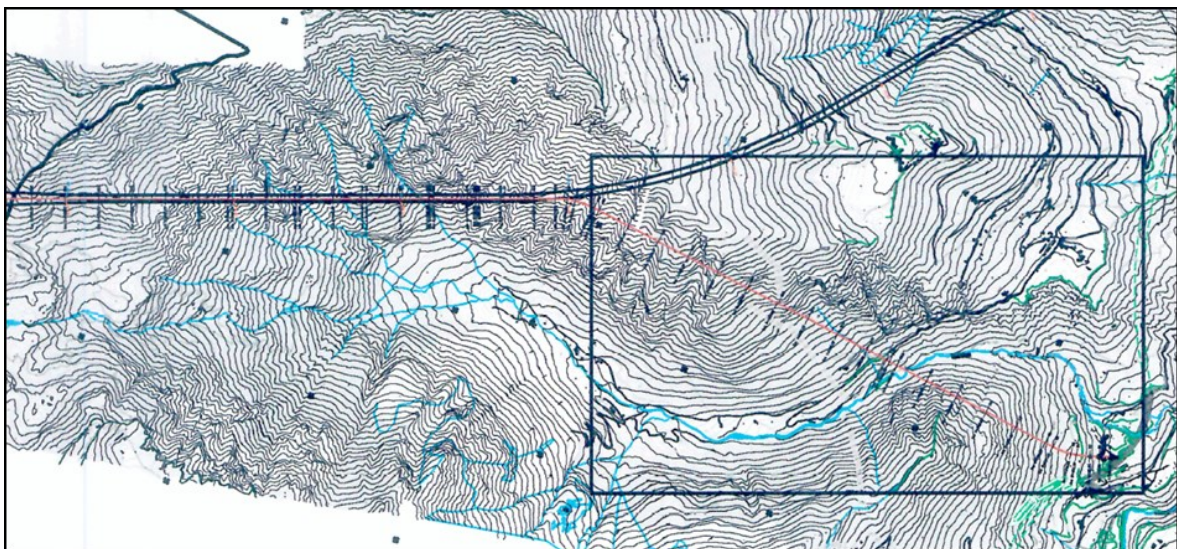


Figure 3.6 La Maddalena route (red line) and MCBT one (double blue line); scale 1:5000.

3.2 La Maddalena exploratory tunnel

3.2.4 Encountered rock mass lithologies

In this section the lithologies encountered during La Maddalena excavation have been listed. The detailed description is provided in the following chapters.

From Pk. 0 + 198,0 m to 0 + 967,0 m the lithological formation is gneiss belonging to the Ambin complex (following identified as Domain I, DI, reported in literature as AMC); from Pk. 1 + 360.0 m rock mass consists of micaschist belonging to Clarea complex (following identified as Domain III, DIII, reported in literature as CLR), between Pk. 0 + 967.0 m and 1 + 360.0 m a transition zone characterized by an alternation of gneiss and micaschist was encountered (following identified as Domain II, DII, reported in literature as AMD).

Table 3.1 summarises the acronyms proposed by literature, the ones adopted in this work and the formal names of geological complex.

Lithology	Formal Name	Main lithology	Acronym	Initial (used in the present thesis)
Gneiss	Ambin complex	aplitic gneiss	AMC	DI
Gneiss-Micaschist	Transition zone	aplitic gneiss, minuti gneiss, micaschist	AMD	DII
Micaschist	Clarea complex	micaschist and gneiss minuti reequilibrated in blueschist facies	CLR	DIII

Table 3.1 Lithologies, formal names, acronyms and initials of rock masses encountered during La Maddalena excavation.

The preliminary geological section has been reported in Figure 3.7.

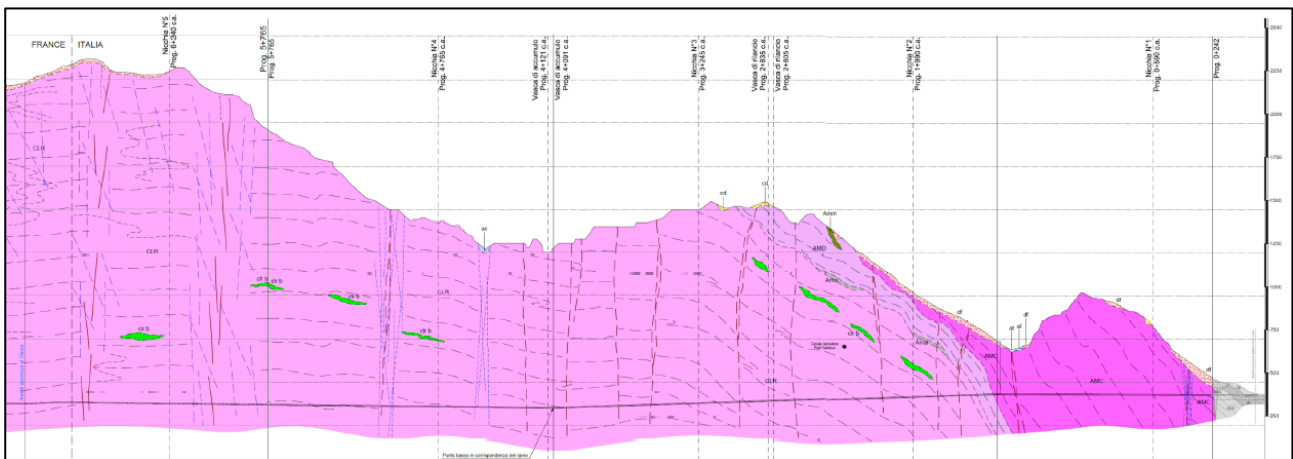


Figure 3.7 Preliminary geological section of La Maddalena tunnel (Padovese et al., 2017).

3.2.5 Rock supports and reinforcements

In order to guarantee long term stability and safety during construction, rock supports and reinforcements have been provided for La Maddalena excavation. The rock mass stability conditions changes from stable to local instability conditions of blocks or wedges and the most relevant support systems involved are rock bolts and steel ribs.

Nine support section types have been applied on the basis of rock mass conditions (Table 3.2).


	Section Type	Rock Support
STABLE  INSTABLE	F1	Occasional Bolting
	F2	
	F3a	Systematic Bolting
	F3b	
	F3c	
	F3c1	Light steel ribs
	FMV	
	F4	Heavy steel ribs
	F5	

Table 3.2 Section types and rock supports and reinforcements applied during La Maddalena construction.

Sections F1 and F2 are the more light ones and they have been adopted where rock mass are characterised by good quality and it is self-sustaining. These conditions occur in the gneiss of DI and part of transition zone (DII) and the first sector of micaschist of Clarea complex.

Sections F3a and F3b require systematic bolting on the roof, they are occasionally utilised in the transition zone crossing. Section F3c includes systematic bolting both on the roof and on the walls and steel wire mesh have been applied in addition to the bolts on the roof (Figure 3.8).

This section was adopted in jointed sections of DI and DIII (Padovese et al., 2017).

3.2 La Maddalena exploratory tunnel



Figure 3.8 Example of F3c section application. Rock bolts and wire mesh have been installed; on the right bolts are being applied.

F3c1 was involved when jointed conditions make blocks of rock detach from tunnel roof, it was installed during the excavation of Clarea micaschist, in particular from Pk. 1399.0 m and pk. 4575.0 m. It includes rock bolts, wire meshes and single steel ribs.

The section FMV has been adopted to micaschist of Clarea complex crossing from Pk. 4895 meters. This section needs the introduction of a specific support (similar to the one proposed by C&M McNally Engineering Company, known as McNally Support System). Specifically, it is characterised by systematic bolting and single steel ribs longitudinally jointed by steel bars, steel bars are parallel to tunnel axis and they are put in the roof and in the upper parts of walls (Figure 3.9).

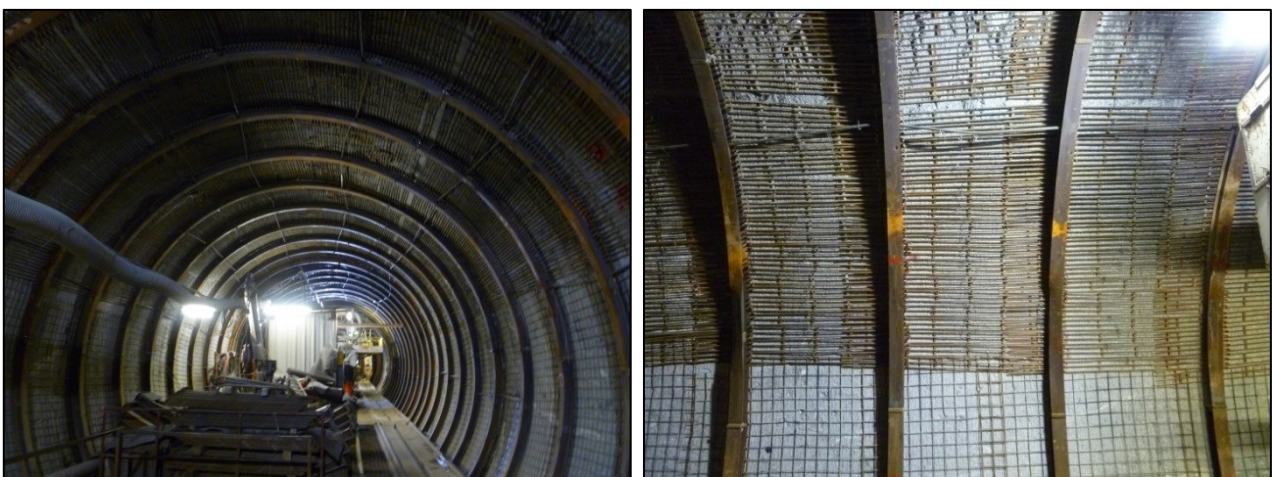


Figure 3.9 FMV section. On the left, tract of tunnel where FMV section has been installed; on the right, detail of this section utilization.

The bars between ribs work as a shield and they avoid rock wedge and chip falling into the tunnel void.

F4 and F5 section types have been applied only in those situations where very jointed masses occur, for example during fault and cataclastic zones crossing, encountered during DIII excavation (Padovese et al 2017). They require the installation of coupled steel ribs (0.5 m or 1.4 m spaced) together with bars (previously described) or wire mesh (Figure 3.10).



Figure 3.10 Coupled steel ribs and bars, F4 and F5 section types.

The support and reinforcement elements adopted during La Maddalena tunnel construction have been synthetically described in this paragraph.

All of them, when put to work, allow the operators to observe the tunnel walls, in order to collect geological, geomechanical and structural rock mass data by direct surveys, given that rock mass is accessible in accordance with the open TBM type utilized to La Maddalena realisation.

3.2 La Maddalena exploratory tunnel

3.2.6 The Tunnel Boring Machine “Gea”

Gea is the name of the Tunnel Boring Machine involved in La Maddalena excavation.

It is an open type main beam gripper TBM produced by Robbin’s Company and it has been specifically designed to be applied in mixed rock masses and therefore it is equipped with tools suitable for this utilization. It has a total length equal to 240.0 meters.

The specifications of “Gea” have been listed in the Table 3.3.

Machine Diameter	6.30 m
Cutters	Series 17 (431.8 mm)
- Number of disc cutters	43
- Max recommended individual cutter load	311.5 kN
Cutterhead	
- Normal operating cutterhead thrust	12,756.5 kN
- Periodic maximum cutterhead thrust	13,667 kN
- Cutterhead drive	Electric motors
- Cutterhead power	2205 kW
- Cutterhead speed	0.0 – 9.3 rpm
- Cutterhead torque	2,706 kNm
Main thrust cylinders	
- Stroke	1.83 m
- Number of main thrust cylinders	4
Hydraulic System – Power	
- Maximum system pressure	365 bar
Electrical system	
- Motor circuit	690 VAC
- Primary voltage	15 kV
- Secondary voltage	400 V
Machine conveyor	
- Width	914.4 mm
TBM weight	250 Ton (approximately)

Table 3.3 specifications of Gea, after Robbins Company, 2005.

The selection of this type of machine is due both to global good quality of rock masses and to the necessity to have a direct access to the tunnel walls and make direct geological surveys possible.

On a rotary cutterhead 43 disc cutter (17") are mounted, of which 33 are single cutter, 4 are double ones and 2 are used for overcutting (Figure 3.11); the cutterhead area is covered by a five meters long roof shield, behind which support and reinforcement installation is performed (where necessary). Rotary power is supplied by seven three-phase electric motors, they are cooled by water system.

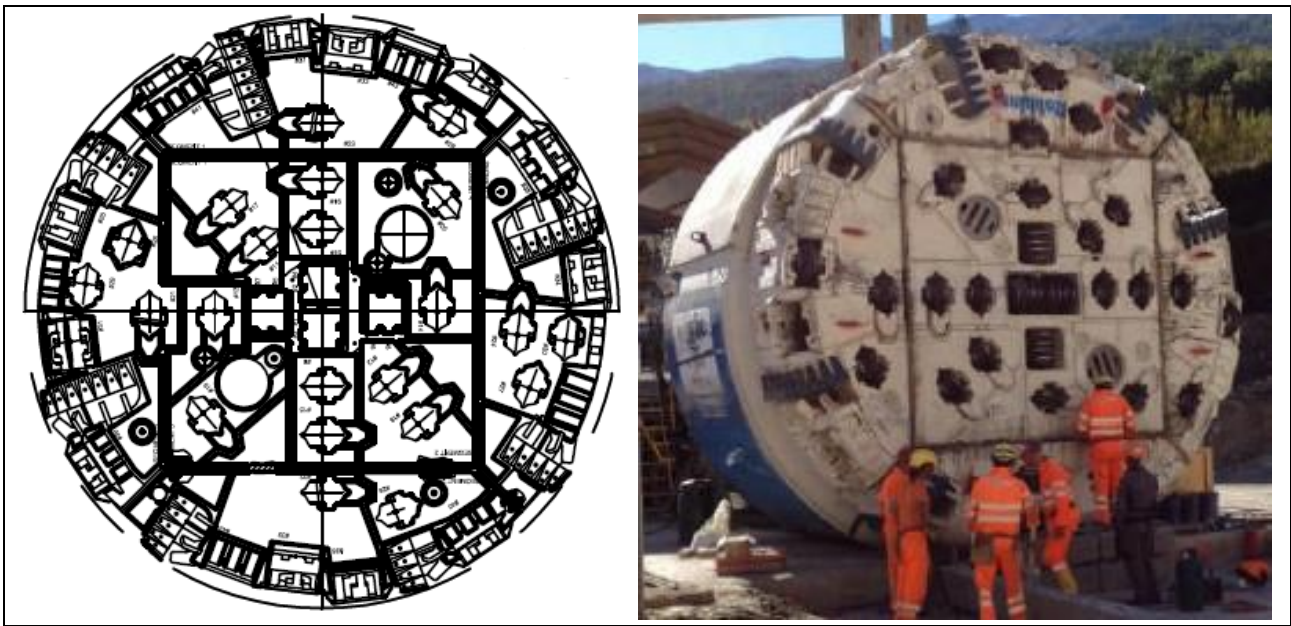


Figure 3.11 TBM Chutterhead. On the left cutterhead section (Robbins Company, 2005), on the right a photo of cutterhead taken during its assembly.

The cutterhead thrust is furnished by four main thrust cylinders, each with a stroke of 1.83 meters. When competent ground conditions occur (as in the case of La Maddalena) cutterhead thrust is transferred to the tunnel walls through hydraulically extended gripper shoes (Figure 3.12).

The four main thrust cylinders are linked between the gripper shoes and the main beam.

3.2 La Maddalena exploratory tunnel

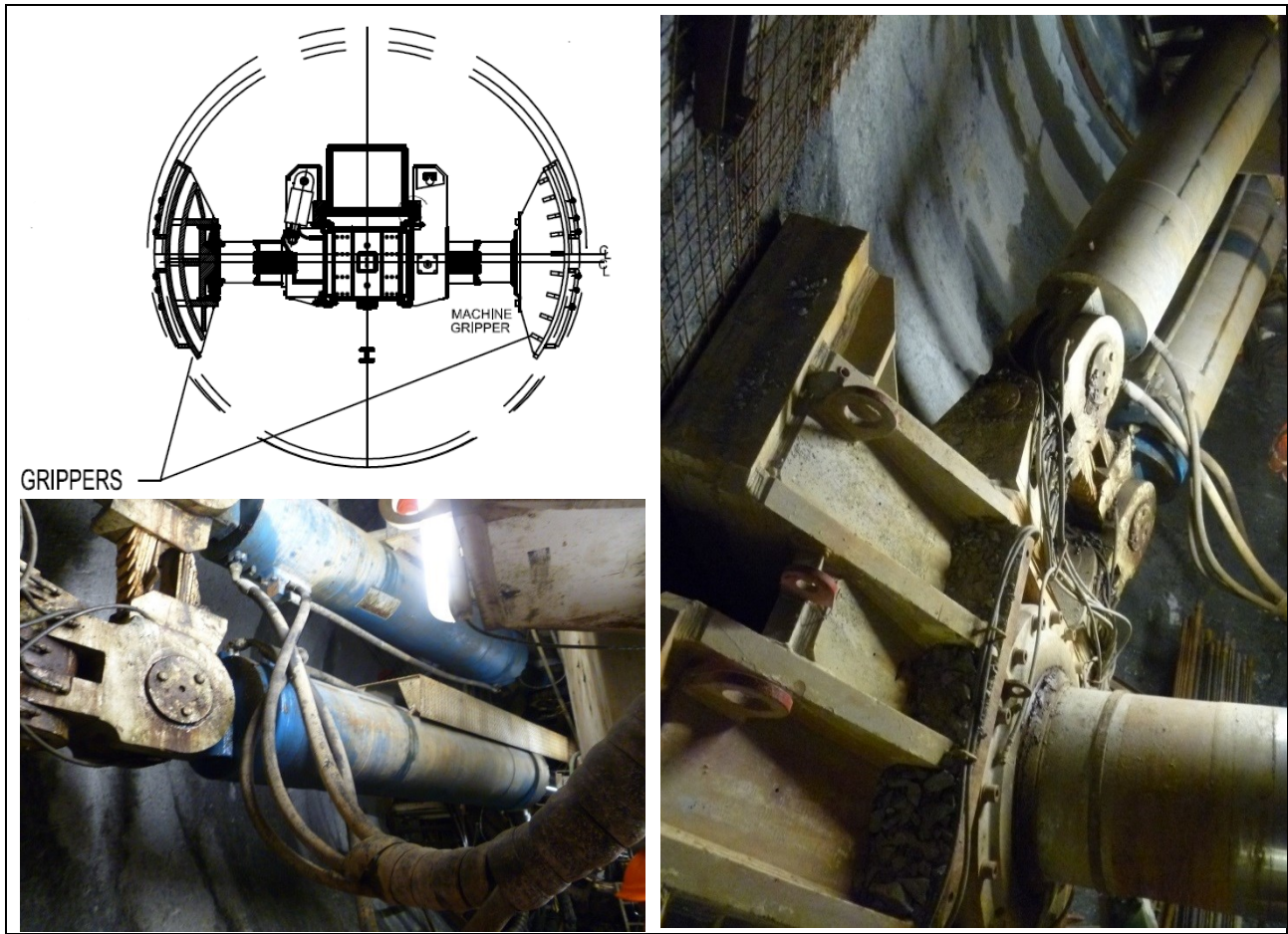


Figure 3.12 Gripper and thrust cylinders. In the top left hand corner, gripper section (Robbins Company, 2005); in the bottom left corner main thrust cylinders, on the right cylinders and gripper.

The TBM is equipped with front and rear laser targets in order to monitor the machine position.

A conveyor belt is used to remove rock cuttings from cutterhead area to the rear of the TBM then the excavation materials are moved out of the tunnel by means of other conveyors and stocked in the proper site (Figure 3.13).



Figure 3.13 Rock cutting moving. On the left, conveyor belt; on the right, rock cutting provisory storage site.

Finally, the machine area that includes bolting rigs, rib erector, the rib that allow pre-drilling ahead the cutterhead (so ahead the tunnel face) and ground treatments is named L1 zone and it is immediately behind the cutterhead (Figure 3.14).

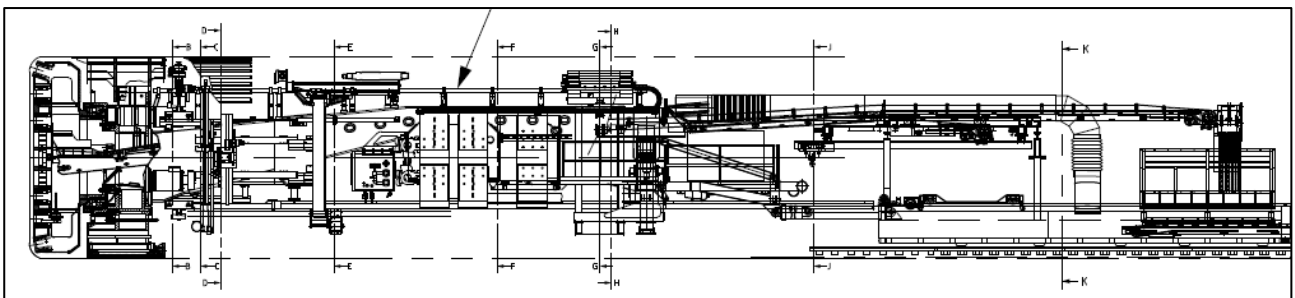


Figure 3.14 Scheme of Gea L1 zone (Robbin's Company, 2005).

In this area a vibrating screen is present (Figure 3.15), with the purpose to select rock cuttings in order not to damage the conveyor belt; in this way the largest pieces of rock can be removed before to be charged on the conveyor.

3.2 La Maddalena exploratory tunnel



Figure 3.15 Vibrating screen, on the left the original version, on the right the modified one.

The area that begins 40 meters away the cutterhead and includes the ribs for shotcrete application is named L2 (Figure 3.16).

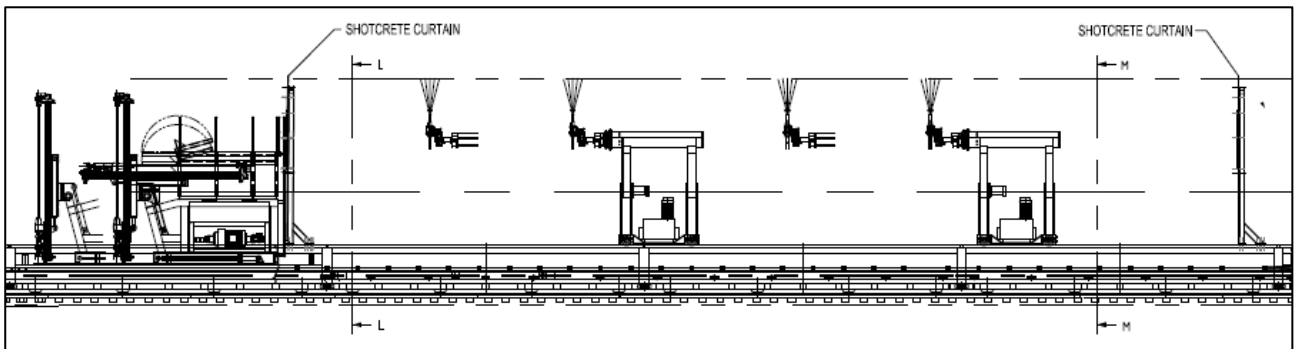


Figure 3.16 Scheme of Gea L2 zone (Robbin's Company, 2005).

Back – up includes air tanks, electric components, transformers, ventilation assy, evaporators, booster fans, compressors, rescue chamber, scrubber and scrubber fans, water reels and water tanks.

4 GEOLOGICAL SETTING

4.1 Introduction

In this chapter, a general description of the geological context in which La Maddalena exploratory tunnel was excavated has been provided. Furthermore, the geological processes that do not directly affect the tunnel are briefly cited for the sake of comprehensiveness.

For obvious reasons, the geological units excavated during La Maddalena construction and the events responsible to their formation have been described with more accuracy.

La Maddalena exploratory tunnel has been excavated in the Ambin Massif, which is part of the Gran San Bernardo Nappe that structurally pertains to the middle Penninic domain (Figure 4.1).

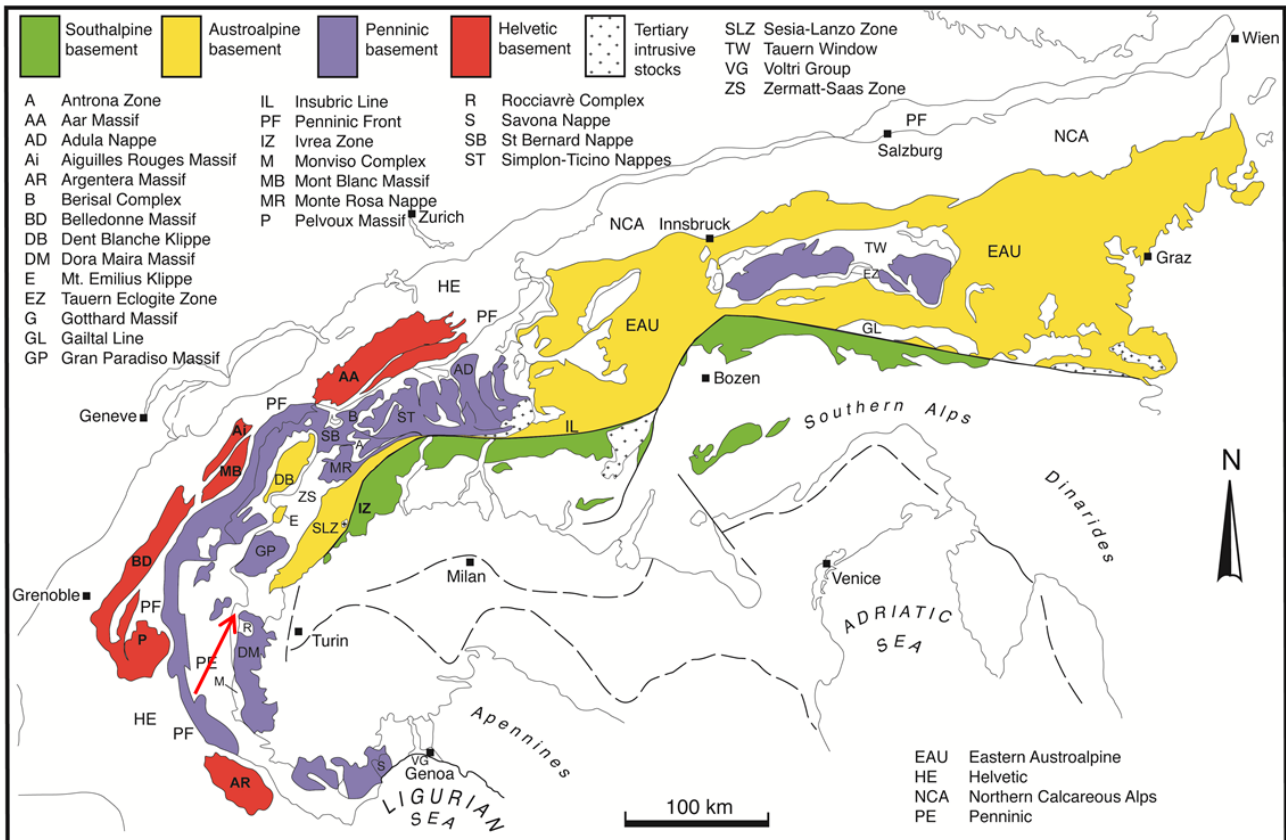


Figure 4.1 Structure of Alpine belt. The red arrow indicates the localization of La Maddalena tunnel (after Spalla et al. 2014).

La Maddalena is located in the central part of the Western Alps named Cottian Alps.

4.2 Penninic domain

4.2 Penninic domain

The Penninic domain is one of the four sectors in which the Alps are divided: the Southalpine, Austroalpine, Penninic and Helvetic domains. The Penninic domain consists of a multi-nappe system, in fact it is divided into units that preserve continental crust material (Piedmontese zone and Calc-schist zone) and into a system of three basement nappes; they are (Polino et al., 2002):

- The *Upper Penninic* nappes: Monte Rosa, Gran Paradiso and Dora Maira nappes;
- The *Middle Penninic* (Briançonnais) nappes: it consists of Grand Saint Bernard nappe;
- The *Lower Penninic* (Valais) nappes: Antigorio, Monte Leone and Lebendun,

4.2.1 Grand Saint Bernard nappe

The Grand Saint Bernard multi-nappe system is located in the Middle Penninic nappe. It extends along the external sector of Western Alps from Valais to Briançon and outcrops close to Acceglio and to Ligurian coasts.

Grand Saint Bernard nappe is made up of a pre-Triassic basement and a Triassic succession of carbonates. The basement consists of carbonaceous schists associated with volcanic materials. It outcrops in the Acceglio zone, in the Ambin Massif zone, near to Sapey and in the zones of Southern Vanoise (Chasseforet Massif) and Northern Vanoise (Mont Pourri-Bellecote) and in Aosta Valley.

4.2.1.1 Pre-Mesozoic basement

The pre-Mesozoic basement is divided into two principal complexes: one is considered polymetamorphic and one monometamorphic (Bocquet et al., 1974). The first complex is made up by paraschists and acid and basic magmatic rocks. The monometamorphic complex consists of successions based on polymetamorphic one; the contact between the two complexes is considered a primary type contact (Guillot and Raoult, 1984; Gay, 1970).

4.2.1.2 Meso-Cenozoic covers

The Meso-Cenozoic covers confirm the evolution of a subsiding basin under extensional regime (Stampfli and Marthaler, 1990). At the base of succession there are quartzites, covered by a succession of carbonate platform and evaporitic and lagoon deposits.

During Middle and Upper Jurassic the collapse of the carbonate platform and the subsequent pelagic deposition characterised by large volumes of breccias as result of syn-sedimentary tectonic activity began.

4.2.1.3 *Ambin Massif*

The Ambin Massif emerges at the border between Italy and France, and forms a large antiform in the Cottian Alps. The Massif outcrops in correspondence of a wide axial culmination under more tectonics elements belonging to Piedmontese nappe.

Argand et al. (1911) related the Massif to the upper Penninic nappe of Dora Maira on the basis of the lithological evidences; afterwards, Staub (1937) and Ellenberger (1958), asserted that the Ambin Massif belongs to Briançonnais zone, according to the Mesozoic cover characteristic. By taking into account for the lithostratigraphic affinities, the Ambin Massif is jointed to Pontis nappe (Thelin et al., 1990) and with Chasseforet Massif (Desmons and Mercier, 1993).

4.3 Tectono-stratigraphic unit of Ambin

4.3 Tectono-stratigraphic unit of Ambin

The tectonostratigraphic unit of Ambin represents the lowest unit of Gran Saint Bernardo nappe; it is formed by a pre-Triassic crystalline basement on which limited Mesozoic metasediments are rested. The Ambin unit outcrops between Chiomonte and Oulx municipalities, on the left bank of the Dora Riparia Valley.

The basement is subdivided into two complexes:

- A base complex known as *Clarea complex* characterised by polymetamorphic schists with relicts of pre-Alpine metamorphism;
- An upper complex, named *Ambin complex*, which is mainly composed of Permian metavolcanic rocks.

The dividing horizon between the two units is in the order of tens of meters in thickness and it is made up of metaconglomerates (Carboniferous-Permian) with quartz pebbles principally, passing to metaconglomeratic quartzites. The origin of this contact can be considered of stratigraphic type, in this case the metaconglomerate level should be considered as the relict of the Late-Varisic transgression in discordance on the metamorphic basement (Goguel, 1958; Gay, 1970). The previous interpretation agrees with the monometamorphic evolution of Ambin Massif (Kretz, 1983).

The Mesozoic cover of the Ambin Massif is poorly conserved on its South side and rests in discordance with the pre-Triassic basement; it consists of a carbonate sequence 20 m thick (Polino et al., 2002).

The structural scheme of the Ambin Massif area has been reported in Figure 4.2.

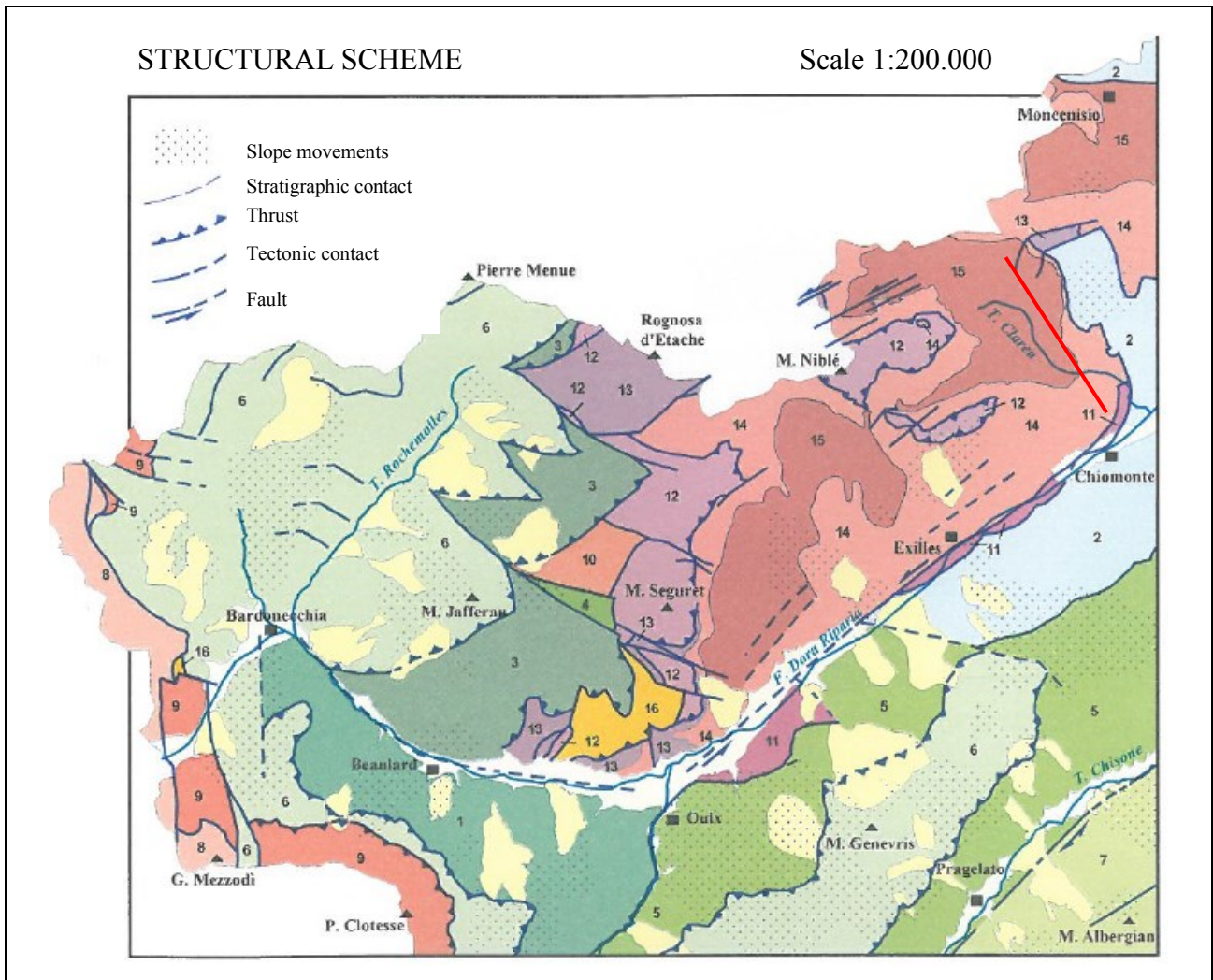


Figure 4.2 Regional structural scheme. 1: Puys complex, 2: Venaus complex, 3: Aigle unit, 4: Vin Vert unit, 5: Cerogne-Ciantiplagna unit, 6: Lago Nero unit, 7: Albergian unit, 8: Re Magi unit, 9: Chaberton unit, 10: Valfredda unit, 11: Gad unit, 12: Vallonetto unit, 13: Mesozoic cover (Ambin unit), 14: Ambin complex (Ambin unit), 15: Clarea complex (Ambin unit), 16: Gypsum, red line: La Maddalena tunnel. (Geological Map of Italy, Bardonecchia; Polino et al., 2002).

4.3 Tectono-stratigraphic unit of Ambin

4.3.1 Clarea complex

The Clarea complex represents the lowest element belonging to the metamorphic basement of the Ambin Massif. It emerges in Clarea Valley, Tiraculo Valley, in Rio Pontè and Rio Geronda areas, in Susa Valley and in Gran Boursey zone. The minimum thickness of the outcrops is about 700-800 metres (Polino et al., 2002).

The Clarea complex is formed by metasediments represented by micaschists, and gneiss minuti. Some pre-Alpine relicts are present in the lower part of the complex; in these relicts some evidences of pre-Alpine foliation have been preserved. The Alpine tectonometamorphic deformation becomes more significant in the upper levels of the complex and it has deleted every trace of pre-Alpine deformation.

The pre-Alpine foliation, typical of the lowest levels, is considered Cambrian by Desmons and Fabre (1998) and Desmons (1992). Moniè (1990) conducted radiometric analysis Ar/Ar which suggested a Varisian Period (310-350 My) and so it is possible to consider Permo-Carboniferous the monometamorphic complex of Ambin Massif.

The Clarea complex has been subdivided into the following informal units:

4.3.1.1 Micaschist and gneiss minuti reequilibrated in blueschist facies

They emerge in the upper levels of the Clarea complex, close to the contact with the Ambin complex. The principal forming minerals are quartz, albite, white mica, chlorite, amphibole, chloritoid and garnet. The schistosity is developed in HP-LT conditions and it is defined by the orientation of white mica, chlorite and glaucophane.

Levels of quartz are located parallel to the schistosity. The decompression event at LP-LT causes the mica substitution with albite. This process determines the micaschist transformation into gneiss minuti albitized.

4.3.1.2 Micaschist with pre-Alpine parageneses

The micaschist with pre-Alpine parageneses represents the most common unit in the lowest sectors of Clarea complex. Where the quartz content is relevant rocks, are quite massive and where white mica content is high the schistosity is dominant.

The principal forming minerals are quartz, muscovite, plagioclase, biotite, chlorite and garnet. The foliation is defined by the layering of muscovite and biotite levels and quartz-feldspar ones.

4.3.1.3 Metabasites with pre-Alpine relicts

This unit consists of dark green metabasites characterised by metamorphic layering defined by the alternation of amphibolitic domains (in the order of centimetres in thickness) and albite and epidote ones (in the order of millimetres in thickness).

The unit is characterised by variable thickness, in the order of metres and tens of metres. In some cases an Alpine foliation has been recognised, due to the HP event.

4.3.1.4 Polymetamorphic ortogneiss

The polymetamorphic ortogneiss unit emerges in the area of Monache Lakes, Clot delle Selle, Rio Geronda and Rio Clapier (Polino et al., 2002). If Alpine parageneses is preserved, rocks are whitish, medium fine grained, rich in quartz, white mica and feldspar. In some cases, the original magmatic fabric is recognisable.

The ortogneiss is characterised by a foliation defined by muscovite and biotite, subsequently substituted by Alpine aggregates formed by phengite + glaucophane + chlorite.

4.3 Tectono-stratigraphic unit of Ambin

4.3.2 Ambin complex

The Ambin complex is principally formed by albitic-cloritic gneiss characterised by textural and compositional homogeneity and leucocratic gneiss with jadeite (Gay, 1970; Callegari et al., 1980), considered of magmatic, volcanic and volcanoclastic origins and belonging to the same magmatic complex. They are considered as the metamorphic result of effusive or sub-intrusive magmatic bodies.

There are also levels of quartz-micaschist with chlorite and quartz-micaschist. The metaconglomerate and the carbonate levels are rarer.

The thickness of the units composing the Ambin complex is extremely variable.

The Ambin complex has been subdivided into the following informal units:

4.3.2.1 Metaconglomerates and conglomeratic quartzites

These whitish rocks are located at the basis of Ambin Massif and they have a thickness of tens of metres. Both metaconglomerates and conglomeratic quartzites contain clasts of quartz and lithic fragments (made up by quartz and gneiss) oriented in parallel with respect to the regional foliation.

In some cases, this unit is altered and the global colour can become brownish.

4.3.2.2 Quartz-micaschists, quartzites and marbles

This rock emerges between Chiomonte and Salbertrand municipalities and in Vaccarone area. The unit is formed by quartz-micaschist, passing to quartzites, the quartzite levels are less of 10 metres in thickness. Into these levels there are levels (with the same thickness) of micaschist with glaucophane, mica, chlorite and carbonate (Polino et al., 2002). Sometimes the carbonate level is as relevant as make the rock considered as a calc-schist.

Some levels of micaceous marble have been observed in Ruinas-Maison area.

4.3.2.3 Leucocratic gneiss with jadeite

This gneiss is very compact, whitish and fine grained; it largely emerges in Clarea Valley. These rocks are homogenous and consist of quartz, albite, white mica and plagioclase. Jadeite (previously described by Gay in 1972) is very fine grained and often associated with the quartz. The rock is poorly foliated, due to the mica orientation.

Several interpretations of their origin were proposed (Gay, 1970-1972; Callegari et al., 1980); their composition is alkaline-granitic (Pognante et al 1984).

4.3.2.4 Augen gneiss with albite and chlorite

This is the prevalent lithotype occurring in the Ambin complex. It consists of light green gneiss formed by quartz, albite, white mica chlorite and relicts of chloritoid.

These rocks are characterised by well-marked foliation, defined by chlorite and white mica. The texture is characterised by the occurrence of granoblastic aggregates (measurable in tens of millimetres) made up by albite, quartz, chlorite (large sized) and magnetite. Desmond and Mercier (1993) considered them as metamorphic result of clastic sedimentary rocks (greywacke), however at these days they are interpreted as metamorphosed volcanic/volcanoclastic rocks.

4.3.2.5 Quartz-micaschist with chlorite

These rocks outcrop in Gambara Valley, Punta Sommeiller and Vaccarone-Gros Muttet-Col Clapier. They have medium grain size, they are whitish and very homogeneous. They are affected by marched foliation and the principal constitutive minerals are quartz, white mica, chlorite, chloritoid and carbonates (rarely).

Rare boudins of glaucophane schist are detected surveying this lithotype.

4.3.2.6 Metadiorites with magmatic relicts

Tabular corps of metadiorites and metagabbros have been individuated in the Ambin complex and in Clarea one (Pognante et al., 1984). They have been observed in Susa Valley between Exilles and La Ramat. These rocks are dark green, massive and medium-fine grained.

This unit is poorly foliated; the foliation is defined by the iso-orientation of amphibole, chlorite and titanite.

Polino et al. (2002) interpreted them as dike, on the basis of the relationship between these rocks and the hosting ones.

4.4 Structural evolution of Ambin

The structural evolution of Western Alps is characterised by a complex polyphase deformation history. Each unit is affected by an initial independent evolution, and then the deformation processes become common to all the units (Polino et al., 1999).

In particular the polyphase evolution of the Ambin unit can be summarised as follows (Lorenzoni, 1965; Gay, 1970; Callegari et al., 1980; Allenbach and Caron, 1986; Borghi and Gattiglio, 1997):

- Pre-Alpine structural evolution;
- Development of the first two phases of Alpine deformation;
- Third phase of Alpine deformation;
- Late phases of massif uplift.

4.4.1 Pre-Alpine evolution

The first foliation consists of microstructural relicts as microlithons and sigmoidal tectonic surfaces. The successive deformation phase is defined by amphibolite facies minerals, related to an axial foliation. This defines the schistosity that characterises the lowest structural levels of Ambin unit (Polino et al., 2002).

4.4.2 Ductile Alpine evolution

The first Alpine deformation developed in blueschist condition. Its intensity is higher in the upper levels of Clarea complex and it deforms the pre-Alpine schistosity, generating folds North-South oriented, in the lowest levels.

The second phase has created isoclinal folds and an extensional lineation oriented East-West. The axial plane foliation is the prevalent one; it was evolved in high pressure-low temperature conditions (lawsonite blueschists).

The third Alpine deformation phase gives as result the principal planar elements about the upper levels of Ambin Massif. The axes of the folds developed during the third deformation phase have orientation North-South. Some linear structures are a consequence of this phase, for instance the glaucophane (East-West oriented).

The fourth phase is characterised by low grade metamorphism and it is typical of exhumation events.

4.4.3 Brittle Alpine evolution

The brittle Alpine deformation consists of a series of mechanical discontinuities occurring both at small and large scale. In particular, three main systems of fractures have been distinguished:

- N60 system: it is characterised by planes immerging NW-SE and evidences of sinistral strike-slip;
- N100/N140 system: it is affected by distensional movements;
- A system ranging between N160/N10 and affected by distensional movements.

One of the most relevant fault systems is the so called “Modane-Termignon-Ruisseau de la Chavière”, described by Fudral (1998) which takes place along the Arc Valley at the NW border of the Ambin Massif.

This is delimited by regional fault systems: the Arc Valley Fault, the system with direction ranging from N120 to N180 (Susa-Condove area) and the Susa Valley deformation zone (N60), the last one is very persistent in the Ambin Massif (Fudral, 1998).

4.4 Structural evolution of Ambin

4.4.4 Neotectonics

In the area in which the Ambin Massif takes place, stress field is considered extensional type and it is characterised by two extensional processes.

The first phase is described as a lateral extrusion of the inner Western Alpine Arc, the second event is caused by body forces in the belt root and gravitational re-equilibration (Sue et al., 2007).

The neotectonic map of the Western and Central Alps carried out by Sue et al. (2007) is provided in Figure 4.3.

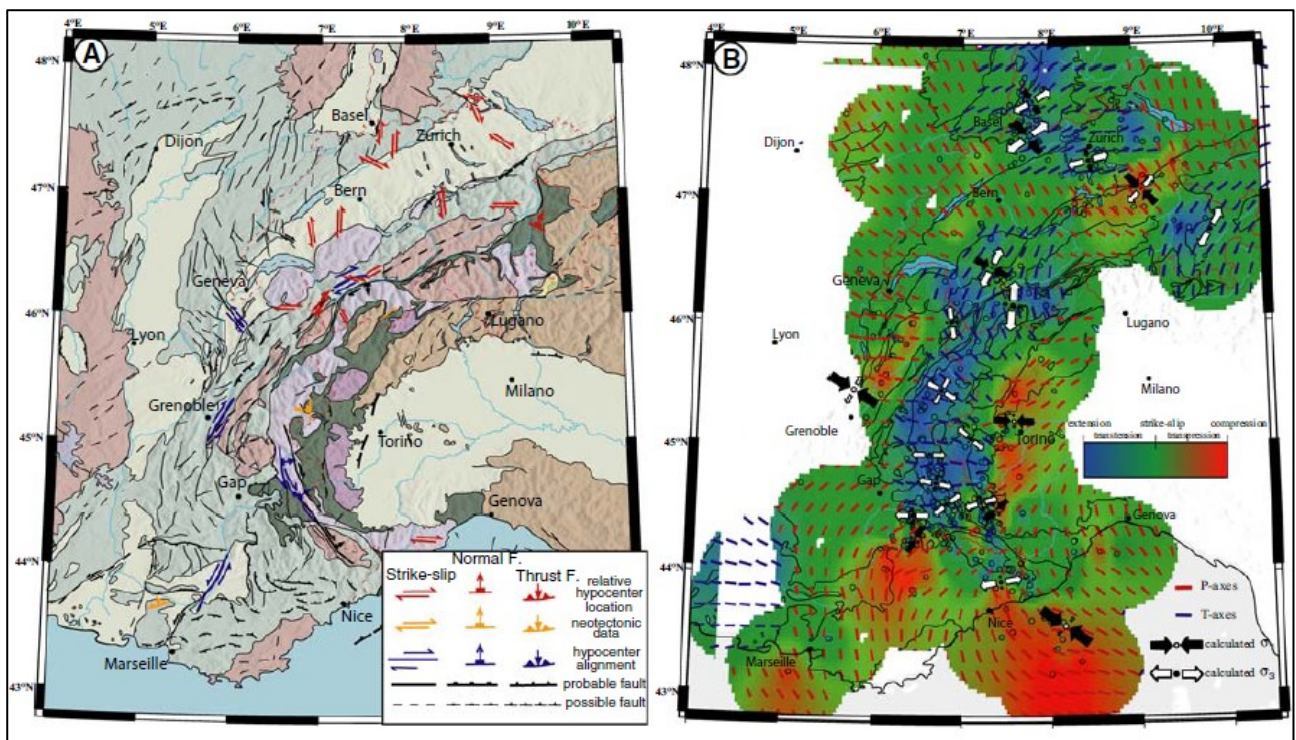


Figure 4.3 Neotectonic map of Western and Central Alps. Figure B orange lines: faults observed, blue: seismic alignments, black: possible and probable ones (Sue et al., 2007).

The neotectonic scheme about the area studied during this research work is provided in Figure 4.4.

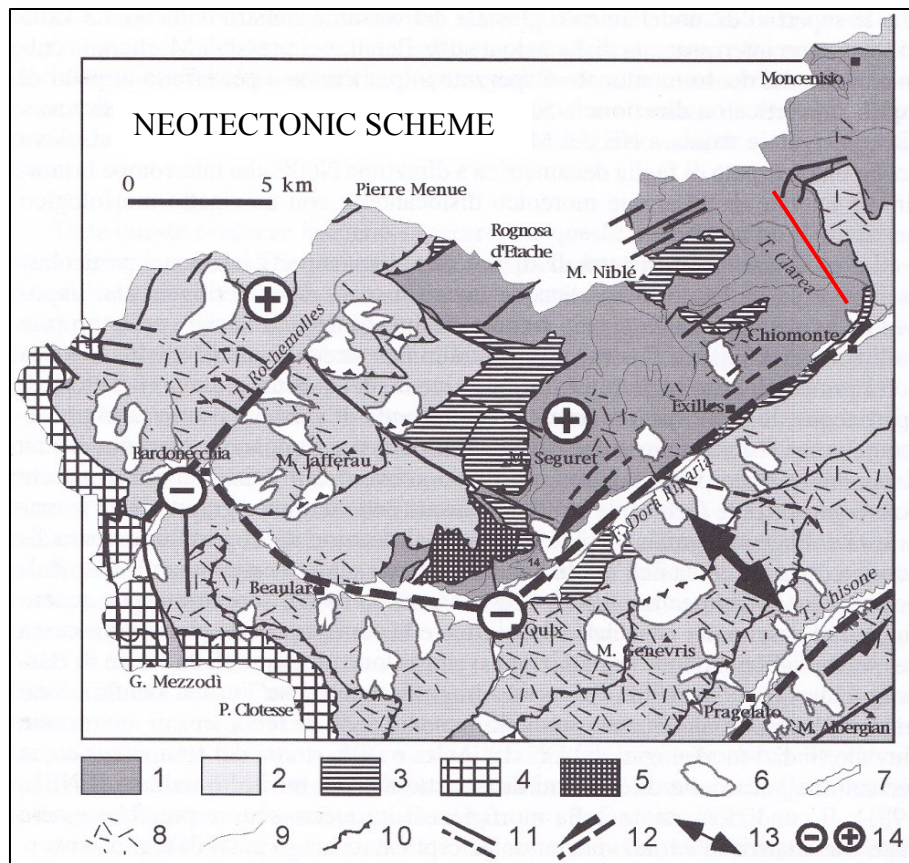


Figure 4.4 Neotectonic map of Ambin Massif. 1: Ambin Massif and cover, 2: Piedmontese Domain, 3: lower tectonostratigraphic units, 4: upper tectonostratigraphic units, 5: gypsum and anhydrite, 6-7: Quaternary, 8: deep seated gravitational slope deformation, 9: stratigraphic limits, 10: thrust, 11: tectonic contacts, 12: strike-slip faults, 13: Susa-Chisone shear zone, 14: subsidence and uplift, red line: La Maddalena tunnel (Geological Map of Italy, Bardonecchia area; Polino et al., 2002).

The area in which La Maddalena tunnel has been excavated is affected by three main fault systems: the “Mompantero-Colle delle Finestre” the “Medium Susa Valley-Upper Chisone Valley” and “Sangone” shear zones.

4.4.4.1 The “Mompantero-Colle delle Finestre” fault system

The “Mompantero-Colle delle Finestre” fault system is a relevant system of faults with mean direction NNE-SSW, the structure is probably related to “Cenischia-Nizza line”, as described by Casati and Giovacchini (1977). Mompantero-Colle delle Finestre system is characterise by a mean direction of N20 and it is observable in the upper sector of Susa Valley and Mouriennne, where there are N-S faults with reject evaluated in the order of kilometres. These faults were dextral strike-slip during Oligocene and Miocene and then they have been reactivated as normal faults (Polino et al., 2002; Malusà 2004). This system corresponds to the normal fault system of Modane-Termignon-Ruisseau de Chaviere and at Bessans-Pont Andagn Fault (Fudral et al., 1998).

4.4 Structural evolution of Ambin

4.4.4.2 “Medium Susa Valley – Upper Chisone Valley”

The “Medium Susa Valley-Upper Chisone Valley” fault system develops in Medium Susa Valley and Upper Chisone Valley and has a mean direction of N60. It is characterized by kilometres length structures that displace the preexisting structural and stratigraphic disposition (Polino et al., 2002; Giardino and Polino, 1997). The activity of this system was dextral strike-slip during Oligocene-Miocene and then evolved in normal activity (Malusà, 2004).

Both Col Clapier and Venaus faults are related to this system.

The stereographic projections of the principal neotectonic deformation elements registered in Medium Susa Valley (Figure 4.5 A) and in Segurét-Vallonetto sector (Figure 4.5 B) have been reported below.

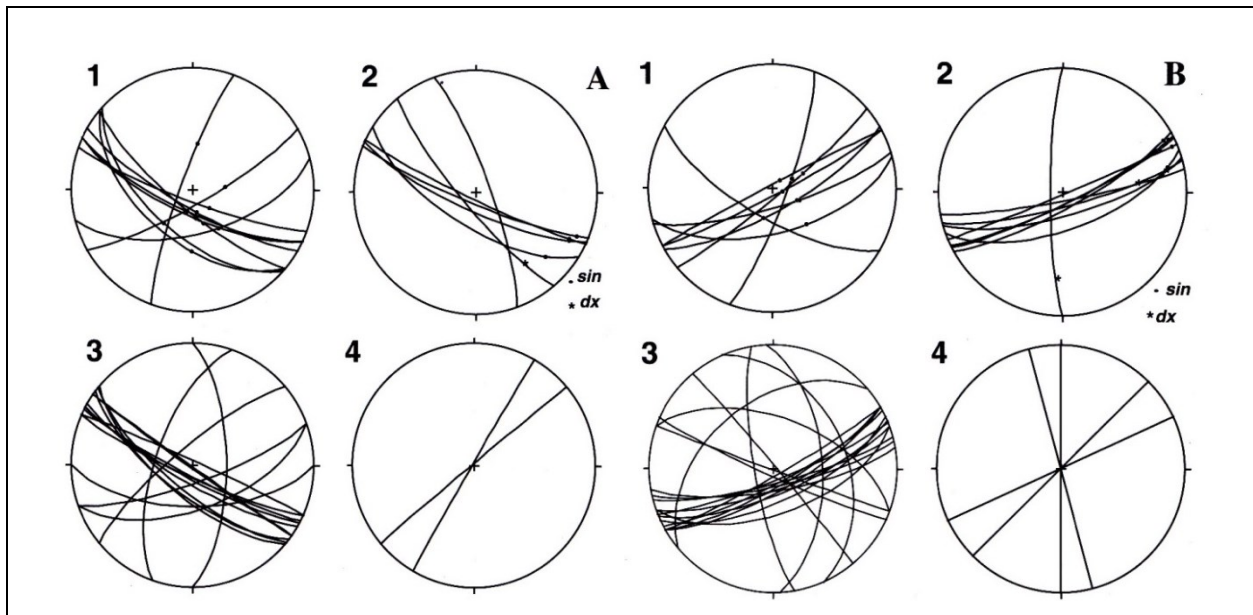


Figure 4.5 A) Deformation elements observed in Medium Susa Valley. 1: normal faults, 2: strike-slip faults, 3: random faults, 4: deep seated gravitational slope deformation. B) Deformation elements observed in Segurét-Vallonetto sector. 1: normal faults, 2: strike-slip faults, 3: random faults, 4: axes of collapse structures (Geological Map of Italy, Bardonecchia area; Polino et al., 2002).

4.4.4.3 “Sangone” shear zone

The fault system named “Sangone” shear zone is defined by a mean direction of N110-N120. It has been observed between Oulx and Bardonecchia and it is characterised by extensional movements (Malusà, 2004). In Sangone Valley, the kinematic indicators detected show normal and sinistral strike-slip movements.

The maximum extension of this shear zone is about 4 kilometres in length.

5 ROCK MASS CHARACTERIZATION

5.1 Introduction

The main purpose of this research work is to carry out the relationships between rock mass features and TBM performances: for this reason, a detailed rock mass characterisation plays a fundamental role.

The rock mass characterisation focuses both on intact rock properties determination and on the mapping and the description of discontinuities.

The first phase of this work consisted into a detailed tunnel wall mapping; in fact, several geological surveys have been carried out continuously along the entire tunnel length. During each survey, the geometry and properties of discontinuities and matrix features have been detected. Their length is equal to the tunnel length excavated the day before of the geological mapping, in this way, each geological survey generates a “rock mass section”, their mean length ranges between 10 and 20 meters. The decision to make the rock mass section long as a daily excavated tract is due to the fact that in this way we are able to evaluate the TBM indices for each of them.

The scheme used to perform the tunnel wall mapping is reported in Appendix I.

At the end of the field work, a total of 502 rock mass sections has been surveyed.

For each rock mass section, a series of geological, structural, mechanical and TBM data is available. The types of data about intact rock, discontinuities, and machine available for each rock section have been listed in Table 5.1.

For each rock mass section, the geological survey allows to classify rock mass using Rock Mass Rating (RMR; Bieniawski, 1989) system and Geological Strength Index (GSI; Hoek and Marinos, 2000).

The results of surveys have been provided referring both to the entire tunnel length and to each encountered geological domain. The geological domains are:

- Gneiss domain, (DI): ranging between Pk. 0 + 198 m and Pk. 0 + 967 m;
- Gneiss-micaschist alternation domain, (DII): ranging from Pk. 0 + 967 m to Pk. 1 + 360 m;
- Micaschist domain, (DIII): ranging between Pk. 1 + 360 m and Pk. 6 + 897 m.

5.1 Introduction

All data collected in the Domain I (DI, gneiss), in Domain II (DII, alternation of gneiss and micaschist) and part of data, from Pk. 1 + 360 m to Pk. 2 + 003 m, collected in Domain III (DIII, micaschist) have been used in the subsequently regression analysis. All data surveyed in the remaining part of DIII (from Pk. 2 + 003 m to 6 + 897 m) have been used to validate the obtained models. For this reason, the description of each geological and geomechanical parameter about the first tract of DIII is also provided. This part of DIII is identified as DIIIa.

List of parameters available for each rock section		
Intact rock	Discontinuity	TBM
<ul style="list-style-type: none"> - Lithological description; - UCS; - Quartz content*; - Thin sections; - CAI*; - CHI*; - Poisson ratio*; - Young modulus*; - Density*; - Seismic wave velocity. <p>* data measured each 200 m</p>	<ul style="list-style-type: none"> - Type of discontinuity; - Orientation; - Spacing; - Number of sets; - Block size; - Persistence; - Waviness; - Angle between discontinuity and tunnel axis; - Degree of weathering; - Aperture; - Type of infilling material; - Groundwater condition. 	<ul style="list-style-type: none"> - ROP; - FPI; - Prev; - SP; - Torque; - Cutterhead thrust.
<p>Tunnel data: Tunnel depth, Tunnel axis orientation, Seismic wave velocity.</p>		

Table 5.1 List of parameters available for each rock section.

In the following paragraphs a brief description of the methods followed in order to describe the parameters listed above is provided.

5.2 Intact rock property determination

The purpose of laboratory tests on intact rock or rock sample macroscopic and microscopic description is to organise, from a geological point of view, the rocks in different classes which represent the mechanical and hydraulic behaviour, and to assess the deformation and strength features.

A brief description of the basic observation or laboratory measurements that have been conducted in order to determine the physical and mechanical properties of the rock matrix excavated during La Maddalena construction has been provided in this section.

The results of laboratory tests have been provided by construction company.

5.2.1 Lithological description

General lithological description of rock has been carried out for each rock section; the description is based on tunnel walls and samples macroscopic examination.

Particular attention is given to:

- Colour;
- Petrographic composition;
- Texture;
- Grain size and shape;
- Presence of planes of foliation (schistosity), layering, lining, orientation of minerals;
- Presence of folds;
- Intact rock weathering degree.

The macroscopic observations listed above allow to define the lithological type of rock.

5.2 Intact rock property determination

5.2.2 Micro-petrographic description

The micro-petrographic description of rocks has the purpose to determine the mineral content, to determinate the presence of microfractures, the degree of weathering, and the grain size and shape. The grain contacts, cement or matrix have also to be analysed. Generally micro-petrographic description has the purpose to focus on all parameters which cannot be carried out from macroscopic observation of a sample of rock.

In order to determine the volumetric proportion of the minerals that make up the excavated geological units quantitative modal analysis has been used, determined by areal analysis of thin section.

Thin section studying allows the individuation of dangerous minerals, as fibrous ones, and to evaluate the content of abrasive mineral, as quartz.

Figure 5.1 shows an example of thin section observed at parallel and crossed Nicols.

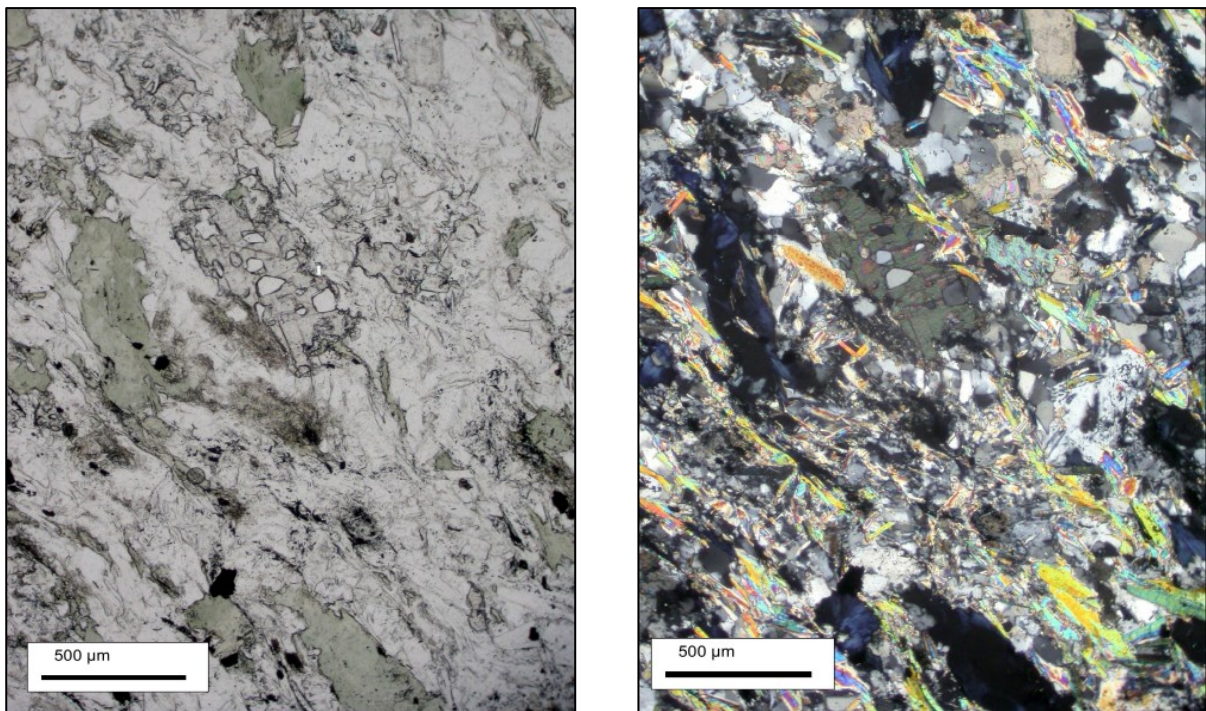


Figure 5.1 Thin section in parallel (left) and crossed (right) Nicols.

Thin section examination for rock engineering purpose should be carried out following the Suggested Methods proposed by ISRM (1978).

Results

Quantitative modal analysis by areal analysis of thin section have been carried out during La Maddalena tunnel excavation in order to determine the volumetric proportion of minerals and the occurrence of dangerous one.

Here the results of 36 thin section analyses are presented, with particular attention to the quartz content, considered largely affecting the TBM performance (Table 5.2).

QUARTZ CONTENT [%]	TUNNEL (n = 36)	Domain I (n = 7)	Domain II (n = 4)	Domain III (n = 25)
Range	15.00 – 80.00	37.00 – 80.00	15.00 – 50.00	20.00 – 35.00
Median	30.00	45.00	30.00	25.00
Mean	32.19	49.86	31.25	27.40
Q1-Q3	25.00 – 35.00	40.00 – 52.00	18.75 – 45.00	25.00 – 30.00

Table 5.2 Quartz content measured by areal analysis of thin sections.

The highest content of quartz has been detected into DI, formed by gneiss. In this domain, a portion with high occurrence of quartz veins has been mapped and in this area a band characterised by 80% of quartz. DI quartz content is 45.0-50.0%, the others constituting minerals are alkaline feldspars, muscovite and plagioclase. Quartz content in DII is lower than in DI (30.0%), however the lowest values have been noted in the third domain (25%). The other minerals forming the rocks of DIII are white mica, chlorite, and albite (and other minerals in lower percentage).

About DIII, there are not significantly differences between the data collected in DIIIa.

Figure 5.2 shows the quartz content distribution through the tunnel excavation.

5.2 Intact rock property determination

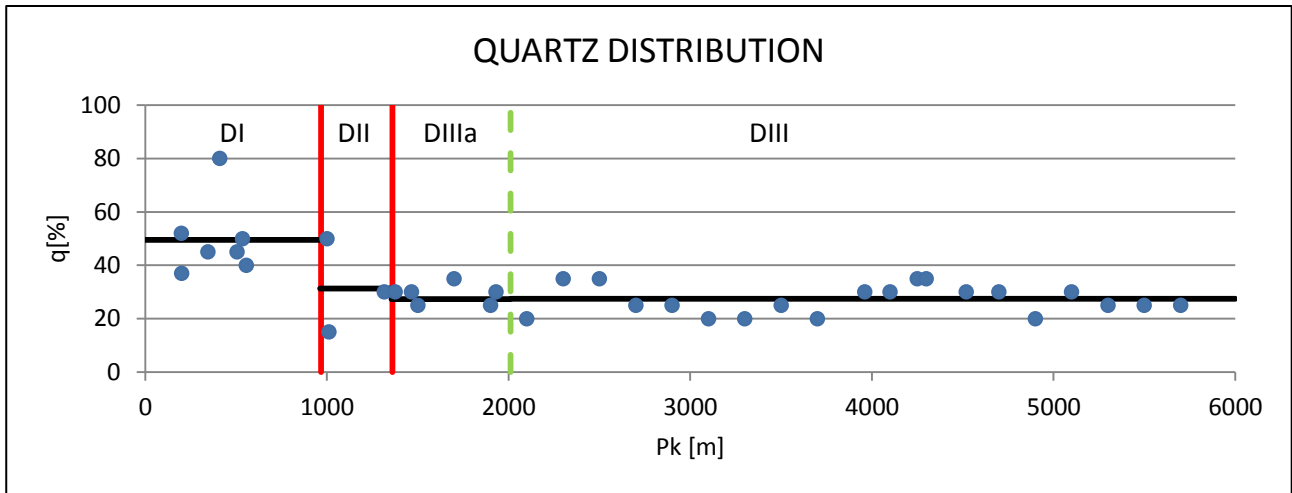


Figure 5.2 Quartz content distribution. Red lines represent the domain changes, green line delimits DIIIa, black ones represent the mean value for each domain.

The quartz content of excavated rocks has been determined also by means of macroscopical observation of rock samples, during tunnel excavation. This allowed to assign a quartz content value to each rock mass section detected.

5.2.3 Uniaxial compressive strength

Uniaxial compressive strength is one of the most required rock parameters; it can be measured by means of uniaxial compression test (ISRM, 1979) which is one of the most common laboratory tests, or by means of the point load test (ISRM, 1985).

5.2.3.1 Uniaxial compression test

This test has the purpose to measure the uniaxial compressive strength of a rock sample and, if sample is opportunely equipped, this test is able to determine stress-strain curves and Young's modulus and Poisson's ratio in uniaxial loading conditions. The test is mainly intended for strength and deformability classification and characterisation of intact rock materials.

The diameter of specimen has to be at least 20 times larger than the maximum grain size. The faces of sample should be perfectly plane parallel and perpendicular to the specimen axis, in particular the lateral one must be smoothed and regular. The sample has to be measured and the basis area has to be computed. The number of specimens to be tested has to be representative to take the variability of the rock strength into account. It is recommended to test 5 specimens for each rock type.

The sample of rock is put between two platens and the axial load is incremented, two loading procedures can be followed, the first is constant load increment and the second is constant axial deformation increment. The radial and axial strains are measured by dial gauge.

The rock specimen can be instrumented with electrical gauges for the deformation measurements and with a control unit to gather the results and, when the interpretation is not manual, with a computer to interpret the obtained data.

The measurements of axial and radial strains allow to determine the rock pseudo-elastic constants.

The axial force registered during the test is divided by the initial cross-section of the specimen to get the average axial stress (σ_a). This latter is plotted versus the overall axial strain (ϵ_a) and versus radial strain (ϵ_r).

The stress strain curve shows four stages:

- Crack closure and initial bedding down;
- Elastic deformation until uniaxial stress σ_{ci} is reached: stable crack propagation begins;
- Crack propagation continues until the axial stress reached σ_{cd} : irrecoverable deformations begin;

5.2 Intact rock property determination

- Irrecoverable deformations increase until the peak and UCS, σ_c , is reached.

By analysing stress-strain curve deformation moduli, Young's modulus and Poisson's ratio, can be obtained (Figure 5.3). Since Young's modulus varies throughout the loading history, stress – strain curve is not linear so three Young's moduli have to be determined:

- Tangent Young's modulus (E_t) is the slope of the axial stress-axial strain curve at 50% of the peak strength;
- Average Young's modulus (E_{av}) is the average slope of the straight line portion of the axial stress-axial strain curve;
- Secant Young's modulus (E_s) is the slope of a straight line linking the origin of the axial stress-axial strain curve to the point on the curve at 50% of the peak strength.

Poisson's ratio is defined as:

$$v = -\frac{(\Delta\varepsilon_r)}{(\Delta\varepsilon_a)} \quad (5.1)$$

The volume variation can be calculated in accordance with the following equation:

$$\varepsilon_v = \frac{\Delta V}{V} \quad (5.2)$$

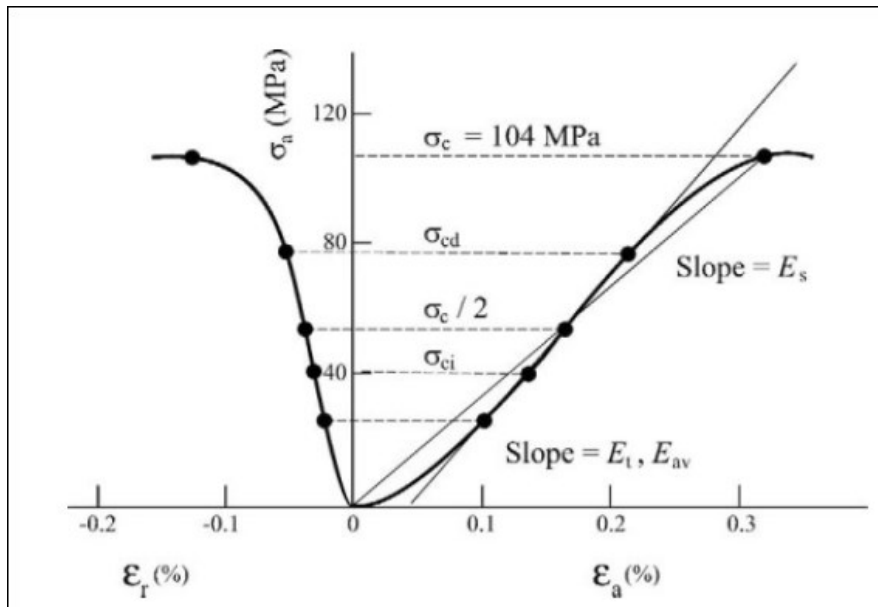


Figure 5.3 Elaboration of strain – stress curve (Brady and Brown, 2004).

Tests have to be carried out following the ISRM suggested methods (1979).

Results

During La Maddalena construction uniaxial compressive strength tests have been carried out by external testing laboratories.

These tests allow the estimation of the uniaxial compressive strength and deformation moduli, Young's modulus and Poisson's ratio. In this work the results of tests on rocks excavated between Pk. 0 + 198 m and 5 + 700 m have been analysed.

The UCS results are listed in Table 5.3: they are proposed both about the entire tunnel tract and for each geological domain (ad exception of DII where no tests have been carried out).

UCS [MPa]	TUNNEL (n = 36)	Domain I (n = 13)	Domain III (n = 23)
Range	41.20 – 235.98	140.30 – 235.98	41.20 – 232.15
Median	125.76	198.40	100.26
Mean	135.68	190.96	104.43
Q1-Q3	81.73 – 187.190	166.30 – 210.00	71.08 – 124.75

Table 5.3 UCS test results.

Globally, the rocks excavated during La Maddalena realisation could be classified as “high strength rocks” (Deere and Mille, 1966, classification).

It possible to note that, a significant reduction of UCS values occurs from DI to DIII. DI gneiss can be considered “high-very high strength rocks” (Deere and Mille, 1966, classification) and micaschist (DIII) are characterised by “moderately hard rocks”.

Figure 5.4 clearly shows the reduction of UCS in the direction of tunnel excavation.

5.2 Intact rock property determination

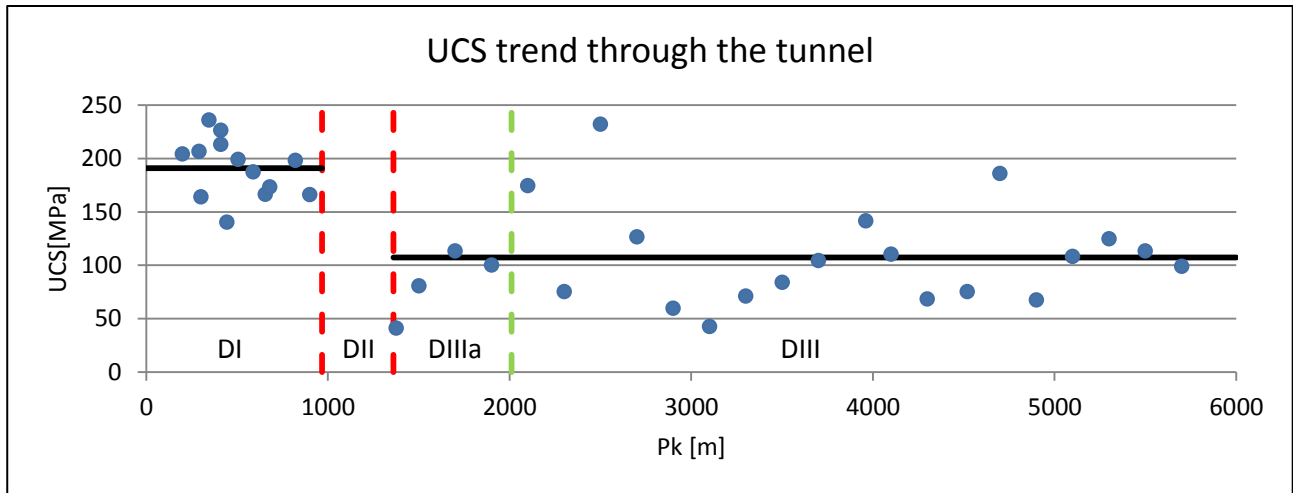


Figure 5.4 UCS distribution along the tunnel. Red lines represent the domain changes; green line delimits DIIIa; black horizontal lines represent the mean values in DI and DIII.

In addition, deformation moduli (E_t , E_s , ν_t , ν_s) have been estimated and their average values have been listed in Table 5.4.

No values have been reported for DII because of no tests have been carried out in this sector.

	TUNNEL (mean)	Domain I (mean)	Domain III (mean)
E_t [GPa]	53.50	57.85	52.36
E_s [GPa]	45.35	38.35	47.18
ν_t [-]	0.19	0.18	0.19
ν_s [-]	0.13	0.14	0.13

Table 5.4 Mean values of deformation moduli.

5.2.3.2 Point load test

Point load test is carried out by applying two punctual loads (loading is manually applied by two standardized truncated-conic points) to a rock specimen and breaking it. The test allows the indirect estimation of uniaxial compressive strength. Point load test implies great advantages since it let us determine UCS with a portable machine, directly on site and on irregular specimens.

The test allows the determination of a strength index I_S , which is related to the uniaxial compression strength. I_S is calculated in accordance with:

$$I_S = \frac{P}{D^2} \quad (5.3)$$

Where P is the failure loading [kN], it is read on a pressure gauge incorporated on the machine and D [mm] is the point distance, it is measured by using a graduated pole before and after the failure loading application.

I_S is expressed in MPa.

The specimen shape can be cylindrical or have other shapes and the direction of loading, for cylindrical core, can be axial or diametral (Figure 5.5).

Specimen shape requirements (ISRM SM 1985)	
	<p>a) Diametral test: $L > 0.7 D$</p> <p>b) Axial test: $D/L = 1.1 \pm 0.05$</p> <p>c) Irregular sample: $D/L = 1.0 / 1.4$</p>

Figure 5.5 Specimen shape requirements for a) diametral; b) axial, c) irregular test.

I_S varies as function of D , so that a size correction has to be applied to obtain a unique value of I_S that can be involved for purposes of rock strength calculation; the standard diameter is equal to 50 mm. The index $I_{S(50)}$ can be graphically obtained by using the “size correction chart”.

Point load test has to be carried out on 10 (or more) specimens, then it is necessary to calculate the mean (or median) value of I_{S50} to use it as input for UCS estimation. The mean (or median) value of $I_{S(50)}$ is to be calculate deleting the two lowest and highest values from the 10 (or more) valid tests and computing the mean or median of the remaining values.

5.2 Intact rock property determination

When a rock sample is anisotropic it has to be tested parallel and normal to the planes of anisotropy, these directions give the greatest and least strength values respectively.

$I_{S(50)}$ is empirically related to UCS by the following equation (5.4, Brokch and Franklin, 1972; 5.5, Bieniawski):

$$\sigma_c = 23.7 * I_{S(50)} [MPa] \quad (5.4)$$

$$\sigma_c = 25.0 * I_{S(50)} [MPa] \quad (5.5)$$

Results

For each rock section a datum of UCS is available, it has been obtained by Point load test directly on site. In order to calculate UCS from I_{S50} value the empirical correlation proposed by Brokch and Franklin (Equation 5.4) has been used.

Tests have been carried out following the ISRM suggested methods (1985).

The statistical description of UCS values is provided in Table 5.5.

The description was carried out about the entire excavated length and for each domain.

UCS [MPa] (plt)	TUNNEL (n = 502)	Domain I (n = 83)	Domain II (n = 44)	Domain III (n = 375); *DIIIa	
Range	60.00 – 255.00	68.00 – 219.00	70.00 – 251.00	74.00 – 224.0*	60.00 – 255.00
Median	150.00	143.00	129.00	105.00*	152.00
Mean	149.10	151.02	129.08	112.70*	151.02
Q1	133.50	121.00	101.25	93.00*	143.00
Q3	168.00	174.00	154.25	127.00*	168.50

*Table 5.5 UCS (from point load test) statistical description; * DIIIa data: part of DIII data used in the following predictive model creation.*

The mean value referred to the entire excavated material is about 150.00 MPa, and it allows to classify rock as “high strength” (Deere and Miller, 1966).

In particular, the intact rock samples of gneiss (DI) and of micaschist (DIII) have the same values of UCS. The strength decreases in the tract of tunnel characterised by the alternation of gneiss and micaschist.

By plotting the distribution of UCS values vs. the progressive length (Figure 5.6) it is possible to assert that there are two sectors in micaschist domain in which UCS has values significantly different from the average of the entire domain.

Between the Pk. 1 + 360 m and Pk. 2 + 003 m the mean value of UCS is 112.70 MPa, it makes possible to classify this rock as medium strength.

5.2 Intact rock property determination

The sector between Pk. 2 + 329 m and Pk. 2 + 756 m is characterised by mean value of UCS equal to 194.10 MPa, so rock can be classified as high strength.

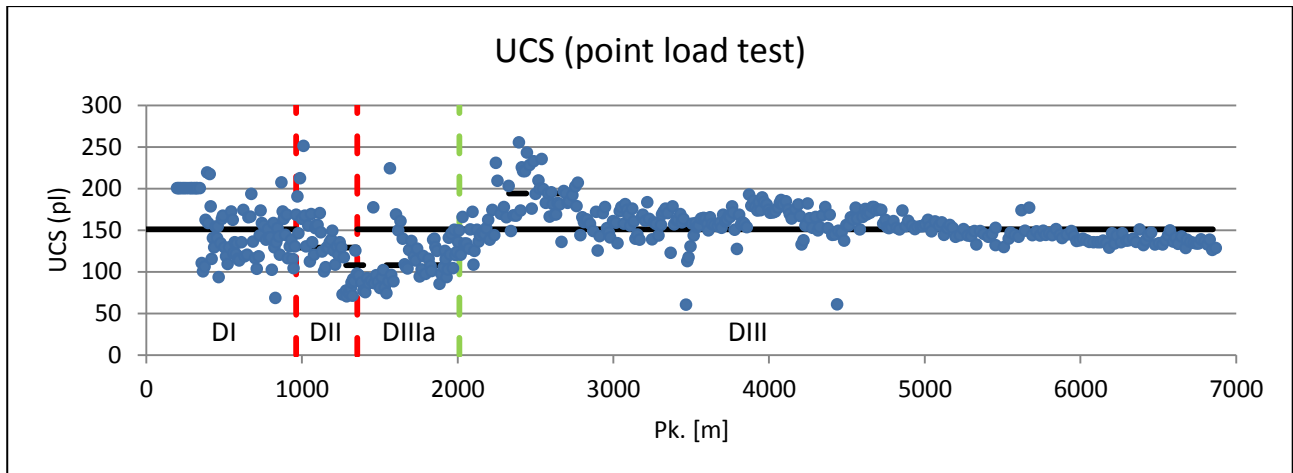


Figure 5.6 UCS (determined by means of point load test) distribution through the tunnel. Red lines represent the domain changes, green line delimits DIIIa, black lines the mean value of UCS for each geological domain, black dotted lines represent two zones in which the average value is significantly different from the mean value of the domain.

5.2.4 Determination of rock abrasivity

Rock abrasivity index are frequently used in TBM tunneling and rock drilling for the estimation of tool wear; the Cerchar abrasivity test is one of the widely used for this purpose. It was introduced by Centre d'Etudes et Recherches des Charbonages de France in 1970s (Valantin, 1973).

The test is based on a steel pin with defined hardness and geometry that scratches the surface of a rock sample under a constant load equal to 70 N.

A scheme of Cerchar testing device is provided in Figure 5.7. Cerchar Abrasivity Index is given by the ratio between the diameter of the wear flat, d [mm] and the unit correction factor, $c = 1$ mm (Figure 5.8); in accordance with the following formulation:

$$CAI = \frac{d}{c} [-] \quad (5.6)$$

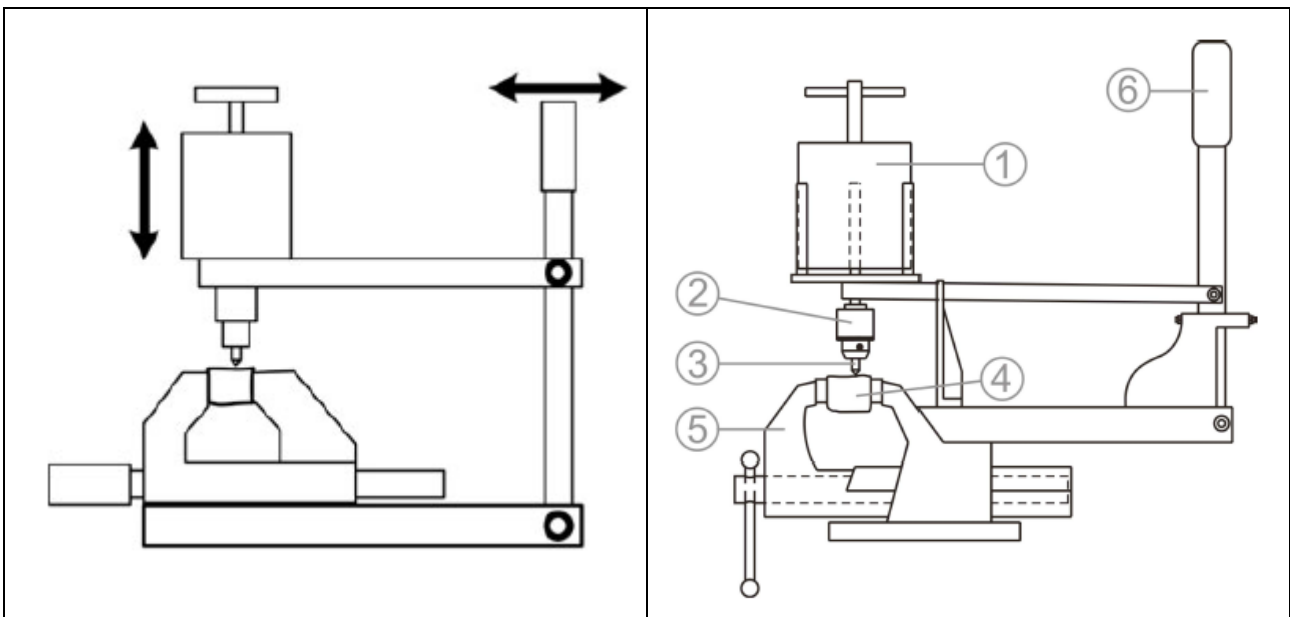


Figure 5.7 Cerchar testing device. 1: weight, 2: pin chuck, 3: steel pin, 4: rock sample, 5: vice, 6: hand level (Alber et al., 2013; Käslin and Thuro, 2010).

Only worn surface measurements obtained from standard profiles should be used, for example in Figure 5.8, *a* and *b* profiles represent sandard situation, nonstandard worn profile is shown in *c*, in this case no measurements have to be recorded.

5.2 Intact rock property determination

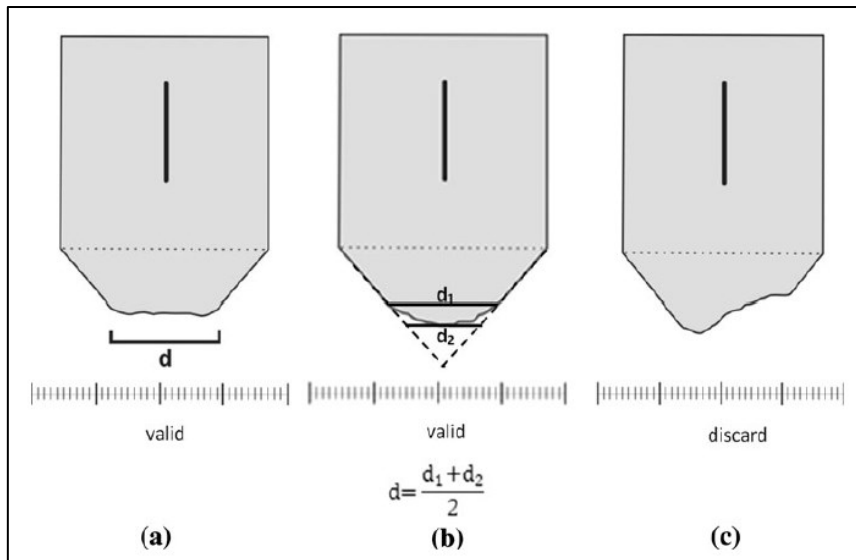


Figure 5.8 Pin shape before and after usage (Alber et al., 2013).

A minimum of five test replications must be made on the rock surface, and then the mean value is considered.

Rock can be classified on the basis of its abrasivity: the classification is proposed in Table 5.6.

Classification of CAI	
CAI	Classification
0.1 – 0.4	Extremely low
0.5 – 0.9	Very low
1.0 – 1.9	Low
2.0 – 2.9	Medium
3.0 – 3.9	High
4.0 – 4.9	Very high
≥ 5.0	Extremely high

Table 5.6 CAI classification, Alber et al., 2013.

Results

In this work the results of Cerchar Abrasivity tests carried out during La Maddalena construction, between Pk. 0 + 198 m and 5 + 700 m have been collected.

The results are listed in Table 5.7, they are proposed both about the entire tunnel tract and for each geological domain.

CAI [-]	TUNNEL (n = 36)	Domain I (n = 11)	Domain II (n = 3)	Domain III (n = 22)
Range	2.19 – 6.10	3.38 – 6.10	3.00 – 3.88	2.19 – 5.50
Median	3.94	5.30	*	3.60
Mean	4.04	4.96	*	3.65
Q1-Q3	3.28 – 4.74	4.13 – 5.70	*	3.19 – 4.21

Table 5.7 Results of Cerchar Abrasivity tests. (in DII only three tests have been performed, for this reason only value range has been provided).*

In general, the abrasivity of rocks encountered during La Maddalena excavation is classified as “high”-“very high”. The most abrasive unit is the gneiss, considered “very high” and “extremely high” abrasive. Generally CAI decreases from DI to DIII, where rock abrasivity is “high”.

In the transition zone (DII) only three tests have been carried out, and the abrasivity is “high” also in this tract.

The lowest class of abrasivity detected during La Maddalena realization has been obtained into micaschist unit, and it is the “medium” one.

The distribution of rock abrasivity reflects the cutter consumption and TBM performance distribution. Where highest classes of abrasivity have been encountered the maximum excavation tool consumption occurs and the lowest machine performance has been registered.

Figure 5.9 shows the rock abrasivity distribution through tunnel excavation.

5.2 Intact rock property determination

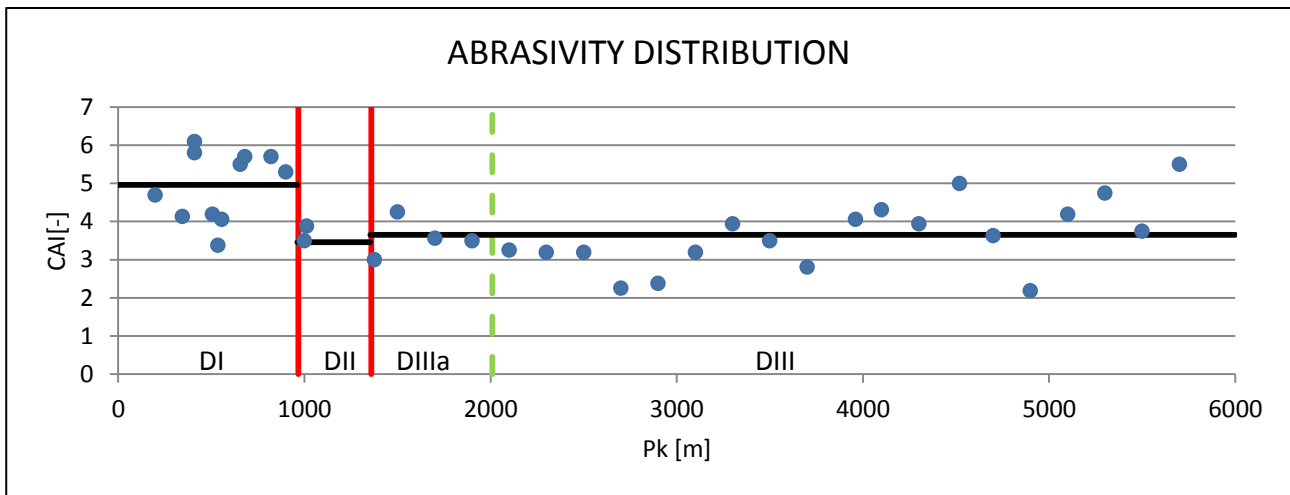


Figure 5.9 Rock abrasivity distribution. Red lines represent the domain changes, green line delimits DIIIa and black ones represent the mean values for each domain.

5.2.5 Determination of rock hardness

The hardness of rock units encountered during La Maddalena exploratory tunnel excavation was determined by means of Cerchar Hardness Test.

The test consists of measuring the indentation time of a bit into the rock sample for 10 mm. A vertical weight of 200 N provides the compressive force to the bit, which has a diameter of 8.0 mm; the test is performed at 200 rev/min of drilling rate.

The scheme of Cechar Hardness Index is provided in Figure 5.10.

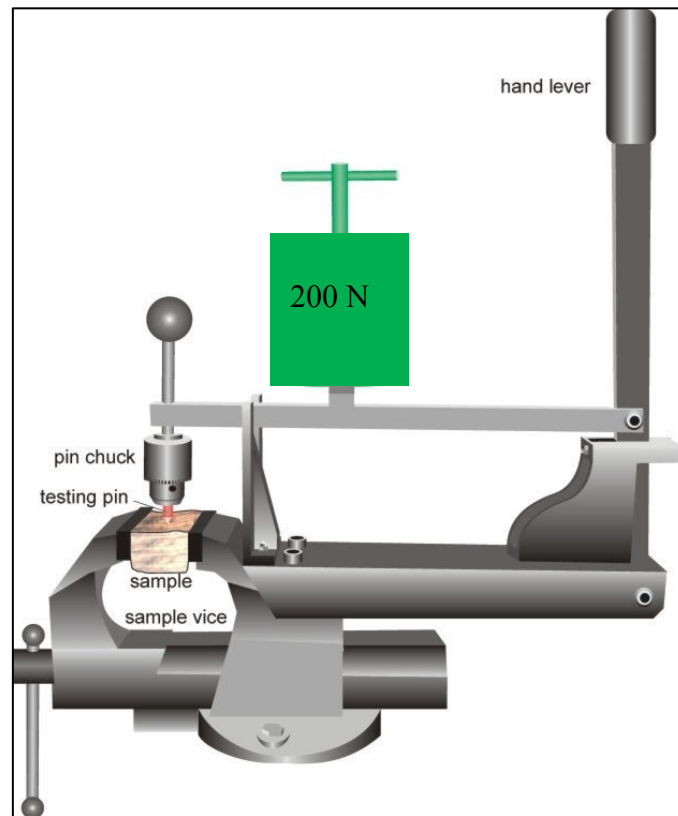


Figure 5.10 Cerchar Hardness Test device (Modified after Plinninger Geotechnik).

The test allows to estimate the Cerchar Hardness Index, CHI, expressed in seconds.

Rock can be classified on the basis of its hardness: the classification is proposed in Table 5.8 CHI classification.

5.2 Intact rock property determination

Classification of CHI	
CHI	Classification
0.0 – 20.0	Soft
20.0 – 40.0	Medium hard
41.0 – 80.0	Hard
81.0 – 120.0	Very hard
≥ 120.0	Extremely hard

Table 5.8 CHI classification.

Results

In this work, the results of Cerchar Hardness tests carried out during La Maddalena construction, between Pk. 0 + 198 m and 5 + 700 m have been collected.

The results are listed in Table 5.9: they are proposed both about the entire tunnel tract and for each geological domain. It is necessary to note that some tests carried out in DI give CHI higher than 1200 s. In these cases, a value of 1200 s has been considered, however in statistical analysis these value have been excluded being considered as out values.

CHI [-]	TUNNEL (n = 36)	Domain I (n = 11*)	Domain II (n = 3)	Domain III (n = 22)
Range	32.30 – 514.70	132.30 – 514.70	42.00 – 55.40	32.30 – 314.30
Median	95.00	362.20	**	90.55
Mean	134.59	342.85	**	108.38
Q1-Q3	52.50 – 158.70	170.83 – 495.53	**	52.85 – 126.28

Table 5.9 Results of Cerchar Abrasivity tests. (* in 7 cases CHI is higher than 1200 s, these results haven't been considered; ** in DII only three tests have been performed, for this reason only value range has been provided).

In general, the rocks excavated during La Maddalena realisation are “very”-“extremely hard”. The hardest formations have been encountered in DI, where eleven tests have been carried out and seven

on them give results of $CHI \geq 1200$ s, the gneiss of DI are classified as “extremely hard”. Hardness decreases in the micaschist domain (DIII) where rocks are classified as “very hard”. A very important difference between gneiss and micaschist hardness has been noted.

Figure 5.11 shows the rock hardness distribution through tunnel excavation.

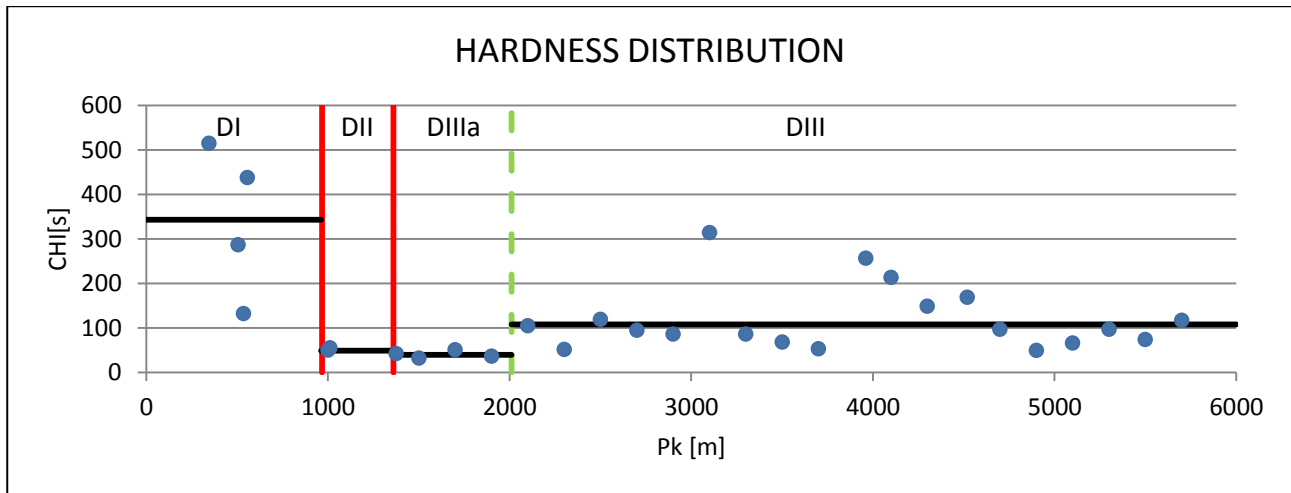


Figure 5.11 Rock hardness distribution. Red lines represent the domain changes, green line delimits DIIIa and black ones represent the mean values for each domain.

5.3 Quantitative description of discontinuities

Discontinuities represent any separation in rock continuum having zero tensile strength.

The intact rocks are subjected to millions of years of thermal, chemical and mechanical processes and during these actions discontinuities have been generated into rocks by geological and tectonics events as a result of different stress levels.

Generally, the geometrical and mechanical properties of discontinuities are determined by the processes by which the discontinuities have been generated, for this reason structural geology principles have to be involved in order to understand the discontinuity formation (Price and Cosgrove, 1990).

In engineering contexts discontinuities can govern the strength, deformability, permeability and global stability of the rock mass both in underground and in surface. For these reasons it is fundamental to study the geometrical and mechanical features of discontinuities and the way in which these influences rock mechanics and hence rock engineering projects.

During this work, La Maddalena tunnel walls have been continuously surveyed and, in this paragraph, a short description of the methods and techniques that have been adopted to characterise rock mass discontinuities and the results obtained after discontinuity feature analysis has been provided.

The described discontinuity properties are:

- *Discontinuity type*;
- *Orientation*: dip and dip direction of foliation planes, joints, shear planes, veins, faults and the orientation of these planes of weakness respect to the tunnel orientation (α angle);
- *Fracturing degree* expressed by means of spacing, joint volumetric number and rock quality designation index;
- *Groundwater circulation*;
- *Joint conditions*: persistence, aperture, filling, roughness, weathering.

5.3 Quantitative description of discontinuities

- *Survey windows*: all the discontinuities that outcrop inside a pre-determined area (window) have to be described (Figure 5.14). This method is used to survey discontinuities at small and medium scale;

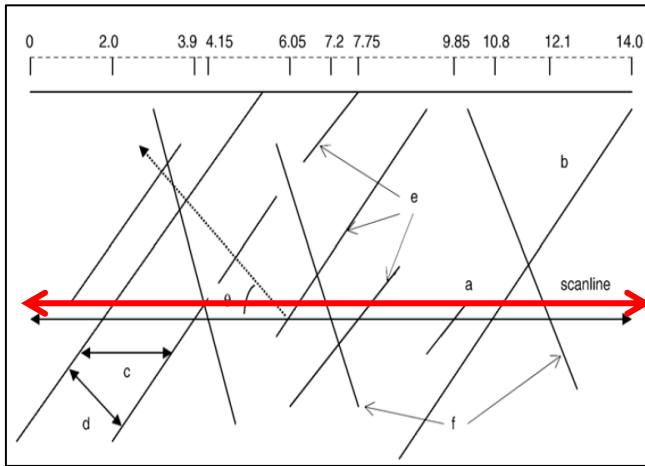


Figure 5.13 Scanline discontinuity survey method (Latham et al., 2006).

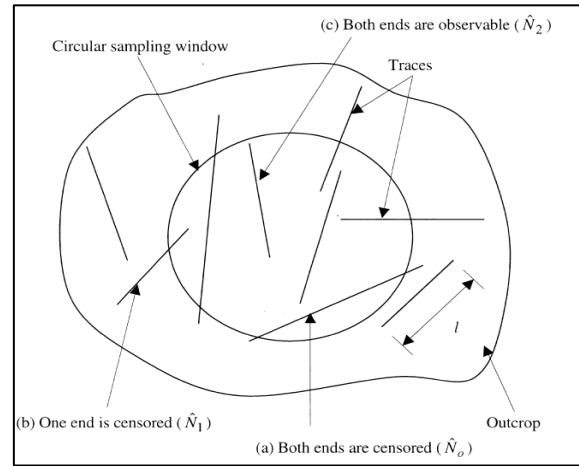


Figure 5.14 Window discontinuity survey method (Zhang and Einstein, 2000).

- *Drilling*: continuous core drilling allows the recovering of intact rock cores and the occurring discontinuities can be analysed; moreover, boreholes can be monitored by TV camera measuring the position and the orientation of the discontinuities (Figure 5.15). This method is used too to survey discontinuities at small and medium scale;
- *Digital surface model*: rock mass discontinuities can be surveyed by means of digital surface model (DSM) like laser scanning and photogrammetry (Figure 5.16). These methods are used to survey discontinuities at large scale and when rock masses are not easy accessible, for example large slopes.

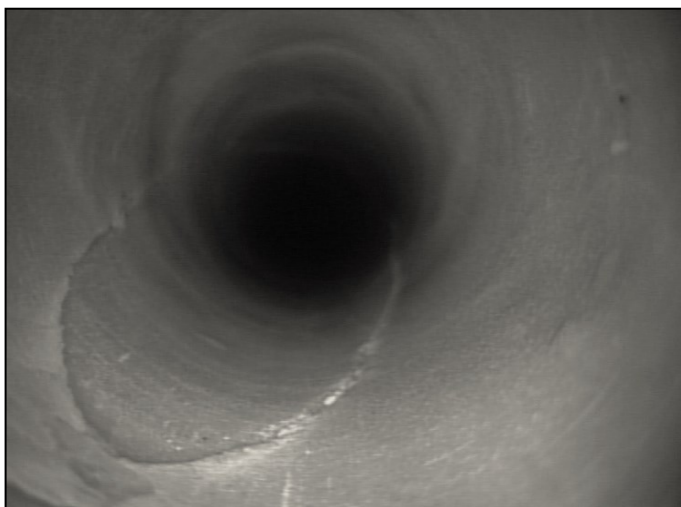


Figure 5.15 TV camera borehole inspection.

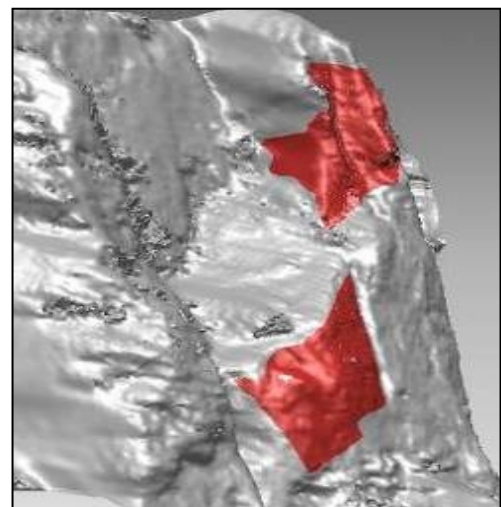


Figure 5.16 DSM discontinuity survey.

5.3 Quantitative description of discontinuities

Discontinuities should be described following the “Suggested Methods for the quantitative description of discontinuity in rock masses” proposed by ISRM (1978).

In the research work the rock mass discontinuities have been surveyed adopting the “window method”. The area (window) where surveys have been carried out consists of La Maddalena tunnel walls, all joints, faults, veins and other planes of weakness encountered during tunnel excavation have been surveyed, then described and analysed.

An example of discontinuity mapping performed during the survey is reported in Figure 5.17, the window of observation coincides with the tunnel wall.

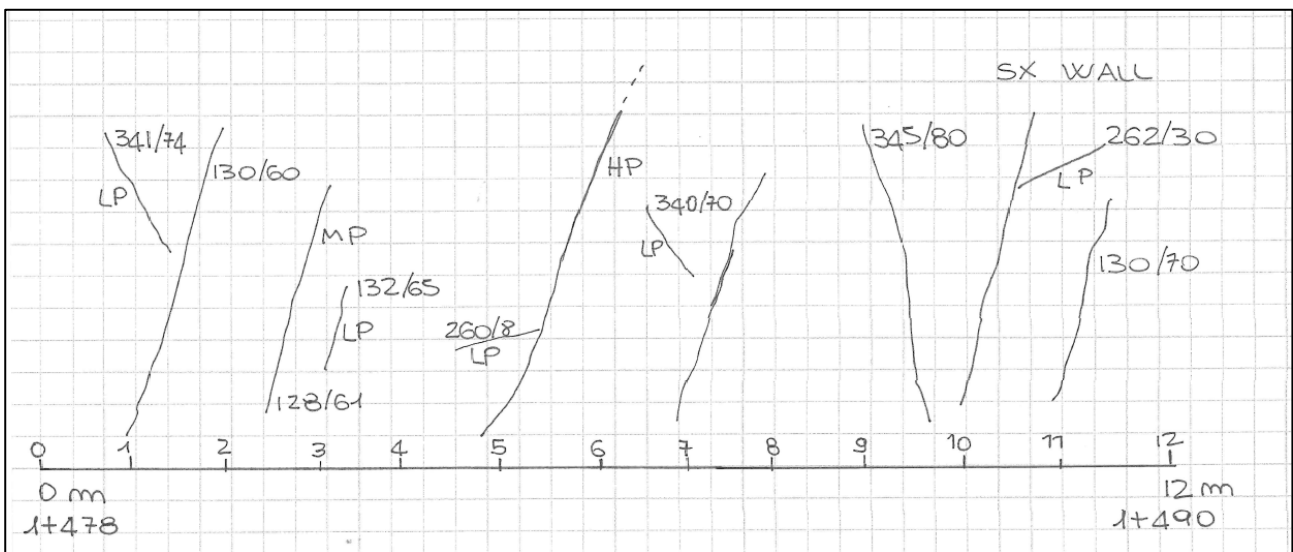


Figure 5.17 Example of discontinuity mapping performed during La Maddalena survey. The initial and final progressive length, the graphical representation of the discontinuities, their orientation and persistence are always noted.

5.3 Quantitative description of discontinuities

5.3.1 Types of discontinuity

The term “discontinuity”, related to a rock mass, indicates any separation in the rock continuum and any mechanical discontinuity in a rock mass having zero (or very low) tensile strength.

It is a collective term, used without any genetic connotation; the principal most appropriate terms to indicate rock mass discontinuity are:

- *Joint*: a break into rock masses along which there has been no visible displacements;
- *Fault*: a fracture, or zone of fractures, where there has been evidence of displacement;
- *Schistosity, cleavage, foliation*: discontinuities generated by metamorphism;
- *Bedding planes, stratification*: discontinuities typical of sedimentary rocks;
- *Unconformity, limit*: discontinuity which occur when there is change of lithology or geological unit.

The largest part of discontinuities mapped and described during the geological survey carried out in this work consists of joints however some faults have been encountered.

Foliation is clearly recognisable into micaschist domain; the principal set of joints develops along foliation planes.

5.3.2 Orientation

The orientation of rock mass discontinuities largely affects the conditions of stability relative to a rock structure, such as a tunnel or a rock slope. The importance of discontinuity orientation has a primary role when more deformation conditions occur, for example when shear strength is low or when a sufficient number of joints for sliding is present.

The orientation of discontinuity in space is described by two angles:

- *Dip (ψ)*: is the maximum inclination of a discontinuity to the horizontal plane (field range $0.0^\circ - 90.0^\circ$);
- *Dip Direction (α)*: is angle between the Northern direction and the horizontal trace of the dip line measured clockwise from the Northern direction (field range $0.0^\circ - 360.0^\circ$).

Another angle is involved in discontinuity orientation definition; it is the *strike (β)*. Strike is the angle between the Northern direction and the trace intersection of the discontinuity plane with a horizontal reference plane (field range $0.0^\circ - 180.0^\circ$).

Graphical representation of terminology used to describe discontinuities plane orientations has been provided in Figure 5.18.

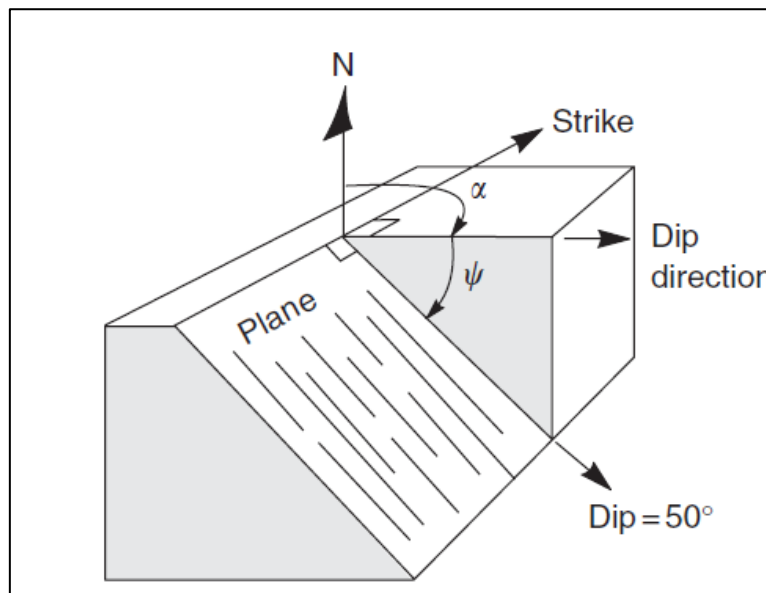


Figure 5.18 Terminology describing discontinuity plane orientation (Willie, 2014).

Dip/dip direction system is largely used in field and tunnel walls mapping, in plotting stereonets and in the analysis of orientation data.

5.3 Quantitative description of discontinuities

During field survey orientation data are usually collected by means of a compass and a clinometer, as recommended by ISRM (1978).

A method widely used to analyse orientation data of discontinuities is the stereographic analysis, in fact stereonet allows to identify the discontinuity sets and their orientation in space (by determining the central value and orientation distribution by cluster analysis); moreover stereographic projection permits to represent and analyse the three-dimensional orientation data in two dimensions.

They consist of a reference sphere where its equatorial plane is horizontal and its orientation is fixed about to the North. There are two types of stereographic projections, the equal area stereographic projections and the equal angle ones:

- *Equal area projection* (Lambert or Schmidt): the areas are maintained, but not the shapes because of the circumference arc becomes a different curve. It is adopted for the statistical analysis of the spatial distribution of the discontinuity planes.
- *Equal angle projection* (Wulf): in which both the angles and the shapes are maintained. It is recommended for the visualization of the rock blocks isolated by discontinuities and excavation surface, and to carry out rock block stability analysis.

A discontinuity plane can be represented as its intersection with the lower half part of the reference sphere, defining a circular arc called “great circle”, or as a point called “pole”. The pole is the intersection of the line perpendicular to the plane with the surface of the sphere (Figure 5.19).

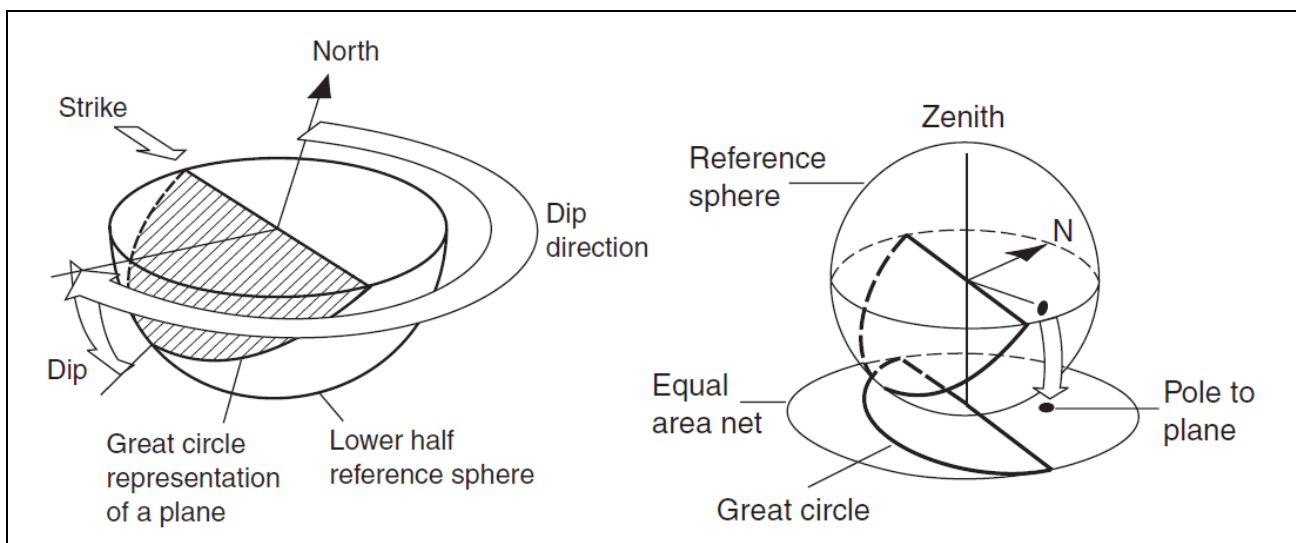


Figure 5.19 Stereographic representation of plane (Wyllie, 2014).

The same group of discontinuity poles has to be analysed in order to determine the central value of the joint set in term of orientation.

For this purpose, a great number of discontinuity planes needs to be analyzed, so it is necessary to consider poles and not great circles. In a spherical projection, a surveyed discontinuity generally belongs to a cloud of poles which are more or less near the central value.

Results

More than 2100 orientation data in terms of dip and dip direction have been collected during “La Maddalena” tunnel wall mapping then they were analysed with the purpose to define the main orientation of each set of joints.

A stereographic projection of all collected orientation data is reported in Figure 5.20.

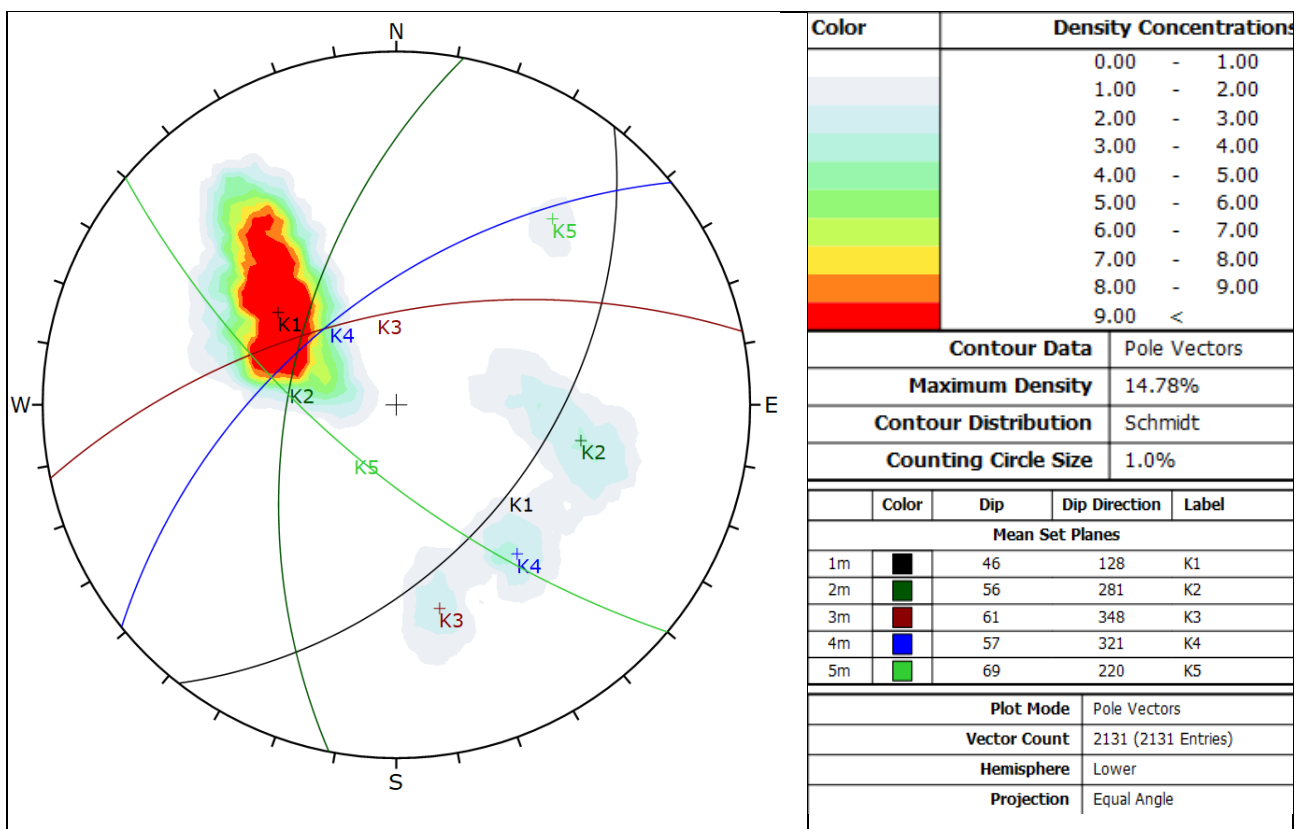


Figure 5.20 Stereographic projection of discontinuity orientation data.

Five sets of fractures have been recognised, their mean orientations do not significantly change through the portion of rock mass investigated during tunnel excavation.

The principal set, named K1, has a mean orientation of 128/47, in terms of dip direction/dip. K1 develops on foliation planes.

The other four sets are less frequent than K1 and their orientation characteristics have been listed in the following table (Table 5.10).

5.3 Quantitative description of discontinuities

Orientation of principal joint sets		
Set	Dip Direction	Dip
K1	128	47
K2	281	56
K3	348	61
K4	321	57
K5	220	69

Table 5.10 Orientation of principal joint set.

The orientation of the planes of foliation has been surveyed. The mean orientation of foliation planes is about 123/50, however this orientation change in occurrence of folds with axes oriented 325/50 – 60, in terms of trend and plunge. However, the folded zones are limited and foliation generally dips towards SE with a medium dip angle, ranging between 30° and 60°.

K4 develops on the planes of folded foliation.

The analysis of data orientation has been performed for each domain.

The stereographic projections related to each geological domain are reported in Figure 5.21 (Domain I), Figure 5.22 (Domain II) and Figure 5.23 (Domain III).

5.3 Quantitative description of discontinuities

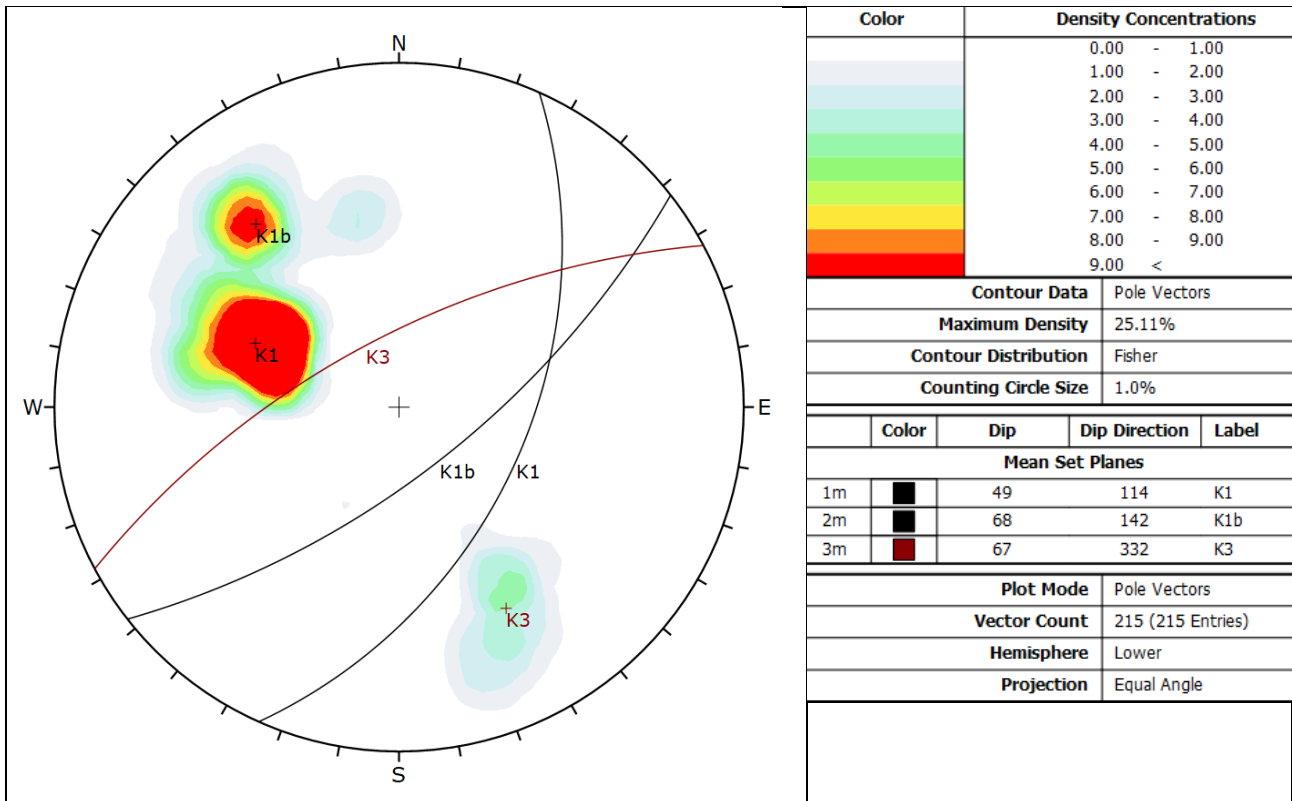


Figure 5.21 Stereographic projection of discontinuity orientation data collected in Domain I.

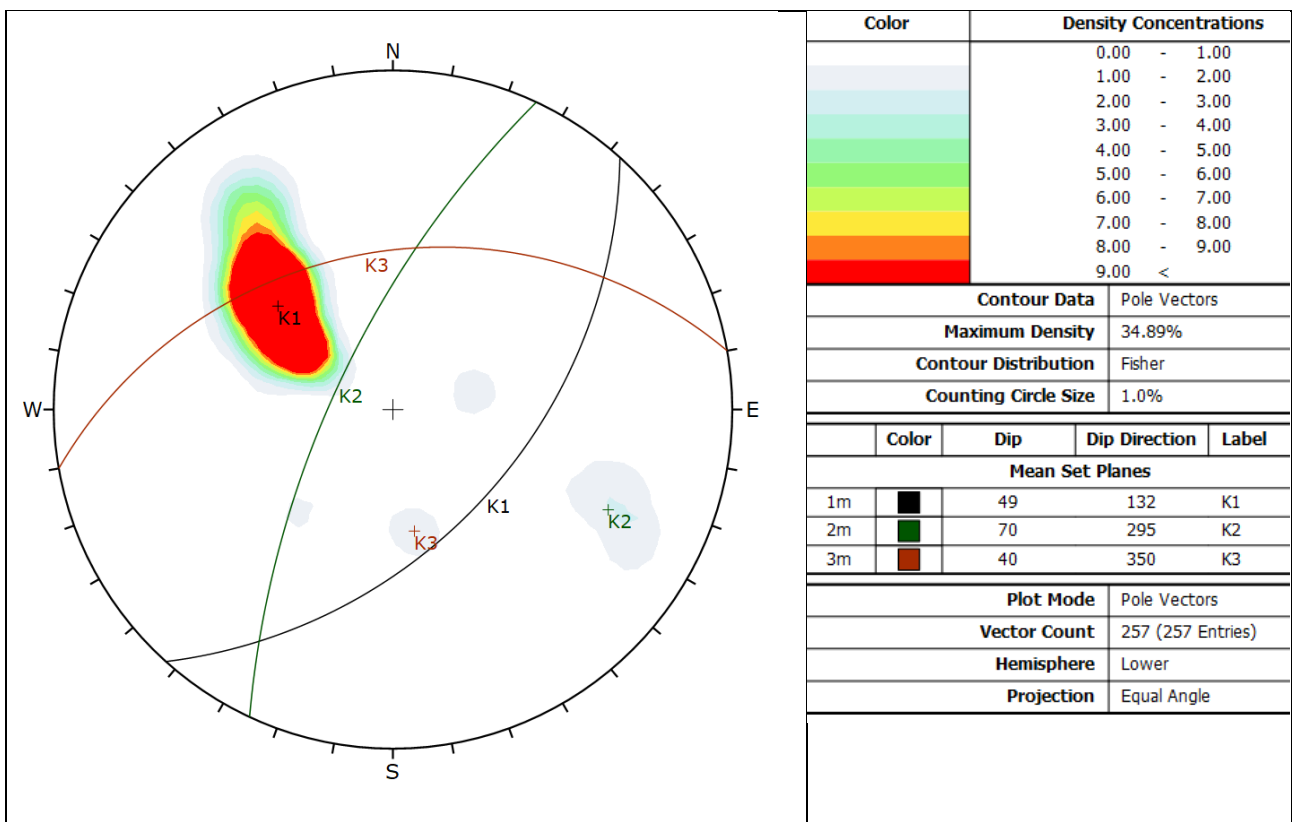


Figure 5.22 Stereographic projection of discontinuity orientation data collected in Domain II.

5.3 Quantitative description of discontinuities

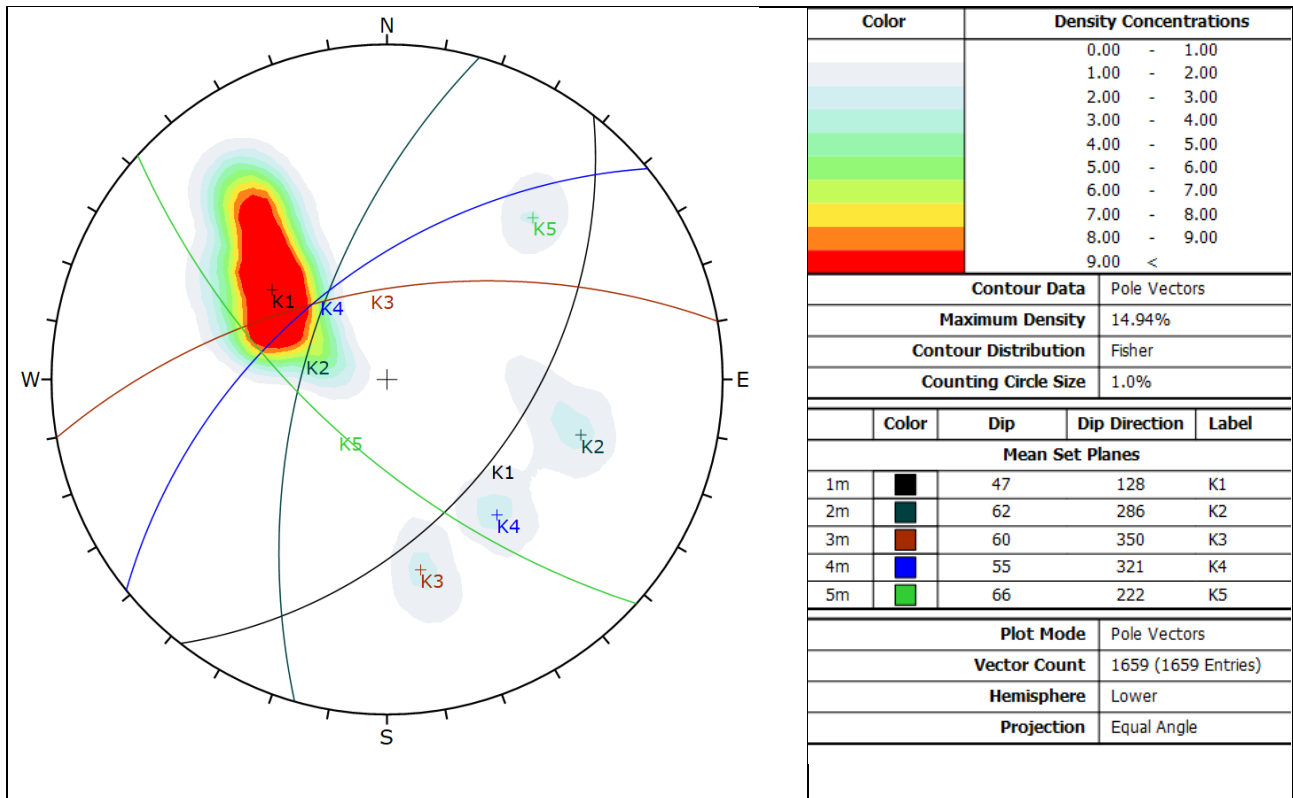


Figure 5.23 Stereographic projection of discontinuity orientation data collected in Domain III.

The summary of joint sets orientation is provided in Table 5.11.

Orientation of principal joint sets (Dip Direction/Dip)			
Set	Domain I	Domain II	Domain III
K1	114/49	132/49	128/47
K1b	142/68		
K2		295/70	286/62
K3	332/67	350/40	350/60
K4			321/55
K5			222/66

Table 5.11 Mean orientation of joint sets, detected in each domain.

5.3.2.1 α angle

The angle between tunnel axis and planes of weakness can affect the TBM performance. This angle, α [°], was introduced by NTNU prediction model and it is calculated by using the following equation (Bruland, 1998; Equation 5.7):

$$\alpha = \sin^{-1}(\sin \alpha_f * \sin(\alpha_t - \alpha_s)) \quad (5.7)$$

where:

- α_f is the dip and α_s is the strike of the planes of weakness;
- α_t is the strike of tunnel axis;

The best tunnelling conditions occur when α is approximately 60° (Bruland et al, 1998; Macias et al., 2014).

For each rock mass section α angle has been calculated considering the mean orientation of the principal set of joints and the tunnel axis orientation in that tract of tunnel. For more information about the tunnel orientation see section 3.2.3. The results of α calculation have been reported in Table 5.12.

α [deg]	TUNNEL (n = 502)	Domain I (n = 83)	Domain II (n = 44)	Domain III (n = 375); *DIIIa	
Range	2.8 – 85.0	18.4 – 85.0	22.5 – 72.0	7.4 – 69.4*	2.8 – 72.6
Median	45.2	48.3	41.6	39.8*	45.0
Mean	44.8	49.8	40.3	40.7*	45.3
Q1-Q3	36.8 – 52.3	42.0 – 56.8	33.8 – 46.0	29.8 – 52.3*	39.4 – 54.4

*Table 5.12 α angle Spacing statistical description; * DIIIa data: part of DIII data used in the following predictive model creation.*

The mean value of α referred to the whole tunnel is 44.8°. The highest mean value has been calculated in DI where the orientation of the principal set of joints taking in consideration for the tunnel axis about 50.0°. In DII and DIIIa it decreases, and it is equal to 40.0° in both domains. However, considering the entire DIII the angle increases and it is equal to 45.0°.

5.3 Quantitative description of discontinuities

The trend of alpha angle through the tunnel is showed in Figure 5.24.

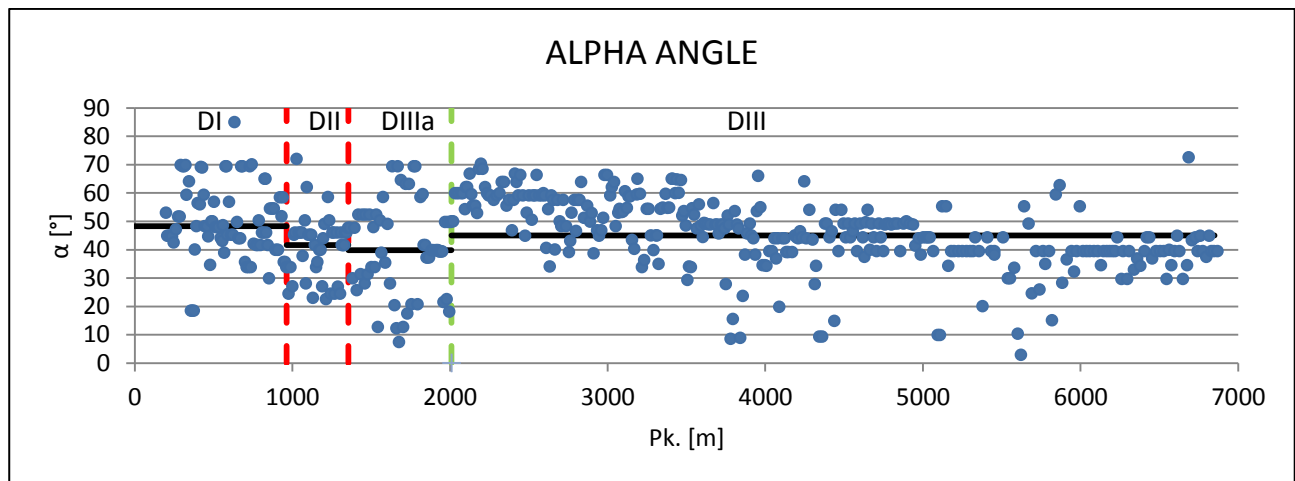


Figure 5.24 Alpha trend through the tunnel. Red lines represent the domain changes, green line delimits DIIIa and black horizontal lines the median values for each domain.

5.3.3 Spacing between discontinuities

The spacing is the minimum orthogonal distance between two adjacent fractures, measured on a scanline. It is an indicator of rock mass fracturing degree, moreover spacing affects the volume of rock blocks, the strength and deformability properties of rock masses and its stability conditions.

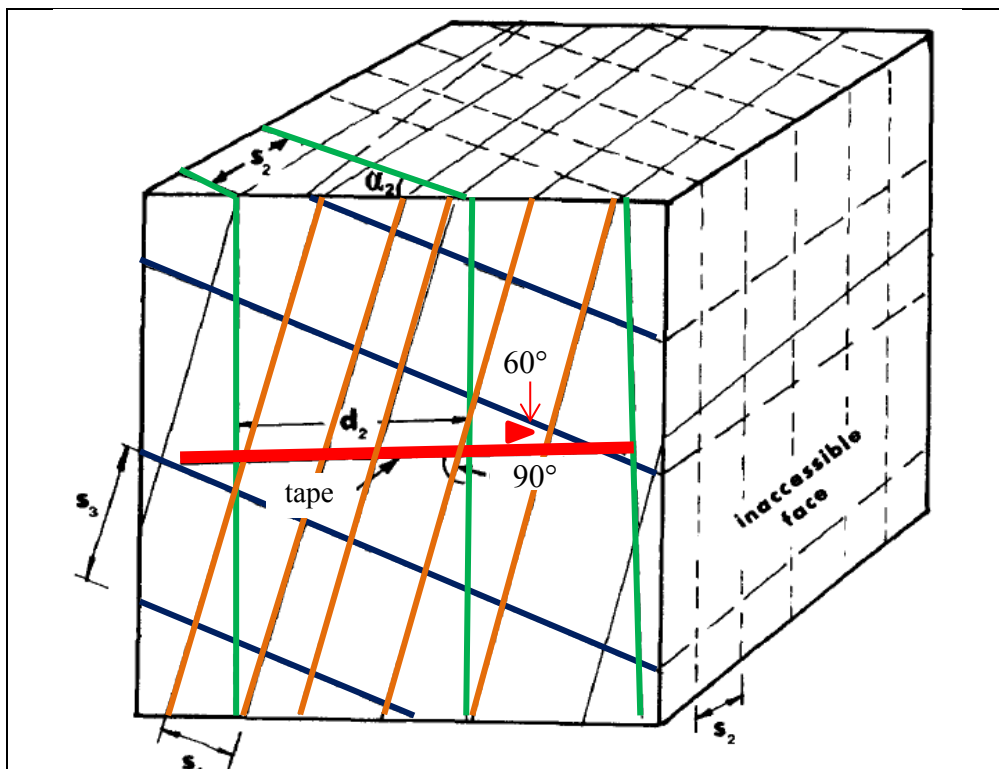
The orientation of the tape used to measure the distances (so the scanline) and the one of the discontinuity should be perpendicular, however, when it is not possible the operator has to apply the “Terzaghi correction” in accordance to:

$$S = d * \sin \alpha \quad (5.8)$$

where:

- S is the spacing between two adjacent discontinuities;
- d is the distance between two adjacent discontinuities;
- α is the angle between discontinuity and scanline.

Figure 5.25 reports discontinuities perpendicular to the scanline for which correction equation is not necessary and sets of discontinuity which form an angle different from 90° with the scanline, for which Equation 5.8 application is necessary.



5.3 Quantitative description of discontinuities

Figure 5.25 Measurement of joint spacing. The red line represents the measuring tape, the green lines represent a set of discontinuities perpendicular to the measuring tape and brown and blue lines represent sets not perpendicular to the tape (modified after ISRM, 1978).

Spacing can be measured for each set of discontinuities, and in this case the average or modal value of each set of joints are considered, or spacing can be referred to all the discontinuities which occur into the examined rock mass.

The mean spacing can be calculated in according to:

$$\bar{x} = \frac{L}{N} \quad (5.9)$$

where L is the scanline length and N is the number of discontinuities occurring in L.

It is also possible to consider the frequency of fracturing as:

$$\lambda = \frac{N}{L} = \frac{1}{\bar{x}} \quad (5.10)$$

So spacing can be calculated as:

$$S = \frac{1}{\lambda} \quad (5.11)$$

Terzaghi correction has to be applied also when spacing frequency is considered, by using the following formulation:

$$\lambda_r = \lambda_a * \sin \alpha \quad (5.12)$$

Where λ_r is the real frequency of fracturing, considering the angle between scanline and joints, λ_a is the apparent λ .

Equation 5.12 has to be applied to each set of joints and the frequency of fracturing related to the entire rock mass has to be calculated as proposed by:

$$\lambda_r = \sum_{i=1}^n \lambda_i * \sin \alpha \quad (5.13)$$

were:

- λ_r is the real frequency of fracturing referred to the entire rock mass;
- n is the number of joint sets;

- λ_i is the frequency of fracturing of each discontinuity set.

Finally, the global spacing between discontinuities can be calculated as the inverse of the frequency of fracturing referred to the entire rock mass:

$$S = \frac{1}{\lambda_r} \quad (5.14)$$

Spacing is measured in metres or in centimetres, the frequency of fracturing in m^{-1} .

On the basis of spacing values, ISRM (1978) suggested to adopt the terminology listed in Table 5.13 in order to describe the classes of spacing of each set.

Spacing [cm]	Description
< 2.0	Extremely close spacing
2.0 – 6.0	Very close spacing
6.0 – 20.0	Close spacing
20.0 – 60.0	Moderate spacing
60.0 – 200.0	Wide spacing
200.0 – 600.0	Very wide spacing
≥ 600.0	Extremely wide spacing

Table 5.13 Spacing description (ISRM, 1978).

5.3 Quantitative description of discontinuities

Results

During La Maddalena discontinuity survey, spacing has been measured by using scanline method. In this case spacing is referred to all the discontinuities occurring in the rock mass: firstly we considered the frequency of fracturing, considering as L the daily excavation advance, an apparent λ was calculated, so it was necessary to correct it by using the Equation 5.12.

The Terzaghi correction has been applied to each discontinuity set and the real frequency of fracturing was calculated by means of Equation 5.13.

The total spacing referred to all the occurring discontinuities has been calculated by using Equation 5.14.

The results of the evaluation of the spacing between discontinuity planes have been reported in Table 5.14.

SPACING [m]	TUNNEL	Domain I	Domain II	Domain III; * DIIIa	
Range	0.20 – 11.80	0.68 – 11.80	0.28 – 10.00	30.0 – 433.30*	0.20 – 4.33
Median	0.90	2.50	1.29	1.00*	0.83
Mean	1.42	3.56	2.00	1.17*	0.88
Q1	0.75	1.50	1.00	0.83*	0.71
Q3	1.29	5.00	2.12	1.40*	1.00

*Table 5.14 Spacing statistical description; * DIIIa data: part of DIII data used in the following predictive model creation.*

Given that data distribution not normal it is necessary to consider median values instead of mean ones.

The distance between discontinuity about the entire investigate tunnel is equal to 0.90 metres and ranges between 0.75 m and 1.29 m (Q1-Q3).

In particular it has been observed that the spacing decreases significantly through the tunnel advance. The discontinuities mapped into the gneiss are the highest spaced, measured equal to 2.50 m, it represents a continuous portion of rock mass. The distance between discontinuity planes decreases into DII, in which a median value of 1.29 m has been calculated. The lowest value of

spacing has been computed into the micaschist belonging to the Clarea complex, characterised by spacing of 0.83 metres.

The results exposed above mean that fracturing degree increase in the same verse of excavation advance, so that micaschist are considerably more fractured than the gneiss.

The spacing calculated through La Maddalena rock mass has been plotted in Figure 5.26.

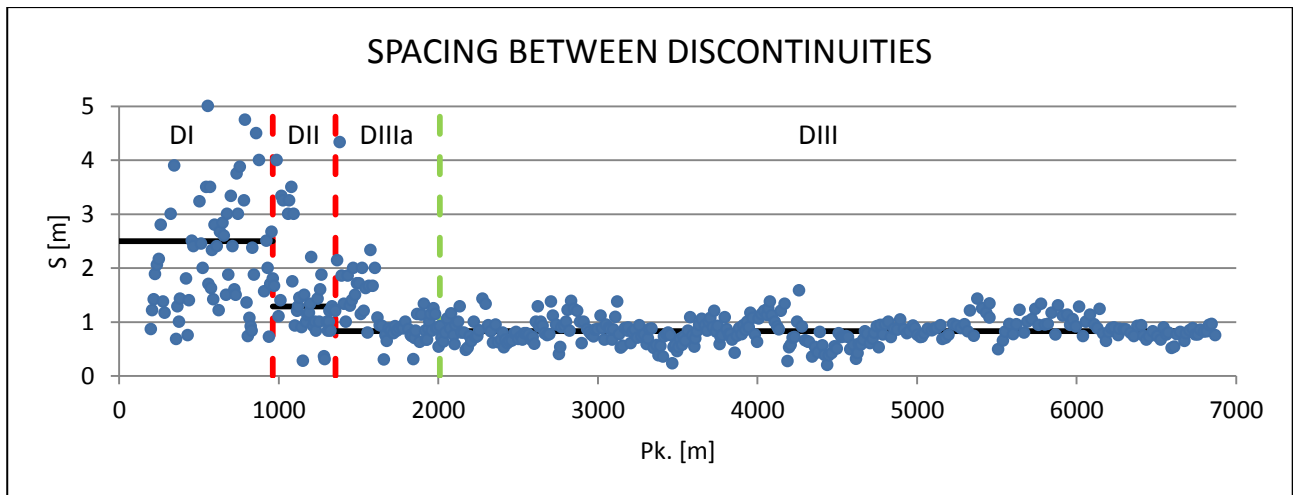


Figure 5.26 Spacing trend. It is necessary to consider that the values higher than 5 metres have not been plotted being them considered as outliers. Red lines represent the domain changes, green line delimits DIIIa and black lines the mean values for each domain.

It can be observed that the most fractured zones are located at Pk. 3 + 780 m, 3 + 860 m, 4 + 440 m and 5 + 500 m; as deduct by tunnel wall mapping and confirmed by Padovese et al. (2017).

Other fractured zones (less visible by the Figure 5.26 observation) has been encountered at about Pk. 1 + 150 m and 1 + 320 m (into the DII), and at Pk. 3.450 m (into the micaschist domain).

DIIIa spacing data are not significantly different from the entire DIII spacing features.

5.3 Quantitative description of discontinuities

5.3.4 Volumetric joint count

Palmström (1982, 1985, 1986) introduced the volumetric joint count, J_v , in order to provide a measure of rock mass jointing.

J_v is a measure of the number of fractures within a unit volume of a rock mass, it is calculated according to the following equation:

$$J_v = \frac{1}{S_1} + \frac{1}{S_2} + \frac{1}{S_3} + \dots + \frac{Nr}{S_r} \quad (5.15)$$

where:

- S_1, S_2, S_3 are joint spacing related to each joint set;
- Nr is the number of random joints;
- S_r is the random joint spacing, Palmström suggests to set $S_r = 5$.

Results

J_v related to La Maddalena rock mass have been calculated on the basis of Equation 5.15.

The results have been listed in Table 5.15.

J_v [$J \cdot m^{-3}$]	TUNNEL	Domain I	Domain II	Domain III	
	(n = 500)	(n = 83)	(n = 44)	(n = 373); *DIIIa	
Range	0.00 – 18.20	0.00 – 14.20	0.00 – 14.50	1.50 – 16.00*	1.50 – 18.20
Median	5.40	0.67	2.50	5.20*	6.40
Mean	5.88	1.59	4.01	5.80*	7.05
Q1-Q3	3.43 – 7.98	0.00 – 2.20	1.13 – 6.33	2.70 – 8.40*	4.60 – 9.00

*Table 5.15 J_v results. statistical description; * DIIIa data: part of DIII data used in the following predictive model creation.*

As a consequence of spacing distribution, also the frequency distribution of J_v is not normal: for this reason it is necessary to consider the median value instead of the mean one.

The mean value referred to the entire tunnel is equal to 5.40 m^{-3} , it is possible to observe that the number of joints per unit of volume increases through the tunnel in the excavation verse, as a result of the reduction of the distance between discontinuity planes.

In the gneiss, where spacing is high and the number of occurring fractures is low, J_v has a median value of $0.67 \text{ J}^* \text{ m}^{-3}$, in the gneiss-micaschist alternation is of $2.50 \text{ J}^* \text{ m}^{-3}$, finally it increases to $6.40 \text{ J}^* \text{ m}^{-3}$ into micaschist domain.

By plotting the J_v values vs. P_k is possible to individuate the most fractured zones, characterised by high values of J_v (Figure 5.27). These zones correspond to those individuated by tunnel wall mapping and and by means of spacing analysis (see section 5.3.3).

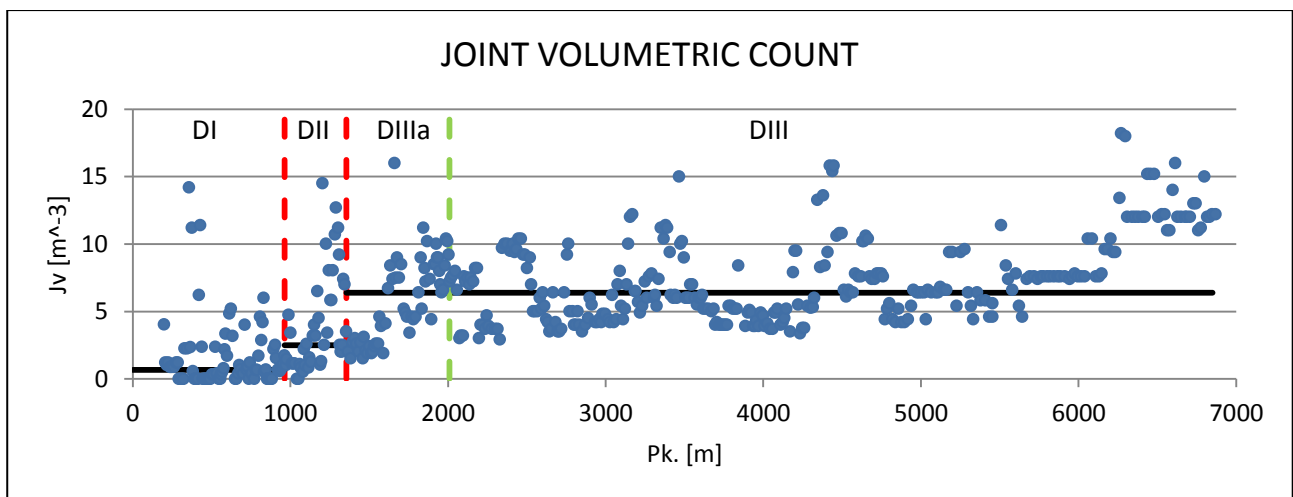


Figure 5.27 J_v distribution through the tunnel. Red lines represent the domain changes and the black ones represent the mean value for each domain.

5.3 Quantitative description of discontinuities

5.3.5 Rock Quality Designation index, RQD

The Rock Quality Designation index, RQD, was introduced by Deere et al. (1967) with the purpose of obtaining a quantitative estimate of rock mass quality by analysing drill core logs, especially in situ. One of the most important RQD use is as parameter of RMR system classification.

RQD is defined as the percentage of intact pieces of core longer than 10.0 cm in the total core length, in accordance with the following formulation:

$$RQD = \frac{\sum \text{Length of core pieces} > 10.0 \text{ cm length}}{\text{Total length of core run}} * 100 \quad (5.16)$$

Where no core is available and traces of discontinuities are visible in surface exposure RQD, is calculable by means of Palmström relationship (Palmström, 1982):

$$RQD = 115 - 3.3 * J_v \quad (5.17)$$

RQD value can change significantly depending upon the borehole orientation, being it a directionally dependent parameter. For this reason, the use of Palmström relationship may be useful in reducing the directional dependence.

Results

Any drill core logs were not available about La Maddalena tunnel, for this reason Equation 5.16 cannot be applied in order to calculate the Rock Quality Designation Index.

We decided to evaluate it by means of Palmström relationship (Equation 5.17).

RQD is always very high in the entire investigated tract; its mean value is equal to 93.32%. However a little difference between DI and DII-DIII has been observed. In particular the highest values characterise the gneiss (mean value of 98.7%) in accordance with the massive structure of this rocks. RQD values reduce through the other two domains; there is not difference between DII and DIII being their mean values 93.36% and 92.13% respectively.

The minimum values of RQD (50%) have been calculated in DIII, it has not a particular significance being an isolated case.

The areas where RDQ is lower respect to the principal trend represent fractured, faulted or cataclastic zones.

The trend of Rock Quality Index through La Maddalena tunnel has been reported in Figure 5.28.

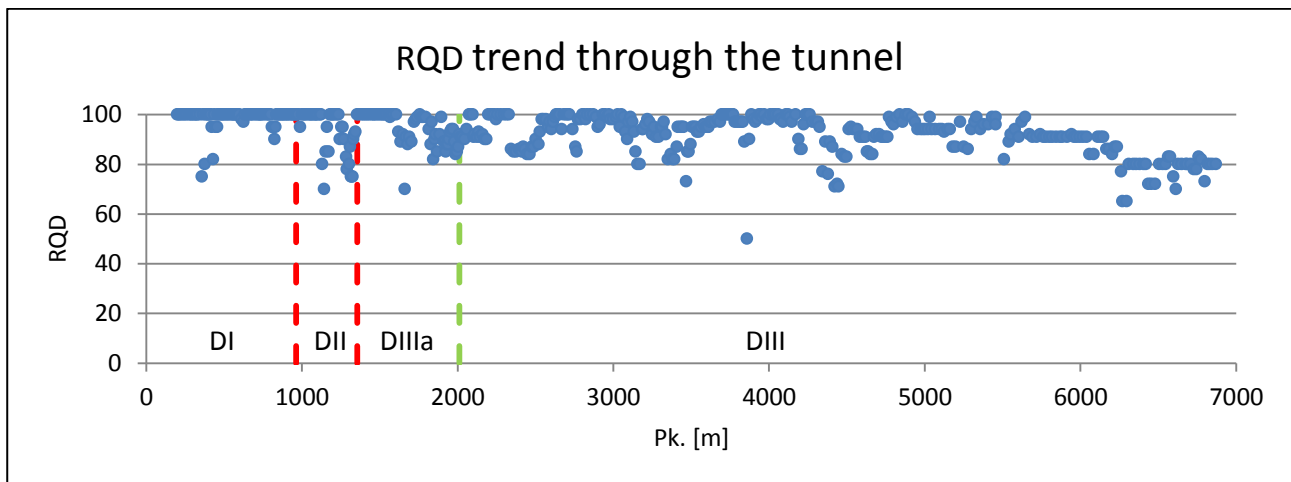


Figure 5.28 RQD trend through the tunnel. Red lines represent the domain changes, green line delimits DIIIa sector.

5.3 Quantitative description of discontinuities

5.3.6 Rock block volume

Block size is considered as one of the most relevant rock mass feature in rock engineering projects, both underground and surface ones. There are several methods that allow to determine rock block volume (V_b); in particular, block volume can be measured in situ where the individual blocks are observable in a surface, moreover, it can be computed from joint spacing or from the volumetric joint count.

The method that allows to estimate V_b from the volumetric joint count has been synthetically described.

V_b can be calculated in accordance to the following equation:

$$V_b = \beta * J_v^{-3} \quad (5.18)$$

where β is the block shape factor, it is usually calculated by means of a method developed by Palmström (1995), as:

$$\beta = 20 + 7 * \frac{S_{max}}{S_{min}} \quad (5.19)$$

where: S_{max} and S_{min} are the maximum and minimum spacing respectively.

Results

The rock block volume about La Maddalena rock mass has been calculated by means of Equation 5.18. However, it was not possible to calculate V_b for each rock mass section, in particular for those ones characterised by high spacing between fractures. This situation frequently occurs in DI and DII; instead for each rock mass section belonging to DIII V_b was calculated.

For this reason, the statistical description of V_b has not been provided.

It was noted that rock block volume is higher into the gneiss (median value equal to 3.62 m^3) than in DII and DIII (median value about 0.17 m^3).

The median V_b referred to the entire excavate length is of 0.18 m^3 .

The trend of Rock Block Volume through La Maddalena tunnel has been reported in Figure 5.29.

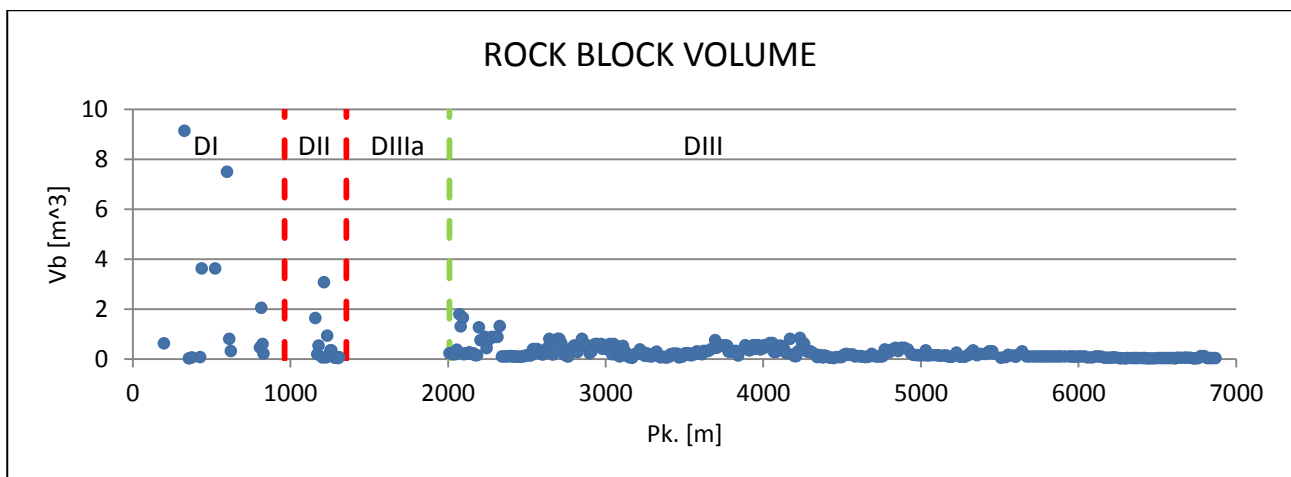


Figure 5.29 V_b trend through the tunnel. Red lines represent the domain changes, green line delimits DIIIa sector.

5.3 *Quantitative description of discontinuities*

5.3.7 Groundwater conditions

Generally, the ground water circulation through rock masses is possible thanks to the secondary permeability, via the discontinuity surfaces.

ISRM (1978) recommend describing seepage from individual or from specific set of discontinuities taking into account for their filling conditions. It is necessary to consider that a tunnel acts as a drain for the rock mass; in this case the overall flow into an individual section has to be described.

The description of groundwater condition about La Maddalena tunnel has been carried out from a qualitative point of view, no inflow or water pressure measurements have been done. Since the ground water circulation is generally poor and evidences of water flow have been observed in correspondence of faults or cataclastic zones.

In particular groundwater conditions have been described using the classes proposed by Rock Mass Rating system (Bieniawski, 1989), described in section 5.4.1.

These classes are:

- Completely dry,
- Damp;
- Wet;
- Dripping;
- Flowing.

As for La Maddalena tunnel the largest part of the surveyed discontinuities belongs to the class damp.

As already mentioned, water flow has been observed in correspondence of faults and cataclastic zones.

5.3.8 Joint conditions

The parameter named “joint conditions”, J_c , takes into account for five parameters which describe some features of discontinuity planes, which are: roughness, persistence (or continuity), aperture, filling and weathering degree.

In this work the parameters listed above have been rated in according to the RMR classification in order to obtain the parameter “ J_c ”, described in RMR related paragraph (5.4.1); in this section a brief description of each of them will be provided.

5.3.8.1 *Persistence*

As it is well known, discontinuity surfaces are not indefinitely continuous through rock masses and the persistence represents their area extension or size inside the rock mass. This parameter can be quantified by observing the trace lengths of discontinuities on the exposure surface; however it is one of the most difficult rock mass parameter to quantify, for example because in some cases exposures are smaller than the length (or area) of discontinuity.

Modal trace length for each set of discontinuity should be measured with a tape. Measurements allow the description of each set according to the classification proposed by ISRM, 1978 (Table 5.16).

Discontinuity persistence	
Length [m]	Classification
< 1.00	Very low persistence
1.00 – 3.00	Low persistence
3.00 – 10.00	Medium persistence
10.00 – 20.00	High persistence
> 20.00	Very high persistence

Table 5.16 Classes of discontinuity persistence proposed by ISRM, 1978.

5.3 Quantitative description of discontinuities

Results

The structural wall mapping of La Maddalena rock mass allows to determine the persistence of detected discontinuities. The measurements could be affected by a systematic error due to the fact that a discontinuity is more extended than the extension of the exposure.

The persistence analysed data regard only the principal set of discontinuity. Persistence has been expressed in terms of classes and not of modal length.

Generally, the largest part of the detected discontinuities has persistence classifiable as medium, given that the length of discontinuity traces is between 3.0 and 10.0 metres. In few cases the persistence is low and these occur in the gneiss (DI) and in the gneiss-micaschist alternation (DII). There are rare cases of very low persistence, mapped in DI.

No one discontinuity is characterised by high or very high persistence. It is probably due to the fact that the tunnel wall exposure is limited and the discontinuity trace length might appear shorter than its real extension (Figure 5.30).

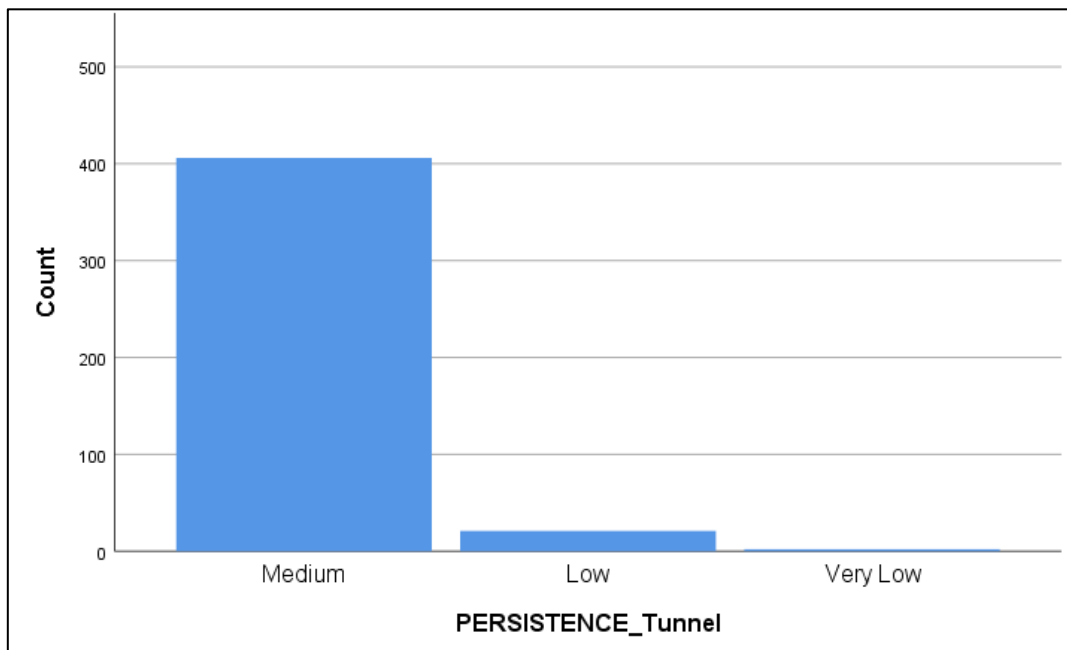


Figure 5.30 Discontinuity persistence distribution (referred to the principal joint set).

5.3.8.2 *Aperture*

The term “aperture” indicates the perpendicular distance separating the adjacent walls of an open discontinuity, the space between walls is filled by water or air (ISRM, 1978).

The largest aperture can be measured by means of a tape calibrated in mm; however in order to measure the width of finest one a feeler gauge is necessary.

Apertures can be divided into three classes (and nine subclasses), in according to ISRM SM (1978; Table 5.17):

Discontinuity aperture	
Aperture [mm]	Classification
< 0.5	Closed
0.5 – 10.0	Gapped
> 10.00	Open

Table 5.17 Classes of discontinuity aperture proposed by ISRM (1978).

Results

During La Maddalena rock wall mapping the aperture of discontinuities belonging to the principal set of fractures has been measured by means of tape and feeler gauge. In this work the aperture values have been divided into three classes in accordance to RMR classification system (Bieniawski, 1989).

Five aperture classes have been considered; their ranges are: 0 mm, < 0.1 mm, 0.1 – 1.0 mm, 1.0 – 5.0 mm and > 5.0 mm.

Discontinuities have prevalently an aperture ranges between 0.1 and 1.0 millimetres and between 1.0 and 5.0 mm. DII is characterised by the highest occurrence of values > 5.0 mm of discontinuity surfaces separation.

5.3 *Quantitative description of discontinuities*

5.3.8.3 *Filling*

ISRM (1978) defines filling as the material that separates the adjacent rock wall of a discontinuity and filling width is considered the perpendicular distance between the adjacent rock walls. Filling materials are usually weaker than the parent rock; however, some exceptions occur when discontinuities are filled with minerals characterised by high strength and deformation feature such as calcite, quartz and pyrite.

The most frequent filling materials are sand, silt, clay and cataclastic rocks. The shear strength of discontinuities is strongly affected by the mechanical features of filling materials.

During a discontinuity mapping the following features about filling material should be recorded: mineralogy, particle size, over-consolidation ratio, water content, previous shear displacement and width (ISRM, 1978).

Results

During La Maddalena rock mass surveys, filling materials were analysed on the basis of the classification proposed by RMR system.

In particular it identifies five classes, these are:

- Absent filling material;
- Hard filling material, width < 5.0 mm;
- Hard filling material, width > 5.0 mm;
- Soft filling material, width < 5.0 mm;
- Soft filling material, width > 5.0 mm.

In the gneiss discontinuities the filling is absent in the largest part of the cases; whereas in the micaschist (DIII) there are some situations in which filling material is soft and its thickness is higher than 5.0 mm, generally this happens in correspondence of faults or cataclastic zones.

Filling material is the result of fault activity.

5.3.8.4 Roughness

The roughness of discontinuity walls can be observed at large scale and at small one. The term “waviness” refers to large scale undulations while the term “unevenness” refers small scale roughness. The roughness of wall discontinuity is one of the most important factors of its shear strength.

ISRM (1978) proposed suggested methods for sampling roughness (the linear profiling method, the compass and disc-clinometer one, the photogrammetric method, etc.), however when logistic and time limitations prevent the use of the recommended roughness measuring techniques the roughness description will be limited to the assignment of two descriptive terms. The first one refers to large scale of observation and the second one to the small observation scale.

In particular, at large scale it can be distinguished three classes or waviness: stepped, undulating and planar; while at small scale it can be recognised three classes of unevenness: rough, smooth and slickenside (Figure 5.31).

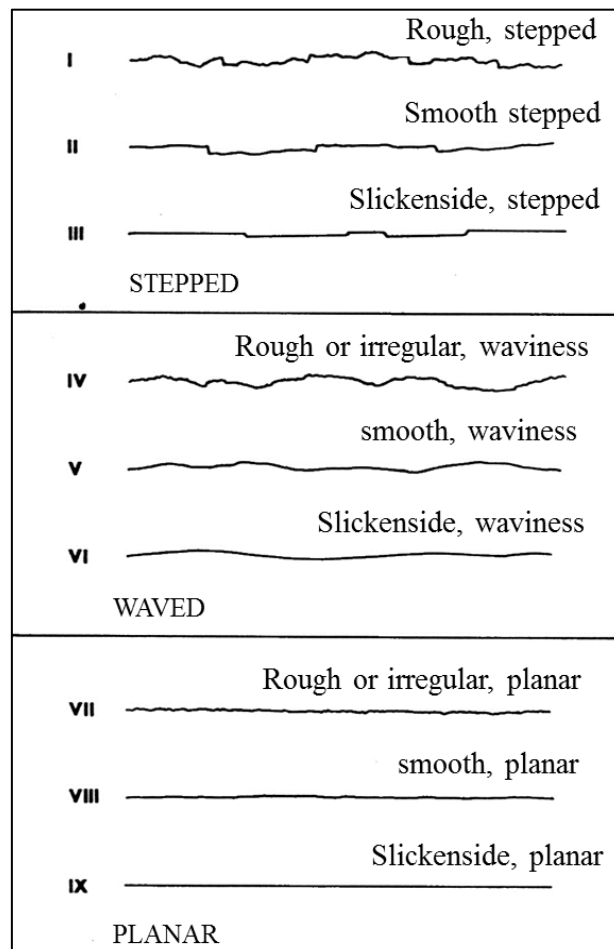


Figure 5.31 Suggested nomenclature for typical roughness profiles (ISRM, 1978).

5.3 Quantitative description of discontinuities

Results

During La Maddalena tunnel wall mapping the description of discontinuity roughness has been carried out considering the purpose of survey: the geomechanical classification of rock mass. For this reason, it was considered both the nomenclature recommended by ISRM SM (1978) and the classes proposed by RMR system (Bieniawski, 1989). The last ones are:

- Very rough;
- Rough;
- Slightly rough;
- Smooth;
- Slickenside.

In particular, for waviness description the nomenclature suggested by ISRM (1978) has been adopted while for unevenness description the classes proposed by Bieniawski have been considered.

Generally, the surfaces of the discontinuities belonging to the principal set are slightly rough (Figure 5.32). In particular, roughness is higher about the gneiss joint surfaces (in which the class “rough” prevails and “very rough” one occurs) and some cases of smooth or slickenside discontinuity surfaces have been recognised mapping the micaschist domain (DIII).

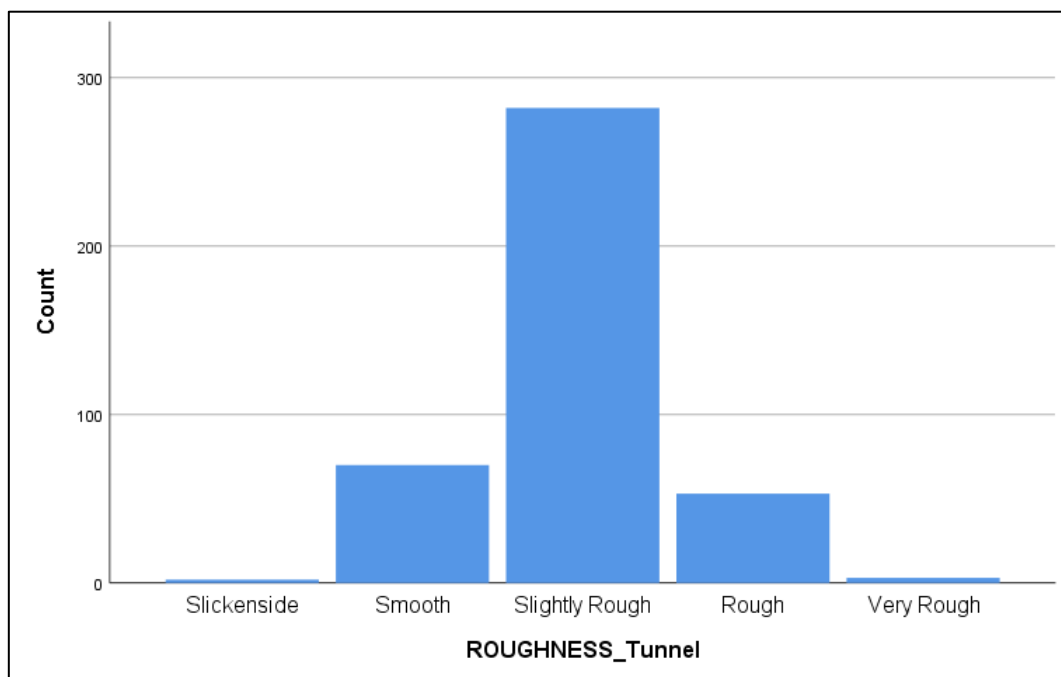


Figure 5.32 Discontinuity roughness distribution.

5.3.8.5 *Weathering degree*

Weathering reduces the shear strength of discontinuities and of the rock mass, given that it reduces also the intact rock strength.

The system used to classify the discontinuity weathering of La Maddalena rock mass is the RMR one. Bieniawski proposed five classes of alteration that range between unweathered and decomposed. The description of these classes coincide with the one of the ISRM classes, Bieniawski includes the ISRM classes “completely weathered” and “residual soil” into a unique group named “decomposed” (Table 5.18).

RMR class	ISRM class	ISRM description
Unweathered	Fresh	No signs of alteration
Slightly weathered	Slightly weathred	Discoloration
Moderately weathered	Moderately weathred	Decomposition < 50%
Highly weathered	Highly weathred	Decomposition > 50%
Decomposed	Completely weathred	Decomposition > 100%
	Residual soil	Rock is converted to soil

Table 5.18 Discontinuity weathering description.

Results

The tunnel surveys allow the description of the weathering condition of the discontinuity surfaces characterizing La Maddalena rock mass.

Generally, the discontinuities result unweathered or slightly weathered; however, in isolated cases, especially where faults occur and where dripping is present, they appear moderately weathered.

No cases of highly weathered or decomposed materials have been recognised.

5.3 Quantitative description of discontinuities

5.3.8.6 Joint condition parameter

The description of joint surfaces in terms of persistence, aperture, filling, roughness and weathering and the rating of this parameter by means of the indication proposed by RMR classification system allow to carry out the fourth parameter of Bieniawski classification, Jc (see section 5.4.1).

In fact, Jc, joint conditions, is the sum of the rate assigned to each of the parameters listed above.

The results of Jc calculation have been reported in Table 5.19.

Jc	TUNNEL	Domain I	Domain II	Domain III; *DIIIa	
Range	7.00 – 29.00	11.00 – 29.00	7.00 – 18.00	10.00 – 21.0*	7.00 – 21.00
Median	18.00	20.00	15.00	19.00*	18.00
Mean	17.04	19.42	15.00	18.00*	16.75
Q1	15.00	17.00	15.00	18.00*	14.00
Q3	19.00	22.00	17.00	19.00*	19.00

*Table 5.19 Jc statistical description; * DIIIa data: part of DIII data used in the following predictive model creation.*

The median Jc value referred to the entire tunnel is of 18.00, the highest value has been calculated in DI, where filling is often absent and discontinuity surfaces are rough of very rough. Joint surfaces show lower quality in DII, where the median value is equal to 15.00.

There is not a significant difference between the features of joint surfaces in the section DIIIa and the entire DIII. In fact, the median values are 19.00 and 18.00 respectively.

Joint conditions tend to be constant for more or less long tract of tunnel; it means that adjacent rock mass sections have the same joint conditions. It was particularly observed in DII and DIII, whereas in DI, Jc changes more rapidly, despite the fact that adjacent tracts characterised by equal values of Jc can be observed (Figure 5.33).

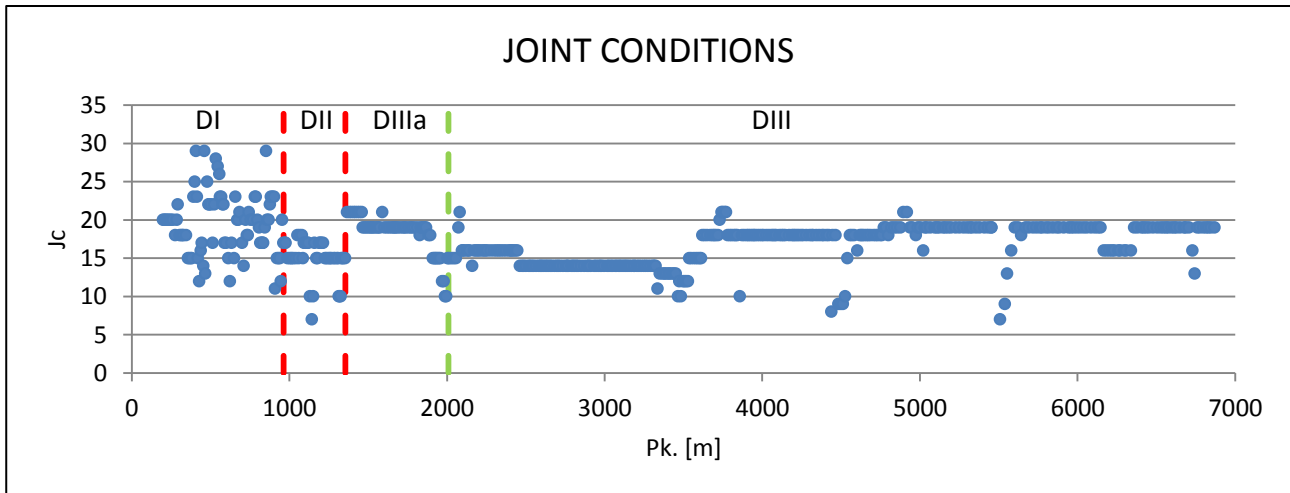


Figure 5.33 Joint conditions distribution, the red lines represent the domain changes.

The lowest J_c values have been calculated in correspondence of fault zones, where:

- Joint surface asperities have been smoothed by fault movements;
- Discontinuity surfaces can be weathered as result of water circulation;
- Filling materials, generated by fault movements, are present;
- Fault dislocation can make the discontinuities open.

The factors listed above make J_c decrease.

5.4 Rock mass classifications

The classification systems are widely applied to the rock masses for the design of civil and mining underground works, rock foundations and dams as a useful engineering tool. In fact, the rock mass classification systems are largely used to assess deformation and strength characteristics of a rock mass considered as a continuous equivalent medium.

The classification methods allow to subdivide the rock masses in different classes of quality: from extremely poor to excellent or exceptionally good.

They are rarely used for rock slope stability analysis since the rock discontinuities play a fundamental role and, for this reason, the rock mass could not be not considered as a continuous equivalent.

Here a brief review of the two rock mass classifications used in this work has been provided. Rock Mass Rating (RMR) system and Geological Strength Index (GSI) will be described.

5.4.1 Rock Mass Rating (RMR) system

Rock Mass Rating (RMR) system was proposed by Bieniawski in 1976; over the years RMR has been refined and significant changes in rating assignment have been made. The version most widely used is the 1989 one: its advantage is that only basic parameter are used in its calculation, they are related to the mechanical conditions and the geometry of rock mass, they are:

- *Uniaxial compressive strength of the rock matrix, σ_c* : it can be evaluated by uniaxial compression tests (UCS) or point load test;
- *Rock Quality Designation, RQD*: it is the percentage ratio obtained by adding all the core rock pieces longer than 10.0 cm and the total length of drill rode;
- *Spacing of Discontinuities*: the whole rock mass discontinuity spacing has to be considered, it can be assessed from scanline discontinuity survey;
- *Condition of Discontinuities*: this parameter considers the overall conditions of discontinuities in terms of roughness, persistence (or continuity), aperture, filling and weathered degree;
- *Groundwater conditions*: this parameter can be considered from a qualitative or from a quantitative point of view. In the first case a qualitative judgment based on the experience of the operator in charge of the rock mass characterization is required. In the second case

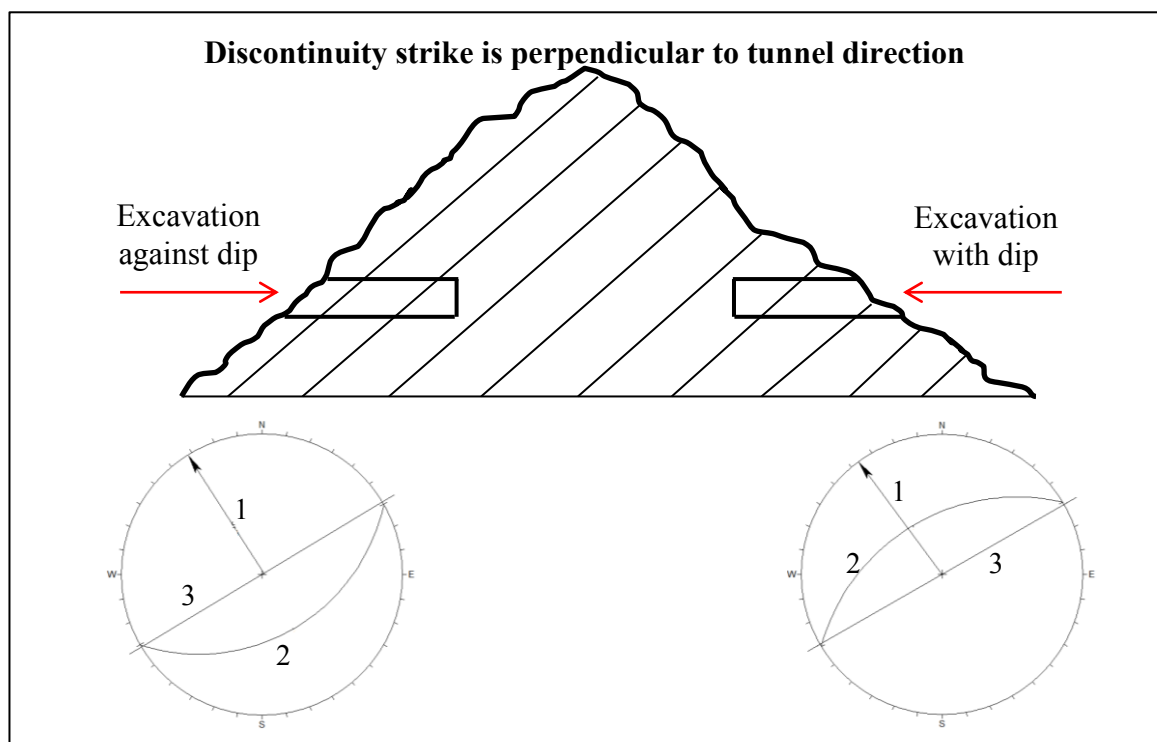
inflow measurement has to be carried out or the ratio between joint water pressure and major principal stress has to be computed.

A score, called rating, has to be given to each value of the five parameters mentioned above and by adding the assigned ratings RMR_{basic} is obtained (section A, *Table 5.20*). This index is used for the rock mass mechanical feature assessment.

It is fundamental to note that discontinuity orientations strongly affect the stability conditions of a “geomechanical work”, for this reason in order to use the RMR system in civil, mining, tunneling or consolidation works, the orientation of discontinuities with respect to the direction of the excavation or the existing rock walls have to be taken into consideration. In section B the rating adjustment for discontinuity orientations have been listed, in particular, in tunneling operations great attention is given to the effect of discontinuity strike and dip orientation (section F, *Table 5.20*).

The two extreme situations for the orientation of the principal discontinuity system are:

- Dip direction parallel to the tunnel excavation direction: in this case two situations can occur. In particular, it is possible to “drive with dip” or “drive against dip”. Drive with dip it is considered favorable because of rock blocks have not the kinematic possibility to slide being directed against the rock mass. Drive against dip it is considered unfavorable because rock blocks can slide from the tunnel crown before to have the time to reinforce the rock mass (Figure 5.34).



5.4 Rock mass classifications

Figure 5.34 Excavation against and with dip when discontinuity strike is perpendicular to tunnel direction. In the stereonet: 1 = tunnel axis, 2 = discontinuity dip direction, 3 = discontinuity strike.

- Dip direction perpendicular to the tunnel excavation direction: in this case the unfavorable condition occurs when the discontinuities are sub-vertical (Figure 5.35).

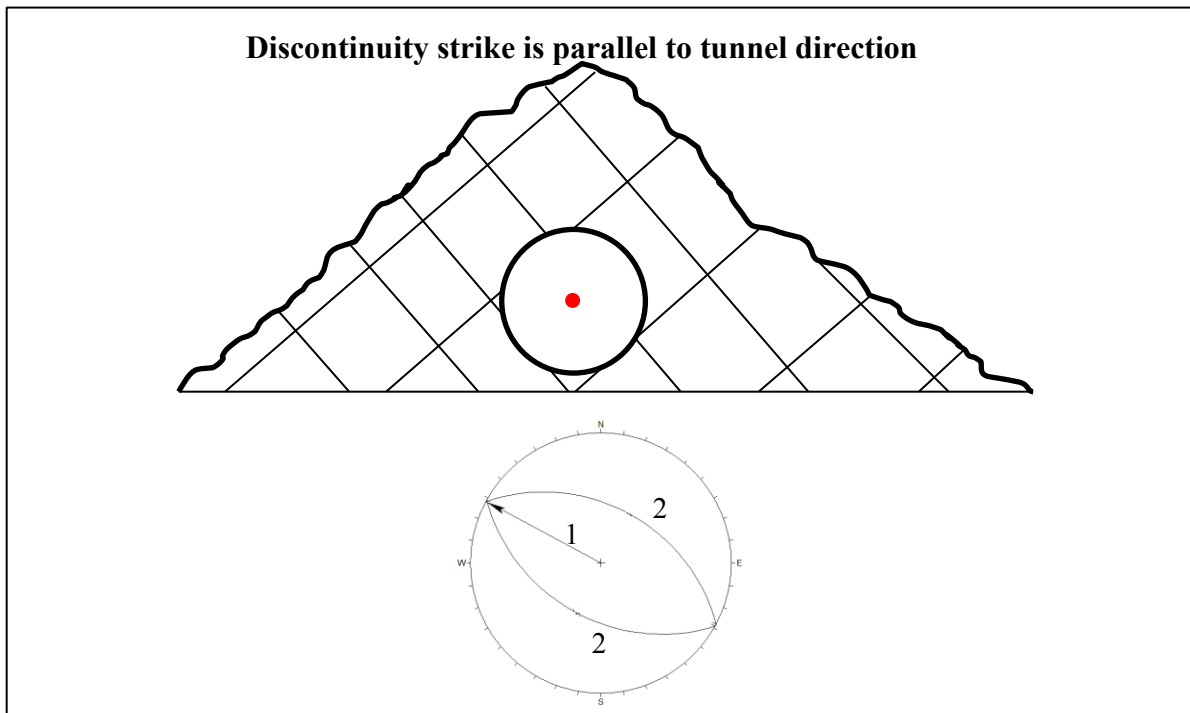


Figure 5.35 Excavation in rock mass where discontinuity strike is parallel to tunnel direction. In the stereonet: 1 = tunnel axis, 2 = discontinuity dip direction.

Considering discontinuity orientation effects $RMR_{corrected}$ can be obtained.

The qualitative judgment of a given rock mass is subdivided into five classes (I – V), where values of RMR from 81 to 100 correspond to very good rock, values between 61 and 80 correspond to good rock, values from 41 to 60 characterise fair rock, values between 21 and 40 correspond to poor rock and very poor rock are characterised by values ranging between 0 and 20 (section C, Table 5.20).

A. CLASSIFICATION PARAMETERS AND THEIR RATINGS									
Parameters			Ranges of Values						
1.	Strength of intact rock material	Point-load strength index (MPa)	>10	4–10	2–4	1–2	For this low range, uniaxial compressive test is preferred		
		Uniaxial compressive strength (MPa)	>250	100–250	50–100	25–50	5–25	1–5	<1
	Rating	>15	12	7	4	2	1	0	
2.	Drill quality RQD (%)		90–100	75–90	50–75	25–50	25		
	Rating		20	17	13	8	3		
3.	Spacing of discontinuities		>0.2 m	0.06–0.2 m	200–600 mm	200–600 mm	<60 mm		
	Rating		20	15	10	8	5		
4.	Condition of discontinuities		Very rough surfaces; Not continuous; No separation; Unweathered wall rock.	Slightly rough surfaces; Separation <1 mm; Slightly weathered wall.	Slightly rough surfaces; Separation <1 mm; Highly weathered wall.	Slickensided Surface or Gouge <5 mm thick or Separation 1–5 mm contours	Soft gouge > 5 mm thick or Separation >5 mm contours		
	Rating		30	25	20	10	0		
5.	Groundwater	Inflow per 10 m tunnel length (min.)	None	<10	10–25	25–125	>125		
		(Joint water Press)/ (Measure principal σ)	0	<0.1	0.1–0.2	0.2–0.5	>0.5		
	General conditions		Completely dry	Damp	Wet	Dripping	Flowing		
	Rating		15	10	7	4	0		
B. RATING ADJUSTMENT FOR DISCONTINUITY ORIENTATIONS									
Strike and Dip Orientations of Discontinuities		Very Favourable	Favourable	Fair	Unfavourable	Very Unfavourable			
Rating	Tunnels and Mines	0	-2	-5	-10	-12			
	Foundations	0	-2	-7	-15	-25			
	Slopes	0	-5	-25	-50	-60			
C. ROCK MASS CLASSES DETERMINED FROM TOTAL RATINGS									
Rating		100–81	80–61	60–41	40–21	<20			
Class no.		I	II	III	IV	V			
Description		Very good rock	Good rock	Fair rock	Poor rock	Very poor rock			
D. MEANING OF ROCK CLASSES									
Class no.		I	II	III	IV	V			
Average stand-up time		20yr for 15m span	1 yr for 10 m span	1wk for 5m span	10 h for 2.5m span	30 min for 1m span			
Cohesion of the rock mass (kPa)		>400	300–400	200–300	100–200	<100			
Friction angle of the rock mass(deg)		>45	35–45	25–35	15–25	<15			
E. GUIDELINES FOR CLASSIFICATION OF DISCONTINUITY CONDITIONS									
Discontinuity length (persistence)		<1 m	1–3 m	3–10 m	10–20 m	>20 m			
Rating		6	4	2	5	0			
Separation (aperture)		None	<0.1 mm	0.1–1.0 mm	1–5 mm	>5 mm			
Rating		6	5	4	1	0			
Roughness		Very rough	Rough	Slightly rough	Smooth	Slickensided			
Rating		6	5	3	1	0			
Infilling (gauge)		None	Hand filling <5 mm	Hand filling >5 mm	Soft filling <5 mm	Soft filling >5 mm			
Rating		6	4	2	2	0			
Weathering		Unweathered	Slightly weathered	Moderately weathered	Highly weathered	Decomposed			
Rating		6	5	3	1	0			
F. EFFECT OF DISCONTINUITY STRIKE AND DIP OREINTATION TUNNELLING**									
Strike perpendicular to tunnel axis					Strike parallel to tunnel axis				
Drive with dip — Dip 45–90°		Drive with dip — Dip 20–45°			Dip 45–90°		Dip 20–45°		
Very favourable		Favourable			Very unfavourable		Fair		
Drive against dip — Dip 45–90°		Drive against dip — Dip 20–45°			Dip 0–20° irrespective of strike				
Fair		Unfavourable			Fair				

* Some conditions are mutually exclusive. For example, if infilling is present, the roughness of the surface will be overshadowed by the influence of the gouge. In such cases use A.4 directly;

** Modified after Wickham et al. (1972)

Table 5.20 RMR system (Bieniawski, 1989).

5.4 Rock mass classifications

In tunnel design, the $RMR_{corrected}$ can be used to assess the self-support time, the roof span and the support installation time.

An example is provided by Table 5.21.

Rock mass class	Excavation	Rock bolts (20 mm diameter, fully grouted)	Shotcrete	Steel sets
I - Very good rock <i>RMR</i> : 81-100	Full face, 3 m advance.	Generally no support required except spot bolting.		
II - Good rock <i>RMR</i> : 61-80	Full face , 1-1.5 m advance. Complete support 20 m from face.	Locally, bolts in crown 3 m long, spaced 2.5 m with occasional wire mesh.	50 mm in crown where required.	None.
III - Fair rock <i>RMR</i> : 41-60	Top heading and bench 1.5-3 m advance in top heading. Commence support after each blast. Complete support 10 m from face.	Systematic bolts 4 m long, spaced 1.5 - 2 m in crown and walls with wire mesh in crown.	50-100 mm in crown and 30 mm in sides.	None.
IV - Poor rock <i>RMR</i> : 21-40	Top heading and bench 1.0-1.5 m advance in top heading. Install support concurrently with excavation, 10 m from face.	Systematic bolts 4-5 m long, spaced 1-1.5 m in crown and walls with wire mesh.	100-150 mm in crown and 100 mm in sides.	Light to medium ribs spaced 1.5 m where required.
V – Very poor rock <i>RMR</i> : < 20	Multiple drifts 0.5-1.5 m advance in top heading. Install support concurrently with excavation. Shotcrete as soon as possible after blasting.	Systematic bolts 5-6 m long, spaced 1-1.5 m in crown and walls with wire mesh. Bolt invert.	150-200 mm in crown, 150 mm in sides, and 50 mm on face.	Medium to heavy ribs spaced 0.75 m with steel lagging and forepoling if required. Close invert.

Table 5.21 Guidelines for excavation and support of tunnels in accordance with the RMR system (Bieniawski, 1989).

Results

The field surveys carried out during La Maddalena tunnel construction allow the collection of a series of geological, structural and mechanical data that have been used to classify the excavated rock mass. For each of the 502 rock sections in which La Maddalena rock mass has been divided, the collected data and the subsequent analysis allow the rock mass to be classified by means of RMR system.

The quality of the excavated rock mass results to be principally fair and good. The most frequent RMR classes are the II and the III; none of the sections belongs to the V class and very few to the IV. Furthermore, there very few instances of rock mass considered of very good quality (Figure 5.36).

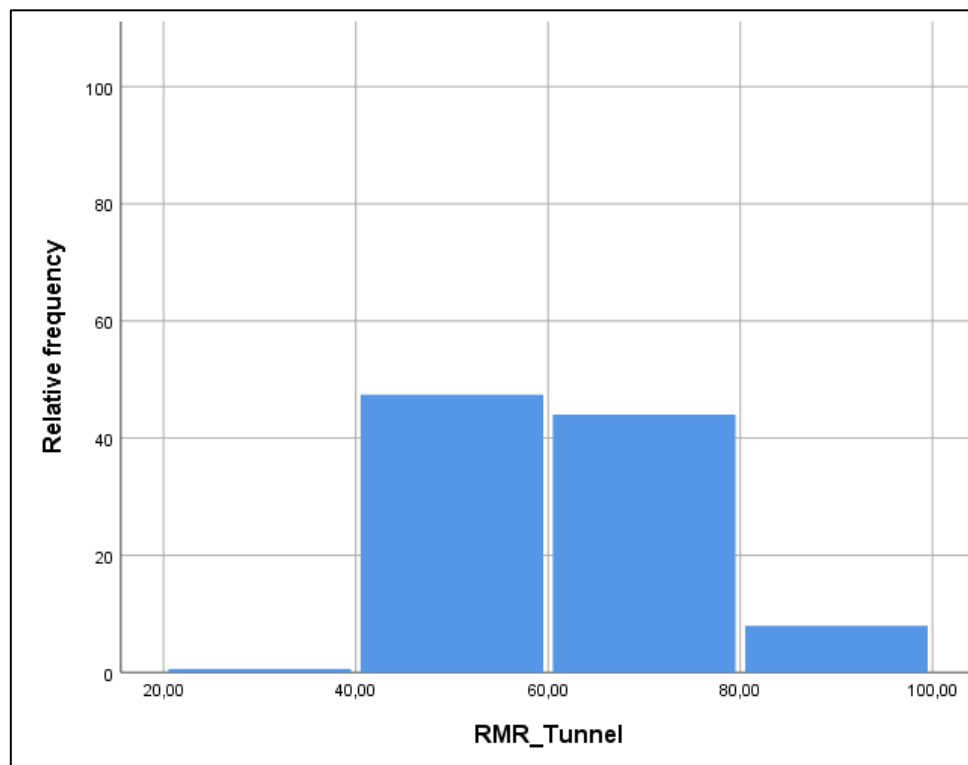


Figure 5.36 Histogram of frequency of RMR distribution.

In particular, the gneiss belonging to Domain I is characterized by higher quality than the quality of the two other domains. In DI there are few rock sections classified as fairly rocks and the largest part of them are considered very good and good rocks.

The quality decreases into the gneiss and micaschist alternation (DII), where the very good quality rock sections are limited; moreover a small decrease can be observed considering RMR values about the Domain III, in which poor quality rock sections occur (Figure 5.37).

5.4 Rock mass classifications

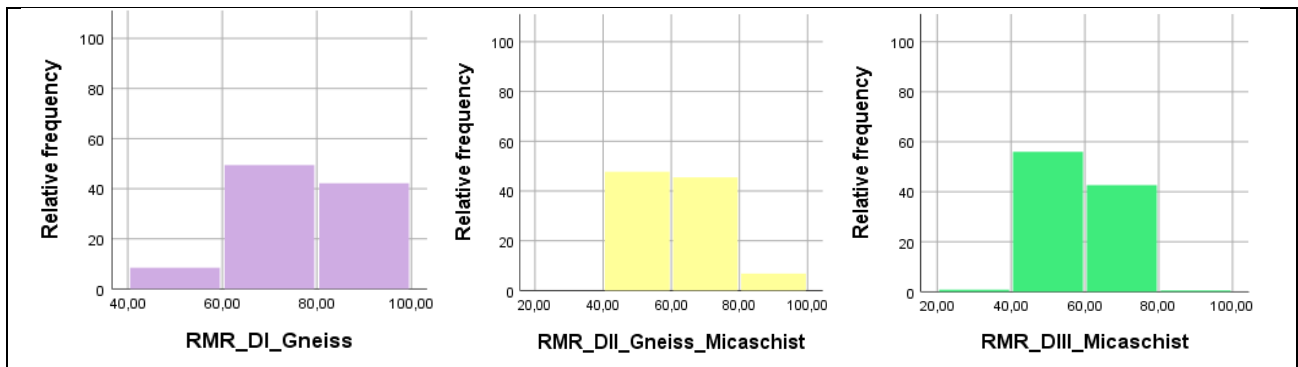


Figure 5.37 Histogram of frequency of RMR distribution about each domain.

The mean RMR value calculated for the entire excavated tunnel is equal to 60, the mean RMR gneiss value is 75 and in the gneiss-micaschist alternation and in the micaschist the values are equal to 62 and 59 respectively.

The RMR trend through the tunnel is showed in Figure 5.38.

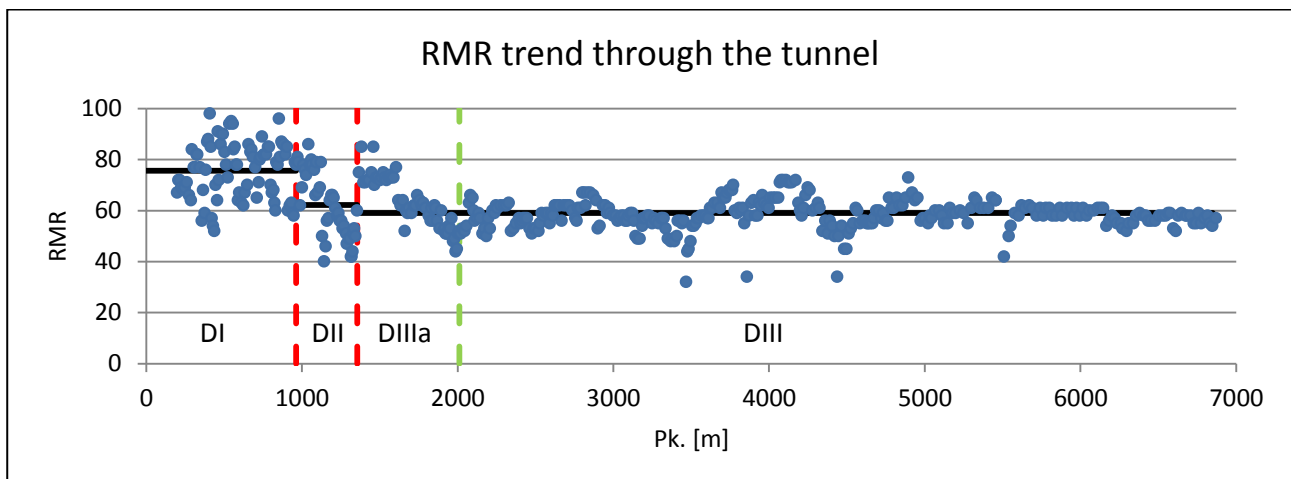


Figure 5.38 RMR trend through the tunnel. Red lines represent the domain changes, green line delimits DIIIa and black lines the mean values for each domain.

5.4.2 Geological Strength Index (GSI)

The Geological Strength Index, GSI, is a rock mass classification scheme introduced by Hoek in 1994 and developed over the years (Hoek et al. 1998; Marinos & Hoek, 2000, 2001; Hoek et al., 2013). It was developed in order to overcome the limitations in rock mass strength criterion that occur by using RMR system. It has a fundamental role in the Hoek and Brown failure criterion and it is an input data for numerical analyses of tunnel, slope or foundation problems. The original GSI chart is based on the field observations. Hoek et al. (2013) proposed a quantification of GSI chart on the basis of two parameters: joint conditions and RQD.

The GSI method takes into account for those properties that determine the strength and the deformability of the rock masses: it gives great emphasis on basic geological observation of rock mass features reflecting the material, its structure and its geological history.

In particular GSI focuses on rock mass structure and on the conditions of the discontinuity surfaces.

As for the structure great attention has to be given to the block interconnection features. Authors consider six situations, these are: intact or massive, blocky, very blocky, blocky/disturbed/seamy, disintegrated and laminated/sheared; the description of each classes is provided in Figure 5.39.

The conditions of the discontinuity surfaces are expressed in terms of roughness and weathering; there are five classes of surface conditions, which are:

- *Very good*: very rough, fresh and unweathered surfaces;
- *Good*: rough and slightly weathered;
- *Fair*: smooth and moderately weathered;
- *Poor*: slickenside and strongly weathered, covered by patina or filled with angular fragment;
- *Very poor*: slickenside, strongly weathered, covered by or filled with clay material.

Using the chart proposed in Figure 5.39 and with some experience, GSI can be obtained by observing rock walls. GSI value is expressed by means of a numerical index associated to every combination of these two parameters. GSI varies in a 0-100 range.

5.4 Rock mass classifications


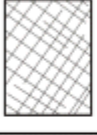




		SURFACE CONDITIONS				
		VERY GOOD	GOOD	FAIR	POOR	VERY POOR
STRUCTURE		DECREASING SURFACE QUALITY →				
	INTACT OR MASSIVE - intact rock specimens or massive in situ rock with few widely spaced discontinuities	90	80	70	N/A	N/A
	BLOCKY - well interlocked undisturbed rock mass consisting of cubical blocks formed by three intersecting discontinuity sets	80	70	60	50	40
	VERY BLOCKY- interlocked, partially disturbed mass with multi-faceted angular blocks formed by 4 or more joint sets	70	60	50	40	30
	BLOCKY/DISTURBED/SEAMY - folded with angular blocks formed by many intersecting discontinuity sets. Persistence of bedding planes or schistosity	60	50	40	30	20
	DISINTEGRATED - poorly interlocked, heavily broken rock mass with mixture of angular and rounded rock pieces	50	40	30	20	10
	LAMINATED/SHEARED - Lack of blockiness due to close spacing of weak schistosity or shear planes	N/A	N/A	10	10	10

Figure 5.39 GSI chart (Marinos and Hoek, 2000).

GSI does not consider UCS of intact rocks and groundwater conditions.

Marinos and Hoek (2000) published a collection of indicative charts which show the most recurrent ranges of GSI for rock masses of a large quantity of rock types (Figure 5.40).

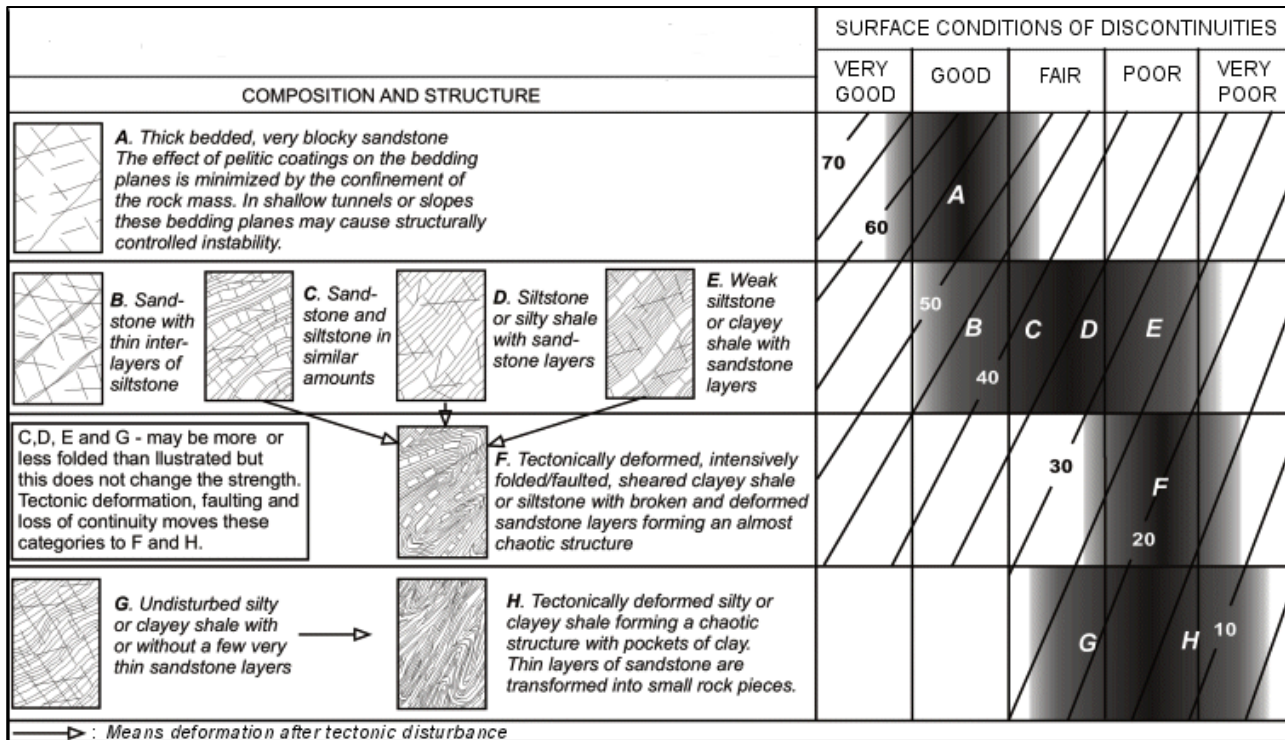


Figure 5.40 GSI chart for flysch (Marinos and Hoek 2000).

Results

By tunnel walls observation and the utilization of the chart proposed by Marinos and Hoek, 2000, (Figure 5.39) it was possible to assign a GSI value at each rock sections surveyed. The latest GSI version (2013) has not been used because it considers Jc and RQD, but in this study, RQD has been empirically obtained by means of Palmström relationship (Palmström, 1982); so GSI-2000 version has been considered.

The results of this classification have been reported in Table 5.22.

GSI	TUNNEL (n = 502)	Domain I (n = 83)	Domain II (n = 44)	Domain III (n = 375)
Range	37.00 – 98.00	54.00 – 98.00	43.00 – 84.00	37.00 – 85.00
Median	65.00	80.00	63.50	65.00
Mean	66.11	77.40	63.93	63.86
Q1-Q3	60.00 – 70.00	70.00 – 85.00	52.00 – 74.25	60.00 – 67.00

Table 5.22 GSI statistical analysis.

5.4 Rock mass classifications

The mean GSI value is about 66; it denotes a good quality rock mass, in particular the highest values have been assigned to the gneiss of DI (mean value equal to 77.40). The GSI decreases through the gneiss-micaschist alternation and micaschist domain. In DII and DIII the mean value is the same (63.93 and 63.86 respectively).

It is possible to assert that on the basis of GSI La Maddalena rock mass can be divided into two principal groups: DI and DII-DIII respectively.

The trend of GSI through La Maddalena tunnel has been reported in the figure below (Figure 5.41).

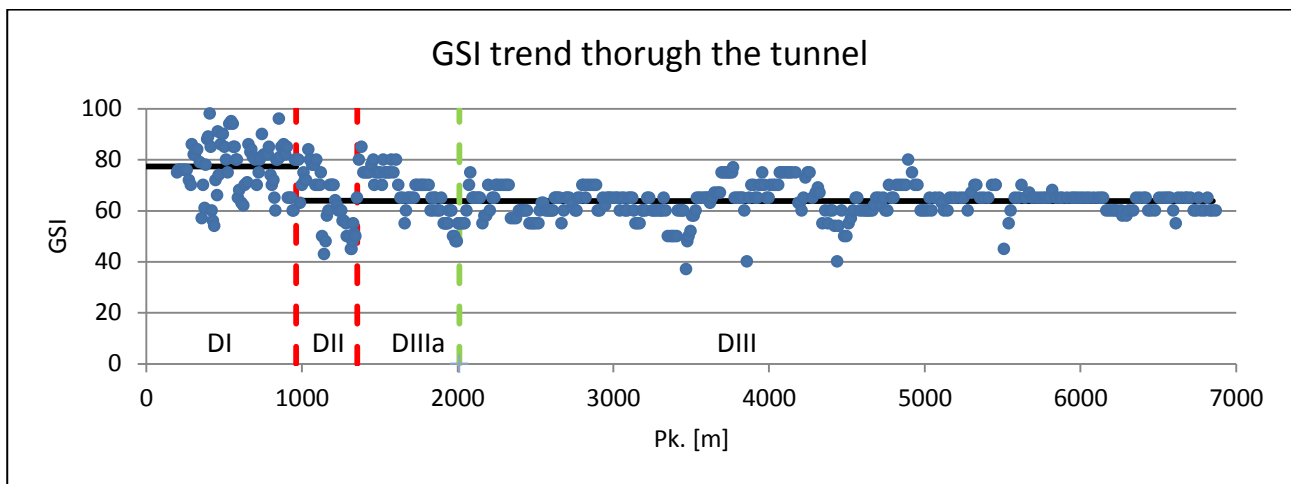


Figure 5.41 GSI trend through the tunnel. Red lines represent the domain changes, green line delimits DIIIa and black lines the mean values for each domain.

5.5 Seismic wave propagation

The velocity of propagation of seismic waves through a rock mass provides fundamental information about the geological characteristics and the mechanical features of the ground, especially when direct survey cannot be done.

Geophysical investigation methods are frequently adopted during excavation works in order to predict the geological framework ahead the tunnel face, with the purpose of avoiding to encountered rock mass conditions different from the expected ones.

During La Maddalena construction seismic investigation methods have been involved for this purpose.

In this work one of them has been taken into account, here a brief description of the methods and the obtained results is provided; its reliability in terms of geological prediction accuracy will be discussed in Chapter 7.

The indirect investigation method considered in this work is the so called “Tunnel Seismic Prediction System”, TSP.

5.5.1 Tunnel Seismic Prediction System

The Tunnel Seismic Prediction System, TSP, is a reflection seismic technique developed by Amberg Technologies AG (Switzerland) and widely and successfully used in underground construction (Dickmann and Tang, 2006; Dickmann, 2005; Dickmann and Krueger, 2013).

24 boreholes need to be drilled aligned in the tunnel wall, each of them has a depth between 1.00 and 1.50 metres and they are 1.50 m spaced. Small explosive charges are fired inside these boreholes, allowing the seismic wave energy to propagate through the rock mass.

Acoustic impedance phenomena, such as significant planes of weakness, faults and shear zones or changes in mechanical and physical properties of rocks, cause the reflection of a portion of signal. The reflected part of signal will arrive at the receivers sited in the tunnel walls.

A schematic representation of the position of source points and receivers is provided Figure 5.42.

5.5 Seismic wave propagation

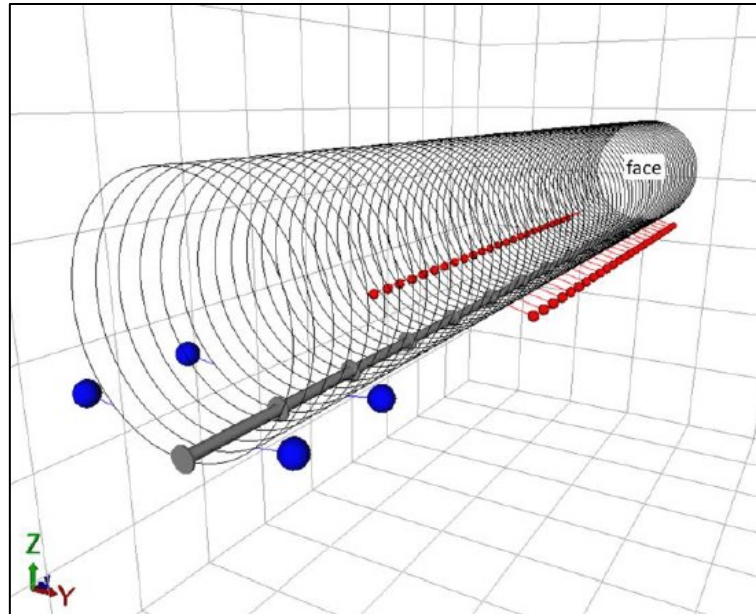


Figure 5.42 Positions of sources (red dots) and receivers (blue dots), Dickmann and Krueger, 2013.

The receiver units are formed by an ultrasensitive triaxial seismic accelerometer, able to convert the seismic signal into electrical voltage ones (Dickmann, 2005). The receiver unit provides the coverage of all three space directions, which allows the recording of the full wave field. The distinction of compressional (P) and shear (S) waves and then their velocity analysis are performed. In this way the reflected signal times are converted into distances allowing us to localise the weakness planes (working as planes of reflection) both in terms of orientation and of distance from the tunnel front (Figure 5.43).

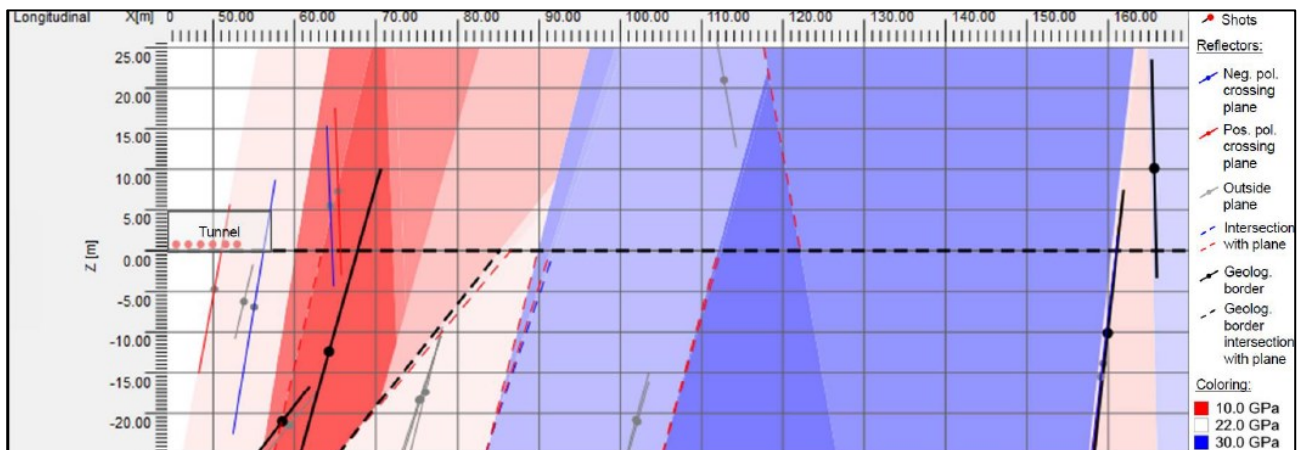


Figure 5.43 TSP survey result (Dickmann and Krueger, 2014).

TSP allows the estimation of some mechanical and physical properties of rocks (for example dynamic Young's modulus, dynamic Poisson's ratio, density), by means of empirical formulation based on seismic wave velocity.

5.5.2 Tunnel Seismic Prediction results

During La Maddalena construction 22 TSP measurements were carried out with the purpose of investigating the geological feature of the rock mass ahead of the tunnel face. The seismic investigated tunnel tract ranges from Pk. 0 + 500 m to Pk. 4 + 980 m.

The results of these measurements have been acquired and a part of them has been used to evaluate their reliability in geological feature prediction: in particular the analysis takes into account the data measured between Pk. 0 + 500 m and Pk. 2 + 000 m (see Chapter 7).

The distribution of seismic data obtained from the 22 TBM measurements has been described in this section.

The following image (Figure 5.44) shows the variation in seismic wave velocities through the tunnel, both in terms of P waves and of S waves.

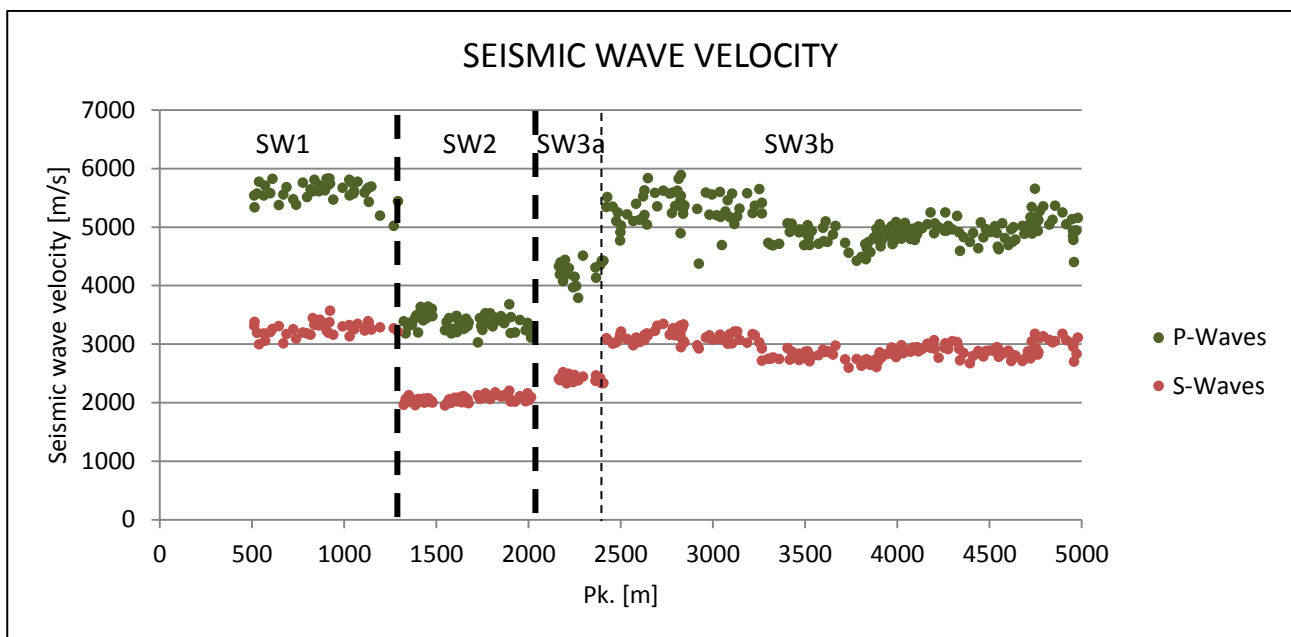


Figure 5.44 Seismic wave velocity measured by TSP technique. Black lines delimit seismic sections.

Rock mass can be divided into three seismic sections, on the basis of the propagation velocity; these sections are:

- SW1: is the section between Pk. 0 + 500 m and Pk. 1 + 360 m. The measured seismic velocity is high and constant into the entire tract. The values about P waves range between 5014 m/s and 5826 m/s (mean value is 5597 m/s) and about S waves they range between 2994 m/s and 3565 m/s (the mean value is equal to 3254 m/s). SW1 corresponds to the geological domain DI and DIII;

5.5 Seismic wave propagation

- SW2: is the rock mass portion from Pk. 1 + 360 m to Pk. 2 + 014 m and it is characterised by P wave velocity ranging between 3028 m/s and 3677 m/s (mean equal to 3370 m/s) and S wave velocity from 1947 m/s to 2202 m/s (mean value of 2054 m/s). SW2 coincides with the first part of DIII;
- SW3: this section covers a total length of 2967 m, from Pk. 2 + 014 m to Pk. 4 + 981 m. It is possible to observe that SW3 velocity distribution is less homogenous than the SW1 and SW2 ones. It is possible to recognise a limited portion of rock mass (between Pk. 2 + 166 m and Pk. 2 + 407 m) in which P and S waves are characterised by lower velocity than the remaining part of SW3. This subsection has been named SW3a, and the principal sector of SW3 is called SW3b.

The SW3a mean values for P and S waves are 4232 m/s and 2413 m/s respectively; whereas referred SW3b the mean values are 5044 m/s, for P waves and 2941 m/s for S waves.

Finally, as far as P waves measured in SW3b are concerned, it is possible to note that a portion is characterised by mean velocity equal to 5326 m/s (from Pk. 2 + 420 m to Pk. 3 + 266 m) and a sector by mean velocity of 4900 m/s (from Pk. 3 + 266 m). The velocities referred to S waves are more constant than the P ones.

Seismic wave velocities obtained by the 22 TSP measurements have been compared with the global quality of the rock mass (expressed by RMR) in which measurements were performed, in order to investigate the relationship between seismic response and rock mass quality (Figure 5.45).

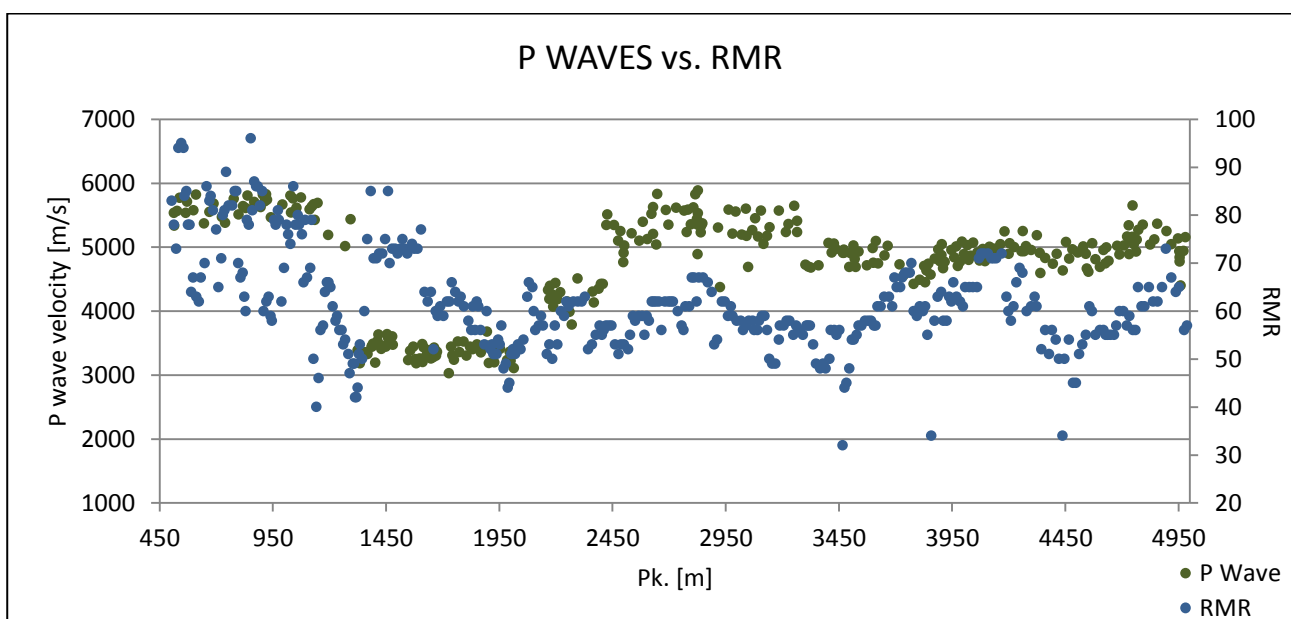


Figure 5.45 Relationship between P wave velocities and RMR.

In the case of the investigated rock mass, the global quality of the ground moderately affects the seismic wave propagation through it.

Generally, it is possible to observe that when RMR decreases also wave velocity becomes lower, on the contrary when the quality increases higher velocities can be measured.

The considerations exposed about P waves and rock mass quality relationship are also valid for S waves.

5.6 Tunnel depth

The depth at which a tunnel is excavated is generally used as a preliminary indicator of in situ stresses; in particular, overbunden is adopted to estimate the lithostatic load σ_1 .

In situ stresses impact the cracks initiation and failure propagation and the formation of chips of rock under TBM disc cutter action. However, there are contrasting opinions on the overall effects of in situ stress and machine performance.

Bordet and Comes (1975), Tarkoy and Marconi (1991), Liu et al. (2002) sustain that if stresses increase the general TBM performance decreases, on the contrary Klein et al. (1995) asserts that high confinement stresses make machine performance increase.

Innaurato et al. (2007) demonstrated that lateral stress has limited effects on the thrust necessary to fragment the rock, therefore on the TBM performances.

The maximum depth reached during La Maddalena construction is over 1990 metres.

The data about tunnel depth have been listed in Table 5.23.

DEPTH [m]	TUNNEL	Domain I	Domain II	Domain III; * DIIIa	
Range	79.4 –1992.6	79.4 – 569.1	273.8 –588.4	256.8 –616.7*	256.8 –1992.6
Median	951.5	360.9	442.2	448.1*	1083.9
Mean	907.6	360.1	435.6	435.5*	1056.4
Q1-Q3	489.9 –1128.8	211.4 – 520.0	346.1 – 516.9	329.4 –539.0*	1056.4-1156.0

Table 5.23 La Maddalena tunnel depth.

A longitudinal profile is provided by Figure 5.46 in order to clearly visualise the overbunden achieved by tunnel excavation.

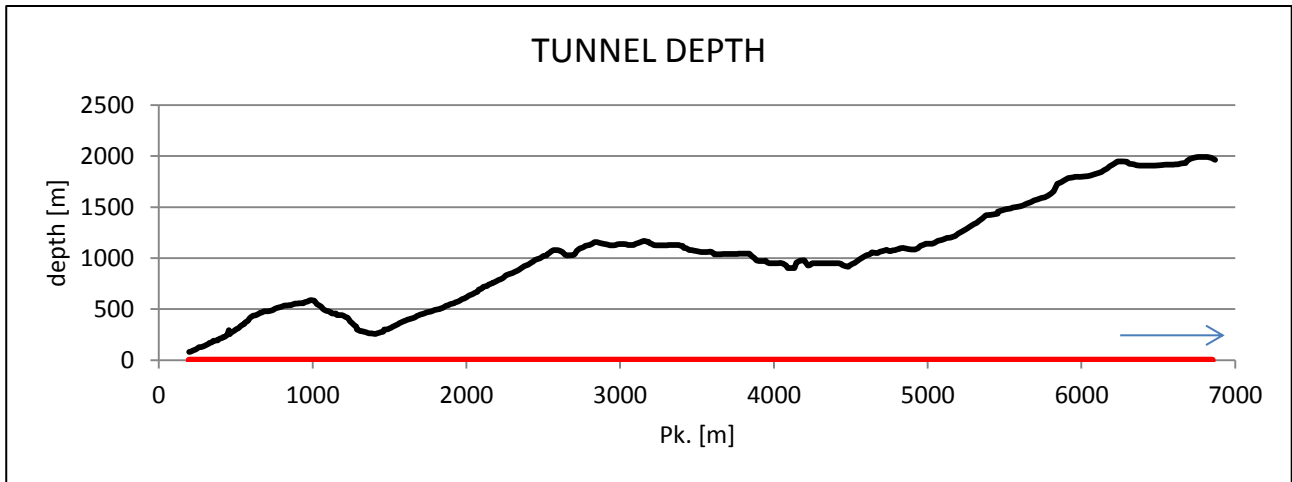


Figure 5.46 La Maddalena depth. Red line represents the tunnel, the arrow represents the excavation verse.

5.7 Conclusive remarks

The field survey work allows the collection of a large amount of information on the lithology, the structure, the conditions and the orientations of discontinuity surfaces and groundwater flow of the Ambin Massif portion hosting La Maddalena tunnel.

These field data, integrated with the results obtained by means of laboratory tests (tests not carried out in person), allow for the qualitative and quantitative description and the classification, in terms of quality classes, of the whole investigated rock mass.

In particular, as already mentioned before, three geological domains have been distinguished:

- From Pk. 0 + 198 m to Pk. 0 + 967 m the main lithology is gneiss and it has been classified as Domain I (DI);
- From Pk. 0 + 967 m to Pk. 1 + 360 m an alternation of gneiss and micaschist has been surveyed and this portion of rock mass has been described as Domain II (DII);
- From Pk. 1 + 360 m to Pk. 6 + 897 m the main lithology consists of micaschist. This tract of tunnel has been named Domain III (DIII).

In the following paragraphs a general overview of the recognized geological domain has been provided.

The histograms for frequency of each parameter detected in each domain are reported in Appendix II and the geological longitudinal section of the portion of Ambin Massif hosting La Maddalena is reported in Appendix III.

5.7.1 Domain I

The portion of rock mass named (in this work) Domain I ranges between Pk. 0 + 198 m and Pk. 0 + 967 m. It consists of a metamorphic rock, mainly characterised by grey colour, but in some sectors rocks present greenish coloration as result of the chlorite occurrence.

Rocks are fine-medium grained and present heteroblastic structure, texture is isotropic and weakly foliated.

The principal forming minerals are quartz, alkaline feldspar, plagioclase, chlorite and muscovite. Calcite has been recognised in limited portion of rock mass, and quartz veins frequently occur.

The foliation is given by the alternation of silic levels consisting of quartz and feldspars and lepidoblastic ones formed by white mica principally. The mean orientation of foliation planes is about 120/50. On the foliation planes develops the principal set of joints. In some situation metric folds occur, their axes are characterised by orientation of 325/60, in terms of trend and plunge.

The described rocks are aplitic gneiss belonging to the Ambin complex (Figure 5.47).

The fracturing degree is the lower than the other two domains, the measured total spacing between weakness planes is 2.50 m (median value), the global joint conditions are good and groundwater circulation is very limited. The levels of rock hardness and abrasivity hare very high, as also UCS.

The velocity of propagation of seismic waves is high both for P (5500 m/s – 6000 m/s) and S waves (3000 m/s – 4000 m/s)

Domain I is characterised by high rock mass quality, in fact the largest part of rock mass sections belong to I and II class of RMR.



Figure 5.47 Aplitic gneiss of Ambin complex.

5.7 Conclusive remarks

5.7.2 Domain II

The Domain II has been recognised between Pk. 0 + 967 m and Pk. 1 + 360 m.

The former consists of a metamorphic rock, dark grey coloured, and medium-fine grained. The foliation is clearly evident due to the alternation between layers in which the principal forming minerals are quartz, albite and white mica (phengite), these rocks can be considered albitic gneiss *minuti*; and layers formed prevalently by white mica and then by quartz, classified as quartz-micaschist (Figure 5.48).

Domain II belongs to the Ambin complex, and represents the transition zone between DI and DIII, and more precisely the passage from the Ambin complex to the Clarea one.

The foliation planes dips towards SE with and a dip angle ranging between 30° and 60° on which the most occurring set of fractures develops.

The general quality of rock mass is lower than the previous domain. Spacing between fractures is shorter than the one of DI (1.30 m), as also the quality of joint surfaces and the mechanical properties of intact rock. RMR values make the rock mass classify into II and III classes.

The velocity of propagation of compressional and shear seismic waves significantly decreases, the mean value for P waves is around 3000 m/s – 3500 m/s and for S ones is roughly equal to 2000 m/s.



Figure 5.48 Rock belonging to DII.

5.7.3 Domain III

The third geological domain recognised during La Maddalena rock mass survey ranges from Pk. 1 + 360 m to the end of the excavated tract, it means that DIII is the geological sector more largely excavated.

The colour of this rocks can variate from light to dark grey and they are generally fine, medium-fine grained. Foliated texture is clearly recognisable and it is principally due to the alternation of silicic and micaceous layers. In this domain micaschist and gneiss minuti have been recognised.

Micaschist are formed principally by quartz, albite, white mica (phengite), chlorite, chloritoid, biotite glaucophane and garnet. The percentage of these minerals is variable, so it was possible to classify rocks as albitic quartz micaschist, glaucophane micaschist, quartz micaschist and micaschist. In some local cases rock has been considered as albitic gneiss minuti (Figure 5.49). These rocks belong to the micaschist and gneiss minuti reequilibrated in blueschist facies of Clarea complex (see section 4.2.1.1).

Foliation and discontinuity orientation do not differ significantly from the previous two domains and metric folds have been observed in limited tracts only.

Spacing between planes of weakness is the lowest of the whole tunnel tract (median value equal to 0.83 m), joint conditions are quite good (mean value 18) and the strength properties of intact rocks are similar to the ones described in DI (UCS mean value 152.00 MPa). The largest parts of rock mass sections belong to class III and II of RMR classification. The seismic wave velocity is similar to the one described in DI, nevertheless more than one seismic response has been detected.



Figure 5.49 Micaschist belonging to the Clarea complex.

6 TBM PERFORMANCE ANALYSIS

In order to investigate the relationship between the rock mass feature and the TBM performance obtained in its excavation it has been necessary to create both a rock mass database (see Chapter 5) and a TBM parameter one.

The machine database is described in this chapter.

It is necessary to anticipate that La Maddalena field TBM database consists of two parts:

- *The first part* (DB1) concerns TBM data, covering a length of about 2.000 metres, from Pk. 0 + 198 m to Pk. 2 + 010 m.

These data have been used to create the predictive models described in the following chapters (see Chapter 9, 10, 11) and they have been personally collected;

- *The second part* (DB2) of La Maddalena field TBM database includes the data referring to a length of about 5.000 metres from Pk. 2 + 010 m to the end of the excavation.

This part of performance data has been used to validate the predictive models created on the basis of the information contained in DB1 (see Chapter 12). These TBM data were derived from the Doctoral Thesis of PhD Andrea Rispoli (Rispoli, 2018); on the contrary the rock mass data have been personally collected.

6.1 Field TBM performance database

During tunnelling, several operational parameters are registered by the automatic acquisition system, which is able to read, visualise and register them. The sampling rate may vary on the basis of the needed analyses and the required representativeness: it can range from one datum every five seconds to one datum every 600 seconds. In this research work, a sampling rate of one datum every five seconds has been selected.

The outliers in TBM data, with respect to DB1, have been manually removed. The biggest errors relative to DB2 have been removed by means of a series of filtering codes.

6.1.1 The first part of the database (DB1)

The most important machine parameters (in relation to this study) are listed below:

- 1) The length of each stroke: it is the length of a continuous advance [mm], measured by the system detecting the start position and the end one of each continuous boring cycle. In particular the system monitors the extension of the thrust cylinders, by means of a wire displacement sensor;
- 2) The actual time of excavation [s]: the system detects the starting time and the ending time of each continuous boring cycle;
- 3) The thrust force [kN];
- 4) The rotation speed of the cutterhead [rpm].

A number of other TBM parameters has been collected (the average motor power [kW], the average motor amperage [A], the gripper pressure [bar], the torque [kN*m], etc...). They have not been involved in the analysis carried out in this research work; some of them are:

The parameters ROP and FPI (see Chapter 2) are calculated taking into account the information obtained by the acquisition system of TBM operating data. In particular, from parameters 1 and 2 it is possible to obtain the net rate of penetration (ROP or PR) through the ratio between the effective bored length and the actual time needed to do it; whereas all the parameters listed above are involved in order to calculate FPI.

Table 6.1 reports an example of the way in which the data were collected and analysed in order to carry out the desired TBM performance indices.

Δt	Stroke In. [mm]	Stroke Fi. [mm]	Δ Stroke [mm]	CHD Force [kN]	Force on cutter [kN]	CHD Speed [rpm]	ROP [mm/min]	Prev [mm/rev]	FPI [kN/cutter/mm/rev]
A	B	C	$D = C - B$	E	$F = E/43$	G	$H = D/A$	$I = H/G$	$J = F/I$
00:05:20	78	282	204	5500	127.91	8.50	38.25	4.50	28.42
00:17:45	1035	1931	896	11000	255.81	9.00	50.48	5.61	45.60
00:26:35	71	1025	954	11800	274.42	8.80	35.89	4.08	67.26
00:07:20	1607	1916	309	11600	269.77	9.20	42.14	4.58	58.90
00:34:40	100	1569	1469	11800	274.42	9.10	42.38	4.66	58.89
00:44:05	73	1922	1849	12000	279.07	8.90	41.94	4.71	59.25
00:39:45	73	1924	1851	12000	279.07	9.10	46.57	5.12	54.51
00:24:35	1101	1925	824	11800	279.42	9.10	33.52	3.68	75.93
00:44:15	75	1092	1017	12000	279.07	8.90	22.98	2.58	108.17
01:03:15	320	1860	1540	10500	244.19	9.10	24.35	2.68	91.12
00:07:25	116	310	194	11400	265.12	9.00	26.16	2.91	91.11

Table 6.1 Example of registration and elaboration of TBM operating data.

The indices calculated as explained above are related to a stroke which is long at maximum 1.80 meters that corresponds to the maximum length of the excavation of the thrust cylinders. It was considered useful obtaining unique value both of ROP and a unique one of FPI for each rock mass section, in such a way comparing TBM performance with the rock mass feature was more immediate. For this reason, a weighted average of all ROP and FPI measurements computed in a length covering a rock mass section has been calculated.

It was considered a length covered by a rock mass section (L_{RMS}) as the sum of n strokes (S_{t_i}), as proposed in Equation 6.1:

$$L_{RMS} = S_{t_1} + S_{t_2} + \dots + S_{t_n} \quad (6.1)$$

At each stroke corresponds a value of ROP, in others words at S_{t_1} corresponds ROP_1 , ..., at S_{t_n} corresponds ROP_n , etc..

So the weighted average ROP registered into a rock mass section (ROP_{RMS}) is given in according to Equation 6.2:

$$ROP_{RMS} = \frac{S_{t_1} * ROP_1 + S_{t_2} * ROP_2 + \dots + S_{t_n} * ROP_n}{L_{RMS}} \quad (6.2)$$

6.1 Field TBM performance database

where L_{RMS} is calculated by means of Equation 6.1.

The same procedure has been adopted to calculate FPI for each rock mass section.

The procedure described allowed to assign to each rock mass section a value of ROP and a FPI one.

A complete database including both geological/geomechanical information and machine data has been created.

6.1.2 The second part of the database (DB2)

The second part of the database was completed with field data obtained from the Ph.D. thesis of Andrea Rispoli (Rispoli, 2018) and was used to validate the predictive models carried out during this work.

Rispoli evaluated eight TBM operating parameters; however, ROP and FPI only have been considered for the purposes of this work.

The Author developed specific calculation codes in order to automatically perform the data filtering with the purpose of removing the anomalous ones. In particular, these codes filter TBM data in two stages. A first filtering allows to remove the most important errors, e.g. the values not compatible with the operating range of the TBM.

During the second filtering phase, a specific code is selected on the basis of the required analysis.

Prior to the utilisation of the acquired data, the Author performed a reliability test that concerns the excavated length measured and the effective time required to do this.

6.2 Measured TBM performances

The ROP and FPI distribution through the tunnel have been analysed, both for DB1 and DB2. Both the indices have been evaluated for the whole excavated length and for each encountered geological domain.

As for the portion of DIII ranging between Pk. 1 + 360 m and Pk. 2 + 003 m (named DIIIa), the machine performances have been calculated on the basis of the modalities discussed for DB1 (see section 6.1.1).

6.2.1 Rate of Penetration distribution

As already described above, the rate of penetration (ROP) or penetration rate (PR) is the ratio between a continuously excavated length and the actual boring time (see section 2.4.1).

Figure 6.1 provides the trend of ROP through the whole tunnel.

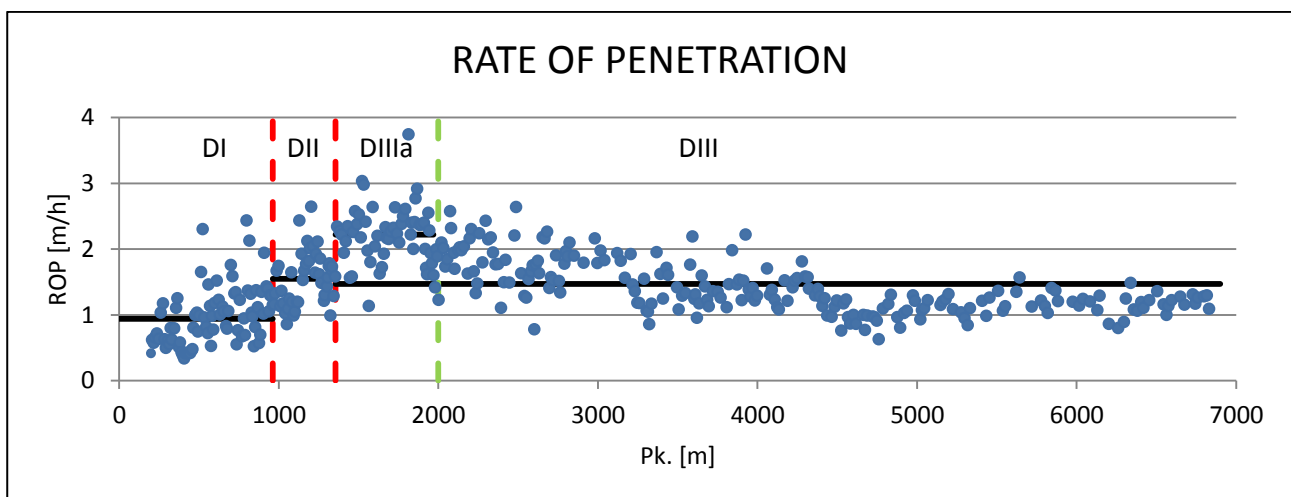


Figure 6.1 ROP distribution through the tunnel. Red lines represent the domain changes, black horizontal lines represent the median values measured in each domain, and dotted black line indicates the median value registered in DIIIa. Green line delimitates DIIIa.

The median value of ROP referred to the entire tunnel length is equal to 1.33 m/h. The lowest ROP have been registered in the gneiss (DI) excavation in which the median values is of 0.94 m/h. This low value is compatible with the high quality of encountered rock mass, which made tunnelling difficult. It is in this domain that the minimum ROP has been registered (0.33 m/h).

The rate of penetration increases boring the gneiss-micaschist alternation characterising DII, a median value of 1.55 m/h has been achieved; that is because in this tract the general quality of rock

6.2 Measured TBM performances

mass and its strength are lower than those observed in the previous domain (as already discussed in Chapter 5).

The highest ROP have been calculated in the first portion of the third domain (DIIIa), where a median of 2.22 m/h has been registered, it is probably due to the decreasing of rock mass quality and strength, with respect to the DII. In the remaining part of micaschist domain, ROP is similar to the one measured in DII, in this tract the median value is 1.47 m/h.

The statistical description of ROP distribution through the tunnel has been reported in Table 6.2.

ROP [m/h]	TUNNEL	Domain I	Domain II	Domain III; * DIIIa	
Range	0.33 – 3.74	0.33 – 2.43	0.85 – 2.64	1.13 – 3.74*	0.62 – 3.74
Median	1.33	0.94	1.55	2.22*	1.47
Mean	1.45	0.96	1.53	2.18*	1.58
Q1-Q3	1.08 – 1.81	0.60 – 1.23	1.19 – 1.78	1.92 – 2.40*	1.18 – 1.97

*Table 6.2 ROP statistical description; * DIIIa data: part of DIII data used in the following predictive model creation.*

6.2.2 Field penetration index

The field penetration index (FPI), is calculated as the ratio between the force acting on each cutter and the penetration rate per revolution (see section 2.4.5).

FPI is strongly affected both by rock mass conditions and by operational ones.

There is in fact a threshold which cannot be exceeded, and it is specific for each machine and that is independent from geological feature of excavated ground. Moreover, in some situations rock mass strength could require high thrusts in order to obtain an acceptable advance, however, FPI is maintained low to avoid machine damages and breakages (also when these thrusts are below the machine threshold).

During faults or cataclastic zones crossing FPI is intentionally maintained low.

For these reasons, the TBM driving decisions and the operator experience may strongly affect the TBM performances in terms of FPI and, in minor part, of ROP.

The FPI distribution for the entire analysed tunnel length is provided by Figure 6.2.

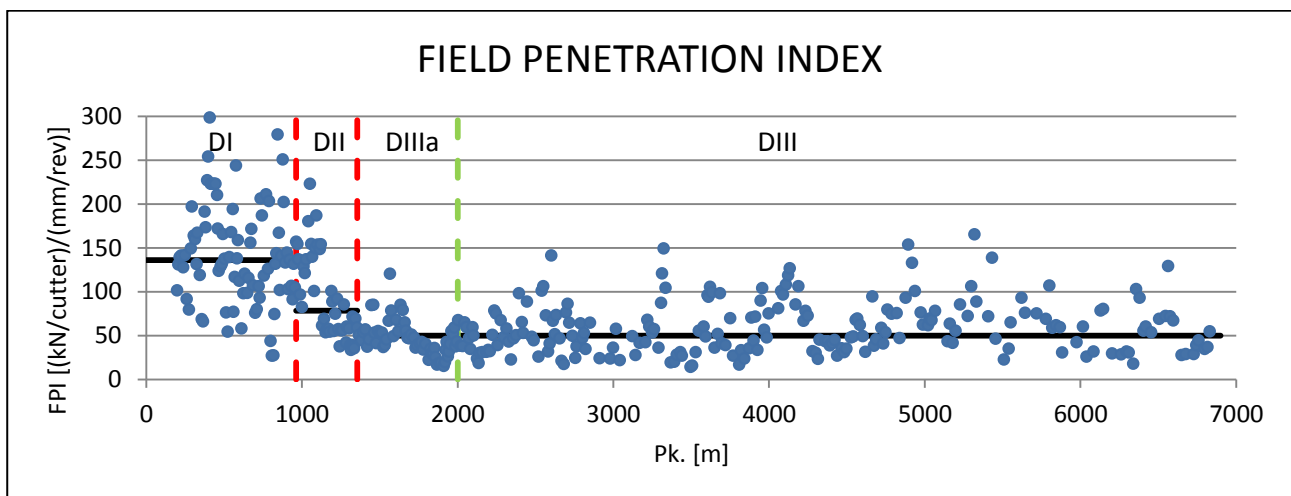


Figure 6.2 Distribution of FPI through the tunnel, red lines represent the geological domain changes. Green line delimitates DIIIa.

The values of FPI calculated during La Maddalena tunnel construction range between 40.90 and 101.15 kN/cutter/mm/rev (in terms of Q1-Q3) and FPI has a median value equal to 61.40 kN/cutter/mm/rev.

6.2 Measured TBM performances

The highest median of FPI has been detected during the excavation of the gneiss domain, where median FPI is of 136.32 kN/cutter/mm/rev. The index significantly decreases through the gneiss-micaschist alternation (DII) which are characterised by median value of 78.52 kN/cutter/mm/rev.

About DIII it was noted that the FPI calculated in the first tract of the domain (DIIIa) does not differ from the index relative to the whole domain, being median values equal to 45.50 and 49.92 kN/cutter/mm/rev respectively.

Table 6.3 provides the statistical description of FPI through the entire excavated length and referred to each geological domain.

FPI [kN/cutter/mm/rev]	TUNNEL	Domain I	Domain II	Domain III; * DIIIa	
Min.	14.20	26.86	33.52	15.16	14.20
Max.	298.61	298.61	222.98	120.42	165.10
Median	61.40	136.32	78.52	45.50	49.92
Mean	78.29	142.73	94.12	47.30	56.07
Q1	40.90	102.68	55.76	35.66	35.40
Q3	101.15	173.25	138.91	55.12	70.95

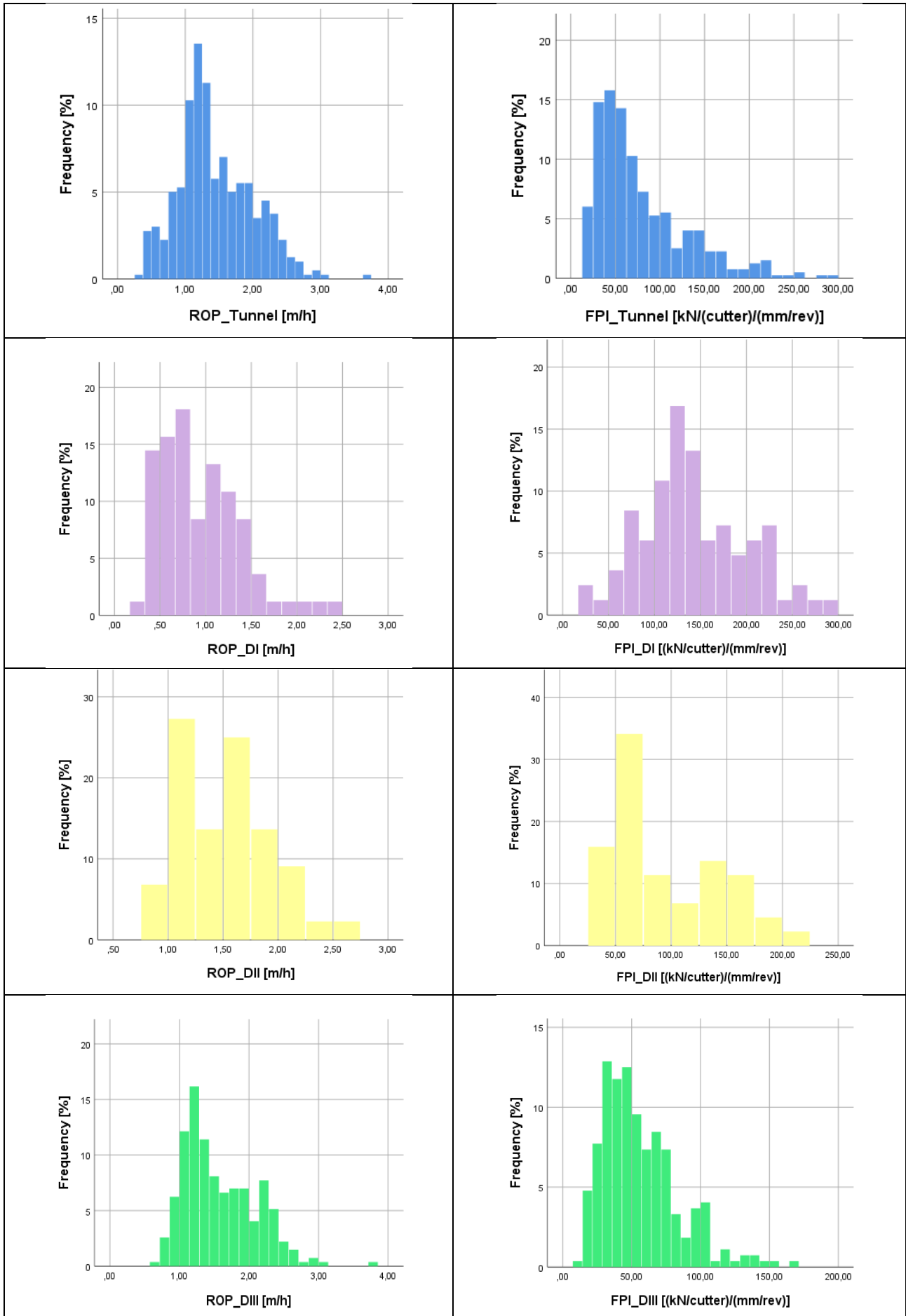
*Table 6.3 FPI statistical description; * DIIIa data: part of DIII data used in the following predictive model creation.*

Generally, it was noted that the FPI trend is related to the one concerning the quality, the strength and the fracturing degree of the rock mass. It is particularly evident by observing the passage from the massive gneiss, characterised by high quality and strength, to the gneiss-micaschist alternation domain, in which the quality decreased and fracturing degree increased. The FPI is high in DI where a high cutterhead force is required to obtain a low penetration and FPI is lower in DII where a reduced thrust is necessary to register a good penetration rate.

The histograms related to the ROP and FPI distribution through the tunnel have been reported in the following page (Figure 6.3).

Figure 6.3 ROP and FPI histograms.

6.2 Measured TBM performances



6.3 Conclusion

During this work, La Maddalena TBM performances have been collected and analysed, in terms of ROP and FPI.

It is possible to note that performances indices improve in the verse of the excavation, in particular, the worst boring conditions have been registered during gneiss excavation, where rock mass high quality make tunnelling difficult.

Generally, in those situations characterised by massive and hard features of ground, TBM performances are low: the thrust required to bore the rock face is high whereas the penetration is low. It determines high levels of FPI and low values of ROP.

Working decisions not related to the geological and geomechanical framework may affect the TBM advance.

7 COMPARISON BETWEEN DIRECT GEOSTRUCTURAL SURVEY AND SEISMIC METHODS FOR PREDICTING GEOLOGICAL FRAMEWORK AHEAD TUNNEL FACE

7.1 Introduction

It is well known that during design phase and tunnel excavation the knowledge of the geological, structural and mechanical properties of rock masses is one of the most important requirements in order to select the best construction method and guarantee the required safety levels.

This is usually accomplished by means of geomechanical and structural observations with local sampling (direct surveys) on site, particularly on the tunnel walls when they are accessible, for example when the excavations is carried out by means of an open type TBM. However, if the access to the tunnel walls is not allowed and the direct surveys not possible (when the excavation is realised by means of a closed type TBM or when the ground conditions are so poor that wall mapping is not safe), indirect methods, like geophysical ones, can be applied. Indirect methods suffer however of uncertainties and resolution limitations that may affect the obtainable results.

This part of the study aims to compare the geological, structural and geotechnical features of rock masses gathered by direct geostructural surveys and the results obtained by an indirect seismic technique; the adopted one is the Tunnel Seismic Prediction (TSP).

In particular, the reliability of TSP in terms of predicting lithological variations, physical and mechanical properties of intact rock, rock mass fracturing degree and orientation of major discontinuity elements have been evaluated and discussed.

With this aim, 8 TSP measurements, covering a total length of 1500 meters, between pk. 500 m and pk. 2000 m, have been analysed. These measurements have been carried out in order to predict the rock mass features ahead of the excavation front.

7.2 Comparison of the results

The purpose of this study is to compare the geological, structural and mechanical data collected during traditional survey and laboratory analyses with the information obtained by the TSP investigation. In particular the purpose is to test the reliability of this method in terms of:

- Prediction of significant lithological changes;
- Estimation of mechanical and physical parameters describing intact rock;
- Estimation of fracturing degree of rock masses and presence of shear or weakness zones prediction;
- Estimation of orientation of the principal elements of discontinuities.

7.2.1 Prediction of significant lithological changes

During “La Maddalena” design phases, many geological field surveys have been performed. These surveys allowed to depict the geological limit between the gneiss of the Ambin complex and the micaschists of Clarea complex. However, given the significant depth of the planned tunnel, it was not possible to establish the exact interaction of this limit with the tunnel axis before tunnel excavation. The mechanical properties of the two rock types are indeed very different so that their boreability is not the same; for this reason, the knowledge of limit location was very important.

TSP measurements showed a significant reduction of P waves (from an average wave velocity of about 5500 m/s to 3500 m/s) and S waves (from about 3250 m/s to 2000 m/s) as shown in Figure 7.1.

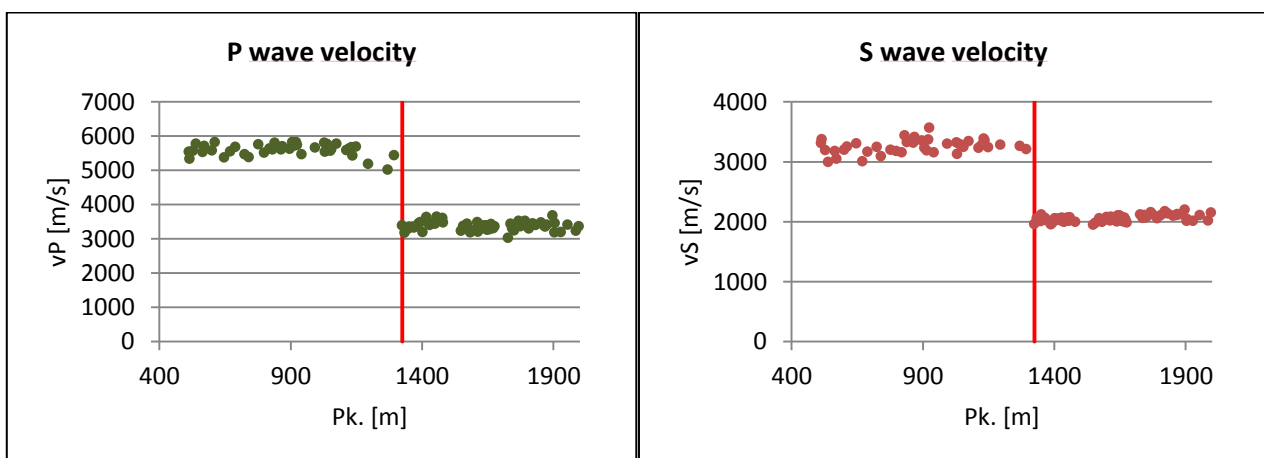


Figure 7.1 P wave velocity (on the left) and S wave velocity (on the right) along the tunnel (Armetti et al., 2017).

This sudden reduction of P and S wave velocities occurs at pk. 1360 m, where also direct geological surveys after the tunnel excavation have detected the passage from gneiss to micaschists. P waves show a little reduction in velocity before the most important one in the transition zone from Ambin to Clarea complex.

7.2.2 Estimation of fracturing degree of rock masses and presence of shear or weakness zones prediction

The occurrence of high fractured zones in rock masses generally reduces the global quality of them and the safety of excavation processes, so that support and reinforcement elements become fundamental in order to guarantee the advance of works and the safety of workers.

The fracturing degree of a given rock mass cannot be evaluated only by observation of tunnel walls and it has to be predicted ahead the excavation front.

Both the type of rock and the characteristics of rock mass (e.g. global quality) affect the velocity of seismic waves; the wave propagation is higher into good quality (low fracturing) grounds and is lower into poor quality (high fracturing) materials. Generally, a low seismic signal velocity propagation denoted a fracturing rock mass.

For each section of homogeneous TSP velocity, the rock mass fracturing degree has been evaluated on the basis of traditional geological survey. The fracturing index has been computed in terms of distance between joints (spacing), by the following formula:

$$S = \frac{L}{n} [cm] \quad (7.1)$$

where L is the length where the velocity of wave is homogeneous (Figure 7.2) and n is the number of joints detected in that distance.

7.2 Comparison of the results

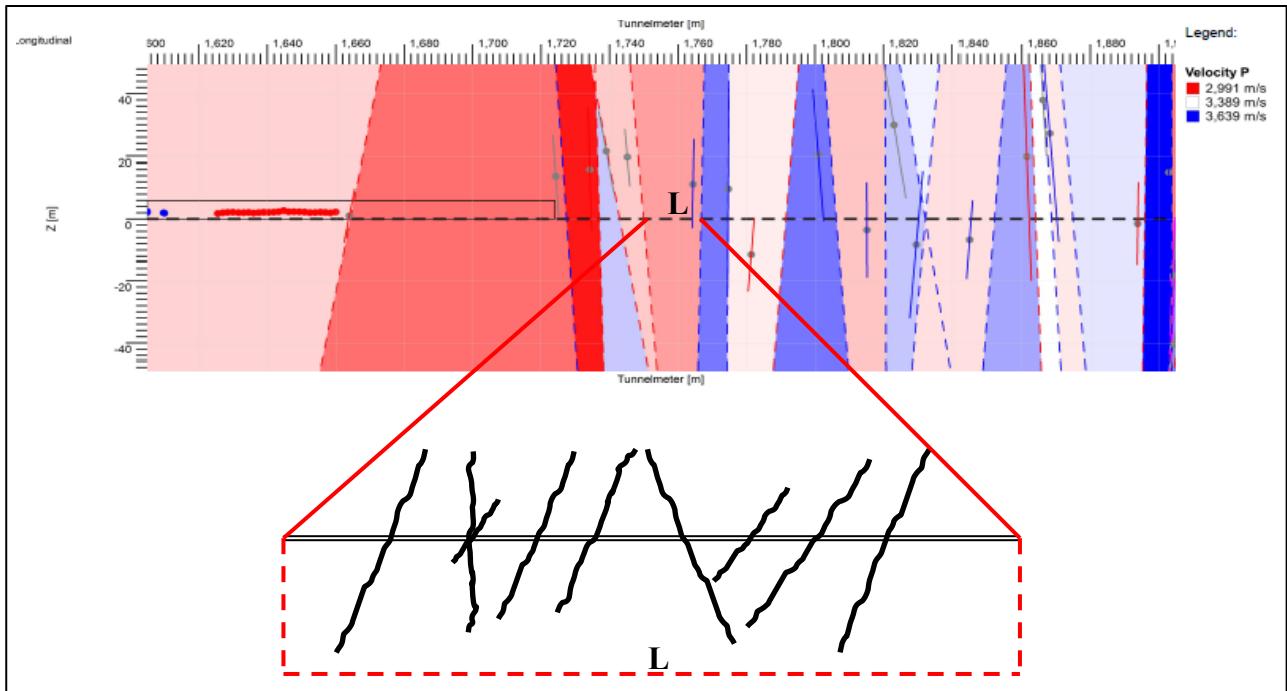


Figure 7.2 The length L considered in Spacing calculation is the one where homogeneous wave velocity has been measured.

The velocity of seismic wave propagation and the spacing values have been compared. From these results, a clear correlation between P and S wave velocity and degree of fracture is not observable in the two investigated rock types (Figure 7.3), probably because the seismic velocity is most affected by the intact rock properties than by its fragmentation degree.

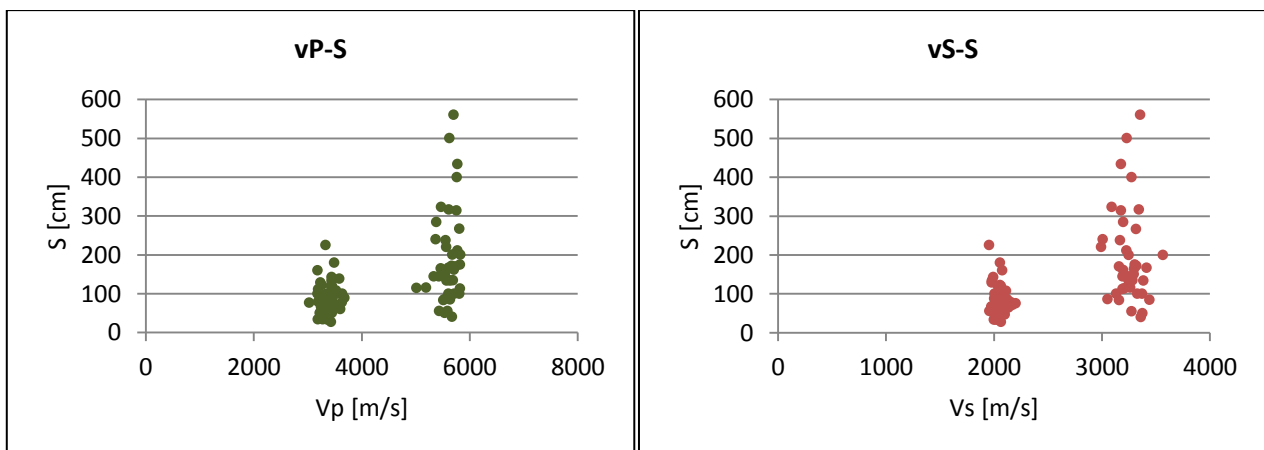


Figure 7.3 P and S wave velocity related to fracture spacing (Armetti et al., 2017).

There was an attempt to evaluate spacing considering a constant L and the calculation has been carried out adopting different L values ($L = 1, 2, 3, 4, 5, 6, 7, 8, 9, 10$ m) but did not allow for more reliable correlations.

The degree of fracturing of rock mass has been also evaluated by means of the volumetric joint count, J_v (Palmström, 1982). It has been related to the wave velocity as reported in Figure 7.4.

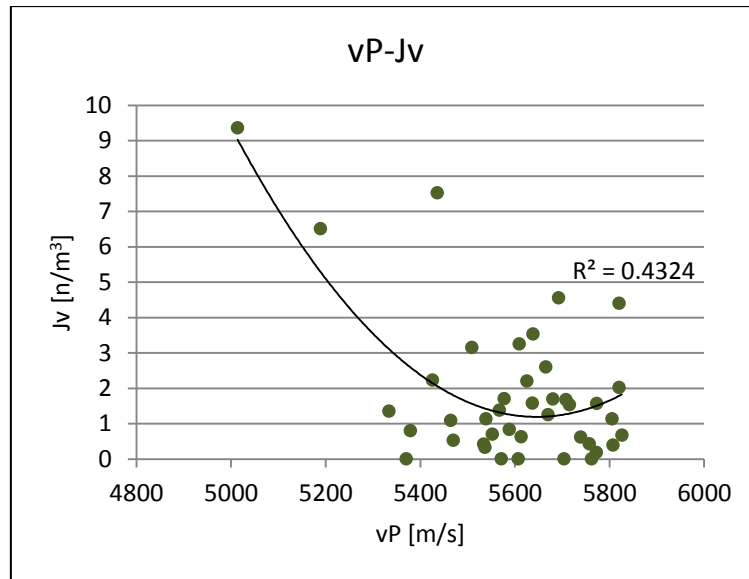


Figure 7.4 P wave velocity related to J_v .

A more reliable correlation between seismic wave velocity and the fracturing degree of rock mass has been obtained by using J_v as indicator of rock mass fragmentation. It is due to the fact that seismic waves propagate into volumes of rock masses and J_v considers the number of discontinuities per unit volume; in other words, waves propagate into three dimensions and J_v represents the fracturing degree into three dimension portion of rock. The extremely poor correlation with spacing is probably because it considers only the linear distance between joints, but the problem of wave propagation has to be considered as three dimensional one.

7.2.3 Estimation of orientation of the principal elements of discontinuities

The intersection angles of principal discontinuities with tunnel axis are one of the most relevant aspects involved in tunnel stability analysis. The orientation of the principal elements of discontinuity (e.g. faults, fractures, cataclastic bands, etc.) is estimated after geostructural surface survey and tunnel walls mapping; however the TSP method is able to give information about the weakness plane orientations, since they are planes of acoustic impedance.

Along the considered tunnel tract, TSP survey detected 103 planes of discontinuities; the method gives the spatial position and the orientation in terms of dip and dip direction for each of them.

The distance between the predicted plane and the mapped one has been evaluated as follows (Equation 7.2) in order to compare these data with data achieved during tunnel walls mapping:

7.2 Comparison of the results

$$\Delta L = |L_{TSP} - L_{MAP}| \quad (7.2)$$

where L_{TSP} is the plane detected by TSP measurements and L_{MAP} is the plane observed during the geological survey.

A graphical representation of ΔL is reported in Figure 7.5.

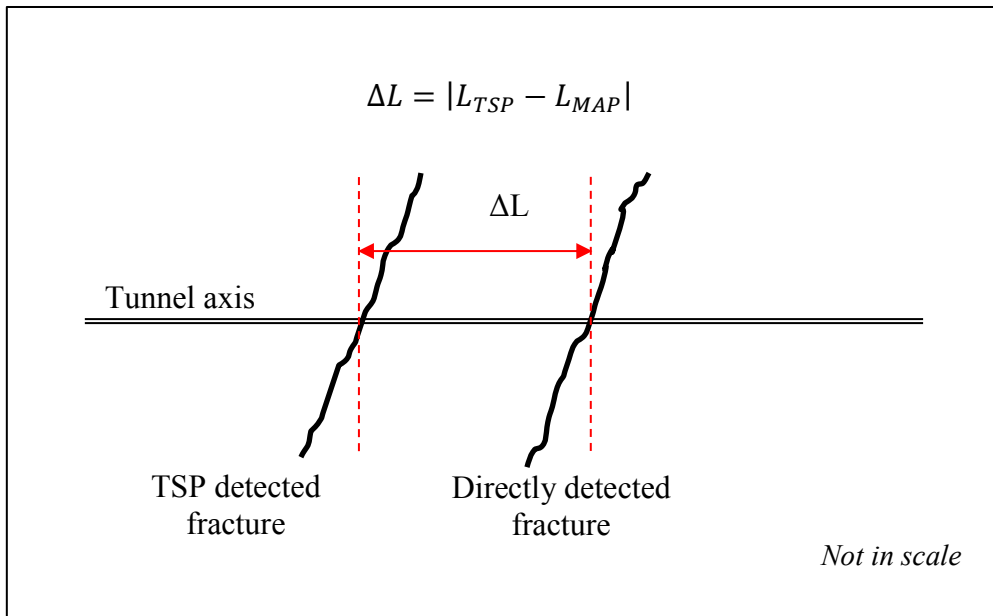


Figure 7.5 Distance between mapped and TSP detected discontinuity.

The fractures have been subdivided into three categories on the basis of ΔL :

- If $\Delta L < 0.30$ m a perfect correspondence among the two methods has considered;
- If $0.30 \text{ m} < \Delta L < 1.00$ m the correspondence is considered acceptable;
- If $\Delta L > 1.00$ m there are no correspondence.

The concept of fracture division into three classes has been graphically explained by means of the schemes in Figure 7.6.

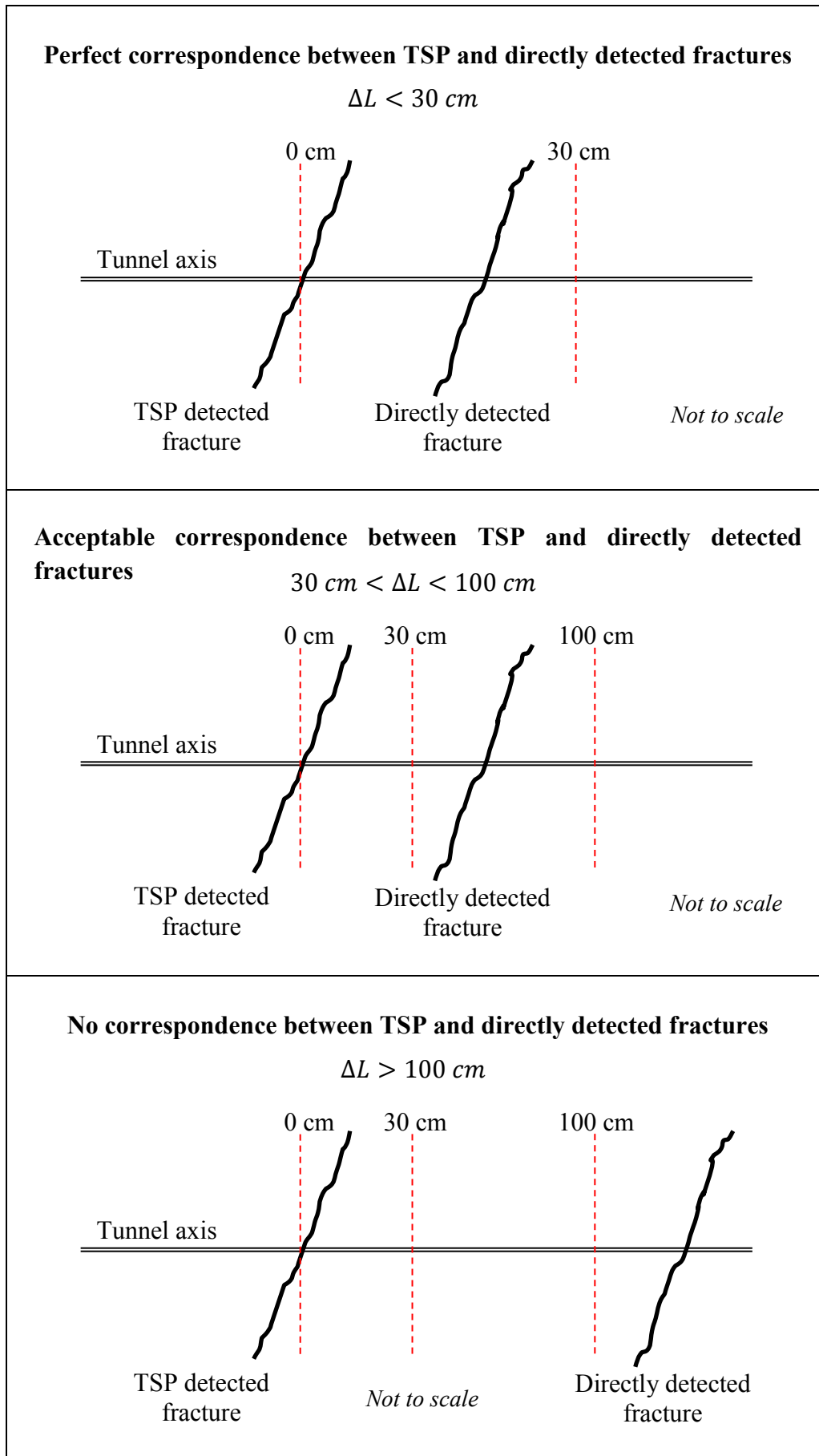


Figure 7.6 Three categories of fractures on the basis of ΔL .

7.2 Comparison of the results

The number of occurrences for each category is summarised in Table 7.1.

ΔL	Number of fractures
$\Delta L < 0.30$	56
$0.30 < \Delta L < 1.00$	35
$\Delta L > 1.00$	21

Table 7.1 Number of discontinuity elements for each ΔL category (Armetti et al., 2017).

A comparison between directly mapped and TSP detected orientations has been attempted only for discontinuities with a $\Delta L < 1.00$ m (“perfect” and “acceptable” correspondence). The results carried out from this comparison show that the dip direction is predicted with good accuracy while the dip is over estimated, as it can be observed by the two stereographic projections reported in Figure 7.7.

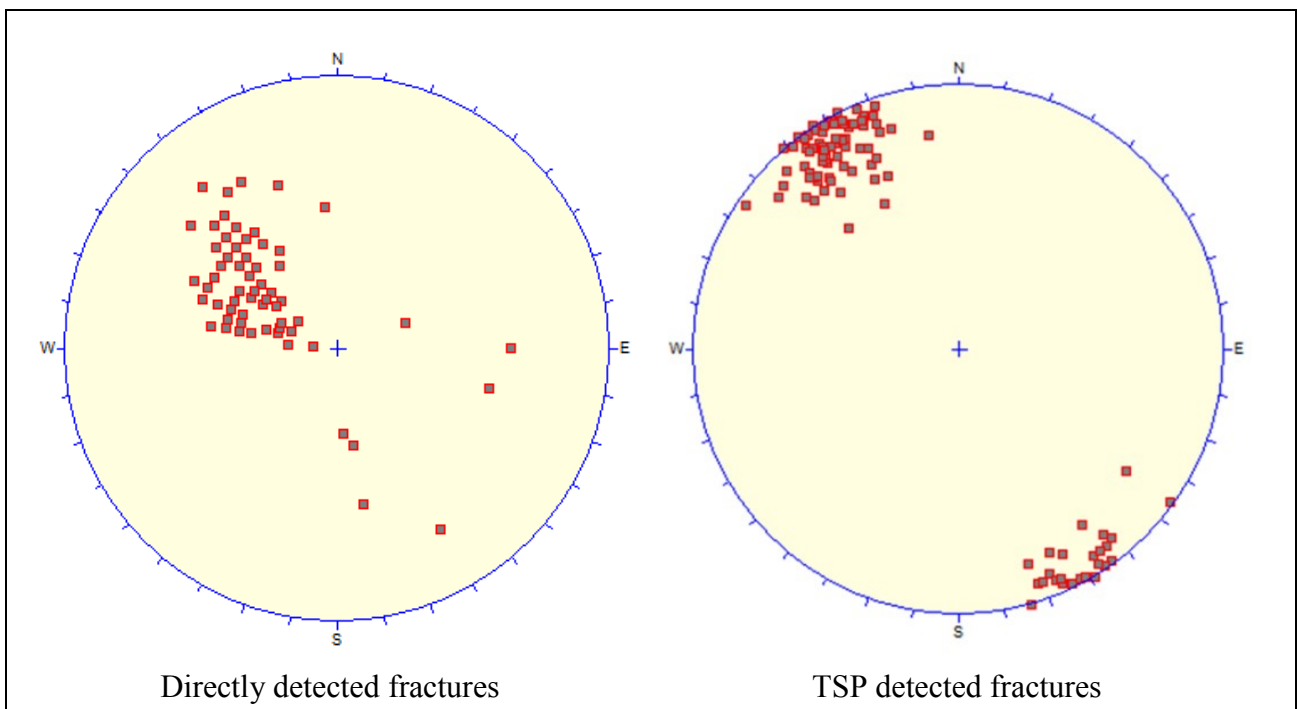


Figure 7.7 Stereographic projection of poles of directly detected discontinuities (left) and poles of discontinuities detected by means of TSP survey (right).

A statistical analysis of joint orientations has been carried out, distinguishing the “perfect correspondence” class ($\Delta L < 0.30$ m) from the “acceptable correspondence” one ($0.30 \text{ m} < \Delta L < 1.00 \text{ m}$). The results are reassumed in the frequency diagrams reported in Figure 7.8.

It is clear that the most frequent difference (Δ dip direction) between observed and TSP estimated dip direction is 10° .

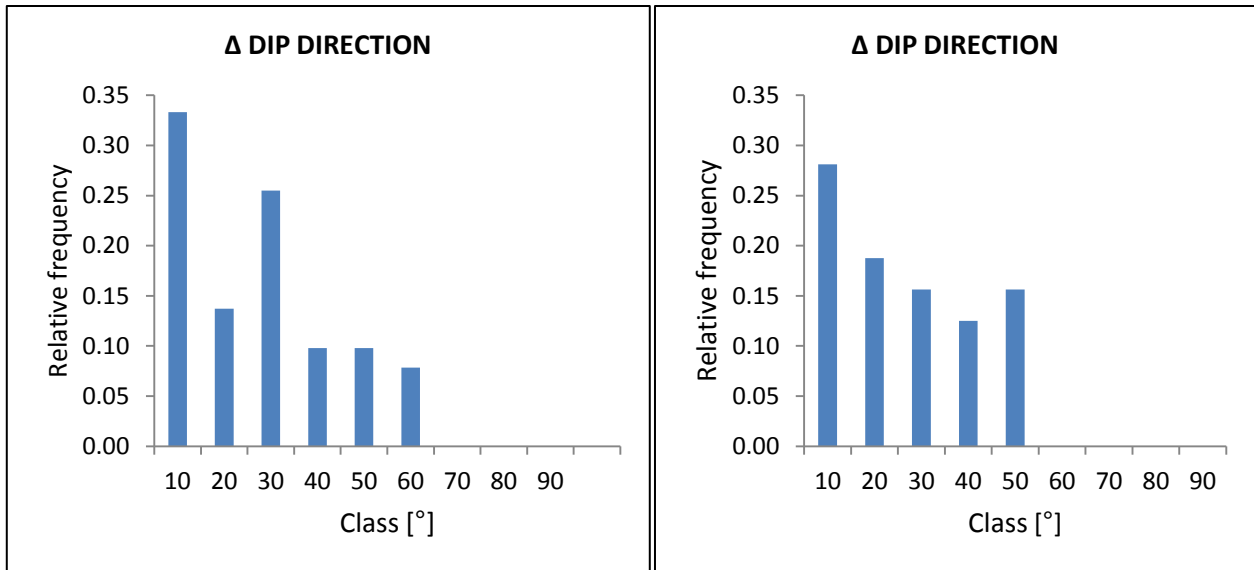


Figure 7.8 Histogram of frequency about the dip direction differences between directly observed and TSP detected fractures $\Delta L < 0.30$ m on the left and $0.30 \text{ m} < \Delta L < 1.00$ m on the right. (Armetti et al., 2017).

The most common differences (Δ dip) between observed and TSP dips are 30° for $\Delta L < 0.30$ m class and 50° for $0.30 \text{ m} < \Delta L < 1.00$ m (as shown in the diagrams of frequency in Figure 7.9).

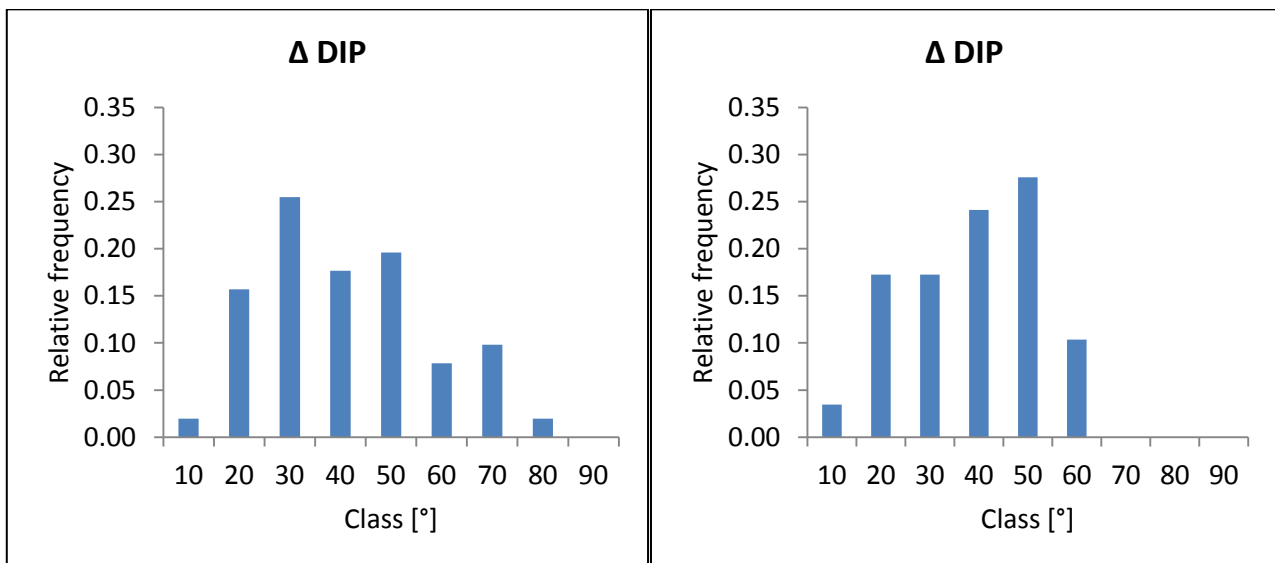


Figure 7.9 Histogram of frequency about the dip differences between directly observed and TSP detected fractures $\Delta L < 0.30$ m on the left and $0.30 \text{ m} < \Delta L < 1.00$ m on the right. (Armetti et al., 2017).

The overestimation fracture dips is probably due to the working principles of TSP system that is most influenced by those planes perpendicular to the tunnel axis than by the parallel and sub-parallel ones.

7.3 Conclusion

The study summarised in this chapter aims to check the reliability of TSP investigation system, adopted during “La Maddalena” tunnel construction to predict the geological and mechanical properties of rock mass ahead the tunnel face, in comparison with direct geostructural surveys.

Three aspects have been investigated during this analysis:

- TSP method was completely reliable as for the individuation of main lithological changes; in fact, the passage from Ambin complex to Clarea one predicted with accuracy;
- A quite relevant relationship between the joint volumetric count (Jv) and P wave velocity has been observed. It means that the seismic velocity obtained with TSP method is also influenced by fracturing degree of rock mass: in other words, the wave velocity can be involved to predict the degree of fragmentation of a given rock mass.
- As for the orientation and the position of the principal planes of weakness, the method has been considered satisfactory; however the angle with tunnel axis is overestimated. This overestimation is because the TSP, due to its principles of working, is mainly affected by the planes perpendicular to tunnel axis.

In conclusion Tunnel Seismic Prediction method can be considered reliable in the scopes for which it has been adopted.

8 LITERATURE MODELS FOR PREDICTING TBM PERFORMANCES AND THEIR APPLICATION TO “LA MADDALENA” EXPLORATORY TUNNEL

This chapter is divided into two parts:

- In the first one, a brief description of the principal TBM performance predictive methods has been provided. The three most relevant groups of predictive models (based on theoretical, empirical and artificial intelligence approaches) have been synthetically illustrated and for each group the models which are mainly involved in tunnel projects have been described. Two tables show what geological, mechanical or technological parameters are considered in the proposed model.
- The second section reports the results of the application of the principal models proposed in literature, to “La Maddalena” case study. In particular the empirical predictive equations proposed by different authors have been considered to predict TBM performance at “La Maddalena” tunnel, then the predicted data have been compared with the measured ones.

8.1 Approaches for predicting TBM performance

8.1.1 Introduction

In mechanized tunnel excavation, Tunnel Boring Machine (TBM) performance has a very dominant impact on the times and costs of tunnel realisation: for this reason they must be accurately predicted. TBM performance prediction is essential to select the most effective method of tunnelling and to generally estimate time and the economic costs of infrastructure realisation.

In other words, the design of tunnel projects and the selection of construction methods require the effective TBM performance prediction to make mechanized tunnelling cheaper, safer and more effective than the “drill and blast” method.

It is well known that the TBM performance is affected by several factors such as geological site conditions (lithological features, fracture frequency, joint orientation, faults and bedding related to tunnel axis, rock bursting, swelling, underground water condition, etc.), geotechnical properties (strength, hardness, brittleness, abrasiveness, etc.) and machine related parameters (machine diameter, cutter disposition and geometry, disc diameter, thrust, torque, etc.).

TBM were introduced in 1950s and since then many researchers (Tarkoy, 1975; Ozdemir, 1977; Blindheim, 1979; Nelson and O'Rourke, 1983; Rostami and Ozdemir, 1993; Alber, 1996, 2000, 2008; Barton, 2000; Sapigni et al., 2002; Yagiz, 2002, 2006, 2008; Gong and Zhao, 2009; Hamidi et al., 2010; Hassanpour et al., 2011; Macias, 2014, Rostami, 2016; Salimi et al., 2016; Adoko et al., 2017; Armetti et al., 2018, and many others) have developed several methods that allow to estimate the TBM performance, by analysing cutting forces (theoretical models) or the interaction between the intact rock and rock mass features and the operating characteristics of the TBM (empirical models).

The TBM performance predictive models are based on different approaches; however the theoretical, based on laboratory tests and cutting forces, and the empirical ones, based on field TBM performance and geotechnical properties of rocks, are the most common, but also artificial intelligence techniques, including artificial neural network, support vector machine, particle swarm optimisation and fuzzy inference systems have been developed for this purpose (Alvarez Grima et al., 2000; Benardos and Kaliampakos, 2004; Yagiz et al., 2009; Yagiz and Karahan, 2011; Mahdevari et al., 2014; Ghasemi et al., 2014).

8.1.2 Theoretical models for predicting TBM performance

The theoretical models are based on the analysis of breakage mechanisms and on the study of the cutting forces acting on cutters to define a force equilibrium relation (Crow, 1975; Ozdemir et al., 1978; Roxborough and Phillips, 1975; Sanio, 1985; Sato et al., 1991; Snowdon et al., 1982). The first developed theoretical models focused on full-scale laboratory cutting tests or indentation tests in various rock types and gave an estimation of cutting forces based on cutter and cutting geometry, spacing and penetration of the cut (Khademi Hamidi et al., 2010). The estimated cutting forces are considered to evaluate cutterhead thrust and torque and to estimate the performance of a TBM with certain specifications (Rostami, 2016).

Nevertheless, these models are difficult to apply, both because they require several laboratory tests, which sometimes do not represent the real rock masses behaviour during tunnels excavation and because the test equipment required is not often available in the research centres. A positive aspect of these methods is that they provide information about rock fragmentation and into applied force-TBM penetration behaviour of rock masses (Khademi Hamidi et al., 2010).

The main advantages and disadvantages of theoretical modes are reported in Table 8.1.

Advantages	Disadvantages
<ul style="list-style-type: none"> - Flexible with machine characteristic and cutter geometry; - Can be adopted for thrust and torque optimization; - Can be used for cutterhead design and its optimization; - Can be involved to understand the effective working condition of the cutters and related forces. 	<ul style="list-style-type: none"> - Unable to easily consider rock mass and intact rock parameters; - Unable to take into account the presence of joints; - Advised against in jointed rock masses; - Unable to account for required field adjustment.

Table 8.1 Principals advantages and disadvantages of theoretical modes (modified after Rostami, 2016).

The model developed by the Colorado School of Mines, CSM (Rostami, 1997; Rostami and Ozdemir, 1993) is the most frequently used one of the group. CSM can be considered as a semi-theoretical model. It begins from the individual cutter force calculation in to define the overall thrust, torque and power requirement of the entire cutterhead (Delisio and Zhao, 2014).

8.1 Approaches for predicting TBM performance

The original model is based only on intact rock properties and later Yagiz (2002) and Ramezanzadeh et al. (2008) modified it taking into account the influence of rock mass parameters as the angle between tunnel axis and weakness planes (α).

The CSM output is the penetration of TBM into rock mass (m/h or mm/min). The list of intact rock and rock mass characteristics and machine related parameters involved in CSM model are summarised in Table 8.2.

Rock and rock mass parameters	Machine parameters	Output
<ul style="list-style-type: none"> - Uniaxial compressive strength (UCS); - Brazilian tensile strength (BTS); - Cerchar Abrasivity Index (CAI); - Rock quartz content (q); - Joint spacing (Js); - Angle between tunnel axis and the planes of weakness (α). 	<ul style="list-style-type: none"> - Cutter load capacity (F_N); - Cutter spacing (S_{cutter}); - Cutter diameter ($\varnothing_{\text{cutter}}$); - Cutter number (n_{cutter}); - Cutter tip width (W_{tip}); - TBM thrust (F_{TBM}); - TBM torque (M_{TBM}). 	<ul style="list-style-type: none"> - Penetration [m/h; mm/min]

Table 8.2 List of intact rock and rock mass characteristics and machine related parameters involved in CSM model.

8.1.3 Empirical models for predicting TBM performance

Empirical models are based on the back-analysis of geological, geotechnical and TBM performance collected during a tunnel realisation and the predictive equations proposed are carried out from the statistical analysis of the dataset. In other words, they consist of empirical correlations between geological-geomechanical parameters and the actual TBM performance. This group of models allows to estimate the TBM performance in a geological site with given features and are generally site-specific.

The main advantages and disadvantages affecting empirical models have been listed in Table 8.3.

Advantages	Disadvantages
<ul style="list-style-type: none"> - Based on field performance of TBM and of rock features; - Consider the TBM as the whole system; - Particular importance is given at geological site condition; - Account of many of field adjustment. 	<ul style="list-style-type: none"> - Very sensitive at joint properties; - Unable to consider machine specifications, cutter geometry and cutter spacing; - Applicable only to similar tunnel project.

Table 8.3 Principals advantages and disadvantages of empirical modes (modified after Rostami, 2016).

The geological, geotechnical and mechanical properties of intact rocks and rock masses are considered as independent variables (input) and the TBM performance as dependent ones (output). The influences of the first ones on the machine operational parameters are evaluated using statistical regression analysis.

Empirical predictive models can be divided into two large groups: the single parameter models and the multiple parameter ones.

The first type of models is easy to apply because it includes a single intact rock parameter such as the uniaxial compressive strength, UCS (Graham, 1976; Farmer and Glossop, 1980; Hughes, 1986; Armetti et al., 2018), or rock matrix index, such as the drilling rate index (DRI), punch penetration, Taber abrasion, brazilian tensile strength, shore harness and point load index (Tarkoy, 1973; Blindheim, 1979; Nelson et al., 1983, 1985; Bamford, 1984; Wijk, 1992; Dollinger et al., 1998) and one machine index. They can be utilised in a limited range of cases and generally tend to

8.1 Approaches for predicting TBM performance

underestimate the actual TBM performance due to the lack of some relevant geological parameters (i.e. because they are hard to collected or not available).

Since the TBM performance does not depend on a single rock feature but by the combination of more of them several multiple parameter models have been proposed later (Sundin and Wanstedt, 1994; Bruland, 1998; Nelson et al., 1999; Alvarez Grima et al. 2000; Zhao et al., 2007; Yagiz, 2008 and many others). This type of approach is able to account for both more than one rock parameters and TBM ones, however the typical disadvantage is to understand the relation type between the rock and machine parameters. Researchers commonly carry out linear or non-linear multiple regression analyses and the best combination of rock mass parameters to predict the TBM behaviour in tunnelling is selected (Alber, 1996; Yagiz, 2008; Gong and Zaho, 2009; Hassanpour et al., 2011; Farrock et al., 2012). The coefficient of determination (R^2) is adopted as indicator of correlation strength.

Some predictive models aim to correlate rock mass geomechanical quality estimating by rock mass classification systems with TBM performances:

- Rock Structure Rating (RSR, Wickham et al., 1972) was considered by Cassinelli et al. (1982) and Innaurato et al. (1991);
- Rock Mass Rating (RMR, Bieniawski, 1989) was used by Sapigni et al. (2002), Ribacchi and Lembo Fazio, (2005), Hassanpour et al. (2009), Armetti et al. (2018);
- Rock Mass Quality Index (Q, Barton et al., 1974) by Burton (2000);
- Geological Strength Index (GSI, Hoek, 1994; Marinos and Hoek, 2000) by Hassanpour et al. (2009) and Armetti et al. (2018).

Bieniawski et al. (2006) developed the Rock Mass Excavability index, RME, based on RMR classification system. RME was carried out from over 400 sections of tunnels and has been updated many times with more case histories up until now (Bieniawski et al., 2007 a,b; Bieniawski and Grandori, 2007).

RME index is based on five input parameters: UCS of intact rock, abrasivity, rock mass fracturing degree, stand-up time of the excavation and groundwater conditions.

The ratings for each of the five parameters are summarised in Table 8.4.

8.1 Approaches for predicting TBM performance

UCS OF INTACT ROCK (0–25 points)										
σ_c (MPa).....	<5	5–30	30–90		90–180		>180			
Average rating	4	14	25		14		0			
DRILLABILITY (0–15 points)										
Drilling Rate Index	>80	80–65	65–50		50–40		<40			
Average rating	15	10	7		3		0			
DISCONTINUITIES AT TUNNEL FACE (0–30 points)										
Homogeneity			Number of joints per meter					Orientation with respect to tunnel axis		
	Homo- geneous	Mixed	0–4	4–8	8–15	15–30	>30	Perpendicular	Oblique	Parallel
Avg. rating	10	0	2	7	15	10	0	5	3	0
STANDUP TIME (0–25 points)										
Hours	<5	5–24	24–96		96–192		>192			
Average rating	0	2	10		15		25			
GROUNDWATER INFLOW (0–5 points)										
L/sec	>100	70–100	30–70		10–30		<10			
Average rating	0	1	2		4		5			
¹ Zero for argillaceous rocks.										

Table 8.4 RME index input ratings (Bieniawski and Celada).

The assigned ratings are summed in order to give the RME value. Several statistical correlations have been carried out between RME and TBM performance index, as coefficient of utilization, average rate, penetration rate and specific energy.

One of the empirical models most widely used nowadays around the world is the Norwegian University of Science and Technology method (NTNU) developed by Bruland (1998); it is based on empirical correlation between geological and geotechnical properties of rock masses and the actual TBM performance. NTNU method takes into account some machine parameters and provides the penetration rate, the advance rate and the utilization factor as the output indices.

The list of intact rock and rock mass characteristics and machine related parameters involved in NTNU method is summarised in Table 8.5.

8.1 Approaches for predicting TBM performance

Rock and rock mass parameters	Machine parameters	Output
<ul style="list-style-type: none"> - Uniaxial compressive strength (UCS); - Cerchar Abrasivity Index (CAI); - Cutter Life Index (CLI); - Drilling Rate Index (DRI); - Porosity; - Rock quartz content (q); - Joint spacing (Js); - Angle between tunnel axis and the planes of weakness (α). 	<ul style="list-style-type: none"> - Cutter thrust (F_N); - Cutter spacing (S_{cutter}); - Cutter diameter (\varnothing_{cutter}); - Cutterhead revolution per minute (RPM); - Installed cutterhead power. 	<ul style="list-style-type: none"> - Penetration Rate (PR); - Advance Rate (AR); - Utilization Factor (U).

Table 8.5 List of intact rock and rock mass characteristics and machine related parameters involved in NTNU model.

Q_{TBM} method proposed by Barton (2000), is based on Q-system with the addition of some parameters as the quartz content, cutter life index and the stress on tunnel face.

Q_{TBM} method is able to predict TBM performance; however it is difficult to use it in practical applications because it includes several parameters, in addition some of them are overlapped (Gong and Zhao, 2009).

The list of intact rock and rock mass characteristics and machine related parameters involved in Q_{TBM} method are summarised in Table 8.6.

Rock and rock mass parameters	Machine parameters	Output
<ul style="list-style-type: none"> - Rock Quality Designation (RQD); - Number of joints (Jn); - Joint roughness (Jr); - Joint alteration (Ja); - Joint water condition (Jw); - Stress Reduction Factor (SRF); - Quartz content (q); - Rock Mass Strength (SIGMA). - Cutter Life Index (CLI); - Average biaxial strength on tunnel face (σ_{θ}) 	<ul style="list-style-type: none"> - Average cutter thrust (F); 	<ul style="list-style-type: none"> - Penetration Rate (PR); - Advance Rate (AR).

Table 8.6 List of intact rock and rock mass characteristics and machine related parameters involved in Q_{TBM} method.

Delisio et al. (2014) developed a predictive model suitable when “blocky rock condition” occurs. “Blocky rock condition” means that there are face instabilities in jointed rock masses, where the combined effect of the structure of rock mass and the in-situ stress conditions causes a fragmentation process of the tunnel face, which can become “blocky” (Delisio et al., 2013).

Blocky rock conditions may entail a significant impact on the TBM performance such as the increase of cutter/cutterhead wear caused by the dynamic impact of the rock blocks against cutters or the damages to the muck conveyor system generated by blocks in the muck.

These conditions may generally result in negative effects that increase the TBM maintenance requirements and lead to higher construction times and costs. (Delisio et al., 2014).

Some of the most common empirical formulations are reported in Table 8.7.

8.1 Approaches for predicting TBM performance

Barton, 2000	$PR = 5 * Q_{TBM}^{-0.2}$ $Q_{TBM} = \frac{RQD}{J_n} * \frac{J_r}{J_a} * \frac{J_w}{SRF} * \frac{20^9 SIGMA}{F^{10}} * \frac{20}{CLI} * \frac{q}{20} * \frac{\sigma_\theta}{5}$
Bieniawski, 2007	$ARA = 0.422RME_{07} - 11.61$
Cassinelli et al., 1982	$PR = -0.0059RSR + 1.59$
Gong and Zhao, 2009	$BI = 37.06 * UCS^{0.26} * Bi^{-0.10} * (0.84e^{-0.05J_v} + e^{-0.09*\sin(\alpha+30)})$
Hamidi et al., 2010	$FPI = 9.401 + 0.397 * Log\alpha + 0.011 * J_c^2 + 1.14E - 5 * RDQ^3 + 1.32E - 8 * UCS^4$
Hassanpour et al. 2009	$FPI = 0.222BRMR + 2.755$ $FPI = 9.273e^{0.008GSI}$ $FPI = 11.718Q^{0.098}$
Hassanpour et al., 2011	$FPI = exp(0.008UCS + 0.015RQD + 1.384)$ $ROP = \frac{0.06 * 200 * 7}{FPI}$
Innaurato et al., 1991	$PR = \sigma_c^{-0.437} - 0.0437RSR + 3.15$
Ribacchi and Fazio, 2005	$SP = 250 * \sigma_{cm}^{-0.66}$ $\sigma_{cm} = \sigma_c * exp\left(\frac{RMR - 100}{18}\right)$
Yagiz, 2008	$ROP = 1.093 + 0.029 * PSI - 0.003UCS + 0.437 * Log(\alpha) - 0.219 * DPW$
<p>PR = Penetration Rate [m/h]; ROP = Rate of Penetration [m/h]; Bi = Boreability Index [(kN/cutter)/(mm/rev)]; CLI = Cutter Life Index; SP = Specific Penetration [(mm/rev)/(kN/cutter)]; FPI = Field Penetration Index [(kN/cutter)/(mm/rev)]; ARA = Average Rate of Advance; Q = Rock Tunnelling Quality Index; Q_{TBM} = Q-system classification applied to TBM; RMR =Rock Mass Rating; RME = Rock Mass Excavability; BRMR = Basic Rock Mass Rating; GSI = Geological Strength Index; RSR = Rock Structure Rating; UCS = Uniaxial Compressive Strength [MPa]; RQD = Rock Quality Designation [%] (Deere et al., 1967); J_n = Joint Set number; J_r = Joint Roughness number; J_w = Joint Water Reduction factor; J_a = Joint Alteration number; SRF = Stress Reduction Factor; SIGMA = Rock Mass Strength [MPa]; F¹⁰ = average cutter force [tnf]; q = quartz content [%]; σ_θ = average biaxial stress on tunnel face [MPa]; J_v = total number of joints per m³ [m⁻³]; J_c = Rating for Joint conditions; PSI = Peak Slope Index [kN/mm]; DPW = Distance between Planes of Weakness (spacing) [m]; σ_c = rock material uniax. compr. strength [MPa]; σ_{cm} = r. m. uniax. compressive strength [MPa]; α = angle fractures/tunnel axes [deg].</p>	

Table 8.7 Principal empirical predictive models.

8.1.3.1 Selection of the most appropriate model

An empirical predictive model is carried out by analysing the relationship between rock and rock masses features (independent variables) and TBM specification measured on site (dependent variables). The literature proposes a large variety of relationships but it is impossible to know beforehand what kind of correlation occurs in each specific case. For example, in a certain case the relation between UCS and ROP is of a linear type while in other cases it may be nonlinear; furthermore, the parameters involved in a model may be different from those of another one. For these reasons several models are usually developed for the same site, trying different combination of input and different relation type: generally the influence of each independent variable on the dependent ones is evaluated using forward stepwise regression analyses; at this point it is necessary to select the most representative model.

A predictive model is reliable if the measured and the calculated data are comparable. There are different ways to choose a formulation:

- Comparison of different coefficient of determination (R^2). Generally, the model with the higher R^2 is considered the most representative; however, this coefficient increases with the number of inputs. This is why the adjusted coefficient determination, R^2_{adj} , that takes into account the number of independents variables, has to be considered;
- T-test is adopted to evaluate the significance of R^2 for each variable comparing the computed and the tabulated t-value, using the null hypothesis. When the computed value is higher than the tabulated one the null hypothesis (that is a testable statement opposed to the hypothesis considered) is rejected and the R^2 is significant. If the greater value is the tabulated one, null hypothesis cannot be refused, so R^2 is not significant and the model should be modified;
- The significance of the regression is tested by means of the analysis of variance, F-test. If the computed F-value is higher than the tabulated one, the null hypothesis will be refused and that signifies a real relationship between independent and dependent variables and the generated model can be used. Otherwise it is not reliable;
- The statistical significance of a model or of an independent variable involved into a model is also evaluated considering the significance value, p-value. If the p-value is less than the significance level the resulted formulation is considered statistically significant, otherwise a new selection of input and relation type must be carried out. Generally, the statistical level is

8.1 Approaches for predicting TBM performance

fixed at 0.05; in other words, it means that a statistically significant results has less than 5% of occurring from chance;

- Exclusion of a formulation as a consequence of multicollinearity that occurs when two or more independent variables are related. In these cases, erroneous results can be obtained because of the redundancy of input. Multicollinearity is evaluated by means of the variance inflation factor, VIF that is the coefficient of determination of each variable to the others. VIF ranges from 1 to infinity; VIF equal to 1 means no linear relation between independent variables and VIF higher than 10 indicates multicollinearity problems (Montgomery and Peck, 1992);
- Some authors (Johnson and Omland, 2004; Feng and Jimenez, 2015) recommend using a selection criterion able to consider the fitness and the complexity of the model, that is a selection criterion based on information criterion (Akaike information criterion, AIC), the deviance information criterion (DIC, Spiegelhalter et al., 2002; Lunn et al., 2012) and the Bayesian information criterion (BIC);
- Graphical method: finally, as additional test the predicted and the measured parameters (as ROP or AR) are plotted on the same Cartesian plane. The empirical model is more able to predict the TBM performances more the calculated and the measured data are closely aligned on the bisector. The Figure 8.1 shows a reliable equation (point closely aligned on the bisector) and an equation that must be refused (calculated and observed data are not comparable).

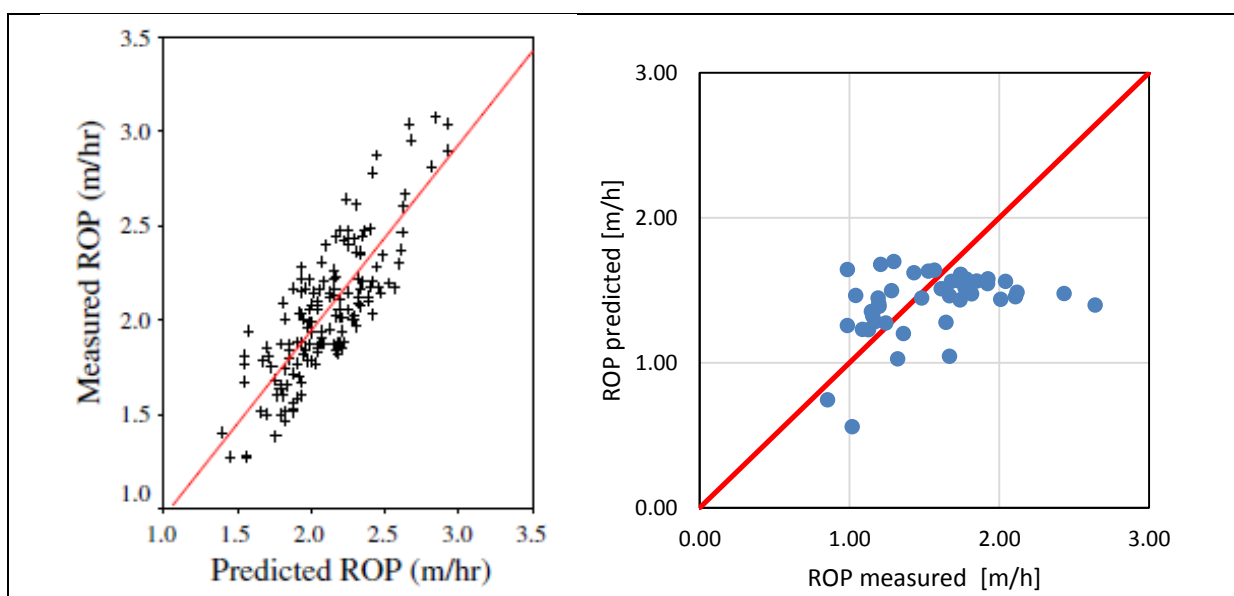


Figure 8.1 Graphical results of reliable equation, on the left (Yagiz, 2007) and not reliable one on the right.

Table 8.8 shows the principal theoretical and empirical predictive model proposed in literature. For each of them the intact rock, rock mass and machine considered parameters are specified.

It is observable that there is a high utilisation of mechanical rock properties and rock masses site characteristics and a low frequency of machine indices is registered.

Uniaxial compressive strength is the most involved parameter, both for its easy determination and representativeness. Great importance is given to the joint sets both in terms of frequency (RQD and spacing) and of their orientation in comparison the tunnel's one.

The largest part of models, in particular the empirical group, does not take into account TBM or cutter specifications to carry out predictive formulation. However, given that also machine features influence the excavation processes, some models consider them and provide a most complete study of all parameters implicated in the boring (CSM, 1993; Gehring, 1995; NTNU, 1998).

The most relevant models and the parameters that they involve have been listed in Table 8.8.

8.1 Approaches for predicting TBM performance

8.1.4 Final observation about theoretical and empirical predictive models

In the table reported in the following page (Table 8.8), the most adopted theoretical and empirical TBM performance predictive models have been listed with the purpose of showing what parameters are more frequently considered into TBM performance prediction equations.

13 studies have been considered and the most of them is based on the empirical approach.

As for intact rock parameters the most utilized is the uniaxial compressive strength followed by the abrasivity index and the quartz content. Other parameters are sometimes considered, such as the Brazilian tensile strength and the peak slope index.

The most frequently considered rock mass features are fragmentation, expressed both by means of spacing and RQD, and the angle between the most relevant set of discontinuities and the orientation of tunnel.

The machine specifications which are more frequently taken in consideration by theoretical and empirical approaches are the diameter of machine, the force acting on cutterhead and the number of cutter.

The most carried out indices are the net penetration rate, the advance rate, FPI and coefficient of utilization are less evaluate.

Barton, CSM and NTNU are the models that involve the largest quantity of rock, rock mass and machine related parameters.

8.1 Approaches for predicting TBM performance

8.1.5 Artificial intelligence techniques for predicting TBM performance

Apart from the theoretical and empirical models, artificial intelligence technique (AI) has been introduced to predict the TBM performance by several researches (Alvarez Grima et al., 2000; Benardos and Kaliampakos, 2004; Yagiz et al., 2009; Yagiz and Kaharan, 2011; Mahdevari et al., 2014; Ghasemi et al., 2014).

Artificial intelligence techniques include:

- Artificial neural network, ANN;
- Particle swarm optimization, PSO;
- Support vector machine;
- Fuzzy logic.

Many authors developed hybrid algorithms such as neuro-fuzzy or PSO-ANN: the aim is to improve the performance of the artificial neural network through the use of algorithms of optimization such as PSO, generic algorithm, GA, or the imperialism competitive algorithm, ICA (Alvarez Grima et al., 2000; Bashir and El-Hawary, 2009; Lin and Hsieh, 2009; Yagiz and Karahan, 2011; Marto et al., 2014; Gordan et al., 2016).

The AI techniques are very flexible and this aspect makes them powerful tools in solving geotechnical problems, in particular when the problem is complex and nonlinear (Armaghani et al., 2017).

8.1.5.1 Artificial Neural Network ANN

Artificial neural network methods are simplified mathematical models that have the purpose of simulating some organisational principles of the nervous system. In tunnelling ANN methods are adopted to predict TBM performances. ANN is able to learn automatically, from provided training patterns, to find the relationship between input and output data (Zurada, 1992).

The constitutive elementary units of an ANN system are the artificial neurons (or nodes): they develop a process of information very similar to the biological brain ones. The elementary units are interconnected in a predefined topology known as layer and neurons work in parallel layers (Alvarez Grima et al., 2000).

Usually, neural network topology is composed by input layer, inner layers and output layer. It is possible to train the network and during the training process the architecture of network and connection weights are modified in order to reduce the output error respecting every output layer node (Armaghani et al., 2017).

On the basis of the network architecture ANN methods are divided into two groups: the feed-forward and the feed-back respectively. Generally speaking, hidden and output neurons are able to accomplish some specific activation functions of network input with the purpose to produce neuron outputs. Each neuron output is considered as input of the next neuron layer. Mathematical equations are able to give the total net input and output to every hidden or output neuron.

Among all artificial intelligence technique, ANN (in combination with other adjusting algorithm, have received great attention because of they are able to solve several geotechnical problems (Momeni et al., 2014; Gordan et al., 2015).

8.1 Approaches for predicting TBM performance

8.1.5.2 Particle swarm optimization

Kennedy and Eberhart in 1995 first developed a sub-field of the swarm and computational intelligence called particle swarm optimization, PSO. It is an optimization algorithm and it has been inspired by the behaviour of some animals (like fish and birds) with regards to food acquisition in nature (Yang, 2010; Brownlee, 2011; Armaghani et al., 2014, 2015). PSO has the advantage of being easier than the other swarm intelligence algorithm. That is because PSO does not consider mutation/crossover and pheromone, as other algorithms do, and it utilizes the real-number and the global communication between swarm particles (Kennedy and Eberhart, 1995). In particle swarm optimization algorithm, the particles (that are the entries) are scattered in the space of objective function (Armaghani et al., 2017).

The algorithm aims to put the particles in optimal spaces; the particles move inside the global current towards their own best position. Figure 8.2 schematically represents the movement of particles in PSO, x_i is the current best for the specific element i and p' is the global best.

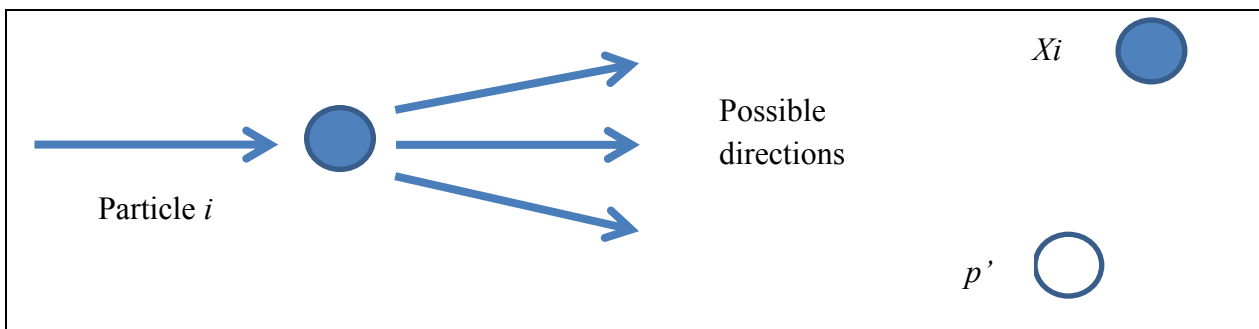


Figure 8.2 Representation of the movement of particles in PSO.

After moving, an element finds a better location than the previous one and the algorithm stops after a certain number of interactions (Armaghani et al., 2017). PSO algorithm is commonly used to predict TBM performance: in this way one of the most important studies was conducted by Yagiz and Karahan in 2011. PSO is usually utilized to optimize the artificial neural network, so ANN and PSO are frequently adopted in combination.

Atashpaz-Gargari and Lucas in 2007 developed one of the best optimizing algorithms available in science and engineering field: the imperialism competitive algorithm, ICA.

For the sake of brevity, in this text the explanation of ICA is not provided. ICA procedure can be seen in other works such as Atashpaz-Gargari et al., 2008; Marto et al., 2014; Armaghani et al., 2015, 2017.

8.1.5.3 *Hybrid techniques*

Many researchers (Alvarez Grima et al., 2000; Bashir and El-Hawary, 2009; Lin and Hsieh, 2009; Gordan, 2015; Armaghani et al., 2017) have developed the so called “Hybrid technique” with the purpose of overcoming the limitations that affect the singular techniques. For example, many algorithms (genetic algorithm and optimization one) are often combined with ANN in order to predict penetration rates with more accuracy.

Alvarez Grima et al. (2000) combined logic and numeric method, the logical component consists of fuzzy set and the numerical one consists of neural network and data analysis (Figure 8.3).

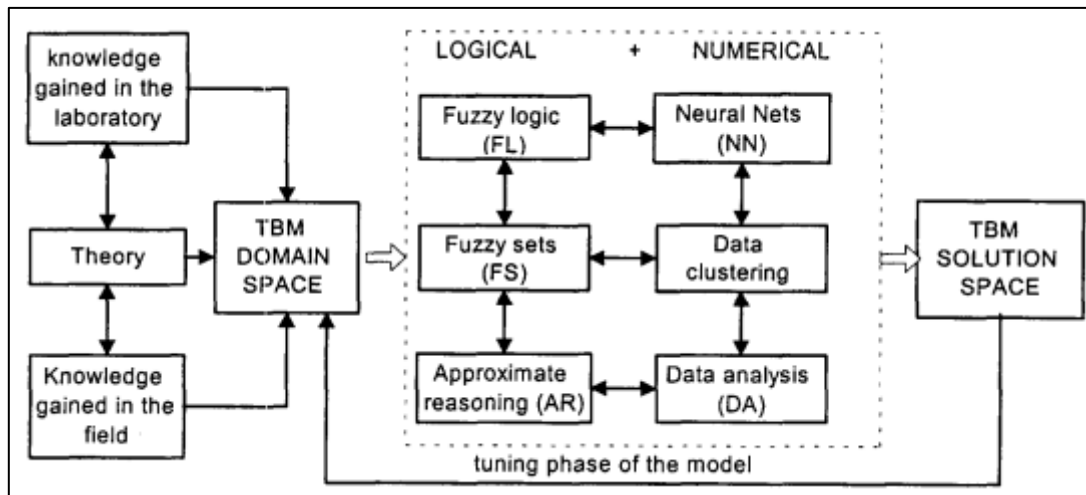


Figure 8.3 Neuro-fuzzy modelling technique (Alvarez Grima et. al, 2000).

Logical component takes into account fuzzy logic, fuzzy sets and approximate reasoning, whereas artificial neural network considers neural nets, data clustering and data analysis, as it is schematised in Figure 8.3.

Fuzzy logic component allows to incorporate expert knowledge, dealing with uncertainty and imprecision, making decision and performing inference. On the other hand, ANN permits to recognise patterns and to adapt methods in case of environment changes (Jang et al. 1997).

8.1 Approaches for predicting TBM performance

8.1.6 Final observation about artificial intelligence technique

Table 8.9 reports the most utilised artificial intelligence predictive methods, summarised with the purpose of showing what parameters are more frequently considered into TBM performance prediction calculation.

Seventeen studies have been considered and the majority of them is based on the artificial neural network technique.

As for intact rock parameters the most utilized is the uniaxial compressive strength followed by the Brazilian tensile strength and by the rock brittleness index. Other parameters are sometimes involved such as the quartz content and the peak slope index.

The most frequently considered rock mass features are fragmentation (expressed by means of spacing and RQD) and the angle between the most relevant set of discontinuities and the orientation of tunnel.

The machine specifications are less considered than rock-rock mass one and some models (Torabi et al., 2013; Yagiz and Karahan, 2011, 2015; Yagiz, 2009; Yavari Mahdavi 2005) do not consider any TBM characteristic. The other ones involve cutter geometry features and operational parameters.

The most carried out index is the net penetration rate, whilst the advance rate and coefficient of utilization are less frequently evaluated.

8.1 Approaches for predicting TBM performance

REFERENCES	TECHNIQUE			ROCK INPUT														TBM INPUT							OUTPUT					
				INTACT ROCK PARAMETERS						ROCK MASS PARAMETERS																				
	ANN	FIS	other	UCS	BTS	PSI	BI	q	p	RQD	DPW	α	J _c	RMW	W	RMR	depth	other	Ø _m	Ø _c	N	TF	CT	RPM	RS	SE	PR	AR	UI	
			[MPa]	[MPa]	kN/mm	[MPa]	[%]	[m ²]	[%]	[m]	[deg]	[-]	[-]	[m]	[-]	[m]		[m]	[mm]	[-]	[kN]	[kNm]	rev/min	[m/s]	[J/kg]	[m/h]	[m/h]	[%]		
Alvarez Grima et al. (2000)			ANFIS																											
Benardos and Kaliampakos (2004)																														
Eftekhari et al. (2010)																														
Ghasemi et al. (2014)																														
Gholami et al. (2012)																														
Gholamnejad and Tayaran (2010)																														
Mahdevari et al. (2014)			SVR																											
Mikaeil et al. (2009)																														
Orace et al. (2012)			ANFIS																											
Salimi and Esmaeili (2013)																														
Shao et al. (2013)			ELM																											
Simoes and Kim (2006)																														
Torabi et al. (2013)																														
Yagiz and Karahan (2011)			PSO																											
Yagiz and Karahan (2015)																														
Yagiz et al. (2009)																														
Yavari and Mahdavi (2005)																														
FREQUENCY	10	3	6	16	6	3	6	1	1	7	12	9	1	1	2	3	1	2	1	1	1	2	2	1	1	1	15	2	2	

ANN = artificial neural network; FIS = fuzzy inference system; ANFIS = neuro – fuzzy inference system; SVR = support vector regression; ELM extreme learning machine; PSO = particle swarm optimization; UCS = Uniaxial Compressive Strength [MPa]; BTS = Brazilian Tensile Strength [MPa]; PSI = Peak Slope Index [kN/mm]; BI = Brittleness Index [MPa]; q = quartz content [%]; p = porosity [m²]; RQD = Rock Quality Designation [%]; DPW = Distance between Planes of Weakness [m]; α = angle between fractures and tunnel axes [deg]; J_c = Rating for Joint conditions; RMW = Rock Mass Weathering [-]; W = position water table; RMR = Rock Mass Rating (Bieniawski, 1989); depth = tunnel depth [m]; Ø_m = TBM diameter [m]; Ø_c = cutter diameter [mm]; N = number of cutter [-]; TF = Total Force to the cutterhead [kN]; CT = Cutterhead Torque [kNm]; RS = Rotational Speed [m/s]; SE = Specific Energy [J/kg]; PR = Penetration Rate [m/h]; AR = Average Rate; UI = Utilization Index [%]; (other: ν = Poisson ratio [-], ϕ = friction angle [deg]).

Table 8.9 List of intact rock, rock mass and machine parameters involved in the most relevant artificial intelligence predictive techniques.

8.2 Evaluation of various TBM performance prediction models based on field data from “La Maddalena” tunnel

Various approaches for predicting field penetration index, FPI, penetration rate, PR or ROP, specific penetration, SP, and other machine performance parameters have been developed by several researchers as mentioned in the previous paragraphs.

In this section, an evaluation of existing performance prediction model will be presented; this evaluation is based on field data from “La Maddalena” tunnel with the purpose of testing the prediction capability of some of the more frequently involved formulations.

Fourteen predictive equations have been selected, based on the availability of required parameters.

The models have been tested on the tunnel sector ranging between Pk. 198 m and 2010 m. This length, as previously described, is subdivided into 186 sections.

The prediction capability of existing models is graphically evaluated; the actual and the calculated machine parameter are plotted into a graph where the bisector line represents the line where the predicted and measured indices are the same. If the plotted points are close to the dashed line, the model is reliable and it is good at predicting TBM performance. If plotted points are under or over the line, the formulation tends to underestimate or overestimate the machine performance, respectively.

The percentage of prediction error has been calculated for each rock section by means of the following equation:

$$E(\%) = \left| \frac{\text{Measured Performance Index} - \text{Predicted Performance Index}}{\text{Measured Performance Index}} \right| \quad (8.1)$$

The error distribution has been evaluated along the investigated tract.

8.2.1 Cassinelli et al. (1982) model

Cassinelli et al. (1982) used Rock Structure Rating (Wickham et al. 1972) and the observed TBM performances to develop an empirical predictive method. They carried out the following equation:

$$PR = -0.0059 * RSR + 1.59 \quad (8.2)$$

where RSR is empirically derived from RMR by means of 8.3, Bieniawski (1989):

$$RSR = 0.77 * RMR + 12.40 \quad (8.3)$$

This formulation has been involved to compute the theoretical TBM performance for “La Maddalena” tunnel; it tends to underestimate the actual penetration per revolution rates, as shown in Figure 8.4.

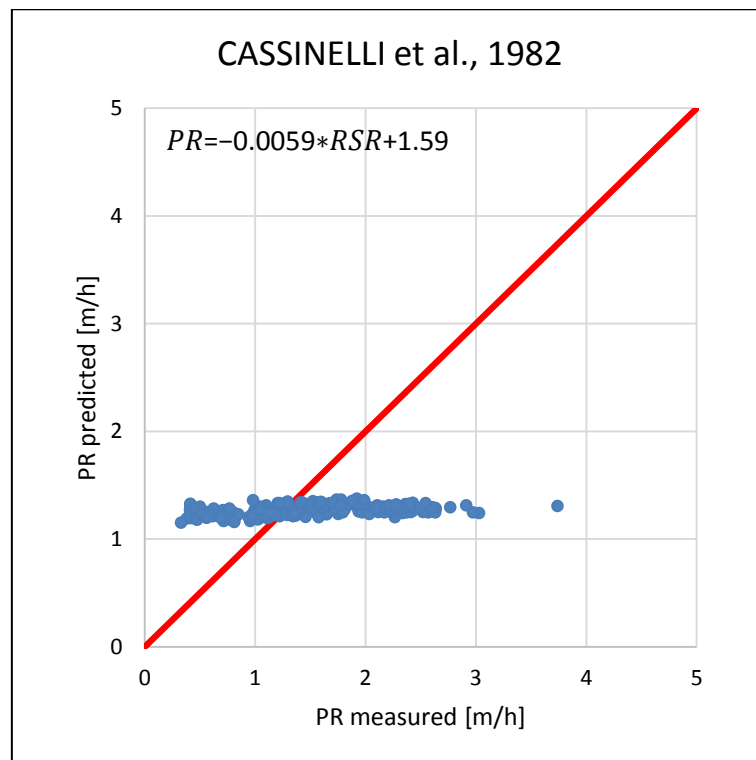


Figure 8.4 Comparison between the measured and predicted PR from the Cassinelli et al., (1982) model.

The results obtained in this study have been compared with the results carried out by the research conducted by Farrokh (Figure 8.5).

8.2 Evaluation of various TBM performance prediction models based on field data from “La Maddalena” tunnel

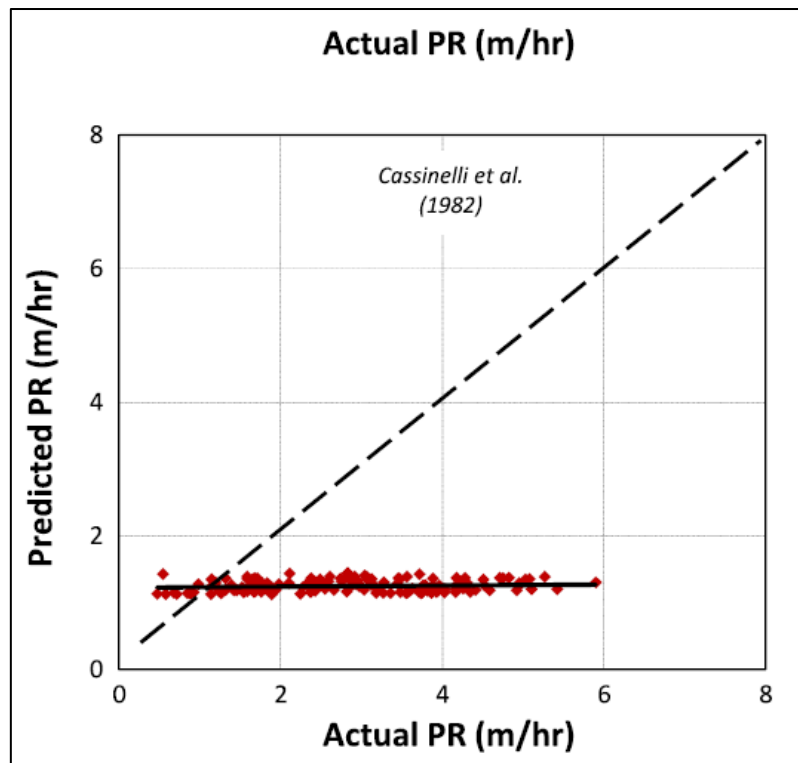


Figure 8.5 Result of comparison for Cassinelli et al., 1982 model. Farrokh et al., 2012.

It is observable that the Cassinelli model produced the same type of prediction both for “La Maddalena” and Farrokh database tunnels.

The predicted value of PR is always the same; it could be due to the fact that RSR is derived by means of an empirical formulation, and not obtained by direct site investigation. Equation 8.3 probably is not appropriate to evaluate RSR about La Maddalena rock mass.

Moreover, the value of RSR, empirically obtained, is more or less constant through the investigated tunnel length, for this reason, the predicted PR results constant, given that RSR is the unique independent variable of the model.

8.2.2 Innaurato et al. (1991) model

Innaurato et al. (1991) modified the model proposed by Cassinelli et al. (1982) by including UCS. The utilized database consists of 19 km bored in five tunnels excavated in igneous, sedimentary and metamorphic rocks with UCS values in the range 50-150 MPa. They found a strong relation between PR, uniaxial compressive strength and rock structure rating, RSR, as reported in Equation 8.4:

$$PR = UCS^{-0.437} - 0.047 * RSR + 3.15 \quad (8.4)$$

where RSR has been calculated according to Equation 8.3

The machine performance parameter carried out is PR, measured in m/h.

The prediction results carried out by means of Equation 8.4 are reported in Figure 8.6.

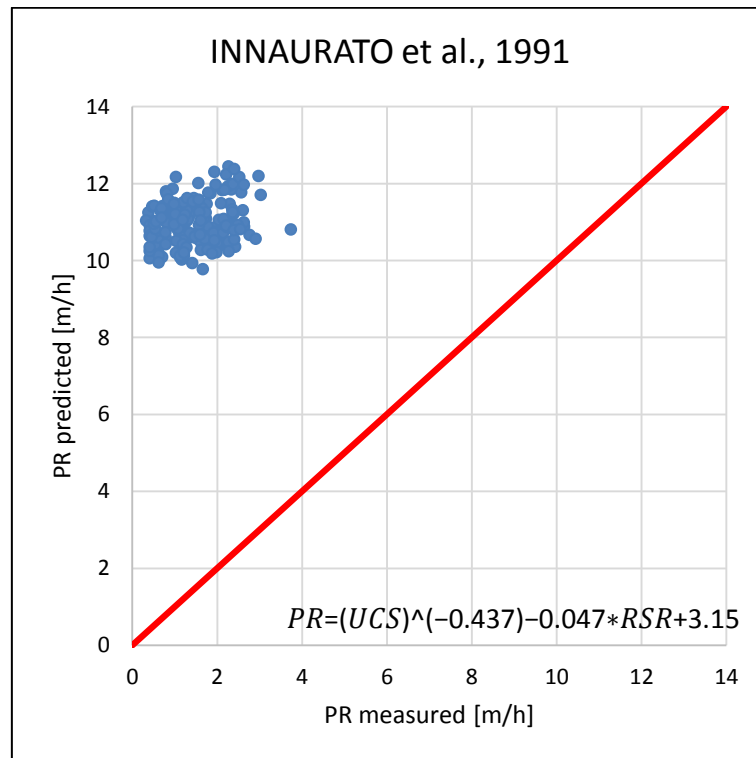


Figure 8.6 Comparison between the measured and predicted PR from the for Innaurato et al. (1991) model.

The formulation proposed by Innaurato tends to overestimate the actual TBM performances of “La Maddalena” tunnel; all points are clearly plotted above the bisector line. The use of RSR as an independent variable implies the same limitations discussed in section 8.2.1.

8.2 Evaluation of various TBM performance prediction models based on field data from “La Maddalena” tunnel

The median value of the percentage of error (evaluate according to Equation 8.4) is equal to 278.16%.

Sapigni et al. (2002) use the Innaurato model to compute the theoretical PR for Mean, Pieve and Varzo tunnels in Italy and then compared them with the recorded ones. They observed that the predicted parameters are much higher than the registered ones (Figure 8.7 left). Farrokh (2012) used the Innaurato model to predict the TBM performance for more than 300 tunnels and observed an underestimation of penetration rates (Figure 8.7 right).

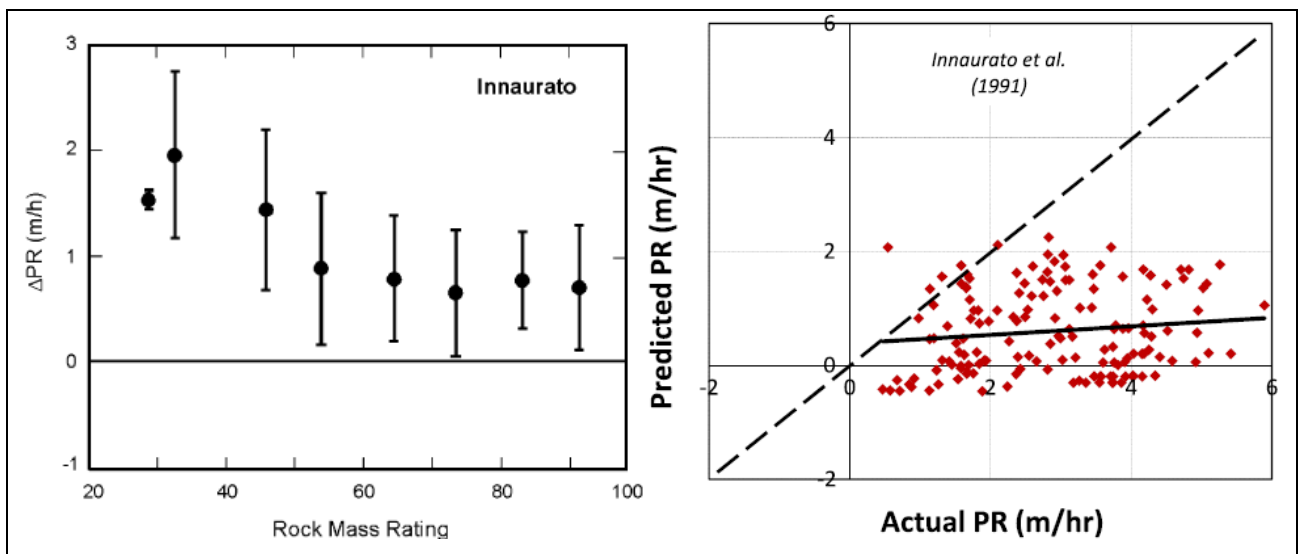


Figure 8.7 Difference between actual and predicted penetration rates for the Innaurato model. Left Sapigni et al. (2002); right Farrokh et al. (2012).

Farrokh asserts that one of the potential problems that affects the Cassinelli and the Innaurato models may be the absence of any parameters able to take into account the TBM diameter (Farrokh et al., 2012). Generally, if the diameter of TBM is large, the penetration rates will be lower than in those of small machines.

The empirical formulation proposed by Innaurato cannot be used to predict the TBM performance in “La Maddalena” tunnel and it could not be adopted to estimate the penetration rates both in the tunnels studied by Sapigni and by Farrokh.

8.2.3 Khademi Hamidi et al. (2010) models

Khademi Hamidi et al. (2010) collected rock mass and TBM performance data about 8.5 km of the Zagros tunnel excavated in sedimentary rocks by means of double shield TBM. Authors carried out linear and nonlinear multiple regression analysis based on RMR system and the angle between the principal set of discontinuities and tunnel axes, α .

8.2.3.1 Linear model

“La Maddalena” parameters have been entered in the linear type equation (Equation 8.6) proposed by Khademi Hamidi et al. (2010).

$$FPI = 4.161 + 0.091 * UCS + 0.077 * RQD + 0.117 * JC + 1.077 * Log\alpha \quad (8.6)$$

RQD related to La Maddalena rock mass has been empirically calculated by means of the equation proposed by Palmström, 1982, (Equation 5.19: $RQD=115-3.3*J_v$).

The comparison between actual and computed FPI has been plotted in Figure 8.8.

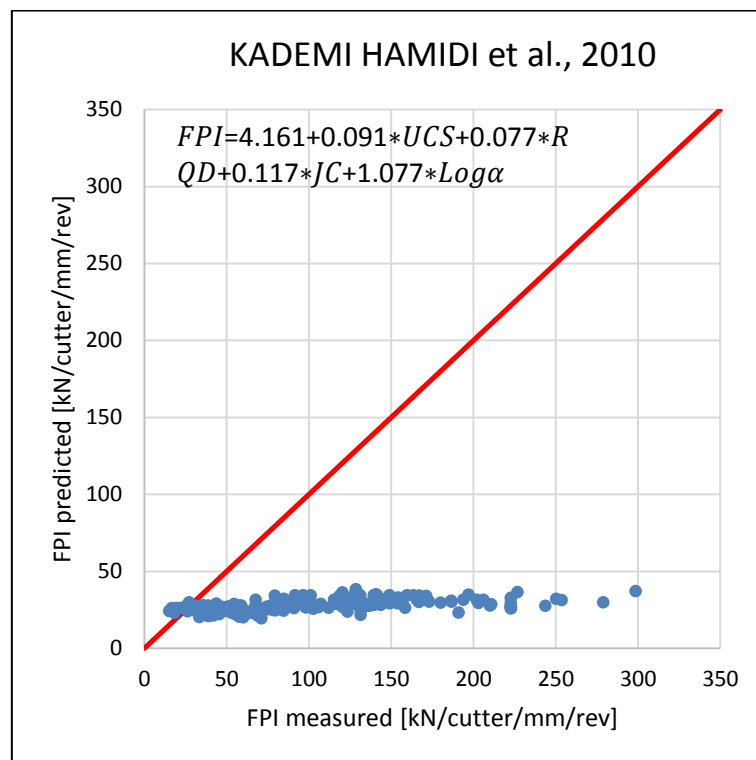


Figure 8.8 Comparison between the measured and predicted FPI from the Khademi Hamidi et al (2010) linear model.

The formulation (8.6) proposed by Khademi Hamidi et al. (2010) is not able to estimate the actual performance of “La Maddalena” TBM.

8.2 Evaluation of various TBM performance prediction models based on field data from “La Maddalena” tunnel

8.2.3.2 Nonlinear models

Khademi Hamidi et al. (2010) proposed also nonlinear formulation, exponential (Equation 8.7) and polynomial (Equation 8.8) type respectively.

$$FPI = EXP(1.995 + 0.004 * UCS + 0.005 * RQD + 0.01 * Jc + 0.068 * Log\alpha) \quad (8.7)$$

$$FPI = 9.401 + 0.397 * Log\alpha + 0.011 * Jc^2 + 1.14E - 5 * RQD^3 + 1.32 - 8 * UCS^4 \quad (8.8)$$

The prediction results obtained by means of Equation 8.7 and Equation 8.8 are reported in Figure 8.9 and Figure 8.10 respectively.

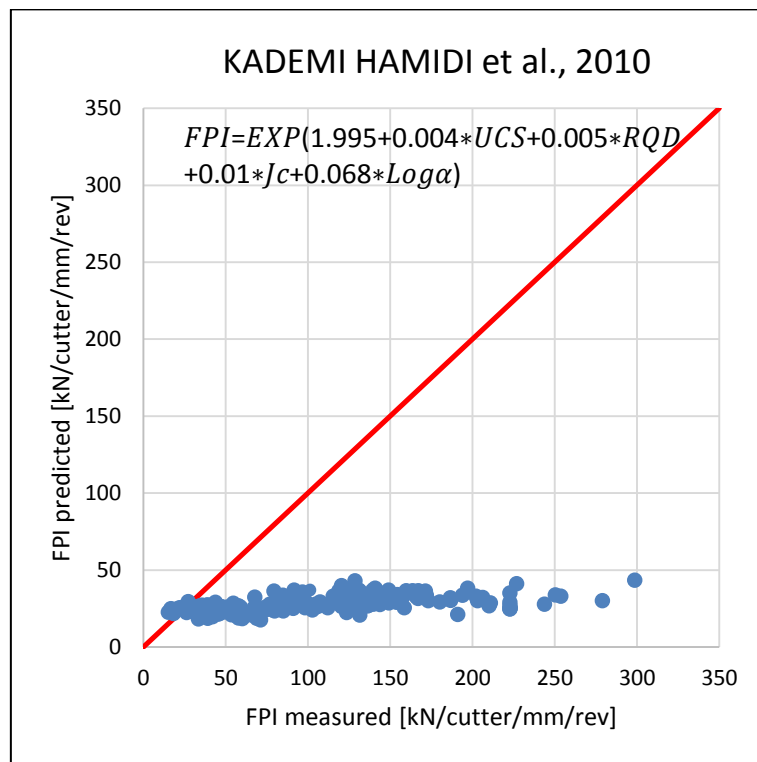


Figure 8.9 Comparison between the measured and predicted FPI from the Khademi Hamidi et al. (2010) exponential model.

8.2 Evaluation of various TBM performance prediction models based on field data from “La Maddalena” tunnel

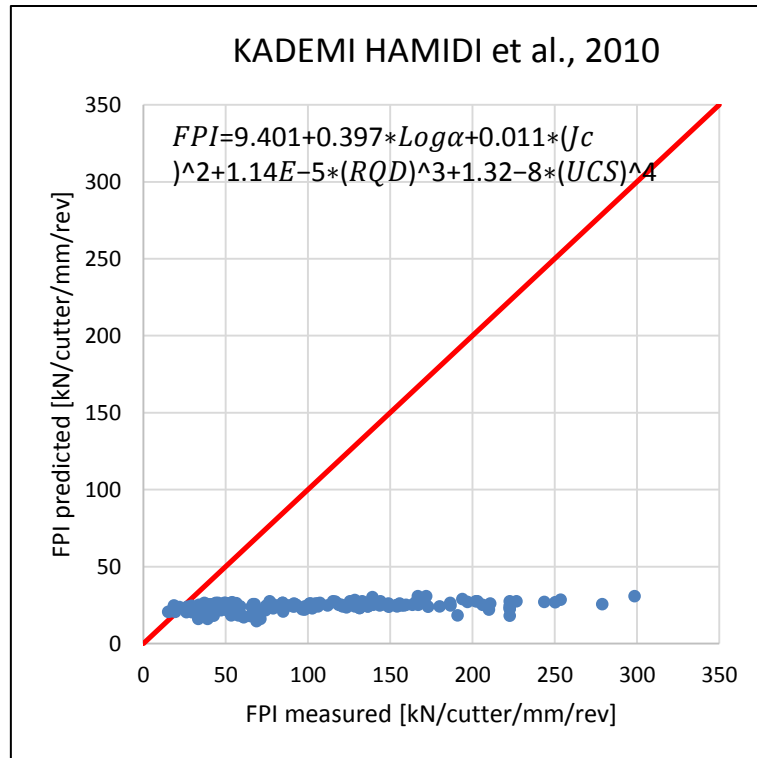


Figure 8.10 Comparison between the measured and predicted FPI from the Khademi Hamidi et al. (2010) polynomial model.

The median percentage of error relative to Equation 8.7 and 8.8 prediction is equal to 68.19% and 73.32% respectively. Both the exponential and polynomial formulations proposed by Khademi Hamidi et al. (2010) are not able to predict the actual TBM performance in the case of “La Maddalena”. In all three cases a significant inability in prediction can be observed. RQD is empirically calculated and it could determine the reliability of input data.

Farrokh et al. (2012) evaluated these models based on field data from more than 300 tunnels and an overestimation of penetration rate can be observed, Figure 8.11.

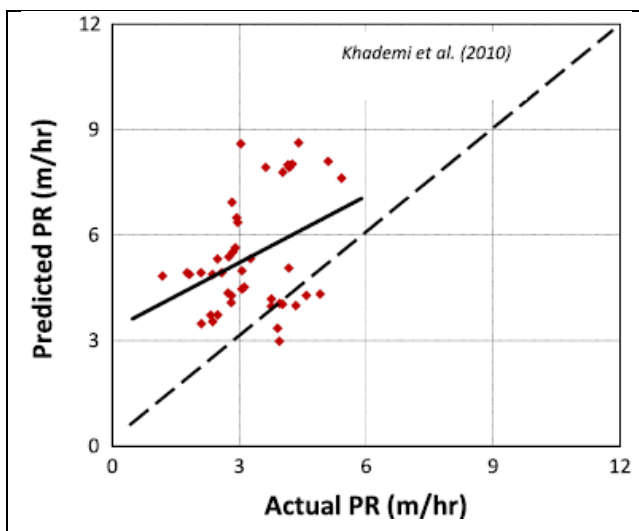


Figure 8.11 Result of comparison for Khademi Hamidi et al. (2010) linear model carried out by Farrokh et al. (2012) based on field data from more than 300 tunnels. Farrokh et al. (2012).

8.2 Evaluation of various TBM performance prediction models based on field data from “La Maddalena” tunnel

8.2.4 Hassanpour models

Hassanpour et al., carried out four empirical predictive equations based on four different tunnel projects, each of them realized in different geological and mechanical conditions; Authors developed a “general model” on the basis of these four models.

8.2.4.1 Zagross tunnel

In 2009 Hassanpour et al., the researchers analysed the Zagross water conveyance tunnel excavation, in Iran. The tunnel passes through the Zagross Simply folded zone and the encountered lithologies are limestone, shale and limy shales belonging to the Carbonate-Argillaceous rocks of Padbeh, Gurpi and Ilam Formations (Hassanpour et al., 2009). The UCS values range from 15 to 150 MPa and the maximum overburden is 650 meters. The excavation was realized by means of a double shield TBM. The empirical equation (Equation 8.9) carried out by Hassanpour et al. (2009) allows to predict FPI:

$$FPI = \exp(0.004 * UCS + 0.008 * RQD + 2.077) \quad (8.9)$$

“La Maddalena” FPI values have been calculated according the previous formula, then the predicted and measured values have been compared (Figure 8.12).

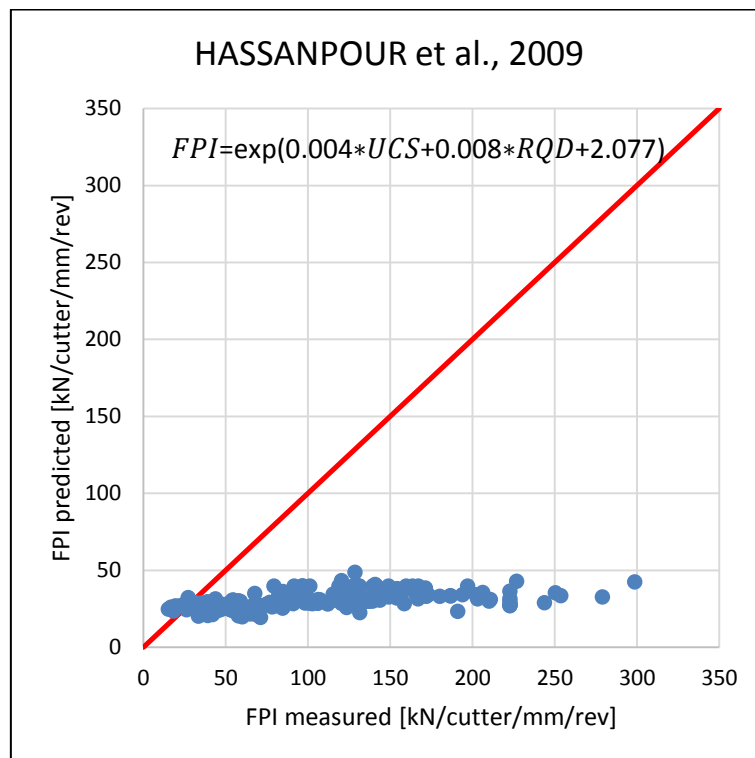


Figure 8.12 Comparison between the measured and predicted FPI from the Hassanpuor et al. (2009) exponential model.

8.2 Evaluation of various TBM performance prediction models based on field data from “La Maddalena” tunnel

The median of percentage of error generated by using Equation 8.9 in predicting “La Maddalena” performance is 64.42%.

The inability of this method to predict “La Maddalena” FPI values is probably due to the different lithology of excavated rock masses and to the different (lower) UCS range.

8.2.4.2 Karaj tunnel

Karaj water conveyance tunnel, Iran, is located in Central Alborz geological zone and passes through the pyroclastic rocks of Karaj formation that consist of tuffs, agglomerate, shaly and sandy tuffs. The UCS values range from 30 to 150 MPa and the maximum overburden is 600 meters.

The excavation is realized by means of a 4.65 m in diameter double shield TBM (Hassanpour et al., 2010). Hassanpour et al., collected and analysed rock mass and TBM parameters and developed a new predictive model in order to predict FPI. The following equation was carried out:

$$FPI = \exp(0.005 * UCS + 0.002 * RQD + 2.129) \quad (8.10)$$

The previous formula (Equation 8.10) has been used to calculate “La Maddalena” FPI values, the error that affects the prediction is defined by a median value equal to 75.98%. The calculated and measured values have been compared (Figure 8.13).

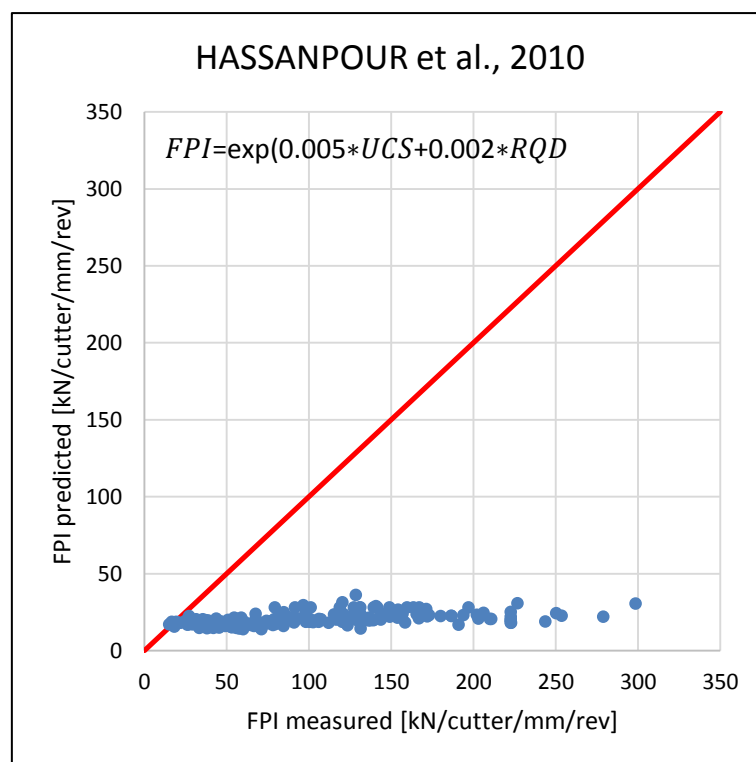


Figure 8.13 Comparison between the measured and predicted FPI from the Hassanpuor et al. (2010) exponential model

8.2 Evaluation of various TBM performance prediction models based on field data from “La Maddalena” tunnel

In this case too, the formulation proposed by Hassanpour et al. (2010) tends to underestimate the actual values of FPI about “La Maddalena” tunnel.

This lack is probably due to different lithology of excavated rock masses and to the different (lower) UCS range.

8.2.4.3 Ghomrood tunnel

Ghomrood water conveyance tunnel (Iran) is 24.5 km length and passes through the Sanandaj-Sirjan metamorphic belt characterized by Jurassic metamorphic rocks (low to medium grade) and Cretaceous limestone.

The encountered lithologies are limestone, shale, slate, sandstone, phyllite and schist with quartzitic veins (Hassanpour, 2010). The tunnel is constructed by means of a double shield TBM (4.52 m in diameter), it is 700 meters deep (maximum value).

The minimum value of UCS is 25 MPa and the maximum one is 150 MPa (Hassanpour, 2010).

Hassanpour analysed both geological-geomechanical features and TBM parameters in order to obtain an empirical predictive equation to pre-estimate FPI index, he proposed the following formula:

$$FPI = \exp(0.004 * UCS + 0.023 * RQD + 1.003) \quad (8.11)$$

The proposed formulation (Equation 8.11) has been utilized to predict FPI of “La Maddalena” tunnel. The error calculated for this model is 53.84%. The comparison between measured and predicted FPI values is shown in Figure 8.14.

8.2 Evaluation of various TBM performance prediction models based on field data from “La Maddalena” tunnel

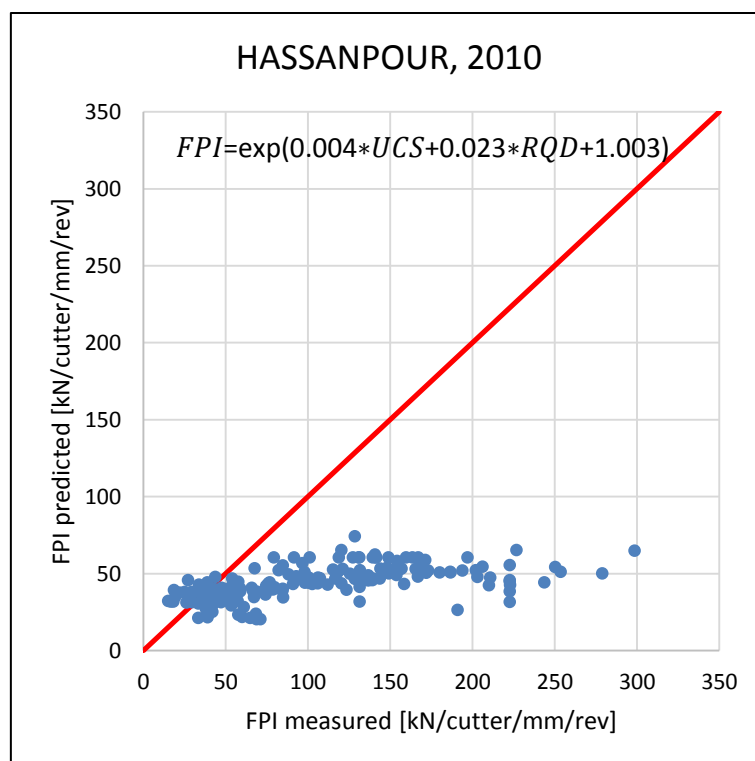


Figure 8.14 Comparison between the measured and predicted FPI from the Hassanpuor (2010) exponential model.

The comparison between actual and computed FPI values gives a result similar to the previous ones: a significant underestimation is induced.

8.2.4.4 Manapouri tunnel

Manapouri Second Trailrace tunnel in New Zeland is excavated into gneiss, intrusive rocks like gabbro and diorite, calc-silicate and quartzite belonging to the Paleozoic metamorphic and igneous rocks of the Fiordland Complex (Hassanpour et al., 2011). The encountered rocks are characterised by UCS values ranging from 100 to 225 MPa.

Tunnel maximum deep is 1200 meters from surfaces. The excavation is realized by means of a main beam open TBM, 10 meters in diameters.

In this case study Authors carried out a new equation to predict TBM performance, it is as follows:

$$FPI = \exp(0.005 * UCS + 0.020 * RQD + 1.644) \quad (8.12)$$

Equation 8.12 has been involved to predict FPI of “La Maddalena” tunnel and the comparison between measured and predicted values is shown in Figure 8.15.

8.2 Evaluation of various TBM performance prediction models based on field data from “La Maddalena” tunnel

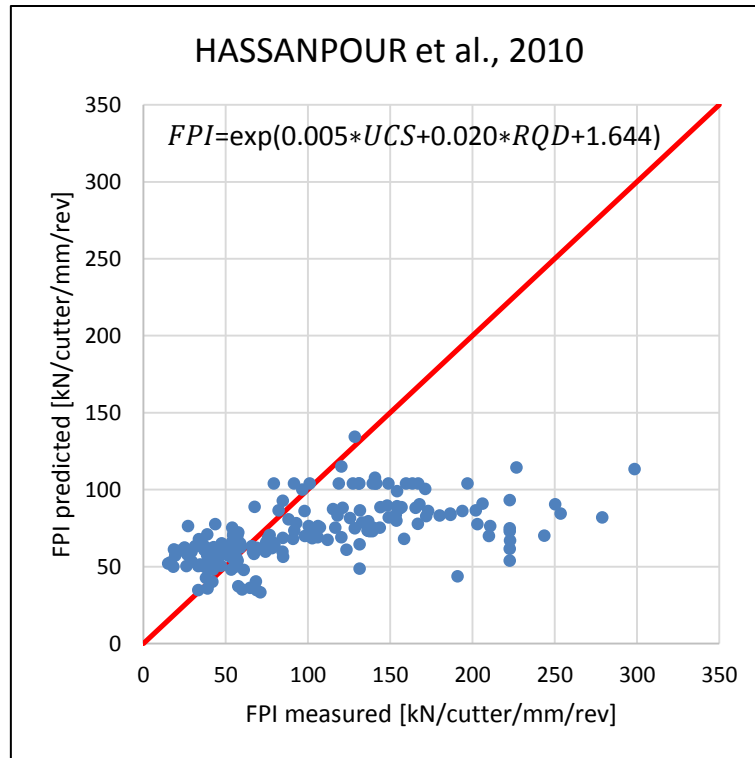


Figure 8.15 Comparison between the measured and predicted FPI from the Hassanpuor et al. (2010) exponential model.

The plot shows that there is a group of points plotted close to the bisector line. This means that in some cases the proposed formulation has been able to predict FPI, however this method cannot be used to calculate the TBM performance of “la Maddalena” because in several cases they are underestimated. The error in prediction (35.79%) is much more reduced in comparison to the other models.

8.2.4.5 Hassanpour general method

As it is known, predictive models are usually specific-site, they are carried out for specific condition and they cannot be used to predict TBM performance in conditions different from those in which they have been produced. For this reason, data from the previous projects with different rock mass features were collected and compiled in a database in order to develop a more accurate TBM performance prediction model that can be used in different geological and geotechnical conditions.

Hassanpour et al., in 2011, developed a model based on Zagross, Karaj, Ghomrood and Manapouri Tunnels database.

A multivariable regression analysis was used to relate the machine parameters and the geological ones.

8.2 Evaluation of various TBM performance prediction models based on field data from “La Maddalena” tunnel

As a result, an empirical equation was introduced; it is as follows:

$$FPI = \exp(0.008 * UCS + 0.015 * RQD + 1.384) \quad (8.13)$$

Equation 8.13 has been used to predict PFI for “La Maddalena” tunnel, and calculated and actual FPI have been compared, an error in prediction equal to 48.00% has been observed. The result is shown in Figure 8.16:

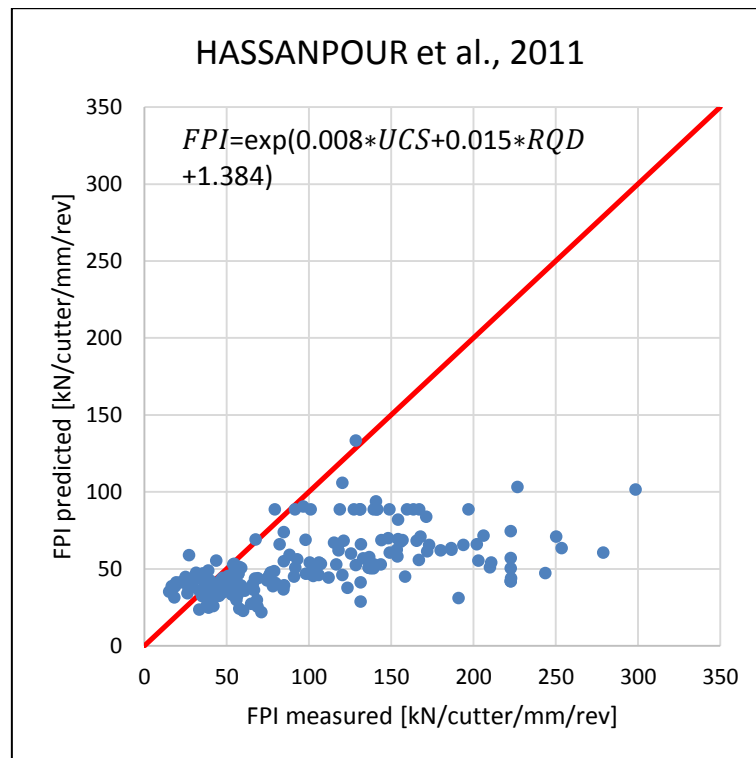


Figure 8.16. Comparison between the measured and predicted FPI from the Hassanpuor et al. (2011) exponential model.

In some cases, the FPI values are correctly predicted applying the previous formulation, in other cases there is an underestimation in prediction. In particular low FPI are best predicted than higher one.

The error that affects predictions is defined by a median values equal to 44.19%.

Authors developed a new formulation (Equation 8.14) in order to calculate ROP, based on FPI, by assuming practical values for:

- Average disc cutter load, $F_n = 200$ kN/cutter;
- Revolution per Minute, RPM = 7 rev/min.

8.2 Evaluation of various TBM performance prediction models based on field data from “La Maddalena” tunnel

ROP is calculated as:

$$ROP = \frac{0.06 * 200 * 7}{FPI} \tag{8.14}$$

The FPI measured at “La Maddalena” tunnel has been involved in Hassanpour predictive formulation, then computed and registered values have been compared, the error in calculation is reduced (30.96%).

The result of comparison is shown in Figure 8.17.

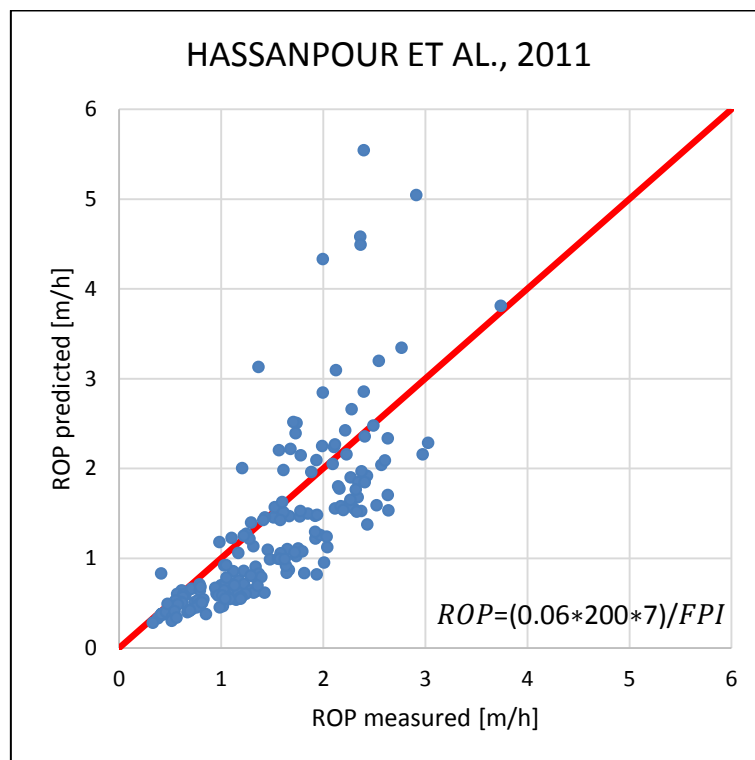


Figure 8.17 Comparison between the measured and predicted ROP from the Hassanpuor et al. (2011) linear model.

As it can be seen, the equation proposed by Hassanpour is able to calculate ROP with accuracy. Most of the points are plotted close to 1:1 line (bisector) and the measured and the predicted ROP are very similar.

8.2.5 Delisio et al., models

Delisio et al. (2013, 2014) developed TBM predictive models for jointed rock masses, where “blocky conditions” occur. They introduced a new TBM performance index, the FPI_{blocky} .

FPI_{blocky} is defined according to:

$$FPI_{blocky} = \frac{FN}{p} \quad (8.15)$$

where FN is the TBM thrust force [kN] and p is the penetration per revolution [mm/rev].

Authors proposed a deviation from standard definition of the Field Penetration Index, which is as follows:

$$FPI = \frac{Fn}{p} \quad (8.16)$$

where Fn is the average cutter load [kN/cutter].

Delisio proposed to consider TBM thrust force, FN, instead of average cutter load, Fn, where blocky conditions are verified. The modification of standard FPI definition is justified by Authors by the fact that especially in blocky rock masses tunnel face is not regular and plane so not all cutters are in contact with the face. If some discs are not in contact with the rock, the load will be distributed on the cutters touching the face and Fn cannot be evaluated to be constant anymore (Delisio et al., 2013).

8.2.5.1 Lötschberg Base Tunnel model

In 2013, Delisio et al., analysed field geological and machine related data collected during the excavation of Lötschberg Base Tunnel in Switzerland. The considered section is composed by rock units belonging to Aar Massif. It is formed by three lithological units (Delisio et al., 2013):

- Gneiss and granodiorite, Baltschieder granodiorite;
- Grained granite, Central Aar granite;
- Crystalline sector composed of granite, gneiss and amphibolite.

In the Aar Massif blocky conditions occurred, because of the volumetric joint count, J_v , ranges between 4 to 25 joints/m³ (Delisio et al., 2013). The mean UCS ranges between 108 and 220 MPa,

8.2 Evaluation of various TBM performance prediction models based on field data from “La Maddalena” tunnel

BTS between 11 and 19 MPa, CAI between 3.3 and 5.2; these characteristics define very strong and highly rock masses.

Maximum depth is 1950 meters and the excavation was realized by means of two gripper TBMs.

Authors performed a multivariate regression analysis to determine an empirical relationship to predict the FPI_{blocky} , taking into account the joint counts (n/m^3) and UCS of intact material. The following equation has been carried out.

$$FPI_{blocky} = 5952 - 1794 * \ln Jv + USC \quad (8.17)$$

The gneiss domain of “La Maddalena” tunnel consist of massive gneiss where blocky conditions do not occur; for this reason, the previous formulation has been applied to predict FPI in gneiss-micaschist and micaschist domains. The comparison between calculated and predicted values is shown in Figure 8.18.

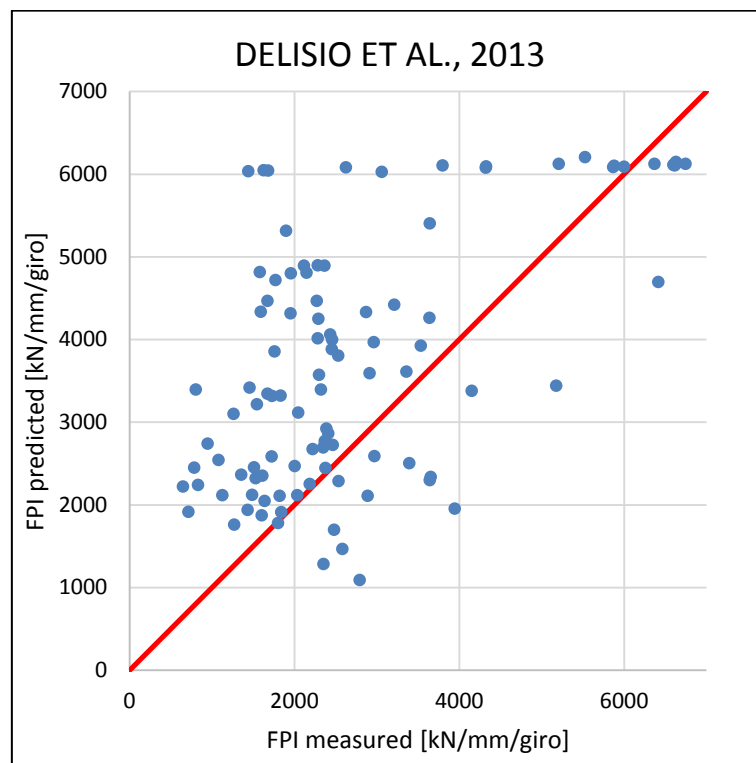


Figure 8.18 Comparison between the measured and predicted FPI_{blocky} from the Delisio et al. (2013) model.

As shown in Figure 8.18, the predicted FPI_{blocky} ranges between the same ranges of measured FPI_{blocky} furthermore the median value of calculated error is 34.71%; however Delisio formulation could not be utilised for “La Maddalena” case study because of significant data dispersion and only few cases able to predict FPI with high accuracy.

8.2 Evaluation of various TBM performance prediction models based on field data from “La Maddalena” tunnel

Generally, Delisio model tends to overestimate FPI, this is probably due to the fact that “La Maddalena” rock mass J_v is lower than the Löttschberg one.

8.2.5.2 Löttschberg and Second Manapouri Trailrace Tunnels model

In 2014 Delisio and Zhao developed a new model based on field data collected at Löttschberg Base Tunnel (see 8.2.5.1 paragraph) and at Second Manapouri Trailrace Tunnel (see 8.2.4.4 paragraph).

Authors have carried out two predictive empirical equations, the first (Equation 8.18) suitable for rock masses where blocky conditions are verified and the second (Equation 8.19) that allow us to evaluate FPI starting from FPI_{blocky} .

$$FPI_{blocky} = e^6 * J_v^{-0.82} * UCS^{0.17} \quad (8.18)$$

$$FPI = \frac{D}{c} * FPI_{blocky} \quad (8.19)$$

where D is the diameter of TBM [m] and c is the number of cutters put on the cutterhead.

Equation 8.18 has been used to predict FPI at “La Maddalena” tunnel, then the comparison between predicted and measured FPI have been carried out (Figure 8.19).

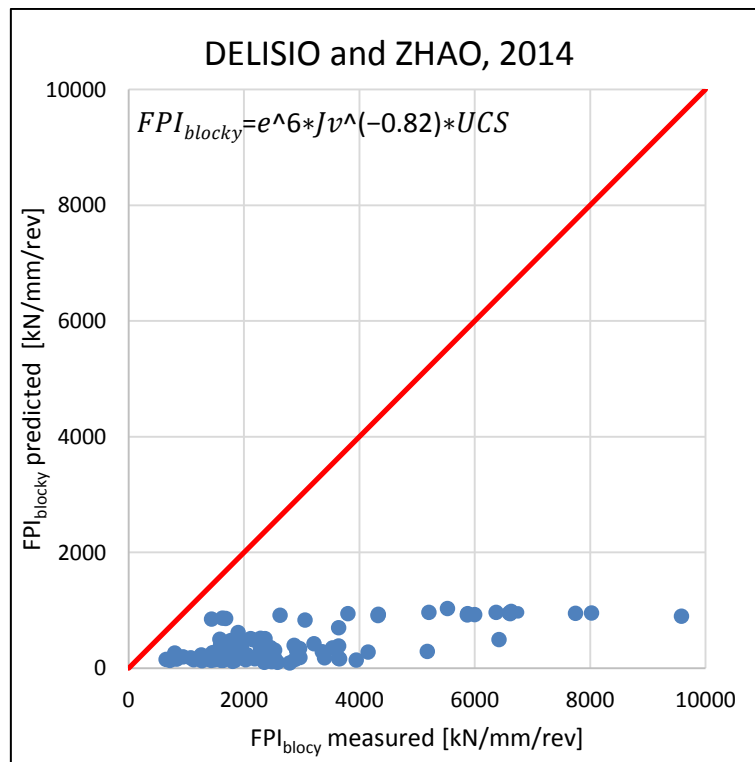


Figure 8.19 Comparison between the measured and predicted FPI_{blocky} from the Delisio and Zhao (2014) model.

8.2 Evaluation of various TBM performance prediction models based on field data from “La Maddalena” tunnel

The equation proposed by Delisio and Zhao (2014) produces a very relevant underestimation of FPI characterised by median percentage of error equal to 86.34%: for this reason, it is not utilisable to predict FPI at “La Maddalena” tunnel.

The formulation 8.19 carried out to estimate the FPI starting from FPI_{blocky} was also used to predict FPI at “La Maddalena”.

This formulation considers both the TBM diameter (6.30 meters) and the number of cutters installed on the machine cutterhead (43 cutters). A comparison between predicted and registered FPI has been carried out, the result is shown in Figure 8.20.

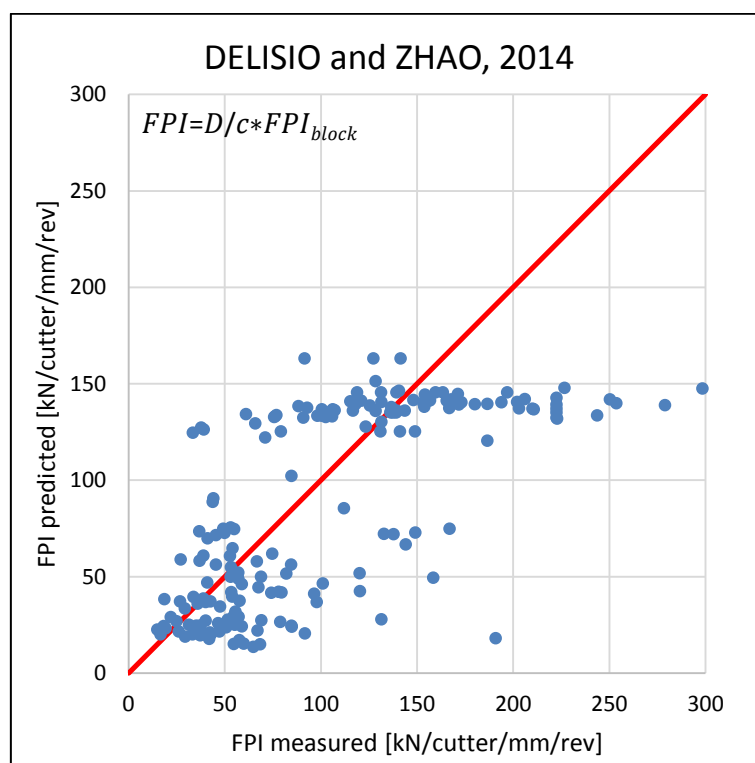


Figure 8.20 Comparison between the measured and predicted FPI from the Delisio and Zhao (2014) model.

As it is possible to note in Figure 8.20, the predicted FPI ranges between the same ranges of measured FPI, the median error in prediction is evaluated equal to 34.86%, however the plot shows a great data dispersion that made it not utilisable to predict FPI for “La Maddalena” exploratory tunnel. In some cases, points are plotted close to the 1:1 line and it means that in these situations the model has been able to correctly calculate FPI.

8.3 Conclusion

During this study, fourteen empirical TBM predictive models have been selected and their capacity to predict the TBM performances at “La Maddalena” exploratory tunnel has been tested.

Three models aim to predict the net penetration rate (ROP or PR) of a TBM and eleven are intended to calculate FPI. The number of FPI models is higher than the ROP one because of FPI is a composite parameter, for this reason, it is considered more representative. It is based both on rock masses parameters and machine ones (diameter and number of cutters).

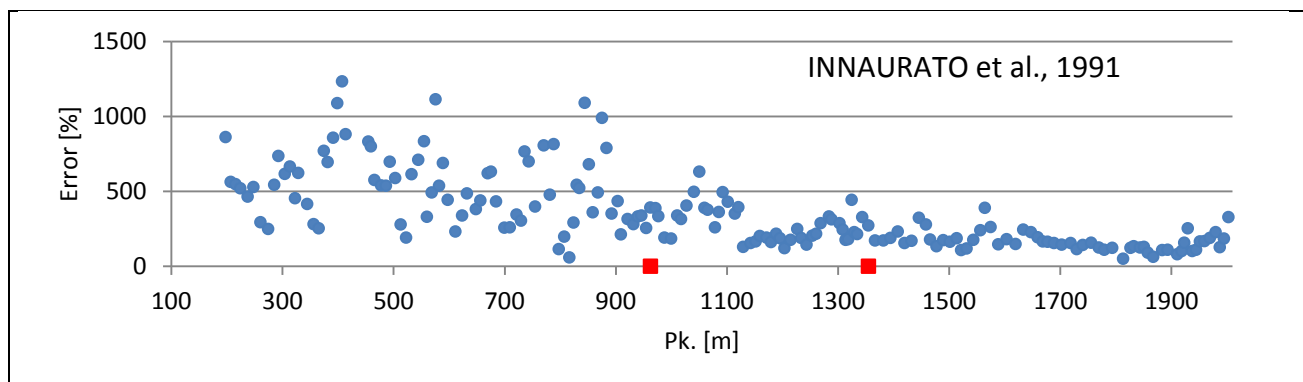
One model gives significantly overestimation of the selected indices as a result, nine generate a constant result and in three cases great data dispersion is observable; in these situations, the ranges of predicted and observed values are comparable, however these models are not applicable for “La Maddalena” case study because the differences between actual and computed values can be very high. Only one model, proposed by Hassanpour in 2011, was able to predict with accuracy “La Maddalena” TBM performances.

The errors generated by using literature proposed models to predict “La Maddalena” TBM performances are generally high, as expressed by median values in the previous paragraphs.

As already explained, the error in prediction of TBM performance, computed by using the mentioned models, has been evaluated for each rock section. Then the spatial distribution of the errors has been evaluated.

Generally, error in prediction is higher in gneiss domain (it occurs eight in cases); however, some models show constant distribution of percentage of error (two cases) and in some cases the higher percentage of error has been measured into micascist domain (four cases).

An example for each of the three types of distribution has been reported in Figure 8.21.



8.3 Conclusion

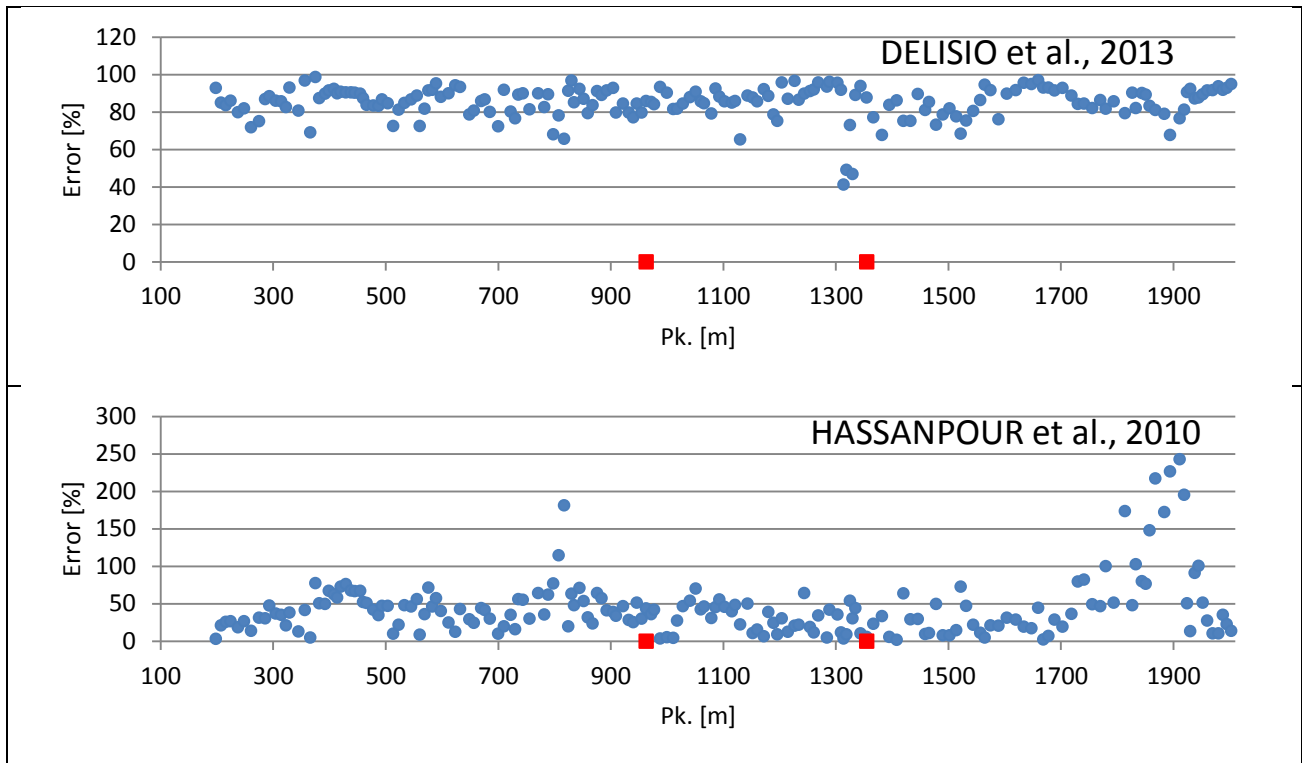


Figure 8.21 Spatial distribution of error in prediction. Red points represent the passage from DI to DII and from DII to DIII.

The use of empirically calculated parameters as independent variables is not suitable, because the formulation selected to calculate the parameter could be not appropriated.

It is confirmable that model limitations are caused by limited database used in the development of the models; in fact, the acceptable formulation was carried out focusing on a large database (four tunnels and 55.4 km of available data). Farrokh asserts that utilizing a large database of machine field performance records that considers an ample range of ground conditions and tunnel diameters can generate models able to offer better accuracy than the existing one.

Some common causes of the inability of a model to predict TBM performance in a tunnel different from that where the model has been carried out are:

- High site-specificity: they are valid only if the geological and mechanical contexts similar to the ones in which they have been developed;
- Exclusion of relevant parameters or introduction of inappropriate parameters: related to the decisions of the operators and to the availability of the data;
- Introduction of too many inputs in the model;

- Lack of distinction between the rock masses conditions and the work constraints that affect TBM performance.

Nevertheless, the site specificity of prediction models do not have to be considered as a negative aspect only because they are the best method to estimate the TBM performance in a given tunnel project (Hassanpour et al., 2016).

The following graphs show:

- The ranges of ROP values obtained from Cassinelli, Innaurato and Hassanpour models (Figure 8.22);
- The ranges of predicted FPI obtained from Kademi Hamidi and Hassanpour models (Figure 8.23);
- The ranges of predicted FPI_{blocky} from Delisio et al. models (Figure 8.24).

These ranges have been compared with measured one; the actual range of TBM performance has been reported.

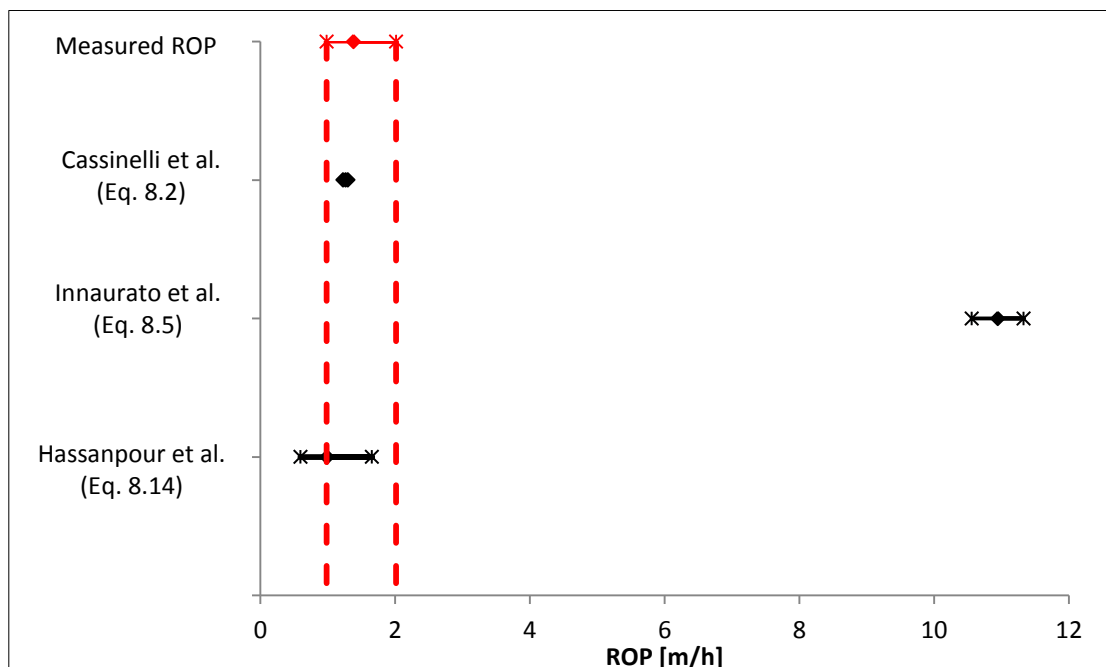


Figure 8.22 Ranges of values of ROP predicted from the models listed on the left. Asterisks represent the 25th and 75th percentile of ROP, diamond boxes represent the median. Measured values of ROP have been represented in red. Red dashed line demarcates the ranges of observed values.

8.3 Conclusion

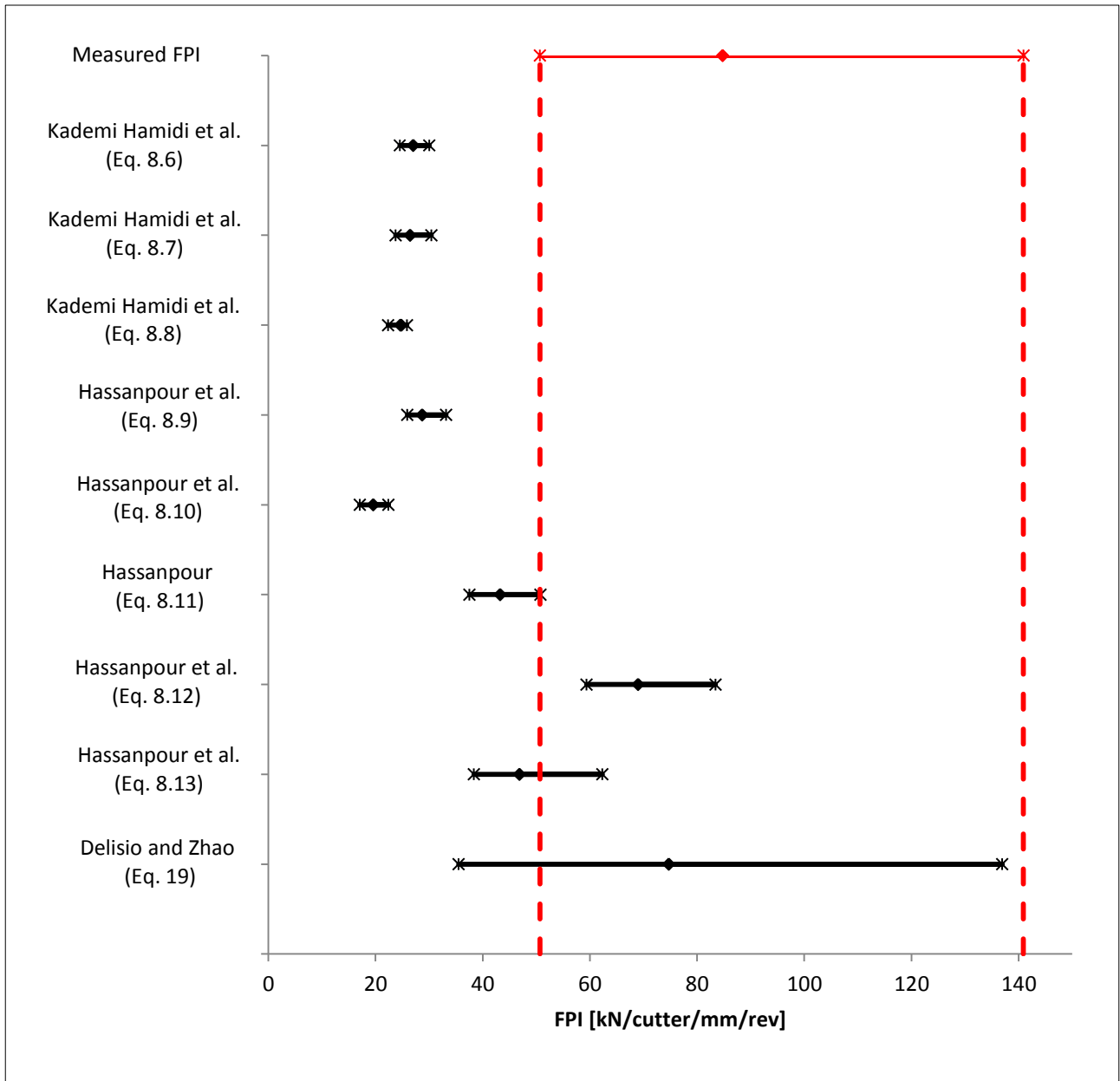


Figure 8.23 Ranges of values of FPI predicted from the models listed on the left. Asterisks represent the 25th and 75th percentile of FPI, diamond boxes represent the median. Measured values of FPI have been represented in red. Red dashed line demarcates the ranges of observed values.

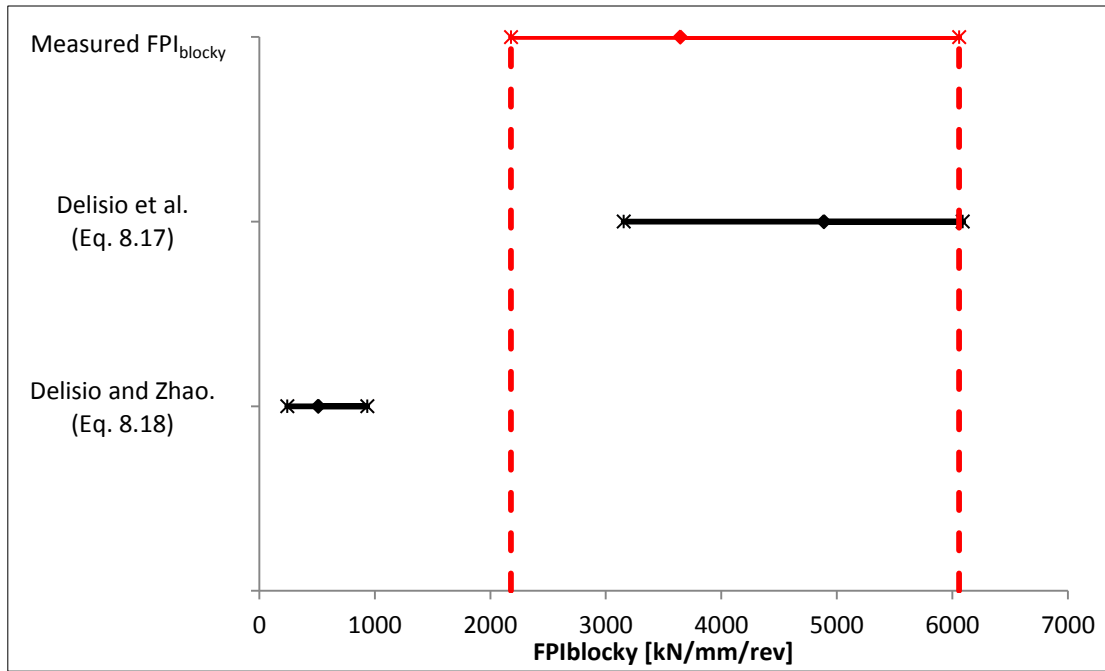


Figure 8.24 Ranges of values of FPI_{blocky} predicted from the models listed on the left. Asterisks represent the 25th and 75th percentile of FPI_{blocky} , diamond boxes represent the median. Measured values of FPI_{blocky} have been represented in red. Red dashed line demarcates the ranges of observed values.

9 DEVELOPMENT OF TBM PERFORMANCE PREDICTIVE MODELS

9.1 Introduction

The relationship between the geological, mechanical and structural frameworks concerning a given rock mass and the performance of the TBM used to construct a tunnel have been investigated with the purpose of carrying out empirical models able both to explain the relationship and to predict the behavior of the TMB working into a specific ground.

For this purpose, simple and multivariate regression analyses (both linear and nonlinear) have been carried out and discussed in this chapter.

The models obtained have been validated and the results of validation have been reported in Chapter 12.

The models have been developed using geological and machine data collected from Pk. 0 + 197 m to Pk. 2 + 010 m, as described in Chapter 5. The geological information contained in each of the 186 rock mass section surveyed has been input into the model as independent variables and the machine parameters, attributed to each section, as independent ones.

The reliability of the obtained models in TBM performance prediction has been tested on the data collected from Pk. 2 + 010 m to Pk. 6 + 776 m, this length is divided into 212 rock mass sections

A brief theoretical introduction about statistical methods and tests involved in the analyses has been provided, prior to the presentation and discussion of the obtained models.

9.2 Theoretical concepts

When two or more variables related to the same problem are detected, the relationship between them can be generally investigated in two different ways.

If it is necessary to study the level of association between two variables, the statistic technique adopted is the correlation; instead, if it is necessary to carry out an equation able to link two or more variables, the statistical procedure adopted is the regression analysis. The best way has to be selected on the basis of the purpose of the study.

9.2.1 Correlation between variables

The correlation aims to investigate if a relationship between two variables occurs, and to numerically quantify the association level. Generally, the first step is to create a scatterplot and to observe the disposition of the points.

If the points are principally plotted into the quadrant I and III, the association between the two variables is positive; on the contrary, if the points are distribute between II and IV the correlation is negative (Figure 9.1).

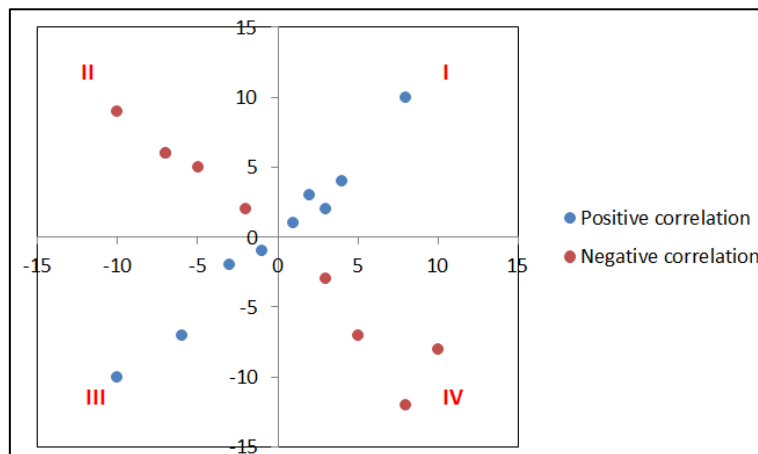


Figure 9.1 Positive (blue dots) and negative (red dots) correlation.

If the points are equally distributed among the quadrants, there are not any associations.

By observing the point distribution, it is possible to understand whether the correlation is linear (the points are aligned on a line) or not.

If the correlation is linear and the distribution is Gaussian type, it can be quantified by means of Pearson coefficient, calculated as:

$$r = \frac{COV_{XY}}{S_X S_Y} \quad (9.1)$$

where: COV_{XY} is the covariance between X and Y and S_X and S_Y are the standard deviations of X and Y respectively.

The Pearson coefficient ranges between -1 and $+1$. If r is equal to $+1$ or -1 , there is a perfect correlation and points are perfectly aligned on a line; the more distant the points from the line are, the weaker the correlation is, values near to 0 indicate no correlation between the studied variables (Figure 9.2).

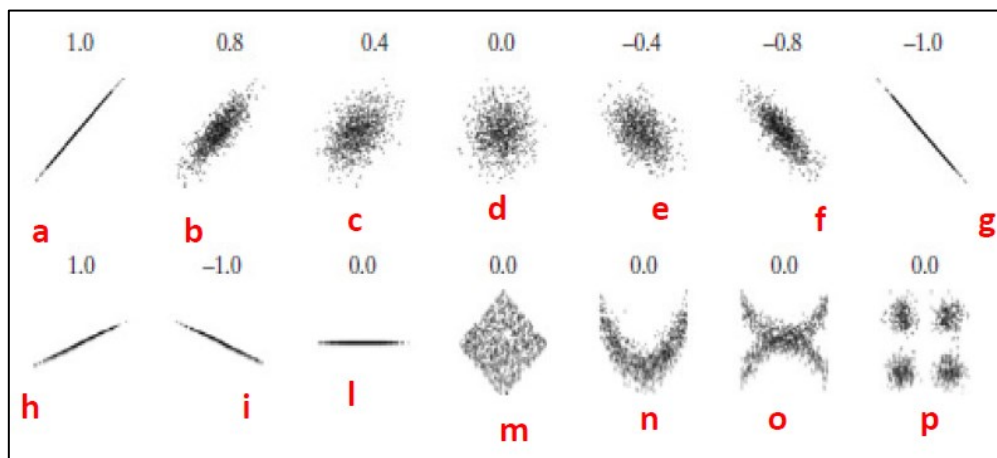


Figure 9.2 Example of data scatterplots with a variety of correlation values. In a,g,h,i points are perfectly aligned on a line and in these case r is $+1$ or -1 . In d, l, m, p there is no correlation and $r=0$. In n and o there is correlation but $r=0$ because of the correlation is not linear (Boracchi et al., 2015).

When the relation between variables is not linear, or at least one variable is not normally distributed, or at least one of them is an ordinal variable, the Pearson coefficient cannot be considered. In these cases, the Spearman rank correlation coefficient ρ_s should be used. ρ_s is calculated as:

$$\rho_s = 1 - \frac{6 * \sum_i D_i^2}{N(N^2 - 1)} \quad (9.2)$$

where D_i is the difference between the ranks and N is the number of the observations. ρ_s ranges from -1 (negative correlation) to $+1$ (positive correlation); ρ_s equal to zero means absence of correlation.

9.2 Theoretical concepts

Correlation analysis represents a preliminary stage in the investigation of the relationship between variables: in fact at the end of the analysis it is possible to assert if relationship occurs, and to understand the type and the level of correlation.

If a relationship between variables is recognised by plotting data, the study can be continued. It has a dual purpose:

- *Explanation*: the aim is to comprehend and evaluate the effects of the independent variable on the dependent one, on the basis of a mathematical function;
- *Predictive*: the aim is to individuate a combination of dependent variables in order to predict the value of the dependent one.

For these purposes, regression analyses are largely adopted.

9.2.2 Simple linear regression analysis

Regression analysis is a group of statistical techniques that allows to explain the relationship between one or more independent variables and a dependent one.

The simple regression analysis considers one independent variable only and its effects on the dependent one, on the contrary, if the purpose is to investigate the relations between more than one independent variables and a dependent parameter a multiple regression analysis has to be performed.

The objective of linear regression analysis is to find a line that minimises the distance between the observed data and the line; which is calculated by means of the least square method, as follows:

$$y_i = a + bx_i + e_i \quad (9.3)$$

where:

b is calculated as:

$$b = \frac{\sum(x_i - \bar{x})(y_i - \bar{y})}{\sum(x_i - \bar{x})^2} \quad (9.4)$$

a is calculated as:

$$a = \bar{y} - b\bar{x} \quad (9.5)$$

and e_i is the distance between the point and the line and it should be as small as possible:

$$\min(\sum e_i^2) \quad (9.6)$$

A graphical explanation of least square method has been reported in Figure 9.3.

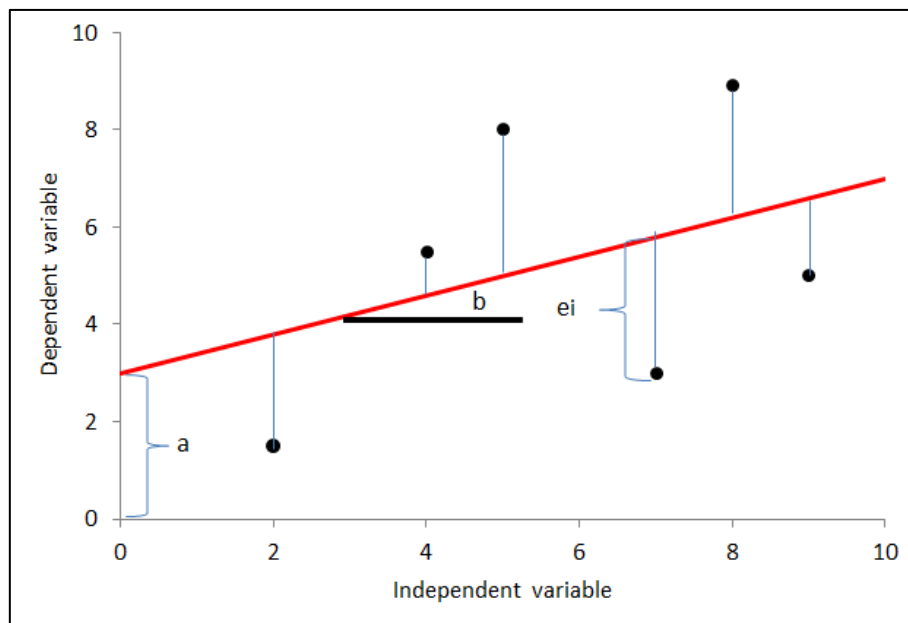


Figure 9.3 Least square method.

9.2.2.1 Coefficient of determination

The coefficient of determination, R^2 , is one of the measures used to assess the ability of a regression in explaining the relationship between a dependent and an independent variable. R^2 expresses the proportion of variance (the variance is the square of the standard deviation of a set of data) in the dependent variable that is explained by the regression and the predictor variable.

The coefficient of determination is calculated as follows:

$$R^2 = \frac{SS_R}{SS_T} \quad (9.7)$$

where:

- SS_R is the sum of squares of the model or the explained sum of squares, and it is obtained by the total sum of squares minus the residual sum of squares;
- SS_T is the total sum of squares.

R^2 ranges between 0 and 1; R^2 equal to zero means that the regression does not explain any percentage of variance, on the contrary R^2 of 1 means that all the variance is explained by the regression.

9.2 Theoretical concepts

9.2.2.2 Model assumptions

In order to carry out a linear regression model it is necessary that three assumptions are verified, which are:

- *Independence*: the response variables (y_i) are independent;
- *Normality*: the values of the response variables are normally distributed;
- *Homoscedasticity*: the response variables have the same variance.

The assumptions are usually tested on the random errors, they have to be independent and normally distributed, they have to have a constant variance, σ^2 , for all settings of the independent variables (homoscedasticity) and their mean has to be equal to zero. The verification of the assumption can be performed considering the residuals (e_i); however considering the standardised residuals is suitable.

Normality can be checked graphically or numerically.

In the first case box-plots (normal distribution occurs when they are symmetric), QQ-norm diagrams (normal distribution occurs if the points are aligned on the bisector line) and histograms (observing the probable distribution) are widely used. Figure 9.4 reports an example of QQ plot, which shows a normal distribution and two histograms: the first one is about a normal distribution, while normality is not verified in the second one.

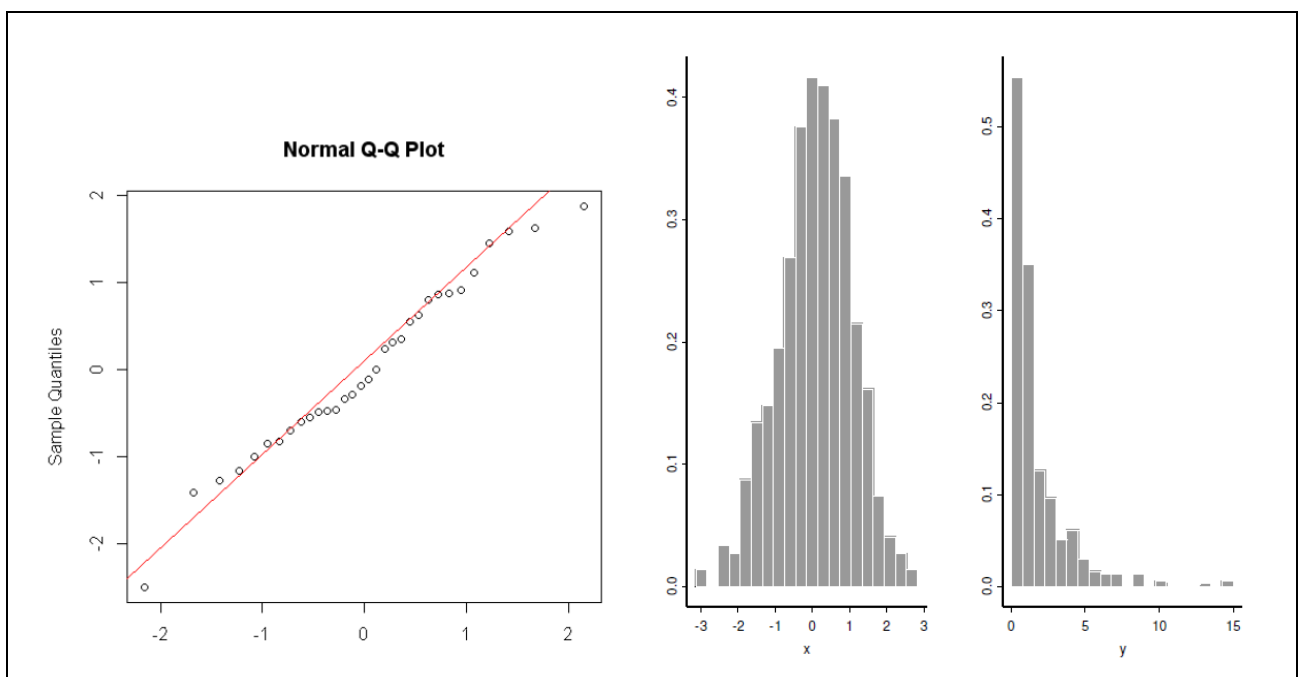


Figure 9.4 From left to right: normal QQ plot, histogram showing normal distribution, histogram showing not normal distribution.

Normal distribution can be numerically tested by means of tests that compare the shape of a given distribution to the one of a normal curve, a significant result means that the distribution is not shaped as a normal curve.

The normality test which is most frequently applied is the “Shapiro-Wilk normality test”. Its null hypothesis is that data are normally distributed, so if p-value is higher than 0.05 the null hypothesis has to be rejected and data are normally distributed, on the contrary the population is not normally distributed. Shapiro-Wilk, W , is calculated as follow:

$$W = \frac{\left(\sum_{i=1}^n a_i x_{(i)}\right)^2}{\sum_{i=1}^n (x_i - \bar{x})^2} \tag{9.8}$$

where a_i is a constant.

Homoscedasticity can be checked producing a scatterplot of the standardised residuals vs. the fitted values or standardised values vs. each of the independent variables. When the assumptions are satisfied, residuals vary randomly around zero and their spread is the same throughout the plot (Figure 9.5).

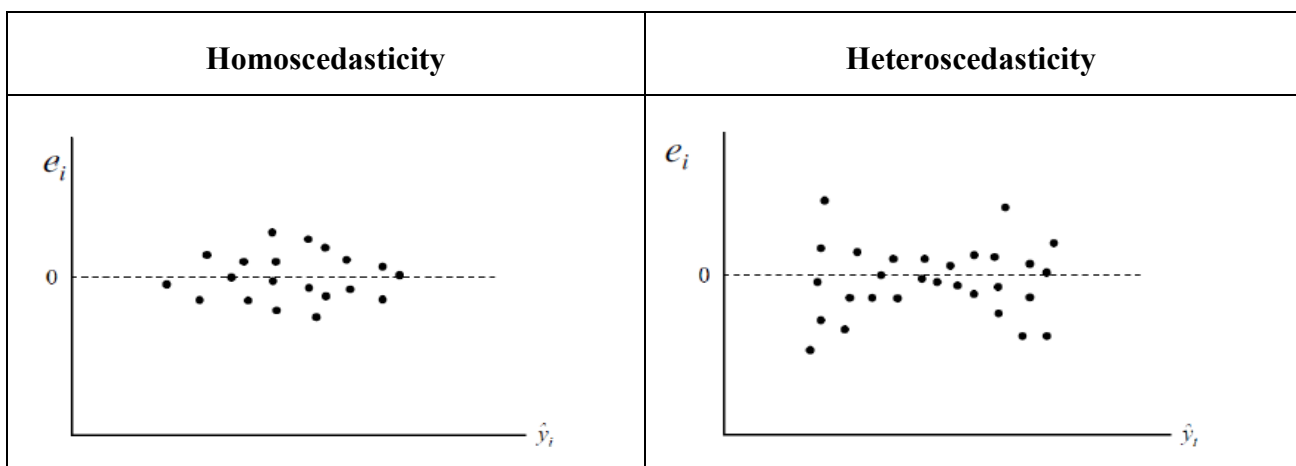


Figure 9.5 *Homoscedasticity verified (on the left), and not verified (on the right); Boracchi et al., 2015.*

Homoscedasticity is numerically tested by means of the White test. It carries out a regression analysis on the residual values as follows:

$$e_i^2 = a_r + b_r x_i + b_{r2} x_i^2 \tag{9.9}$$

Where a and b have been obtained by means of leas square method.

9.2 Theoretical concepts

The R^2 about Equation 9.9 has to be calculated and if $n \cdot R^2$ is higher than x^2 there is evidence of heteroscedasticity.

9.2.3 Multiple linear regression analysis

A multiple regression analysis is carried out when the combined effect of more independent variables on the dependent one is investigated; it is considered as an extension on the simple regression.

There are many situations, in statistics, in which one variable is able to predict very accurately another single variable. However, the predictions usually improve when additional relevant information is considered. The most widely used mathematical functions with the purpose of expressing the relationships among more than two variables are equations as:

$$y = b_0 + b_1x_1 + b_2x_2 + \dots + b_kx_k \quad (9.10)$$

where:

- y is the variable of response (the dependent one);
- x_1, x_2, \dots, x_k are the explanatory variables (the independent ones);
- b_0, b_1, \dots, b_k : are the regression coefficients. They are obtained by means of the least-squares method.

The sum of the squared difference between the measured y_i and the residual (y_i predicted by the model) has to be as low as possible:

$$\sum [y_i - (b_0 + b_1x_{1i} + b_2x_{2i} + \dots + b_kx_{ki})]^2 \text{ minimum} \quad (9.11)$$

where y_i is the i^{th} data value for y , x_{1i} is the i^{th} data value for x_1, \dots, x_{ki} is the i^{th} data value for x_k . The value of b_0, b_1, \dots, b_k which satisfy this property are the least square estimates of the regression.

9.2.3.1 T-test and F-test

T-test is frequently used to evaluate the influence of each predictor and its significance. The index t is equal to the ratio between the estimated value and the standard deviation.

T-test is used to assess only one regression coefficient at a time; on the contrary, the F-test can assess multiple coefficients simultaneously.

The F-test is carried out to evaluate the utility of the regression, comparing the fits of different linear models. F-tests assess the overall significance of the regression model, based on the following hypothesis:

- Null hypothesis: the fit of the obtained model is equal of the intercept- only model (in which no coefficients are present);
- Alternative hypothesis: the fit of the regression model is significantly improved compared to the intercept-only one.

If the p-value related to the F-test is less than the selected significance level the null hypothesis can be rejected, and it means that at least one of the independent variables significantly affects the dependent variable.

Generally, if t-test is not significant, the F-test will not be significant either.

R^2 provides some information about the strength of the relationship between the regression model and the dependent variable and it does not provide a hypothesis test about this relation. On the contrary, the F-test determines if this relationship is statistically significant. When the p-value related to the F-test is less than the selected significance level the R^2 is significantly different from zero.

9.2.3.2 Coefficient of determination

When a multiple regression analysis is carried out, there is more than one dependent variable, so it is necessary to adopt a modified version of the coefficient of determination, the so called R^2_{adjusted} , which considers the number of predictors, because the coefficient of the determination tends to increase with the number of dependent variables included into the model.

9.2.3.3 Multicollinearity

Multicollinearity occurs when two or more independent variables are associated or highly correlated to each other, if it is present, the performed regression is not reliable. In geomechanics multicollinearity occurs if a variable is computed from another one in the same dataset, or when two variables represent the same aspect. When this problem takes place, the partial regression coefficient may not be estimated correctly, and it makes difficult to assess the relative influence that an independent variable has on the dependent one.

9.2 Theoretical concepts

Multicollinearity can be detected by means of tolerance and the variance inflation factor, VIF, which is the reciprocal of the tolerance. When tolerance is less than 0.1 – 0.2 VIF is higher than 10 and it indicates that there are problems of multicollinearity.

The researchers have to select with great accuracy the independent variables that will be input into the regression analysis in order to avoid the problem above explained. When VIF is ≥ 10 it is necessary to revise all the input parameters and remove the ones considered redundant.

9.2.3.4 Regression model building

There are different methods to select and enter the variables into a regression model. The most commonly used are: the “Backward elimination”, the “Forward selection” and the “Stepwise regression”.

Backward elimination: it is the so called “top down approach”. Firstly it is necessary to decide a significance level, SLS, which makes the variables stay into the model; this level can be 0.05 however; if it causes too many parameters to be removed, it can be elevated at 0.20. All independent variables are input into the model, then the predictor characterised by the highest p-value has to be considered. If it is higher than SLS the variable has to be removed and the model has to be fitted without it. On the contrary if the highest p-value is \leq SLS the variable has to be maintained.

The procedure continues until all independent variables have p-values less than SLS.

Forward stepwise: it is also known as “bottom up approach”. In this case too, it is necessary to choose a significance level, SLE, so that the variables are inserted in the model, it can be 0.05 but for this method it may be too low and cause too few predictors to be entered; for this reason the suitable SLE is equal to 0.20. Then the variables are added to the equation one at a time: it is necessary to consider the parameter with the lowest p-value. If it is less than SLE this predictor has to be included into the model, whereas if p-value $>$ SLE it is necessary to stop and consider the previous model.

The procedure has to be continued until none of the new independent variables have p-values less than SLE.

Stepwise regression: this method combines the backward and forward ones. It is necessary to consider both SLS and SLE and choose them in such a way that $SLE < SLS$. The procedure starts as the bottom up process (forward selection).

The new variable must have $p\text{-value} \leq \text{SLE}$ to be entered, at this point all the variables that have already been input have to be re-tested and their $p\text{-values}$ have to be less than SLS to allow them to stay into the model.

The process continues until none of the new variables can be input and none of the old ones have to be removed.

9.2.3.5 *Model assumption*

The assumptions for multiple linear regression models are that the response variables have to be independent, the values of the response variable have to be normally distributed and they have to be characterized by the same variance.

In order to check these assumptions, the same methods described for simple linear regression analysis are adopted (see section 9.2.2.2).

9.2.4 **Nonlinear regression analysis**

Generally, the linear regression analysis is used in order to investigate the relation between independent variables and a dependent one; however, if the relationship between the dependent variable and at least some of the independent ones is not linear, or when the assumptions for linear regressions are not satisfied, a nonlinear regression analysis should be performed.

Nonlinear regression requires estimating the coefficients in a not linear relation between independent variables and dependent one.

The nonlinear models considered in the commercial statistical software are: logarithmic, inverse, quadratic, cubic, polynomial, compound, logistic and exponential mathematical forms. The mathematical function that best represents the relation between dependent and independent variable can be individuated by analysing a scatterplot of the collected data.

Once the mathematical function has been determined, the coefficients are generally calculated on the basis of the Levenberg-Marquardt nonlinear least squares algorithm (Nash, 1987).

Obviously, the assumptions of normality are not required and the unique assumption is that the data are well represented by the selected model.

9.3 Effects of single rock/rock mass properties on TBM performances

The effect of single intact rock properties or rock mass parameters on the TBM performances has been investigated by means of correlations and simple regression analyses.

The geological parameters involved in this study are: UCS, quartz content, α , spacing J_v , RDQ, J_c RMR, GSI and tunnel depth; these are the independent variables. ROP and FPI are the dependent ones.

All the analyses have been performed by means of the commercial statistical software “IBM SPSS Statistics 25”.

9.3.1 Uniaxial compressive strength

The relationship between the uniaxial compressive strength of the intact rock and ROP and FPI has been analysed and the result is reported in Figure 9.6.

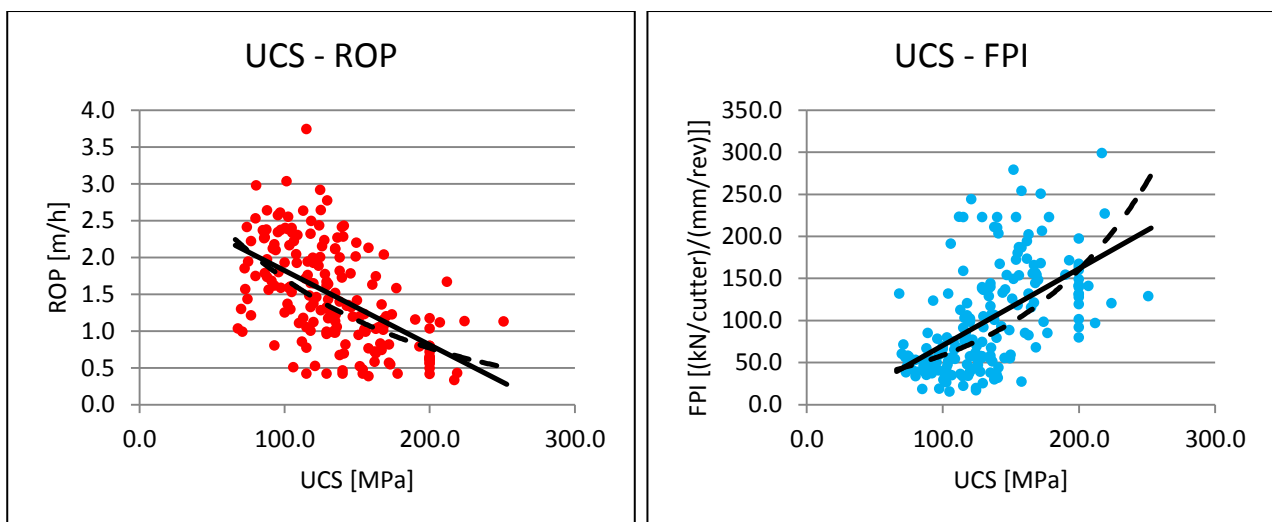


Figure 9.6 UCS vs. ROP (on the left); UCS vs. FPI (on the right), modified after Armetti et al. 2018.

As it is possible to expect, when rock strength increases the performances of the TBM decrease. In particular when high values of UCS characterise the intact rock, the net penetration rate is generally low because of the chip rock formation is more difficult; on the contrary FPI increases because a high thrust has to be applied in order to guarantee the penetration. It is necessary to consider that there is a threshold of thrust which cannot be exceeded in order to avoid machine damages.

Linear and exponential mathematical functions have been selected as the most representative ones to explain the relation between UCS and ROP-FPI. Previous studies described linear relationship

9.3 Effects of single rock/rock mass properties on TBM performances

(e.g. Khademi Hamidi et al., 2010) and the exponential one (Graham, 1976; Farmer and Glossop, 1980; Hughes, 1986; Gong and Zhao, 2009; Hamidi et al., 2010).

The assumptions for linear regression analysis have been checked and they result satisfied. The regression analyses allow to carry out 4 empirical equations (linear and exponential equations both for ROP and FPI) listed in Table 9.1.

Equation	r	R ²	F	Reference
$ROP = -0.010 * UCS + 2.829$	0.550	0.306	81.305	9.12
$ROP = 3.809 * e^{-0.080*UCS}$	-	0.322	87.424	9.13
$FPI = 0.912 * UCS - 20.973$	0.554	0.307	81.502	9.14
$FPI = 21.553 * e^{0.010*UCS}$	-	0.324	88.048	9.15

Table 9.1 Results of regression analyses. For each equation the coefficient of determination and F values are reported. Coefficient of correlation is listed only for linear models.

The coefficients of determination R² are medium-low, it means that UCS alone cannot totally determine the performances of a TBM and then UCS cannot be utilised as unique TBM performance predictor.

9.3 Effects of single rock/rock mass properties on TBM performances

9.3.2 Quartz content

The quartz content of the rocks excavated during La Maddalena construction has been related to the obtained TBM performances. The relationship is shown in Figure 9.7.

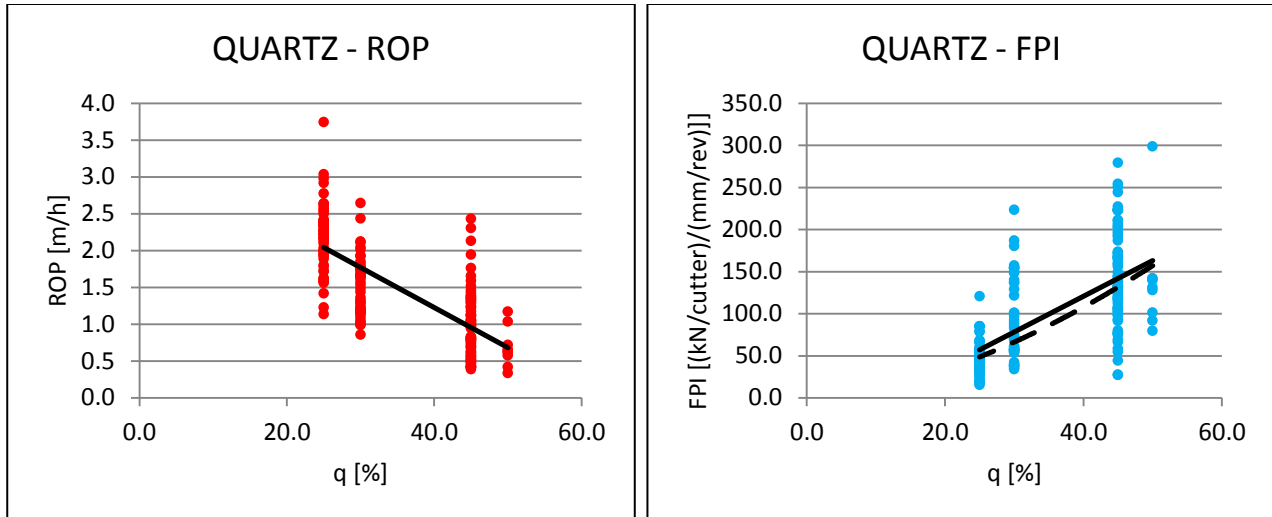


Figure 9.7 q vs. ROP (on the left); q vs. FPI (on the right), modified after Armetti et al. 2018.

It is possible to observe that if quartz content increases, the performances of TBM decrease. This mineral is seriously responsible for the hardness, the strength and the abrasivity of the rocks, so its determination is fundamental in order to predict tool consumption and machine penetration.

In this case, selecting a mathematical function is not completely correct in order to describe the relation between rock quartz content and machine performance, due to the distribution of data. However, if it is necessary to select a regression model, the linear one can be considered only for ROP, given that the assumption of linear regression not satisfied for FPI.

The power function could be considered as the regression model able to examine the relation between quartz content and FPI.

The models obtained by means of the regression analyses are listed in Table 9.2.

Equation	r	R^2	F	Reference
$ROP = -0.055 * q + 3.408$	0.747	0.558	232.330	9.16
$FPI = 0.213 * q^{1.689}$	-	0.468	161.656	9.17

Table 9.2 Results of regression analyses. r , R^2 and F value are reported.

9.3.3 Alpha angle

The alpha angle represents the orientation of discontinuities with respect to the tunnel axis; its calculation has been explained in Chapter 5. Here the relation between α and TBM performances has been proposed (Figure 9.8).

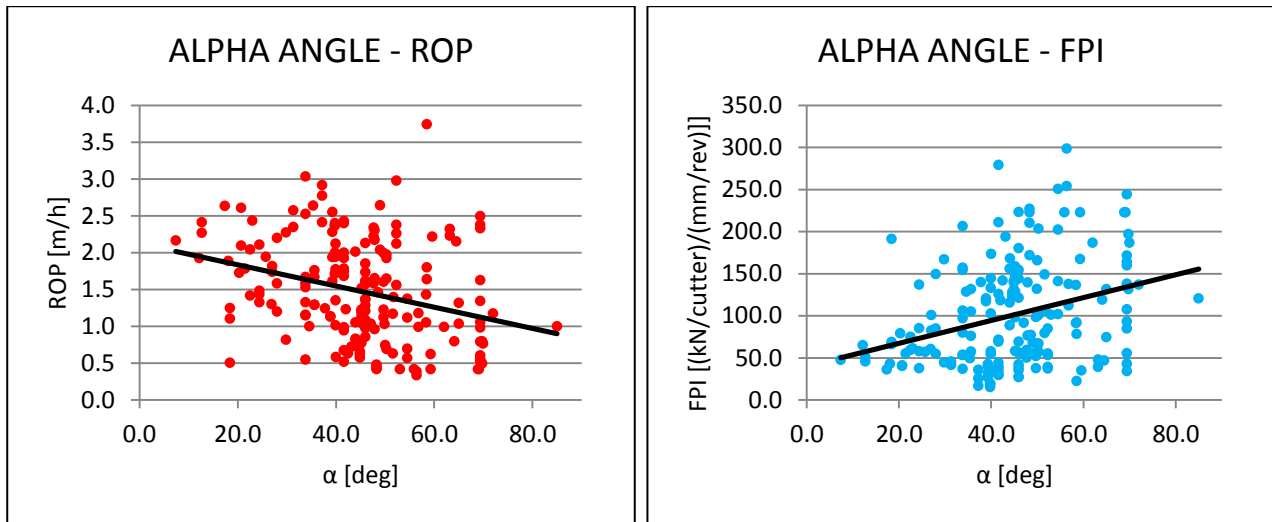


Figure 9.8 Alpha angle vs. ROP (on the left); α vs. FPI (on the right).

The relation between alpha and ROP-FPI is weak, since the effects of discontinuity orientation has not to be evaluated alone but combined with the distance between the discontinuity planes. It means that the role of the discontinuity planes has to be investigated in terms of orientation and frequency at the same time.

It was noted that when α increases the machine performances decrease. The assumptions for the linear regression have been verified and two simple linear regression analyses have been carried out: the results obtained have been reported in Table 9.3.

Equation	r	R ²	F	Reference
$ROP = -0.014 * \alpha + 2.123$	0.296	0.088	17.668	9.18
$FPI = 1.357 * \alpha + 40.326$	0.310	0.096	19.498	9.19

Table 9.3 Results of regression analyses. For each equation r, R² and F value are reported.

As expected, the coefficients of regression and F value are very low.

9.3 Effects of single rock/rock mass properties on TBM performances

9.3.4 Spacing between weakness planes

The rock mass fracturing degree may seriously affect the TBM performances: for this reason, in this work three parameters representing the ground fracturing conditions have been correlated to the measured ROP and FPI.

The scatterplots about the spacing between the discontinuity planes and TBM indices are provided in Figure 9.9.

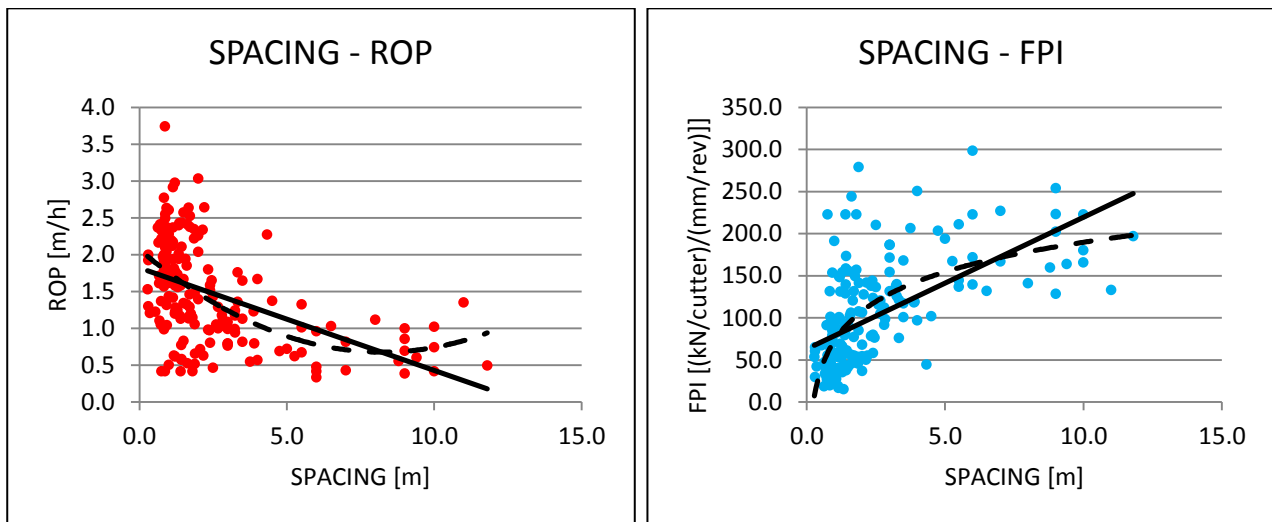


Figure 9.9 Spacing between discontinuities vs. ROP (on the left); S vs. FPI (on the right).

When the distance between the planes of weakness (spacing) is low, ROP covers a large range of values, since the machine could potentially advance rapidly and easily given that fractures frequently occur and chips formation is advantaged by weak planes. However, in case of high fragmentation, the machine cannot be driven at maximum speed due to the fact that the muck removal system would not be able to move too much muck in a short time.

FPI generally increases when fractures are highly spaced; however data distribution shows the presence of a threshold that cannot be exceeded even when rock mass is compact and potentially a high thrust might be requested. On the contrary, fractured rock mass sections do not require high levels of thrust on the cutterhead.

The mathematical forms selected to explain the relation between spacing and ROP are the linear and the polynomial ones, whereas for FPI linear model and logarithmic one (on the basis of the threshold occurrence) have been considered.

The assumptions for linear regression are satisfied, so the empirical equations related to the correlation between spacing and TBM performances have been reported in Table 9.4.

9.3 Effects of single rock/rock mass properties on TBM performances

Equation	r	R ²	F	Reference
$ROP = -0.139 * S + 1.820$	0.477	0.227	54.126	9.20
$ROP = 0.020 * S^2 - 0.338 * S + 2.069$	-	0.268	33.569	9.21
$FPI = 15.654 * S + 62.824$	0.593	0.352	100.034	9.22
$FPI = 50.871 * \ln S + 72.669$	-	0.412	128.778	9.23

Table 9.4 Results of regression analyses. For each equation R² and F value are reported.

Coefficient of correlation is listed only for linear models.

The relation between FPI and fracture spacing is stronger than the ROP-spacing one.

9.3 Effects of single rock/rock mass properties on TBM performances

9.3.5 Joint volumetric count

The joint volumetric count, J_v , has been calculated on the basis of spacing data, as reported in Chapter 5. The influence of J_v on the TBM performances has been investigated.

An appreciable correlation between J_v and TBM indices has been noted (Figure 9.10).

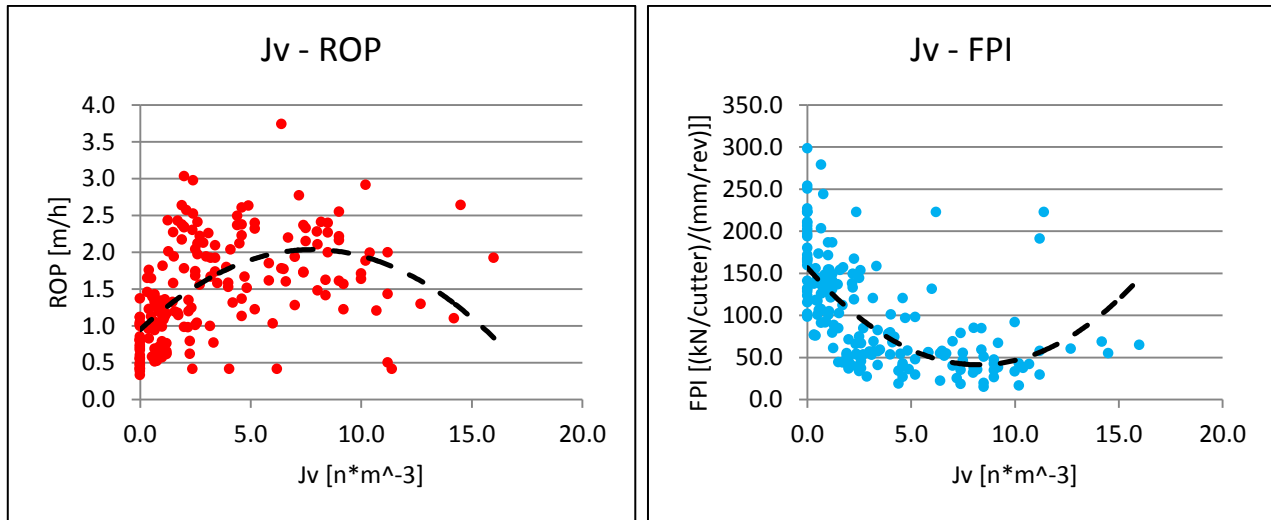


Figure 9.10 J_v vs. ROP (on the left); J_v vs. FPI (on the right).

As it is possible to observe, the highest machine performances occur when the number of joints per unit of volume ranges between 5 and 10 joints $\cdot m^{-3}$. In this situation the net rate of penetration is high and the thrust which has to be applied to guarantee a specific rate per revolution is low. When J_v is lower than 5.0 – 10.0 joints $\cdot m^{-3}$, rock mass is compact and difficult to penetrate, on the contrary, when J_v is higher than 5.0 – 10.0 joints $\cdot m^{-3}$, the degree of fracturing is elevated, so the same observation exposed for low levels of spacing can be considered. The best mathematical function able to explain the relationship between J_v and ROP-FPI is the polynomial one. In this case, J_v represents the influence of the rock mass fracturing degree on the performances of the TBM more clearly than spacing. A polynomial regression analysis has been carried out both with ROP and FPI as dependent variables. The results have been listed in Table 9.5.

Equation	R^2	F	Reference
$ROP = -0.018 * J_v^2 + 0.279 * J_v + 0.949$	0.312	41.579	9.24
$FPI = 1.701 * J_v^2 - 28.014 * J_v + 156.665$	0.428	68.420	9.25

Table 9.5 Results of polynomial regression analysis. R^2 and F values are reported.

9.3.6 Rock quality designation index

The Rock Quality Designation index, RQD, (Deere et al., 1967) has been also considered in order to evaluate the influence of rock mass fracturing degree on the TBM performances.

No one correlation between RQD and ROP or FPI has been observed, it is clearly represented by the scatterplots in Figure 9.11.

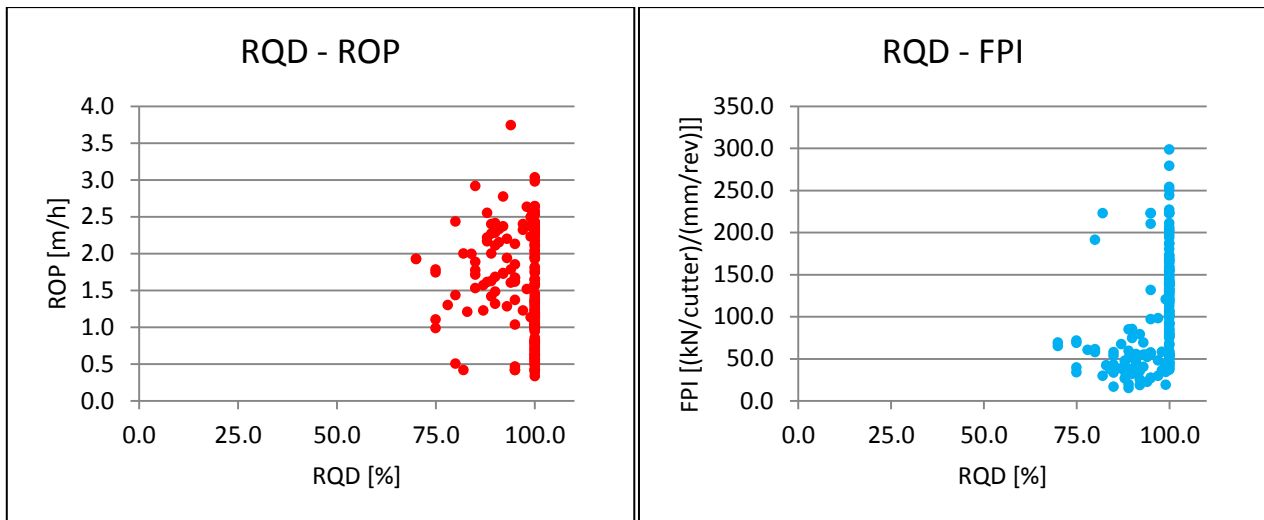


Figure 9.11 RQD vs. ROP (on the left); RQD vs. FPI (on the right).

The RQD index about La Maddalena rock mass has been calculated by means of the empirical equation proposed by Palmström, 1982. The results obtained are almost always very high, even in those situations in which an intense fracturing degree has been observed, as explained in Chapter 5.

By relating RQD with TBM performance measured during the excavation, it is not possible to observe the machine behavior where jointing level is high, so where RQD should be low. For this reason, RQD cannot be used as prediction in a regression analysis.

Moreover, when RQD is empirically calculated (for example by means of the Palmström equation), its use as predictor in an empirical model is not suitable because using an empirically derived variable into a regression analysis might not be useful.

9.3 Effects of single rock/rock mass properties on TBM performances

9.3.7 Joint conditions

The joint conditions parameter, J_c , takes into account for five discontinuity surface features (persistence, aperture, roughness, filling and weathering); for this reason, relating it with the TBM performance indices, it may be useful to investigate the effect of the general conditions of weakness planes on the behavior of the machine involved in tunnel excavation.

The relationship between joint conditions and ROP-FPI has been represented by the scatterplots reported in Figure 9.12.

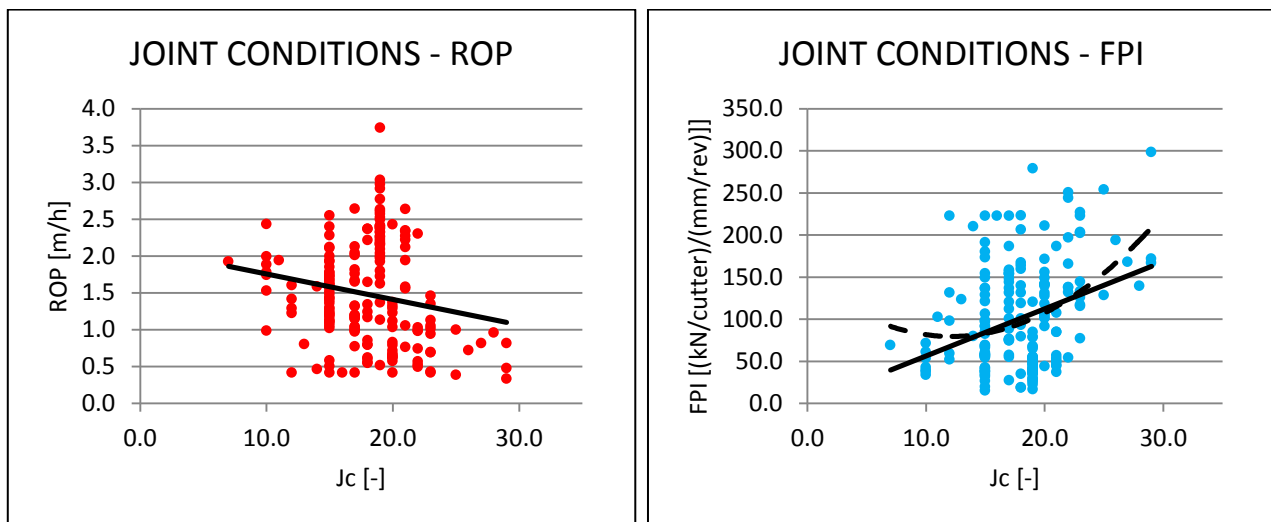


Figure 9.12 J_c vs. ROP (on the left); J_c vs. FPI (on the right).

It is observable that the J_c parameter and the machine ones are barely related; however, it is possible to recognise that where the global quality of joint surfaces increases the TBM performances decrease.

The effect of J_c on the machine performances should not be evaluated alone, but together with the other parameters describing the geometry (in terms of orientation respect to the tunnel axis) and the frequency of joint occurrence. The quality of fracture surface gives limited information if considered alone.

Regression analysis has been performed even through the low correlation between the independent variables and dependent ones. Only the results obtained for FPI have been reported, given that the coefficient of regression related to J_c -ROP relationship is very low (Table 9.6).

9.3 Effects of single rock/rock mass properties on TBM performances

Equation	r	R ²	F	Reference
$FPI = 5.600 * Jc + 0.514$	0.335	0.107	23.277	9.26
$FPI = 0.455 * Jc^2 - 11.060 * Jc + 146.646$	-	0.141	15.054	9.27

Table 9.6 Result of linear and polynomial regression analysis. For each equation R² and F value are reported. Coefficient of correlation is listed only for linear model.

9.3 Effects of single rock/rock mass properties on TBM performances

9.3.8 Tunnel Depth

The depth of excavation is a first indicator of in situ stress condition: it is clear that this parameter is not enough alone to predict the performance of a TBM boring at a certain depth.

The correlation between the depth achieved by La Maddalena tunnel and the performances measured at the relative depths has been studied (Figure 9.13).

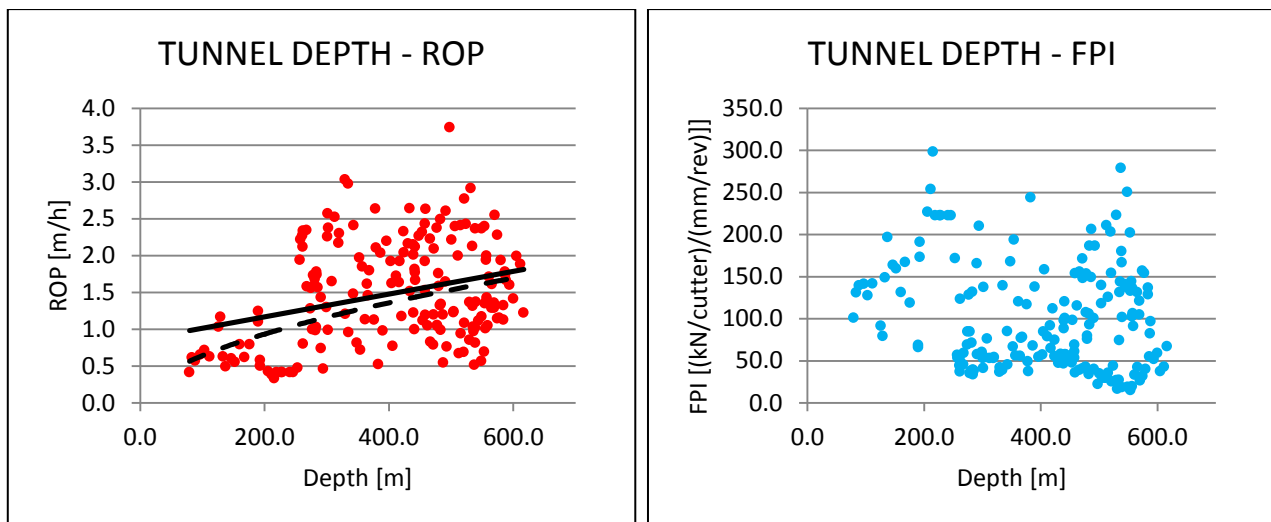


Figure 9.13 Tunnel depth vs. ROP (on the left); Tunnel depth vs. FPI (on the right).

By observing the depth-ROP scatterplot, the rate of penetration appears to increase with the overburden. The correlation is poor and it means that the vertical stress affects the performance of the TBM but its effect has to be evaluated in addition to other geological and mechanical parameters.

Tunnel depth appears not to influence FPI; however this absence of evident correlation does not mean that FPI is not influenced by vertical stress, but it means that the vertical stress alone does not significantly affect boring machine. Linear and nonlinear regression analyses have been carried out in order to explain the relation between tunnel depth and the rate of penetration. The results are summarised in Table 9.7.

Equation	r	R ²	F	Reference
$ROP = 0.002 * depth + 0.858$	0.314	0.098	20.063	9.28
$ROP = 0.053 * depth^{0.541}$	-	0.207	48.038	9.29

Table 9.7 Results of linear and not linear regression analysis. R² and F value are reported.

9.3.9 Rock Mass Rating

The effect of the global quality of rock mass on the TBM performances has been evaluated by means of correlate the RMR index with the machine parameters. The scatterplots obtained have been reported in Figure 9.14.

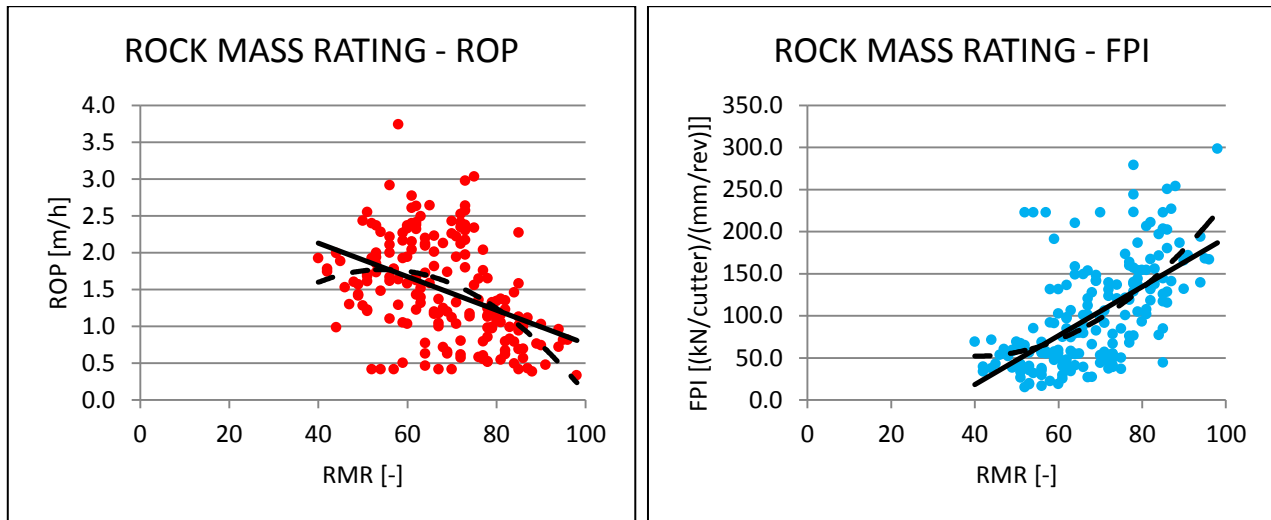


Figure 9.14 RMR vs. ROP (on the left); RMR vs. FPI (on the right), modified after Armetti et al., 2018.

By increasing the rock mass quality, here expressed by means of RMR system, the performances of the TBM generally decreases, in particular ROP reduces and FPI increases. However; the machine performances become lower not only when rock mass sections characterised by high quality occur, but also in low quality grounds because highly jointed or weak rock walls cannot contrast the gripper thrust without make tunnel walls instable. In these situations, FPI is reduced so also ROP is low.

The top TBM performances have been measured in class II (good) as also observed by Sapigni et al. (2002).

The TBM behaviour in poor quality classes is not describable due to the general good or very good quality of La Maddalena rock mass. The performances in lower classes are predictable by observing the polynomial regression curve related to the RMR-ROP analysis.

In order to quantify the correlation between RMR and the performance indices two linear regression analysis and two polynomial ones have been carried out. The results have been proposed in Table 9.8.

9.3 Effects of single rock/rock mass properties on TBM performances

Equation	r	R ²	F	Reference
$ROP = -0.023 * RMR + 3.038$	0.425	0.180	40.516	9.30
$ROP = -0.001 * RMR^2 + 0.089 * RMR - 0.665$	-	0.228	27.000	9.31
$FPI = 2.900 * RMR - 97.590$	0.599	0.359	103.093	9.32
$FPI = 0.052 * RMR^2 - 4.222 * RMR + 137.889$		0.383	56.696	9.33

Table 9.8 Result of linear and polynomial regression analysis. For each equation R² and F values are reported. Coefficient of correlation is listed only for linear models.

9.3.10 Geological Strength Index

The correlation between the Geological Strength Index and ROP and FPI has been evaluated, and the results obtained are very similar to the ones observed for RMR-ROP and RMR-FPI correlations.

For this reason, in this section only the scatterplots (Figure 9.15) and the results of linear and nonlinear regression analyses have been reported (Table 9.9); as for the discussion related to the global rock mass quality effect on the TBM performance, see section 9.3.9.

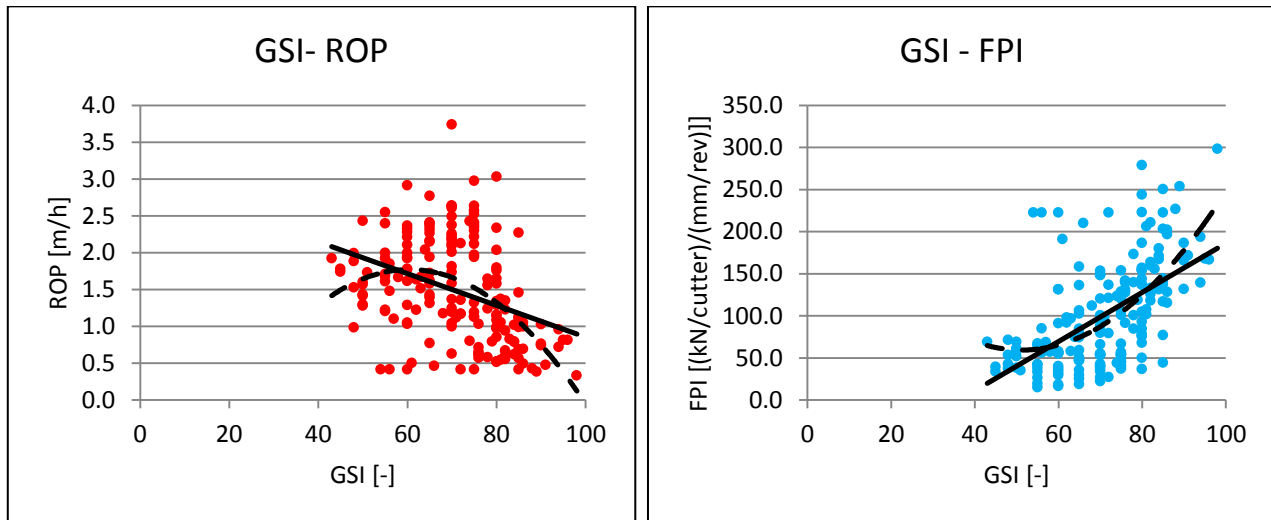


Figure 9.15 GSI vs. ROP (on the left); GSI vs. FPI (on the right), modified after Armetti et al., 2018.

Equation	r	R ²	F	Reference
$ROP = -0.022 * GSI + 3.010$	0.374	0.140	29.936	9.34
$ROP = -0.001 * GSI^2 + 0.141 * GSI - 2.495$	-	0.218	25.450	9.35
$FPI = 2.920 * GSI - 105.901$	0.560	0.313	84.011	9.36
$FPI = 0.079 * GSI^2 - 8.074 * GSI + 265.835$	-	0.357	50.769	9.37

Table 9.9 Result of linear and polynomial regression analysis. For each equation R² and F values are reported. Coefficient of correlation is listed only for linear models.

9.4 Combined effect of rock/rock mass properties on TBM performances

The combined effect of the geological and geotechnical features of a rock mass on the TBM performances registered during its excavation has been investigated by means of multiple regression analyses, which allow to carry out empirical equations.

These equations are the most practical way to explain the relationship between more independent variables and a response one, and are used to predict a parameter from collected data: for this reason they have a great importance during early phases of tunnel design.

During this work, several regression analyses have been performed in order to predict both ROP and FPI. Initially a ROP model and an FPI one has been carried out both for each recognised geological domain and for the entire tunnel length considered to this purpose (models have been obtained on the tunnel tract ranging between Pk. 0 + 197 m and Pk. 2 + 010 m).

It was noted that the most performing models were the ones carried out by considering the geological domains all together and not separately. This is because considering the whole domains more data are involved into the computation and data range is larger, so different situation can be considered at the same time, on the contrary the models related to singular domain take into account for prevalently homogeneous situations.

The results of the regression analyses reported in the following paragraphs have been developed considering the domains all together.

9.4.1 Empirical models to predict the rate of penetration

As mentioned above, in order to obtain an empirical correlation able to represent the relation between rock mass features and ROP, both linear and not linear regression analyses have been performed.

Linear regression models should be preferred in order to investigate the relationship between more than one independent variable and a dependent one, because linear models are the simplest to be carried out and used. For this reason, nonlinear regression analyses have to be developed when linearity assumptions are not satisfied.

9.4.1.1 Multiple linear regression

The geological parameters, considered as predictor, to enter as input in multiple regressions analysis, have been selected on the basis of the single regression results. For this purpose the selected parameters are:

- *UCS*: it gives fundamental information about intact rock strength and affects TBM performances;
- *Quartz content*: it influences the abrasivity and the hardness of rock, so it seriously affects tunnelling;
- *Spacing or Jv*: they are strongly related to each other because they represent the same phenomenon; for this reason they cannot be both inserted in the same model. In this study it was decided to input the spacing between discontinuity as fracturing degree indicator, being Jv a derived parameter;
- *Alpha angle, Jc, Tunnel depth*: these parameters alone are not strongly related to ROP; in this analysis we test their influence when combined with other factors.

RMR and GSI are not included because they consider some of the parameter which have been entered separately.

The model has been generated adopting a stepwise backward selection; at the beginning of the analysis all predictors are included, then the variables that have not significant influence on the response are removed one at a time. The variable is excluded when the null hypothesis (the dependent variable does not influence the independent one) cannot be rejected (p-value >0.05).

9.4 Combined effect of rock/rock mass properties on TBM performances

In this case the parameter that does not affect the rate of penetration is α (p-value >0.05): for this reason a second linear model, named RL2, has been performed.

The results of the analysis have been reported in Table 9.10.

Coefficients										
Model		Unst.ed coefficients		Std.ed coeff.	t	Sign. (p-value)	95,0% C.I. for B		Collinearity statistics	
		B	Std. error	Beta			Bottom Limit	Top Limit	Toler.	VIF
RL 1	(Constant)	2.944	0.248		11.864	0.000	2.455	3.434		
	UCS	-0.004	0.001	-0.236	-4.578	0.000	-0.006	-0.002	0.725	1.380
	q	-0.040	0.004	-0.555	-10.043	0.000	-0.048	-0.033	0.633	1.580
	α	-0.002	0.002	-0.042	-0.896	0.371	-0.006	0.002	0.889	1.124
	S	-0.056	0.016	-0.192	-3.572	0.000	-0.087	-0.025	0.668	1.496
	Jc	0.030	0.009	0.164	3.250	0.001	0.012	0.049	0.761	1.314
	depth	0.001	0.000	0.114	2.445	0.015	0.000	0.001	0.884	1.310
RL 2	(Constant)	2.889	0.240		12.027	0.000	2.415	3.363		
	UCS	-0.004	0.001	-0.239	-4.632	0.000	-0.006	-0.002	0.727	1.376
	q	-0.041	0.004	-0.565	-10.447	0.000	-0.049	-0.033	0.660	1.516
	S	-0.057	0.016	-0.195	-3.636	0.000	-0.088	-0.026	0.671	1.491
	Jc	0.030	0.009	0.163	3.230	0.001	0.012	0.048	0.762	1.313
	depth	0.001	0.000	0.116	2.475	0.014	0.000	0.001	0.885	1.130

Table 9.10 Results of multiple linear regression analysis, red box underlines the no significant parameters.

The second regression gives the coefficient of those variables that significantly influence the rate of penetration (p-value < 0), the null hypothesis is rejected. They are: UCS, quartz content, spacing, joint conditions and tunnel depth.

Problems of multicollinearity do not occur (VIF < 10) and the linear regression assumptions are verified, by testing the random errors; they are independent and normally distributed, they have a mean equal to zero and homoscedasticity has been observed.

9.4 Combined effect of rock/rock mass properties on TBM performances

R^2 (the correlation strength indicator), R^2_{adj} (that takes into account for the number of predictors) and F-value (related to the utility of the overall regression model) are listed in Table 9.11.

r	R^2	R^2_{adj}	F	Sign.
0.809	0.653	0.643	67.683	0.000

Table 9.11 RL2 Model summary.

R^2_{adj} is 0.643, it means that the regression model is able to explain the 64.30% of the total variance of the dataset. F-value is equal to 67.683 and Sign. is 0.000, so the null hypothesis can be rejected.

The equation able to explain the relationship between the five geological parameters and ROP is as follows:

$$ROP = -0.004 * UCS - 0.041 * q - 0.057 * S + 0.030 * Jc + 0.001 * d + 2.889 \quad (9.38)$$

By observing the regression coefficients, it is possible to assert that the equation can be adopted to explain the simultaneous influence of five geological properties on the TBM performance. In Chapter 12, the capability of the model to predict the rate of penetration will be discussed.

9.4.1.2 Multiple nonlinear regression analysis

It has been observed that the relationship between some geological parameters and ROP (or FPI), seems to be nonlinear, on the basis of the analyses of the scatterplots reported in section 9.3.

Carrying out multiple nonlinear regression analyses may be useful in order to evaluate the nonlinear relationship between the geological and geotechnical features of the rock mass and the rate of penetration.

Nonlinear regressions can be performed in two steps: in the first one the mathematical function that best represent the relation between a given independent variable and a dependent one has to be selected. This selection has to be performed for each variable that is necessary to input into the analysis. Then the mathematical functions have to be entered into the model in order to evaluate their combined effects.

In this study the more representative mathematical functions have been recognised by means of the scatterplots (section 9.3). Moreover, to this purpose simple nonlinear regression analyses have been performed, the results have been listed in Table 9.12.

9.4 Combined effect of rock/rock mass properties on TBM performances

Independent Variable	Model	R ²	F	Sign.	Constant	b1	b2
UCS	Linear	0.306	81.305	0.000	2.829	-0.010	
	Logarithmic	0.290	75.243	0.000	7.823	-1.306	
	Quadratic	0.306	40.435	0.000	2.864	-0.011	1.811E-6
	Power	0.303	79.802	0.000	196.760	-1.033	
	Exponential	0.322	87.424	0.000	3.809	-0.008	
q	Linear	0.558	232.330	0.000	3.408	-0.055	
	Logarithmic	0.572	246.176	0.000	8.293	-1.930	
	Quadratic	0.583	127.693	0.000	6.688	-0.250	0.003
	Power	0.565	238.526	0.000	2.465	-1.485	
	Exponential	0.560	234.192	0.000	5.824	-0.042	
α	Linear	0.088	17.688	0.000	2.123	-0.014	
	Logarithmic	0.086	17.356	0.000	3.472	-0.533	
	Quadratic	0.089	8.952	0.000	2.287	9.226E-5	-0.023
	Power	0.100	20.530	0.000	6.897	-0.445	
	Exponential	0.107	22.127	0.000	2.263	-0.012	
S	Linear	0.227	54.126	0.000	1.820	-0.139	
	Logarithmic	0.244	59.433	0.000	1.722	-0.434	
	Quadratic	0.268	33.569	0.000	2.069	-0.338	0.020
	Power	0.262	65.460	0.000	1.584	-0.348	
	Exponential	0.256	63.185	0.000	1.725	-0.114	
Jc	Linear	0.035	6.660	0.011	2.101	-0.035	
	Logarithmic	0.024	4.578	0.034	2.882	-0.489	
	Quadratic	0.073	7.234	0.001	0.240	0.178	-0.006
	Power	0.050	9.701	0.002	6.205	-0.544	
	Exponential	0.066	13.095	0.000	2.532	-0.037	
Depth	Linear	0.098	20.063	0.000	0.858	0.002	
	Logarithmic	0.138	29.573	0.000	-1.901	0.572	
	Quadratic	0.195	22.095	0.000	-0.430	0.010	-1.122E-5
	Power	0.207	48.038	0.000	0.053	0.514	
	Exponential	0.158	34.410	0.000	0.709	0.002	

Table 9.12 Linear and nonlinear models between geological parameters and ROP. In bold the selected models.

9.4 Combined effect of rock/rock mass properties on TBM performances

The equations selected to be entered into the nonlinear model are:

$$ROP = 3.809 * e^{-0.008UCS} \quad (9.39)$$

$$ROP = -1.930 * \ln(q) + 8.293 \quad (9.40)$$

$$ROP = 2.263 * e^{-0.012\alpha} \quad (9.41)$$

$$ROP = 1.584 * S^{-0.348} \quad (9.42)$$

$$ROP = 2.532 * e^{-0.037Jc} \quad (9.43)$$

$$ROP = 0.053 * d^{0.514} \quad (9.44)$$

The global multiple nonlinear equation is as follows (model RNL):

$$\begin{aligned} ROP &= 22.316e^{-2.120E-4UCS} - 1.426\ln(q) + 7.806e^{-0.0003\alpha} + 31.171S^{-0.003} - 1.412e^{-0.094Jc} \\ &+ 0.001d^{1.024} - 53.952 \end{aligned} \quad (9.45)$$

The coefficient of determination, R^2 , related to RNL is equal to 0.655.

9.4 Combined effect of rock/rock mass properties on TBM performances

9.4.2 Empirical models to predict the field penetration index

9.4.2.1 Multiple linear regression

Multiple linear regression analyses have been developed in order to investigate the influence of the principal rock mass parameters on the field penetration index.

The procedures adopted are the same discussed in the paragraphs about ROP models (see section 9.4.1.1), for this reason here only the analyses results and a brief comment on them are reported.

The input parameters are: UCS, quartz content of the rock, spacing between fractures, alpha angle, joint condition parameters, and the depth of the tunnel; these are the independent variables.

The response variable is FPI.

The model has been generated adopting a stepwise backward selection; for this reason, at the beginning all predictors are included, then the not influencing variables (p-value >0.05) are removed one at a time.

In this case the parameter that does not affect the field penetration index are: Jc (Sign. 0.926), tunnel depth (Sign. 0.726) and alpha angle (Sign. 0.143).

The results of the regression analyses have been reported in Table 9.13.

9.4 Combined effect of rock/rock mass properties on TBM performances

Coefficients										
Model		Unst.ed coefficients		Std.ed coeff.	t	Sign. (p-value)	95,0% C.I. for B		Collinearity statistics	
		B	Std. error	Beta			Bottom Limit	Top Limit	Toler.	VIF
FL1	(Constant)	-78.297	24.605		-3.182	0.002	-126.850	-29.744		
	UCS	0.386	0.093	0.234	4.134	0.000	0.202	0.570	0.725	1.380
	q	2.472	0.400	0.375	6.185	0.000	1.683	3.261	0.633	1.580
	α	0.330	0.224	0.075	1.473	0.142	-0.112	0.773	0.889	1.124
	S	8.498	1.556	0.322	5.461	0.000	5.427	11.569	0.668	1.496
	Jc	0.086	0.924	0.005	0.094	0.926	-1.737	1.910	0.761	1.314
	depth	0.008	0.023	0.018	0.360	0.719	-0.037	0.053	0.884	1.131
FL2	(Constant)	-76.917	19.647		-3.915	0.000	-115.686	-38.148		
	UCS	0.386	0.093	0.235	4.165	0.000	0.203	0.569	0.729	1.372
	q	2.474	0.398	0.375	6.215	0.000	1.688	3.259	0.635	1.576
	α	0.331	0.223	0.075	1.480	0.141	-0.110	0.772	0.890	1.124
	S	8.549	1.456	0.324	5.872	0.000	5.676	11.421	0.759	1.317
	depth	0.008	0.023	0.018	.351	0.726	-0.037	0.052	0.905	1.105
	FL3	(Constant)	-72.394	14.803		-4.891	0.000	-101.602	-43.186	
UCS		0.386	0.093	0.235	4.175	0.000	0.204	0.569	0.729	1.372
q		2.439	0.385	0.370	6.339	0.000	1.680	3.199	0.676	1.480
α		0.328	0.223	0.075	1.473	0.143	-0.111	0.768	0.891	1.122
S		8.547	1.452	0.324	5.885	0.000	5.681	11.413	0.759	1.317
FL4		(Constant)	-63.491	13.555		-4.684	0.000	-90.236	-36.745	
	UCS	0.394	0.093	0.239	4.247	0.000	0.211	0.576	0.731	1.368
	q	2.564	0.377	0.389	6.807	0.000	1.821	3.307	0.710	1.408
	S	8.707	1.453	0.330	5.993	0.000	5.840	11.573	0.764	1.310

Table 9.13 Results of multiple linear regression analysis, red boxes underline the no significant parameters.

9.4 Combined effect of rock/rock mass properties on TBM performances

Four models have been created; FL1, FL2 and FL3 involve parameters (J_c , tunnel depth and α) that do not significantly affect the response variable. The model FL4 considers only the influencing independent variables, they are: UCS, quartz content and the spacing between fractures. FL4 is not affected by multicollinearity problems and the linearity assumptions are satisfied.

The carried out empirical equation is as follows:

$$FPI = 0.394 * UCS + 2.564 * q + 8.707 * S - 63.491 \quad (9.46)$$

The regression indices are summarised in Table 9.14.

r	R²	R²_{adj}	F	Sign.
0.761	0.568	0.571	83.222	0.000

Table 9.14 FL4 model summary.

The regression model named FL4 is able to explain the 57.10% of the total variance, it modestly represents the relationship between UCS, q, S and FPI.

9.4 Combined effect of rock/rock mass properties on TBM performances

9.4.2.2 Multiple nonlinear regression

Multiple nonlinear regression analyses have been carried in order to investigate the effects of the geological and mechanical parameters on the FPI.

The procedure is the same of the one discussed about ROP model (see section 9.4.1.2). In this case too, the most representative nonlinear functions have been individuated on the basis of the scatterplots and by means of simple nonlinear regressions.

The results are listed in Table 9.15.

9.4 Combined effect of rock/rock mass properties on TBM performances

Independent Variable	Model	R ²	F	Sign.	Constant	b1	b2
UCS	Linear	0.307	81.502	0.000	-20.973	0.912	
	Logarithmic	0.310	82.756	0.000	121.997	-491.460	
	Quadratic	0.317	42.554	0.000	-91.105	1.967	-0.004
	Power	0.324	88.374	0.000	0.125	1.336	
	Exponential	0.324	88.048	0.000	21.553	0.010	
q	Linear	0.414	129.729	0.000	-48.921	4.240	
	Logarithmic	0.426	136.557	0.000	-430.079	150.462	
	Quadratic	0.444	72.990	0.000	-377.938	23.836	-0.272
	Power	0.468	161.656	0.000	0.213	1.689	
	Exponential	0.450	150.420	0.000	15.444	0.047	
α	Linear	0.096	19.498	0.000	40.326	1.357	
	Logarithmic	0.089	17.887	0.000	-81.448	48.792	
	Quadratic	0.096	9.708	0.000	36.297	1.558	-0.002
	Power	0.073	14.416	0.000	14.045	0.473	
	Exponential	0.082	16.399	0.000	45.215	0.013	
S	Linear	0.352	100.034	0.000	62.824	15.654	
	Logarithmic	0.412	128.778	0.000	72.669	50.871	
	Quadratic	0.423	67.109	0.000	33.244	39.216	-2.431
	Power	0.408	126.951	0.000	60.941	0.543	
	Exponential	0.316	85.002	0.000	55.965	0.159	
Jc	Linear	0.112	23.277	0.000	0.514	5.600	
	Logarithmic	0.092	18.645	0.000	-145.474	86.042	
	Quadratic	0.141	15.054	0.000	146.646	-11.060	0.455
	Power	0.070	13.841	0.000	8.247	0.804	
	Exponential	0.086	17.235	0.000	32.202	0.052	
Depth	Linear	0.034	6.529	0.011	134.180	-0.083	
	Logarithmic	0.045	8.621	0.004	274.663	-29.366	
	Quadratic	0.061	5.969	0.003	195.753	-0.477	0.001
	Power	0.057	11.200	0.001	677.540	-0.356	
	Exponential	0.046	8.771	0.003	124.179	-0.001	

Table 9.15 Linear and nonlinear models between geological parameters and FPI. In bold the selected models.

9.4 Combined effect of rock/rock mass properties on TBM performances

On the basis of the scatterplots reported in section 9.3 and considering the results listed in Table 9.15 alpha and depth have been excluded from the multiple analyses. The equations entered into the model are:

$$FPI = 0.125 * UCS^{1.336} \quad (9.47)$$

$$FPI = 0.213 * q^{1.689} \quad (9.48)$$

$$FPI = 50.871 * \ln(S) + 72.669 \quad (9.49)$$

$$FPI = 0.514 * Jc + 5.600 \quad (9.50)$$

The equations 9.45, 9.46, 9.47 and 9.48 have been considered in order to evaluate the nonlinear effect of multiple parameters on the FPI. The empirical model, named FNL, which has been obtained, is as follows:

$$FPI = 8.408UCS^{0.509} + 7513.902q^{0.011} + 27.552\ln(S) + 0.080Jc - 7818.256 \quad (9.51)$$

The coefficient of determination related to FNL is 0.590.

9.5 Conclusion

In order to evaluate the relationships between the geological and mechanical parameters that characterise the rock mass excavated during La Maddalena construction and the TBM performances registered during tunnel boring regression analyses have been carried out.

The bivariate regression analyses, linear and not linear type, between single rock/rock mass parameters and TBM performance indices (ROP and FPI) have allowed to investigate the effects of the geological conditions on the machine involved to excavate into a specific ground. During this study twenty correlations have been tested: in three cases no correlation has been observed.

When correlation (more or less strong) occurs, simple regression analyses have been developed. These permit both to evaluate the correlation between a single rock parameter and a single TBM one, and the mathematical form that best describes this relation.

Thirteen regression equations have been obtained about the relationship between the geological features of La Maddalena rock mass and the measured ROP; seven of them are linear and six not linear. About FPI, six linear regression equations and seven not linear ones have been carried out.

The geological parameters more related to the TBM indices are UCS, quartz content, spacing and J_v and the parameters which represent the global quality of rock mass (RMR and GSI).

The simple regression analyses do not allow for evaluating the combined effects of all the parameters characterising a rock mass; for this purpose it is necessary to carry out multiple regression analyses. Linear regression analyses have been developed both for ROP and FPI. The $R^2_{adj.}$ of ROP model is slightly higher than the FPI one. Linearity assumptions are satisfied in both cases, for this reason the linear models can be considered able to explain the influence of geology on tunnel excavation.

Furthermore nonlinear multiple regression analyses have been considered and a model has been created for both TBM indices. The type of nonlinear relationship has been imposed: in other words, it has been assumed that the geological parameters and the TBM ones are linked by a specific type of mathematical function. It might be considered as an error, and for this reason it is recommended to avoid the use of nonlinear multiple models. Linear models are simpler to create and use, moreover, when the assumptions that they imply are verified, they are statistically more reliable than the nonlinear ones.

10 CLUSTER ANALYSIS OF ROCK MASS PARAMETERS FOR TBM PERFORMANCE ESTIMATION

In this chapter a method able to estimate the rock mass excavatability is presented.

As it is well known, the performances of a TBM employed to bore a given rock mass depend on a large quantity of geological, structural and mechanical rock mass parameters and on machine specification. The most common way to analyse the combined effect of all these parameters is the multiple regression analysis (as described in Chapter 9); however during this research a new multidimensional geological-TBM data analysis tools has been involved: they are represented by multiple correspondence analysis (MCA) and by clustering.

These statistical tools allowed to divide the rock masses encountered during the construction of “La Maddalena” exploratory tunnel in three homogeneous portions characterised by specific geomechanical features and TBM performances. In this way three classes of excavatability have been defined.

Multiple regression analyses for each cluster have been carried out in order to provide a mathematical function able to relate the geological characteristics of clusters and the performances measured during its boring.

This chapter is divided in two parts: in the first one some theoretical notes on the involved statistical methods have been provided and in the second one their application at “La Maddalena” case study and the obtained results are explained.

10.1 Multidimensional data analysis

10.1.1 Introduction

Survey results are usually summarized in tables by counting the response to a series of questions and the observations (the individuals) are described by several variables; in other words, a group of individuals is described by a set of variables. Very often the specific goal is to describe the data structure under two aspects. The first one is to determine which observations are similar to each other and the second one is to understand the relationship between the variables.

In order to reach this objective, a set of statistical methods is available; they are listed in Figure 10.1.

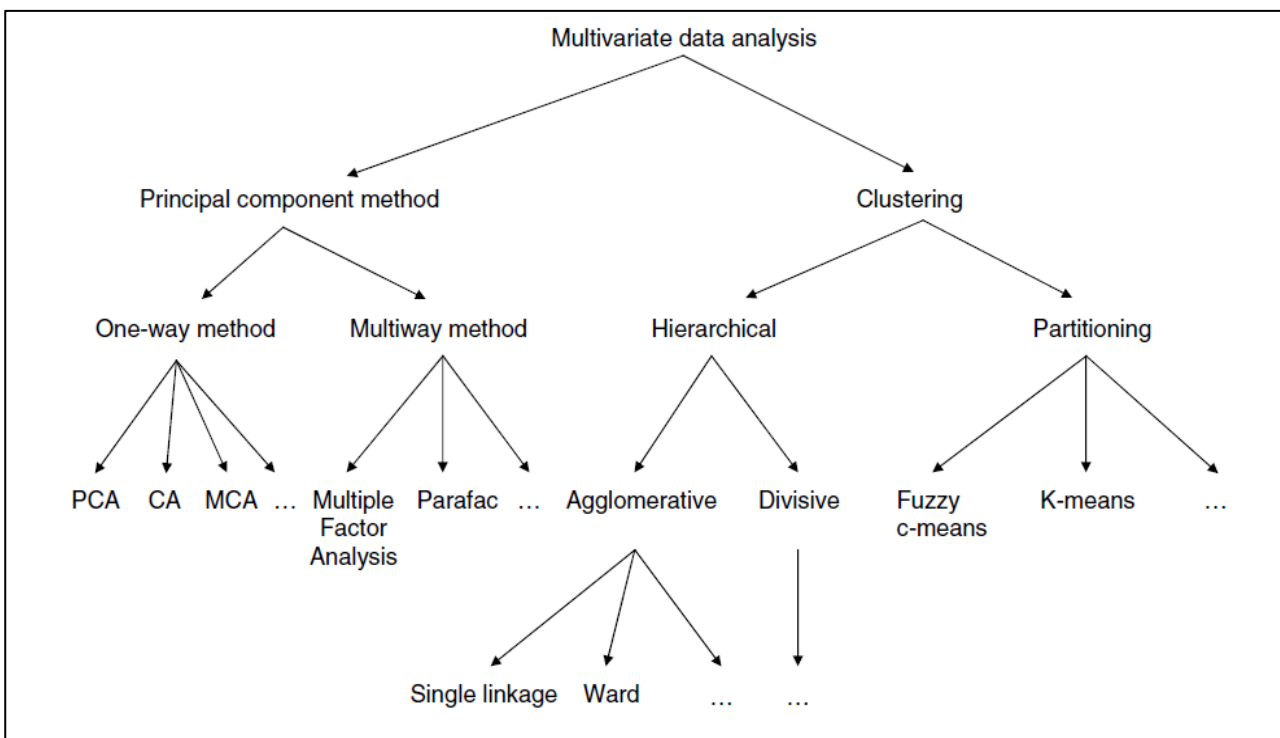


Figure 10.1 Multivariate data analysis methods (Husson et al., 2017).

Exploratory Data Analysis (EDA) and in particular Multivariate Data Analysis (MDA) refer to all descriptive methods for multivariate data set which allow to visualise and describe the data set. In particular these methods permit to study the similarities and the dissimilarities between individuals from a multidimensional point of view (Husson et al., 2010). EDA is fundamental in all statistical analysis both as main aim and as preliminary study.

Two kinds of methods are able to study the similarities between individuals:

- The first one is the *Principal Component Methods* such as Principal Component Analysis (PCA) adopted for continuous variables or Multiple Correspondence Analysis (MCA) for the categorical ones (Greenacre, 2006);
- The second one is the *clustering analysis*. In particular hierarchical and partitional clustering methods can be distinguished. The first one requires to define a distance (Euclidean, Manhattan, etc.) and an agglomeration criterion (Ward, centroid, etc.) (Husson et al., 2010). A tree, named dendrogram, represents the indexed hierarchy. The partitional clustering method is another way to study the similarities between subjects. The most utilised algorithm of this group is based on the Euclidean distance and it is the K-mean algorithm. The clusters of individuals are then described by the variables (Husson et al., 2010).

Principal component methods are frequently used as pre-processing step of clustering with the aim, for example, of denoising data or transform categorical data in continuous ones.

Principal component and clustering methods ones are often combined in order to better understand both the characteristics of collected data and the similarities/dissimilarities between individuals.

10.1.2 Euclidean space

A dataset is a more or less a large collection of information, that are represented as points belonging to some spaces. The most common one is the Euclidean space which has a set of considerable properties useful for clustering, however also the non-Euclidean space has to be considered (see section 10.1.4.4). The points of the Euclidean space are vectors of real numbers; theirs length is the number of the space dimensions. The coordinates of the represented point are the components of the vector. All spaces have a distance measure giving a distance between any two points in the space. In the Euclidean space the most frequently calculated distance is the Euclidean one, computed as the square root of the sum of the squares of the differences between point coordinates in each dimension.

Others distance measures are the Manhattan one (calculated as the magnitude sum of the differences in each dimension, Birant and Kut, 2007) and the L_∞ - distance (calculated as the maximum difference magnitude in any dimension).

A relationship between two points, in order to be the measuring distances function, has to satisfy the following requirements:

- The distance has to be positive;

10.1 Multidimensional data analysis

- Only the distance between a point and itself can be null;
- Distance is symmetric (it is independent from the order that the points are considered during the calculation of distance);
- Distance measures respond on the triangle inequality (it means that the distance from x to y to z is always more than the distance going from x to z directly).

10.1.3 Principal component methods

When one of the principal component methods is chosen in order to perform a statistical analysis, individuals are considered in an Euclidean space of high dimensions and the study of the shape of the point cloud permits to study the similarities between individuals (Husson et al., 2010). Principal component methods approximate the point cloud into a low dimensional Euclidean subspace while maintaining the same distance between individuals.

The main purpose common to all principal component methods is to describe a data set (with individuals and variables) utilizing a small number of variables uncorrelated each other with the aim of obtaining as much information as possible. A brief description of principal component methods has been reported.

- *Correspondence analysis, CA*: it is a multivariate graphical technique that allows to study the relationships between two variables (Abdi and Valentin, 2007). They are compared in pairs and they are not considered all together. As outcome, CA shows a graphic display of the rows and columns of a contingency table that allows to visualize the major relationships among the variable responses in a low-dimensional space (Abdi and Valentin, 2007);
- *Principal component analysis, PCA*: it can be considered as a denoising method which separates noise and signal. In fact, the first dimension extracts the essential information and the second one is related to noise. The following clustering is more stable without the noise than the one carried out from the original distance. The relationships between variables are studied all together, but this approach presents some limitations indeed it considers the linear relationship between variables as the only possible one (actually more complex links can also exist) and it focuses on a Gaussian distribution of variables;
- *Multiple correspondence analysis, MCA*: In this case too, the relationships between variables are studied all together, but the limitations that affect the PCA do not occur. It

focuses both on linear and nonlinear relationship and without distributional assumptions, unlike traditional multivariate technique.

In this study only MCA has been applied, for this reason in the following paragraphs only MCA will be described.

10.1.3.1 Multiple Correspondence Analysis

Multiple Correspondence Analysis is one of the most widespread statistical methods involved to inspect and describe multivariate association among variables and /or patterns of similarity among statistical units or “individuals”. MCA is commonly used to analyse data collected through surveys and it is applied to tables with individuals (in the rows) and categorical variables (in the columns). The target is to identify:

- Groups of individuals with similar profile in their answer to the questions;
- The associations between categorical variables.

MCA is an extension of CA for summarizing a data table containing more than two variables (Abdi and Williams, 2010); in other words MCA is the specific application of correspondence analysis to tables with individuals and their answers to a number of categorical variables (Husson et al. 2017). MCA can be considered as a way to code categorical variable onto a set of continuous ones, the principal components. As for principal component analysis, only the first dimension is usually kept in consideration to stabilize the eventual following clustering by deleting the noise from the data (Husson et al., 2010).

MCA is designed for the analysis of categorical variables; however, numerical variables can be also analysed by subdividing their values in a finite set of classes. In MCA, both the modalities of the variables and the individuals are represented as clouds of points, vectors, in Euclidean spaces, typically of high dimensionality. Then the clouds are projected in low-dimensional spaces (usually characterized by two or three dimensions); however, preserving the highest possible amount of data variability is requested.

As a result, MCA allows to represent a multitude of variables and/or statistical units in few graphical displays (usually one or two), thus achieving the goal of “data reduction”. The displays allow to investigate the association/similarity patterns by the interpretation of the configurations of the clouds of points represented within.

Two essential rules of interpretation are:

10.1 Multidimensional data analysis

- Concerning the association among variables: when two or more points are close to one another, this suggests the possible presence of at least a subgroup of statistical units characterised by these modalities;
- Concerning the similarity among individuals: the lower the distance among two or more points, the higher the similarity among the corresponding units.

As a consequence of the second rule, the coordinates of the points can be involved to identify subgroups of individuals with similar characteristics, or, in other words, to detect the presence of homogeneous clusters.

In MCA, the overall quality of representation of the displays is measured by the index of explained inertia, which quantifies the relative amount (expressed as percentage) of data variability preserved by the low-dimensional spaces. As a rule, a relatively high proportion of explained inertia (e.g. > 50%) usually indicates good quality of representation.

This method does not provide a systematic procedure able to assign the statistical units to the clusters; that is to establish, for each individual, to which cluster it belongs. For this purpose, a frequently adopted procedure consists in performing cluster analysis on the coordinates of the points in the respective displays.

Finally, it must be pointed out that, since MCA is based on a merely geometrical approach, the groups of individuals with similar profiles and the associations between categorical variables can be deduced by observing the graphical displays carried out by MCA method; however, it is known that, sometimes, the displays could show spurious or unrealistic relationships.

Therefore, to rule out the possibility of faulty conclusions, it is of fundamental importance that the results should be evaluated by field experts and in order to make these considerations more objectives clustering procedure can be applied.

Study of individuals

An individual is a row of the data table, composed by a set of K numerical values that evolves within the so called individual's space, a space R^K (Husson et al., 2017). The scatterplot of the individuals in R^K is represented in Figure 10.2.

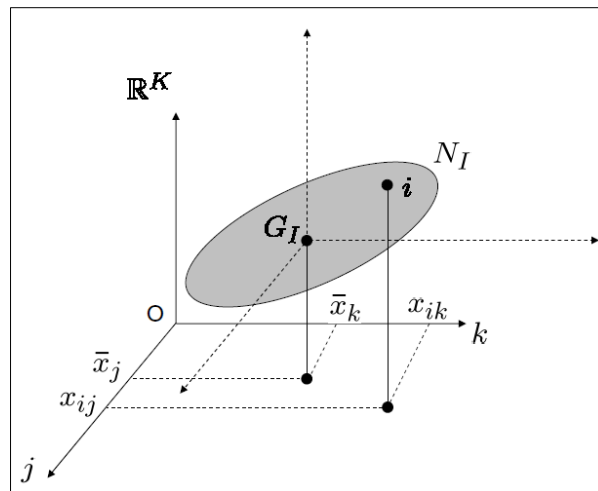


Figure 10.2 Scatterplot of the individuals in R^K ; (Husson et al., 2017).

The study of individuals aims to understand the similarities between the individuals in terms of all variables (which are the most similar/dissimilar individuals) and point out if there are consistent in terms of their similarities.

The Euclidean distance between individuals depends on their characteristics and it gives information about their similarity: for example, if two individuals have similar values within the table of all K variables they are also “close”. The distance is expressed by using an indicator matrix¹ as:

$$d(i, i') = \sqrt{C \sum_{k=1}^K \frac{(x_{ik} - x_{i'k})^2}{I_k}} \quad (10.1)$$

where:

- $(x_{ik} - x_{i'k})$ is the difference between categories;
- I_k is the number of individuals carrying the category k ;
- C is a constant.

¹ From a data table of individuals X categorical variables an indicator matrix with individuals in the rows and all of the categories for every variable in the columns has been constructed. In the table the element x_{ij} has a value 1 if the individual i carries the category k , vice versa it has value 0. For this reason the table $I \times K$ is composed by 1 and 0 only. (Husson et al., 2017).

10.1 Multidimensional data analysis

In order to obtain a graphical representation of the cloud of individuals, N_I (Figure 10.3) they are projected on a plane P of R^K . N_I is made up of many points and it is built to see if it is identifiable a specific shape or particular groups of individuals.

During the representation it is necessary to minimise the N_I distortion: for this reason the distance between the projected points has to be as close as possible to the distance between the original ones.

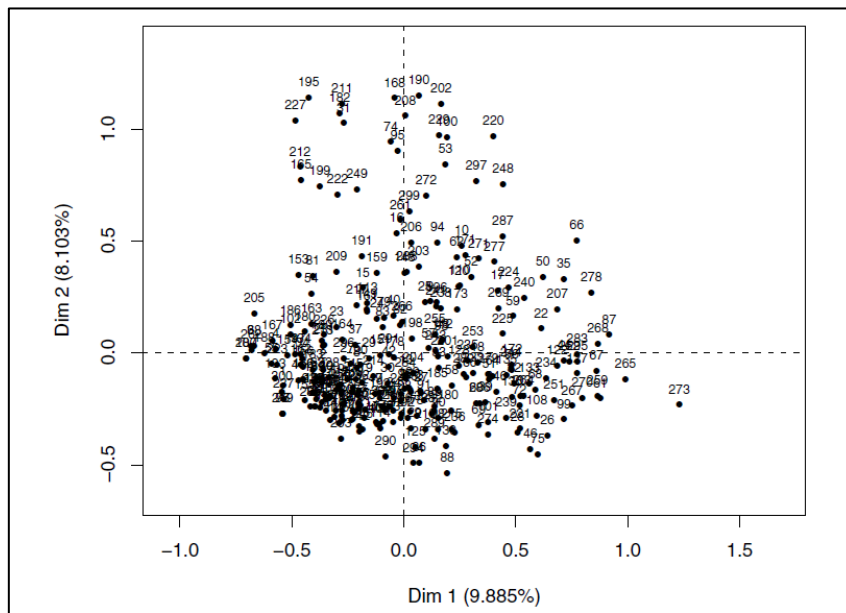


Figure 10.3 Representation of the cloud of individuals, for the two first principal components: Dim 1 and Dim 2. The percentage regards the percentage value of the explained inertia (Husson et al., 2017).

The cloud is constructed maximizing the inertia of individuals projected onto a series of orthogonal axes (Dim 1 and Dim 2 in Figure 10.3).

The study of individuals can be difficult, due to their large number, so commonly it is generalized by studying the categories through the individuals that they represent (Husson, 2017).

Study of categories

The information obtained by a variable can be evaluated in terms of its categories: for this reason, in MCA it is necessary to study the categories as categories present both variables and a group of individuals (Husson et al., 2017). In order to understand how close a category is to others it is fundamental to consider the distance between each other. It has to be taken into account that two categories k and k' are each associated with a group of individuals. If few individuals select, both categories these will be more distant, so more different, contrariwise they will be similar. The

distance between k and k' is based on the count of the number of individual belonging both the two categories. It can be calculated as:

$$d_{k,k'}^2 = C' \frac{I_{k \neq k'}}{I_k I_{k'}} \quad (10.2)$$

where:

C' is a constant and $I_{k \neq k'}$ is the number of individual belonging either k and k' .

Being $x_{ik} = 0$ or 1, the number of individuals selecting only one category is:

$$I_{k \neq k'} = \sum_{i=1}^I (x_{ik} - x_{ik'})^2 \quad (10.3)$$

So:

$$\begin{aligned} d_{k,k'}^2 &= C' \frac{1}{I_k I_{k'}} \sum_{i=1}^I (x_{ik} - x_{ik'})^2, \\ &= C' \frac{\sum_{i=1}^I x_{ik}^2 + \sum_{i=1}^I x_{ik'}^2 - 2 \sum_{i=1}^I x_{ik} x_{ik'}}{I_k I_{k'}} \end{aligned} \quad (10.4)$$

Being $x_{ik} = 0$ or 1; $x_{ik}^2 = x_{ik}$ so $\sum_i x_{ik}^2 = \sum_i x_{ik} = I_k$

$$d_{k,k'}^2 = C' \left(\frac{1}{I_{k'}} + \frac{1}{I_k} - 2 \frac{\sum_{i=1}^I x_{ik} x_{ik'}}{I_k I_{k'}} \right) \quad (10.5)$$

However:

$$\frac{1}{I_k} = \frac{I_k}{I_k^2} = \frac{\sum_{i=1}^I x_{ik}^2}{I_k^2} \quad (10.6)$$

Developing the equation, the distance between two categories can be expressed as:

$$d_{k,k'}^2 = C' \sum_{i=1}^I \left(\frac{x_{ik}}{I_k} - \frac{x_{ik'}}{I_{k'}} \right)^2 \quad (10.7)$$

10.1 Multidimensional data analysis

In MCA the categories can be depicted at the barycentre² of the individuals with those categories. The best use of representation is made when the representation corresponds to the one carried out by maximizing the inertia of the cloud of categories on a sequence of perpendicular axes, as represented in Figure 10.4.

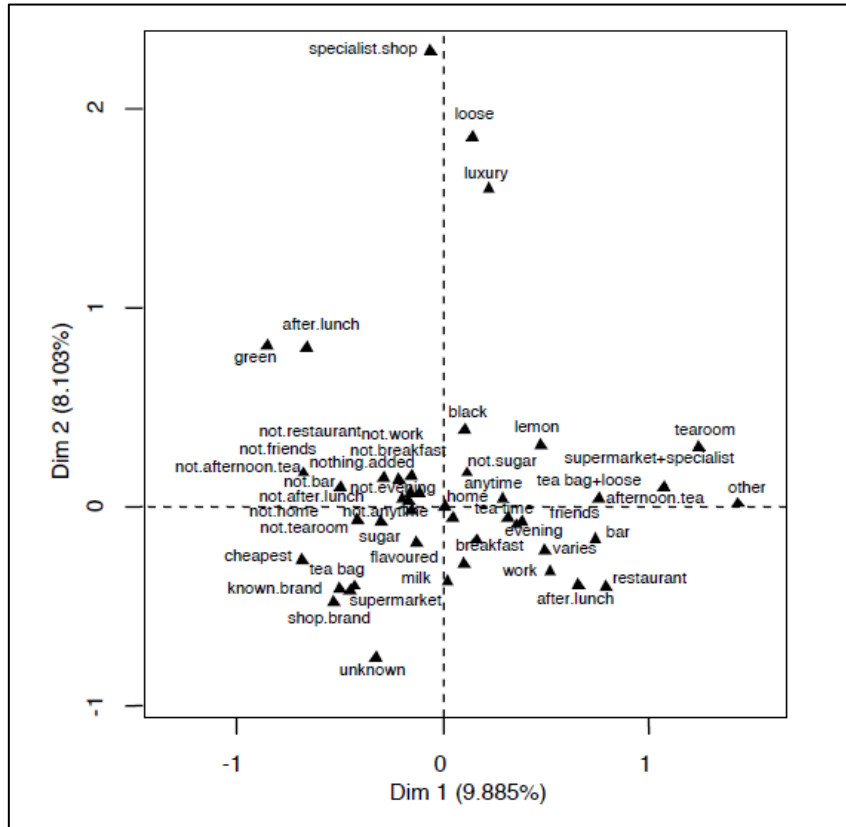


Figure 10.4 Representation of the cloud of categories (Husson, et al., 2017).

The inertia of a category is usually evaluated from the distance from k to the centre of gravity of the categories cloud with coordinates $1/I$, as:

$$\begin{aligned}
 d_{k,G_I}^2 &= I \sum_{i=1}^I \left(\frac{x_{ik}}{I_k} - \frac{1}{I} \right)^2 \\
 &= \frac{I}{I_k} - 1
 \end{aligned} \tag{10.8}$$

The distance increases when very few individuals have taken the category k . The inertia can be expressed as:

² The barycentre of all of categories for a variable is located at the centre of gravity of the cloud of individuals (Husson et al., 2017).

$$\begin{aligned}
Inertia(k) &= d_{k,G_I}^2 * \frac{I_k}{IJ} \\
&= \frac{I_k}{IJ} \left(\frac{I}{I_k} - 1 \right) \\
&= \frac{I - I_k}{IJ} \\
&= \frac{1}{J} \left(1 - \frac{I_k}{I} \right)
\end{aligned} \tag{10.9}$$

The inertia of variable j , which is the inertia of all of the K_j categories for a variable j is equal to:

$$Inertia(j) = \sum_{k=1}^{K_j} \frac{1}{J} \left(1 - \frac{I_k}{I} \right)$$

With $\sum_{k=1}^{K_j} I_k = I$

$$Inertia(j) = \left(\frac{K_j - 1}{J} \right) \tag{10.10}$$

The variable inertia only depends on the category number that makes it up (Husson et al., 2017).

It is recommended to have an equal number of categories for each variable therefore if a variable has a large number of categories the categories are shared over many different dimensions and this variable does not influence the principal axes construction.

The inertia associated with all of the categories is the same of the inertia of the category cloud.

10.1 Multidimensional data analysis

10.1.4 Cluster analysis

PCA, CA and MCA allow to visualize the association between variables and to identify the features of studied characteristics on the basis of graphical displays. In order to make objective this graphical interpretation the cluster analysis method can be adopted.

The objective of cluster analysis is to assign observations to groups (the clusters) so that:

- Observations within each group are similar to one another with respect to variables or attributes of interest;
- Groups themselves stand apart from one another.

Cluster analysis seeks to discover the number and the composition of the groups. The methods that can be used to carry out a cluster analysis can be divided into two groups: the *hierarchical* methods and the *non-hierarchical* ones.

10.1.4.1 Hierarchical clustering methods

The hierarchical clustering method goal is to visualize the links between objects and in order to do that a hierarchical tree (or dendrogram) has to be built (Figure 10.5).

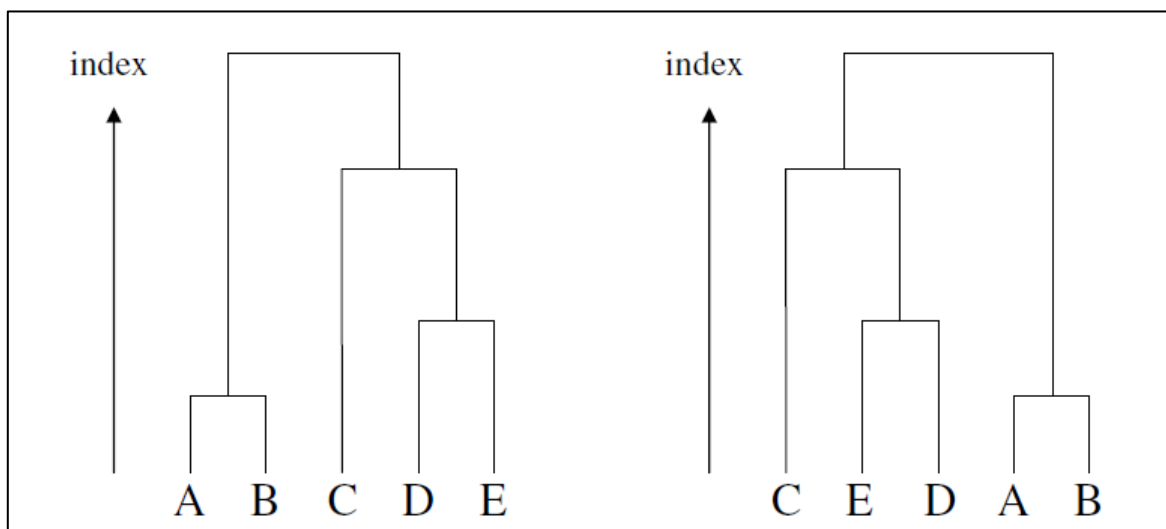


Figure 10.5 Hierarchical tree summarising the associations between 5 objects (Husson et al., 2017).

The hierarchical methods can be divided into two families, based on different algorithms: the agglomerative one and the divisive one. In the first one, subject start in their own separate cluster, then the most similar are combined and this procedure is repeated until all subjects are located in one cluster. At last, the best cluster number is chosen out of all cluster solutions.

There are several algorithms based on the Agglomerative Hierarchical Clustering, AHC; the main ones are:

- *Nearest neighbour method*, also called *single linkage method*: the distance (similarity) between two clusters is defined with the aim to be the one between the two closest groups, the neighbour. This approach is simple to use and it is suitable when the cluster shapes are not spherical or elliptical; as for negative aspects it is criticized because it does not consider the cluster structure;
- *Furthest neighbour* or *complete linkage method*: the distance (similarity) between two clusters is defined with the aim to be the maximum one between members. It is sensitive to outliers and it doesn't consider the cluster structure, it produces compact and similar in size cluster;
- *Average linkage method*: it is a quite robust method where the distance between two groups is evaluated as the average distance between all pairs of members in the two considered clusters;
- *Centroid method*: this approach is based on the distance between centroids (that is the main value for each variable) of each cluster. Groups whose centroids are nearest together are connected. Also this method is robust;
- *Ward's method*: this algorithm is the most largely adopted in AHC. It consists of regrouping two elements by maximizing the quality of the obtained partition (Husson et al., 2017). All possible group couples are arranged and the distance (squared) within each cluster is calculated and summed over all of them. The combination that offers the lowest sum of square is considered. This method is sensitive to outliers and it generally returns equal size clusters.

The *divisive methods*, sometimes called *top-down clustering*, are less used and conceptually more complex than the agglomerative ones. All subjects start into one cluster (at the top) then the cluster is split through a flat clustering algorithm. The procedure is applied until each subject is in its own group (Christopher et al., 2008).

10.1 Multidimensional data analysis

Number of clusters

When the cluster analysis has been obtained, it is necessary to choose the optimal cluster solution; the optimal number of clusters can be selected with several methods (Jolliffe, 2002); however in order to do this operation it is useful to take into account some important concepts:

- The graphical aspect of the dendrogram (Figure 10.6) suggests into how many clusters the partitioning has to be carried out. In fact the tree shows which clusters have been joined at each analysis passage and the distance between clusters at the time of connecting. If a large gap in the distance between clusters occurs from one stage to the following one it means that at one passage clusters that are close together were linked and in the following step the joined clusters were far. This observation suggests that the suitable number of clusters is the one observed just before the significant gap in distance;
- A bar chart can visualize the decrease in the node levels (Figure 10.6), each irregularity in this decrease educes another division;
- The cluster number should not be too high in order not to prevent the succinct nature of the approach;
- Cluster interpretability: it is strongly advisable to maintain only the easy interpretable subdivisions.

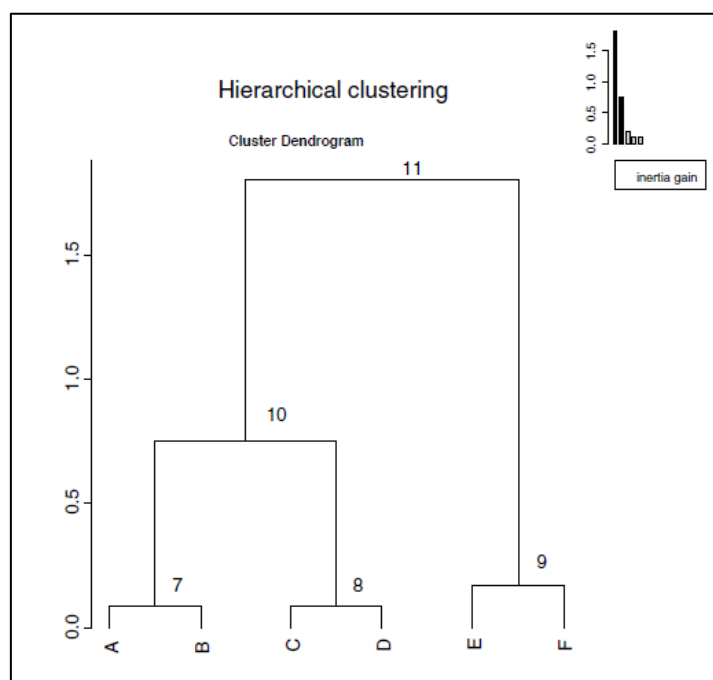


Figure 10.6 Dendrogram of hierarchical clustering, in the top right-hand corner the bar chart representing the level indices (Husson et al., 2017).

At the end a visual examination both of hierarchical tree (dendrogram) and of bar chart of level indices proposes a division into a certain number of cluster (Q) when the inertia between cluster at the passage for Q-1 to a Q cluster partition is much considerable than that from Q to Q + 1 cluster partition (Husson et al., 2017).

10.1.4.2 Non-hierarchical clustering methods

This group of clustering methods, also known as partitioning clustering, is based on the algorithm class of point assignment. Each point is assigned to the cluster into which it best fits. This operation usually comes after a phase in which initial clusters are approximated. Variations allow to split or combining clusters or permit points not to be assigned if there are outliers (elements too far from any of the considered clusters). The most important family of clustering algorithms in this category is known as *k-means* clustering method. These methods assume a Euclidean space. The desired number of clusters, *k*, is specified in advance; it is possible to decide the number of clusters by trial and error.

The steps of such a method are synthetically described in the following rows:

- 1) Choosing the initial cluster centres;
- 2) Assigning each individual to the cluster that is nearest to;
- 3) Finding the centroids of the formed cluster;
- 4) Re-calculating the distance between each centroid and each individual;
- 5) Moving the subjects that are not in the cluster that they are nearest to;
- 6) Continuing this procedure until the centroids become stable.

The *k-means* algorithm procedure for a simple case is graphically shows in Figure 10.7.

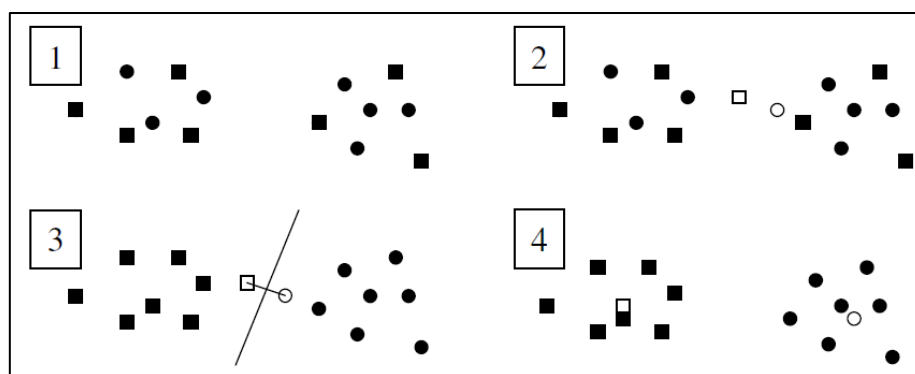


Figure 10.7 Simple illustration of *k-means* algorithm (Husson et al., 2017).

10.1 Multidimensional data analysis

In the case above, the subjects have to be divided into the circle cluster and into the squared one. Firstly, the individuals are divided into two random clusters (1); secondly, the gravity centres are calculated for each of the cluster, the centres of gravity are represented by the white square and circle (2).

Each subject is assigned to the group it is closest to (3) and, in the end, the gravity centres for the new generated clusters are calculated. If step three is reapplied and there are not any changes, it means that the algorithm has converged.

10.1.4.3 Comparison between Hierarchical and Non-hierarchical methods

The non-hierarchical methods present some advantages when compared to hierarchical ones:

- they are suitable when a large number of data are involved into the analysis;
- they permit individuals to move to a cluster to another one while in hierarchical approach once an individual is assigned it cannot move to a different cluster.

On the other hand, non-hierarchical methods present two critical aspects:

- it is complicated to know how many clusters are necessary to carry out a significant analysis, so the procedure may have to be repeated many times;
- the choice of the initial cluster centre can influence too much the analysis. It may be useful to try to use different centroids to understand their impact.

A suitable solution is represented by mixed algorithms, which combine the two approaches to obtain a methodology that includes the advantages of each.

For example, it is possible to adopt a hierarchical approach in the first stages to quantify how many clusters the data must be divided and then to use the centres of the obtained clusters as initial cluster centres in the non-hierarchical method.

Where there is a very large number of individuals, another mixed algorithm can be developed. In a first phase the individuals are partitioned into several groups. On the one hand many of these groups are very close together and on the other hand they are homogeneous and contain subjects that cannot be separated (Husson et al., 2017).

10.1.4.4 Clustering in a Non-Euclidean space

When the space is non-Euclidean it is needed to use some measures of distance that are calculated from points, for example cosine distance, Jaccard or edit distance. In a non-Euclidean space it is not possible to base distance on the location of points. Some problems can emerge if it is needed to represent a cluster, because it is not possible to replace a point collection by their centroid.

In a non-Euclidean space is not permitted to combine points in a cluster but it is only allowed the selection of one of the points of the cluster itself to represent it. The selected point is near to the other ones of the cluster and occurs in the “centre”. This representative point is named “clustroid”. The clustroid can be selected in various ways in order to minimize the distance between it and the other cluster points. The clustroid in the non-Euclidean space is used in place of the centroid (Euclidean space), and the point selected as clustroid has to satisfy the following requirements:

- minimisation of the sum of the distance to the other cluster points;
- minimisation of the maximum distance between itself and another point in the cluster;
- minimisation of the sum of the distance squares to the other points in the cluster.

There are no considerable changes in the option of stopping criteria (the options that make possible to determine when the merging process can be stopped when it has k clusters) from Euclidean to non-Euclidean space.

10.1.5 Observations

As already mentioned, combining the principal component methods and the clustering ones allows to better visualise and to comprehend the data. PCM is not only involved in pre-processing steps (as denoising data, transformation of categorical variables in continuous ones and balancing of the influence of groups of variables) but also to carry out a framework to visualize data. The clustering methods can be represented onto the map carried out by the PCM (Husson et al., 2010).

In other words, the simultaneous use of the principal component methods and the clustering ones enriches the analysis of dataset. Finally, the two described approaches complete one another because: on one hand it is possible to represent both the continuous view (provided by PCM) and the discontinuous one (the clusters) of the same dataset in a unique framework; on the other hand the dendrogram and the clusters, defined from more than two dimensions, provide some information “outside of the map” (Husson et al., 2010), whereas the 2D map does not provide information concerning the position of the subjects in the other dimensions.

10.2 Application to “La Maddalena” case study

10.2.1 Introduction

The statistical tools described in the previous paragraphs have been adopted to analyse the geological, mechanical and TBM related data in order to consider the combined effect of geotechnical rock masses properties on the machine performance.

The analyses were performed using the software R version 3.4.1 (R Core Team, 2017), with the packages FactoMineR (Lê et al., 2008) and quantreg (Koenker, 2017), added.

The considered tract of tunnel has a length of 2010 m and the dataset consist of 186 rock mass section, corresponding to a single site survey (as already described in Chapter 5); each record includes three kinds of variables.

The first one is represented by the geological domain (the lithology) to which the section belongs. The domain has been codified as categorical variable with three modalities I, II, III);

- a) DI gneiss;
- b) DII alternation of gneiss and micaschist;
- c) DIII micaschist.

The second one consists of geological and geomechanical characteristics of detected rock mass. In particular, the geotechnical features selected to carry out the following presented analysis are:

- d) uniaxial compressive strength, UCS [MPa];
- e) quartz content, q [%];
- f) spacing of fractures, S [m];
- g) alpha angle, α [°];
- h) Joint conditions, Jc [-];
- i) tunnel depth [m];

The third type of variables consists of TBM performance indices (considered dependent variables):

- j) rate of penetration (ROP);

10.2 Application to “La Maddalena” case study

k) field penetration index (FPI).

A detailed description of above mentioned parameters have been provided in Chapter 5.

The subsequent analyses have been divided in two steps: the first one aims to assess the association among geological variables (letters from *d* to *i*); in this step MCA and cluster analysis have been carried out. The second one aims to evaluate the relationship between geological and mechanical features of excavated rock masses (from *d* to *i*) and the TBM performance registered during tunnel construction (from *j* to *k*).

10.2.2 Relationship among geological and geomechanical variables

The main goal was to assess the association among geological variables, detect the presence of subgroups of rock sections, and describe the distinctive features of the subgroups possibly found. To such aim a MCA of the geological variables was performed, followed by cluster analysis. The geological variables were converted from numeric variables to categorical ones. The modalities obtained after the conversion are indicated in Table 10.1.

The uniaxial compressive strength values have been divided in four classes; each class has a range of 50 MPa, considering that minimum UCS value is equal to 68.0 MPa.

UNIAXIAL COMPRESSIVE STRENGTH, UCS [MPa]	
Class	Ranges
Low	0.0 – 100.0
Medium	101.0 – 150.0
High	151.0 – 200.0
Very high	201.0 – 250.0

Table 10.1 Classes of UCS utilised in MCA.

Quartz content percentage has been divided in four classes with different amplitudes, as reported in Table 10.2. The class amplitudes have been decided on the basis of the quartz percentage distribution.

QUARTZ CONTENT, q [%]	
Class	Ranges
Low	0.0 – 25.0
Medium	26.0 – 30.0
High	31.0 – 45.0
Very high	46.0 – 100.0

Table 10.2 Classes of quartz content utilised in MCA.

As for discontinuity spacing, both terminology and class ranges proposed by ISRM (Burton, 1978) have been adopted. The classes described by the Suggested Methods as “extremely close spacing” (spacing minor than 0.02 m), the one defined as “very close spacing” (spacing between 0.02 and 0.06 m), the “close” class (0.06 – 0.20 m) and the “moderate spacing” one (0.20 – 0.60 m) have been as a unique class characterised by spacing minor than 0.60 m and named “close-moderate” class.

This decision has been taken because of the minimum spacing observed during tunnel wall mapping was equal to 0.27 m, for this reason extremely close, very close and close spacing have not been considered (Table 10.3).

SPACING OF FRACTURES, S [m]	
Class	Ranges
Close – Moderate spacing	0.00 – 0.60
Wide spacing	0.60 – 2.00
Very wide spacing	2.00 – 6.00
Extremely wide spacing	> 6.00

Table 10.3 Classes of discontinuity spacing utilised in MCA.

The angle between tunnel axis and the main set of fractures orientation, α , can range between 0.0 and 90.0 degrees, this range has been divided in four classes with the same amplitude (22.5°) as it is reported in Table 10.4.

10.2 Application to “La Maddalena” case study

ALPHA ANGLE, α [deg]	
Class	Ranges
Low	0.0 – 22.5
Medium	22.6 – 45.0
High	45.1 – 67.5
Very high	67.6 – 90.0

Table 10.4 Classes of α utilised in MCA.

The parameter identified as “joint conditions” is computed in accordance with the RMR (Bieniawski 1989), in which J_c represents the fourth parameter. Its values have been divided into four classes of different amplitude, as showed in Table 10.5.

JOINT CONDITIONS, J_c [-]	
Class	Ranges
Low	0.0 – 10.0
Medium	11.0 – 20.0
High	21.0 – 25.0
Very high	26.0 – 30.0

Table 10.5 Classes of J_c utilized in MCA.

Tunnel depth has been involved in the present analysis as indicator of in situ stress.

The class have been named taking into account that the maximum depth reached in the considered tunnel tract is equal to 616.7 meters. For this reason the depth values ranging between 501.0 m and 700.0 m have been classified as “very high”.

Actually it is clear that a tunnel 700.0 meters depth cannot be considered as a very high deep tunnel. “La Maddelena” depth classes are listed in Table 10.6.

TUNNEL DEPTH, [m]	
Class	Ranges
Low	0.0 – 100.0
Medium	101.0 – 250.0
High	251.0 – 500.0
Very high	501.0 – 700.0

Table 10.6 Classes of tunnel depth utilized in MCA.

10.2.2.1 Multiple Correspondence Analysis

As the parameter classes as been defined the MCA can be performed.

The number of relevant dimensions was determined by examining the percentages of explained inertia, using the re-evaluation formula illustrated in Benzecri (1979).

Only the dimensions provided of a meaningful geological interpretation were retained in the analysis.

In the MCA the first two dimensions were selected, with proportions of explained inertia equal to 51.2% and 15.7%, respectively; therefore, the overall measure of quality of representation is 66.9% (Table 10.7).

Explained Inertia			
dim	value	%	cum%
1	0.099194	51.2	51.2
2	0.030476	15.7	66.9
3	0.008925	4.6	71.5
4	0.006270	3.2	74.7
5	0.001924	1.0	75.7
6	0.001262	0.7	76.3
7	0.000929	0.5	76.8
8	6.7e-050	0.0	76.9

Table 10.7 Percentage of explained inertia.

The plot of variable modalities is shown in Figure 10.8.

10.2 Application to “La Maddalena” case study

The main feature emerging from the figure is that the higher modalities of the variables (such as: alpha very high, or Jc high and very high), with the exception of the variable depth, lie on the right side of the figure, while the lowest modalities lie on the left side. This indicates an overall positive association among these variables.

In addition, the modalities depth low (i.e. 0 – 100 m) and quartz content very high (46% – 100%) have high coordinates on the y axis, and are thus separated from the rest. This suggests the possible presence of a subgroup of rock sections characterised by these modalities.

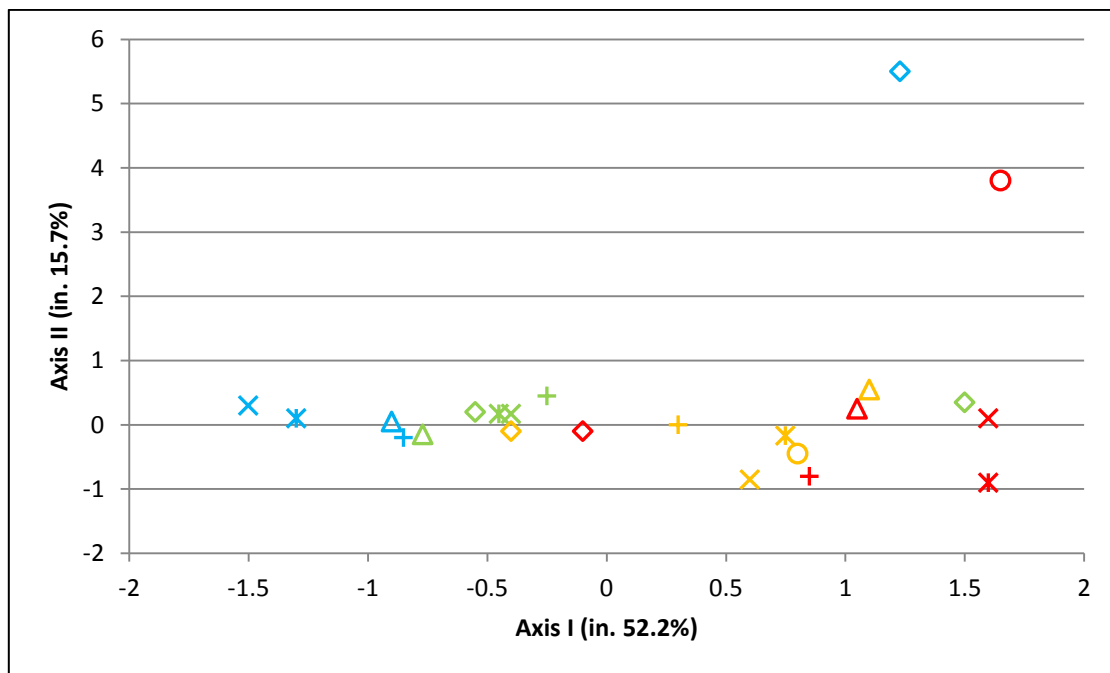


Figure 10.8 Variable map determined in the MCA of geological characteristics. Red symbols: very high modalities, orange: high modalities, green: medium ones, light blue: low modalities. Triangles: UCS, circles: quartz content, crosses: alpha angle, x: Jc, diamonds: depth, asterisks: spacing.

10.2.2.2 Clustering

The considerations presented above are mainly geometric and semi-quantitative, so in order to classify the sections into homogeneous groups (clusters), a cluster analysis was performed on MCA displays. The clustering algorithm was agglomerative nesting with *Ward linkage* (see section 10.1.4.1).

The number of clusters was chosen by visual inspection of MCA displays (Figure 10.8), of cluster analysis displays, i.e. the dendrogram (Figure 10.9), and more formally by evaluating the percentage gains of between cluster inertia (Figure 10.9, upper right corner).

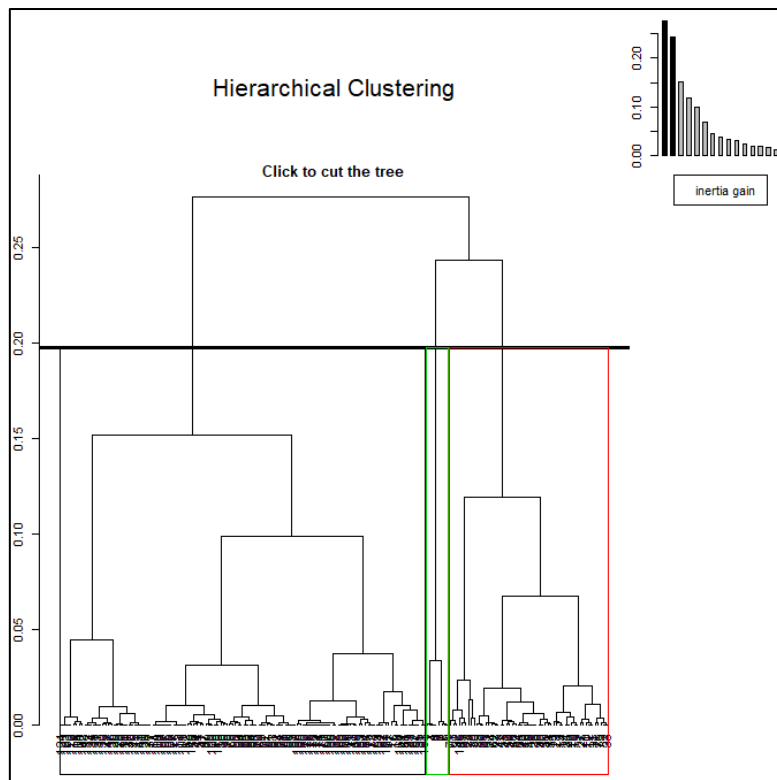


Figure 10.9 Dendrogram of cluster analysis, in the upper right corner the inertia gain.

After these considerations the chosen number of clusters is three. According to the percentage gains of inertia (first four: 25.9%, 24.4%, 15.9%, 11.9%) rock mass sections were divided in three clusters, composed by 111, 66 and 9 rock mass sections respectively (Figure 10.10).

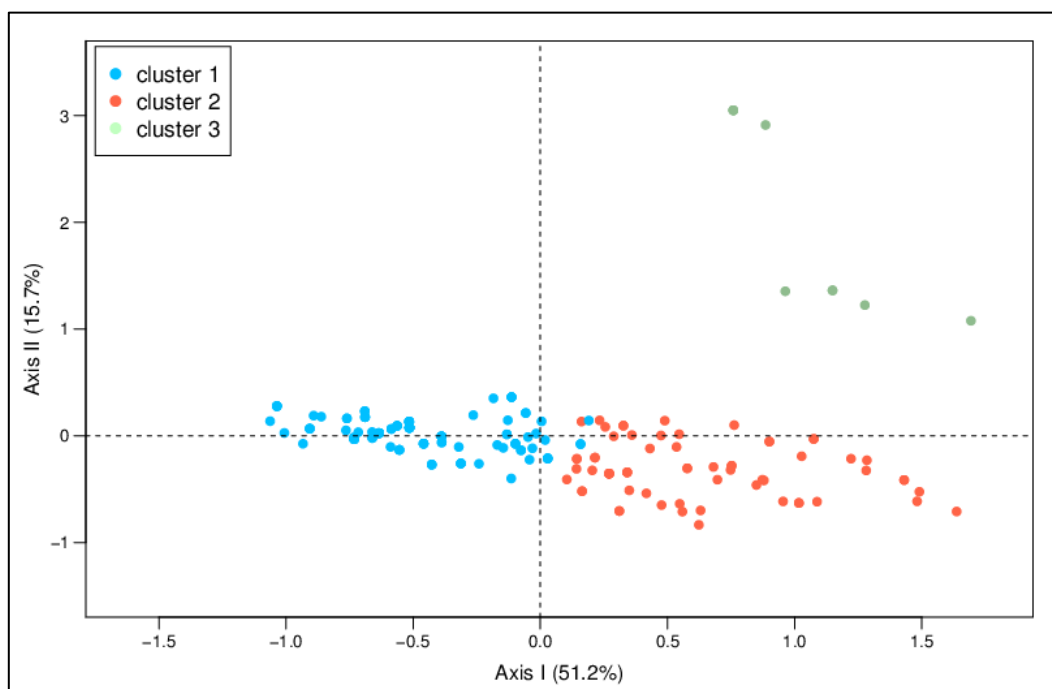


Figure 10.10 Factor map. The three colours identify the three clusters, it is possible to note that cluster I and II are more similar between each other respect to cluster III.

10.2 Application to “La Maddalena” case study

The position of clusters is observable from the factor map. Cluster III is composed by few elements and it is distant, so it is different, from cluster I and II, as it is possible to see by the three-dimensional view of the factor map (Figure 10.11).

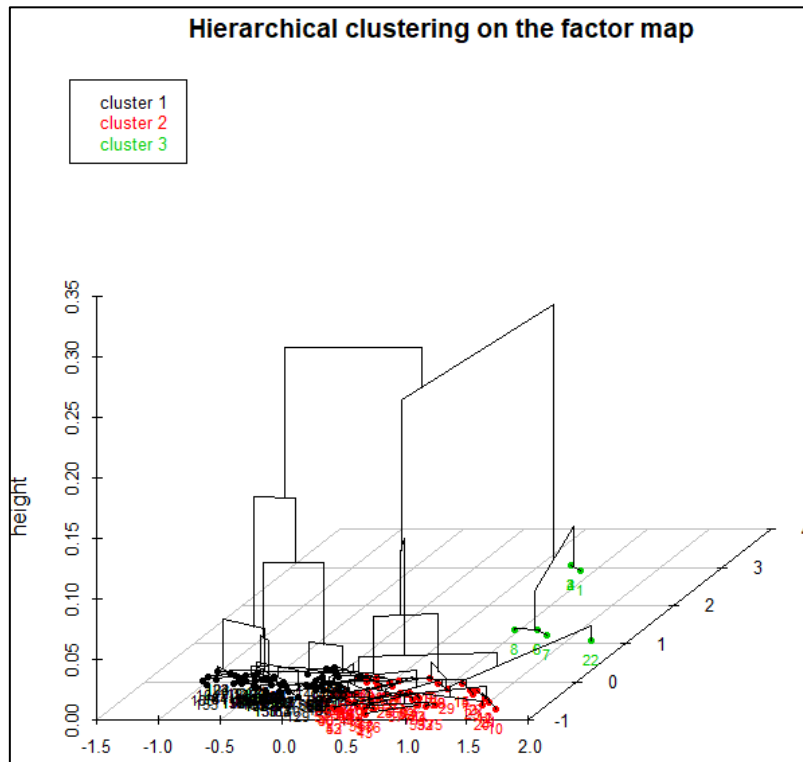


Figure 10.11 Three-dimensional view of the hierarchical clustering on the factor map.

To describe the main characteristics of the clusters, the geological variables were summarized separately for each cluster, using: mean, median, minimum and maximum value, standard deviation, 25th and 75th percentiles (Q1 and Q3) and interquartile range (Q3-Q1).

Furthermore, to evaluate to what extent clusters correspond to distinct geological domains, the frequencies of rock sections belonging to each domain were reported for each cluster (Table 10.8).

The clusters obtained from clustering process and the geological domains defined after traditional surveys have been compared and a good correspondence has been noted.

In particular, cluster I matches the third domain and include part of micaschist sections belonging to the alternation gneiss-micaschist relate to second domain. Cluster II coincides with domain I, in fact 60 sections belong to Ambin gneiss and includes 6 gneiss sections belonging to the gneiss-micaschist alternation.

Cluster III is formed by 9 geological sections belonging to the domain I; this portion of rock mass was not considered as a separated domain but it was surveyed as a very hard tract of gneiss.

MCA showed the significant difference of this portion from the two others both in terms of geotechnical features and TBM performance. In other words: domain I constitutes cluster II, domain II is divided in cluster I and cluster II and the hardest portion on domain I was separate as cluster III. A most detailed description of cluster is reported in Table 10.8.

	Cluster 1 (n=111)	Cluster 2 (n=66)	Cluster 3 (n=9)
UCS [MPa]			
range	68.00 – 251.00	103.00 – 219.00	200.00 – 217.00
median	115.00	153.00	200.00
Q1-Q3	93.00 – 135.00	130.00 – 168.25	200.00 – 200.00
Alpha [°]			
range	7.40 – 69.40	29.80 – 85.00	42.50 – 56.40
median	39.90	48.45	44.90
Q1-Q3	29.80 – 49.00	44.00 – 59.98	44.75 – 52.30
Spacing [m]			
range	0.27 – 5.50	0.75 – 11.80	0.86 – 6.00
median	1.13	3.25	1.88
Q1-Q3	0.84 – 1.56	2.39 – 6.00	1.29 – 2.48
Jc			
range	7.00 – 21.00	12.00 – 29.00	18.00 – 29.00
median	17.00	20.00	20.00
Q1-Q3	15.00 – 19.00	17.00 – 23.00	20.00 – 20.00
quartz[%]			
range	25.00 – 45.00	30.00 – 45.00	50.00 – 80.00
median	25.00	45.00	50.00
Q1-Q3	25.00 – 30.00	45.00 – 45.00	50.00 – 50.00
depth[m]			
range	190.00 – 616.70	133.00 - 569.10	79.40 - 215.30
median	442.00	440.25	103.50
Q1-Q3	329.40 – 531.60	271.03 – 523.20	85.95 – 127.50
geological domain: n (%)			
I	14 (13%)	60 (91%)	9 (100%)
II	38 (34%)	6 (9%)	0 (0%)
III	59 (53%)	0 (0%)	0 (0%)
ROP[m/h]			
range	0.50 – 3.74	0.38 – 2.30	0.33 – 1.17
median	1.88	0.95	0.63
Q1-Q3	1.42 – 2.28	0.60 – 1.17	0.49 – 0.87
FPI[kN/cutter/mm/rev]			
range	15.16 – 190.97	27.15 – 279.10	79.39 – 298.61
median	55.10	146.64	131.03
Q1-Q3	39.19 – 84.70	117.81 – 198.33	96.38 – 141.40

Table 10.8 Statistical description of clusters.

10.2 Application to “La Maddalena” case study

Cluster I is principally composed (53%) by geological sections belonging to the micaschist of Clarea complex (third geological domain), and for the 34% it is composed by rock mass portions defined as an alternation of gneiss and micaschist lithology. Only the 13% of rock sections is characterised by gneiss belonging to Ambin complex.

All range parameters are reported as first quartile (Q1) and third quartile (Q3).

All geomechanical parameters relating to the rock portions characterising cluster I are lower than the same parameters evaluated in the others rock mass sections. Cluster I is characterised by medium values of uniaxial compressive strength, ranging between 93.0 MPa and 135.0 MPa (respectively Q1 and Q3). The angle between principal discontinuity set orientation and tunnel axis ranges between 29.8° and 49.0° and quartz content ranges between 25% and 30%. Fractures are medium spaced (0.84 m – 1.56 m) and generally joint conditions are rated 15.0 – 19.0. Generally, rock mass quality of this cluster is lower than the quality of clusters II and III. These geomechanical and geological features determine TBM performance better than the ones measured in cluster II and cluster III rock masses, ROP is high (1.42 m/h – 2.28 m/h) and FPI is low (39.19 kN/cutter/mm/rev – 84.70 kN/cutter/mm/rev); it means that encountered rocks are easy drillable: the net penetration achieved is good and the thrust required to guarantee a penetration per revolution is low.

Cluster II is mainly characterised by geological section belonging to the Ambin complex, described like domain I (91%). The remaining 9% is formed by portions of rock masses lithologically considered as an alternation of gneiss and micaschist (domain II). Cluster II does not include micaschist sections related to the Clarea complex.

Rock mass portions belonging to cluster II are characterised by general good quality, UCS and quartz content are higher than the ones in cluster I (respectively 130.0 MPa – 168.3 MPa and 45%) and discontinuities are more spaced: Q1 and Q3 are 2.39 m and 6.00 m respectively, they form an angle between 44.0° – 60° with tunnel axis. Jc parameter is slightly higher than the previous one. In general rock mass is compact and hard and it results in a low boreability: ROP is less than 1 m/h (0.6 m/h – 1.2 m/h) and FPI is high (from 117.8 kN/cutter/mm/rev to 198.3 kN/cutter/mm/rev).

Cluster III is defined only by nine geological sections of gneiss belonging to the first domain (Ambin complex); it includes no one portions of micaschist or gneiss-micaschist. It represents the hardest zone of tunnel with the highest levels of UCS (maximum value 217.0 MPa) and of quartz content (50.0%). Discontinuities are medium-high spaced (1.29 m – 2.48 m). The TBM performance in this cluster are the lowest registered, ROP is very low, ranging between 0.5 m/h and 0.9 m/h and FPI is high (96.4 kN/cutter/mm/rev – 141.4 kN/cutter/mm/rev).

10.2.3 Relationship between geological-geomechanical variables and TBM performance

In the second step of the analysis, the relationships between TBM performances (ROP and FPI) and geological characteristics have been assessed through a regression models. In order to account for the joint effect of geotechnical site characteristics on TBM performances, the clusters identified in the previous step were used as independent variable.

The distributions of ROP and FPI were evaluated for each cluster through histograms and the hypothesis of Gaussian distribution was assessed by the Shapiro-Wilks test.

Since the hypothesis of Gaussianity was rejected in some cases, quantile regression models (Koenker and Portnoy, 1996) were fitted for estimating the median values of ROP and FPI for the distinct clusters of rock sections and the respective differences.

Histograms

In order to evaluate the statistical distribution of ROP and FPI for each cluster, histograms of frequency have been created. As we can observe by graphs the normal distribution of data occurs only in three cases (ROP in cluster I and III; FPI in cluster II).

In the other cases TBM performance indices are not normally distributed (Figure 10.12).

10.2 Application to “La Maddalena” case study

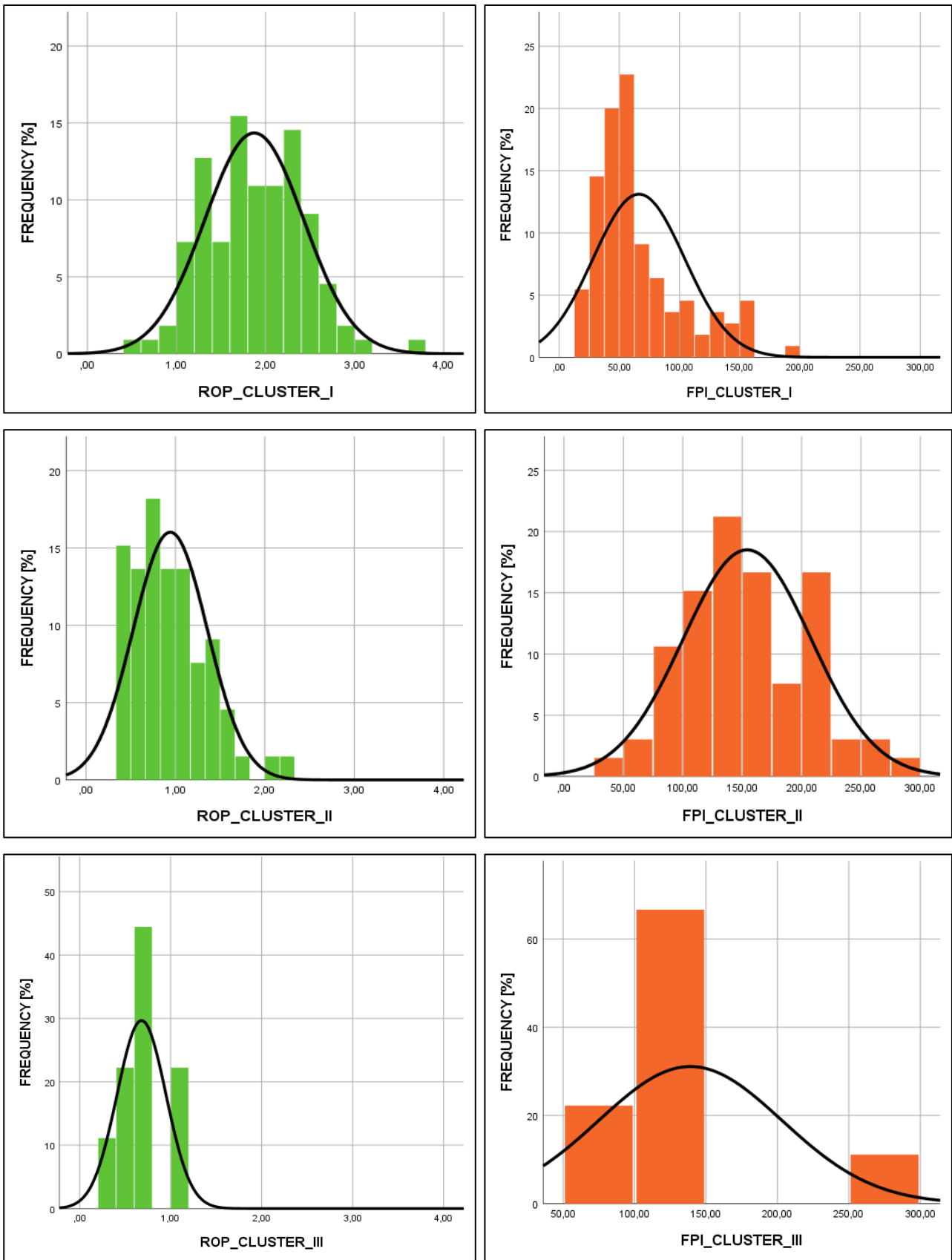


Figure 10.12 Histograms of frequency distribution of ROP and FPI for each cluster.

Normality test

In addition to the histograms, in each cluster “Shapiro-Wilk normality test” has been carried out in order to test the normal distribution of ROP and FPI. It is a normality test that tests if a sample comes from a normally distributed population. The null hypothesis is that the population is normally distributed.

So if the p-value is less than 0.05 the null hypothesis will be rejected and the population will be considered not normally distributed; on the contrary when the p-value is higher than 0.05 the population is considered normally distributed.

The results of “Shapiro-Wilk normality test” are reported in Table 10.9.

TESTED PARAMETER	NUMBER OF CLUSTER	W	p-value	NULL HYPOTHESIS
ROP	I	0.98678	0.348200	accepted
ROP	II	0.93292	0.001489	rejected
ROP	III	0.91223	0.331800	accepted
FPI	I	0.87470	3.188E ⁻⁰⁸	rejected
FPI	II	0.98898	0.827600	accepted
FPI	III	0.72358	0.002673	refused

Table 10.9 Results of Shapiro-Wilk normality test.

As reported in Table 10.9, in some cases p-values are higher than 0.05 so in these cases the null-hypothesis cannot be refused and population is considered normally distributed; however, in three cases p-values are lower than 0.05, it means that population is not normally distributed.

Since the hypothesis of Gaussianity was rejected in some cases, we used quantile regression models (Koenker and Portnoy, 1996) for estimating the median values of ROP and FPI for the distinct clusters of rock sections and the respective differences.

10.2 Application to “La Maddalena” case study

10.2.3.1 Quantile regression

A quantile regression analysis of deviance table was carried out in order to compare the medians both of ROP and FPI of the three clusters and test if they are dissimilar from each other. ANOVA (analysis of variance) test was performed and the considered null hypothesis is that the medians of clusters are all the same. The results obtained by quantile regression (Table 10.10) show significant differences of performance indices between cluster I and II ($p < 0.0001$, for both indices) and between cluster I and III ($p < 0.0001$ for both indices).

	Differences between medians Estimate (95% C. I.)	Test of hypothesis Global test: $p < 0.0001$
ROP[m/h]		
Cluster 2 VS Cluster 1	-0.92 (-1.15, -0.69)	$p < 0.0001$
Cluster 3 VS Cluster 1	-1.25 (-1.52, -0.98)	$p < 0.0001$
Cluster 3 VS Cluster 2	-0.33 (-0.60, -0.06)	$p = 0.0508$
FPI[kN/cutter/mm/rev]		
Cluster 2 VS Cluster 1	144.3 (124.5, 164.1)	$p < 0.0001$
Cluster 3 VS Cluster 1	131.0 (96.3, 165.7)	$p < 0.0001$
Cluster 3 VS Cluster 2	-13.3 (-58.5, 31.9)	$p > 0.999$

Table 10.10 Comparison of median TBM performances among clusters.

The results obtained by quantile regression show that the median values of ROP between cluster I and II, cluster I and III, cluster II and III are significantly different, being p-values less than 0.05 and null hypothesis refused. Also the median values of FPI between cluster I and II, and cluster I and III have been considered dissimilar (p-values < 0.05).

Higher values of ROP belong to rock sections in cluster I (IQR: 1.42 to 2.28 m/h), followed by those in clusters II and III (with IRQs lower than 1.00 m/h). Concerning FPI, cluster I has lower values (IQR: 39.2 to 84.7) than cluster II and II, which overlap one another (IQR: 117.80 to 198.30 and 94.40 to 141.40 kN/cutter/mm/rev, respectively).

The regression analysis shows that FPI of cluster II (146.65 kN/cutter/mm/rev) and FPI of cluster III (131.00 kN/cutter/mm/rev) are not significantly different. Theoretically, keeping in consideration the hardness of cluster III, FPI would have to be higher than the FPI measured during

10.2 Application to “La Maddalena” case study

cluster II excavation because of the excavation of hard rock masses requires high TBM thrust in order to guarantee a penetration per each cutterhead revolution. The same median value of FPI has been registered in cluster II and III is because it is not possible to impart a too high force on very hard rock faces in order to avoid cutter breakage and TBM damages. In other words, there is a force threshold above which TBM cannot be driven in relation to the rock hardness.

At each cluster correspond different TBM performances, so the clusters can be considered as classes of excavability, characterised by specific geological and geomechanical features associated with different ranges of ROP and FPI, as summarised in Table 10.11.

	Geomechanical ranges	ROP [m/h]	FPI [(kN/cutter)/(mm/rev)]
CLUSTER I	UCS = 93.0 – 135.0 MPa $\alpha = 29.8^\circ - 49.0^\circ$ S = 0.84 – 1.56 m q = 25 – 30 % Jc = 15 – 19	1.42 – 2.28	39.19 – 84.70
CLUSTER II	UCS = 130 – 168.3 MPa $\alpha = 44^\circ - 60^\circ$ S = 2.39 – 6.00 m q = 45% Jc = 17 – 23	0.60 – 1.17	117.81 – 198.33
CLUSTER III	UCS = 200 MPa $\alpha = 44.75^\circ - 52.30^\circ$ S = 1.29 – 2.48 m q = 50 % Jc = 20	0.49 – 0.87	96.38 – 141.40

Table 10.11 Ranges (Q1;Q3) of geomechanical properties for each cluster and the corresponding TBM performances.

10.2 Application to “La Maddalena” case study

At this point, three classes of excavatability have been delineated; they allow the prediction of the TBM performances when the geomechanical features describing each class occur.

In order to carry out an empirical formulation able to describe the relationship between geological properties and TBM performance multiple regression analyses have been developed for each cluster.

10.2.4 Regression analyses on clusters

Multiple linear regression analysis has been selected as statistical approach to obtain empirical formulation able to describe the relationship between geological and geotechnical features describing each cluster and the performances of the TBM measured in the same cluster.

The analysis is divided in two groups: in one the dependent variable is ROP, in the other the dependent one is FPI.

In both cases the independent variables are: UCS, q, spacing, alpha angle, Jc, tunnel depth.

The models were generated adopting the stepwise backward selection, and following the procedures described in Chapter 9.

10.2.4.1 Relationship between geological conditions of clusters and ROP

Cluster I

About cluster I the assumptions for linear regression are satisfied. For this reason a multiple linear regression analysis has been carried out. The excluded variables are the spacing between discontinuities and α , they have Sign. 0.996 and Sign. 0.887, respectively.

All coefficient statistics, concerning each model, have been listed in the Table 10.12.

Coefficients										
Model		Unst.ed coefficients		Std.ed coeff.	t	Sign. (p-value)	95,0% C.I. for B		Collinearity statistics	
		B	Std. error	Beta			Bottom Limit	Top limit	Toleranc e	VIF
C1a	(Constant)	2.305	0.408		5.644	0.000	1.495	3.115		
	UCS	-0.006	0.001	-0.348	-4.200	0.000	-0.009	-0.003	0.743	1.346
	α	0.000	0.003	-0.010	-0.141	0.888	-0.006	0.005	0.963	1.039
	S	0.000	0.001	0.000	0.005	0.996	-0.001	0.001	0.922	1.085
	Jc	0.056	0.014	0.303	3.882	0.000	0.027	0.085	0.838	1.193
	q	-0.041	0.007	-0.473	-6.300	0.000	-0.054	-0.028	0.905	1.104
	depth	0.001	0.000	0.258	3.083	0.003	0.000	0.002	0.726	1.378
C1b	(Constant)	2.305	0.406		5.672	0.000	1.499	3.111		
	UCS	-0.006	0.001	-0.348	-4.305	0.000	-0.009	-0.003	0.773	1.293
	alpha	0.000	0.003	-0.010	-0.142	0.887	-0.006	0.005	0.968	1.033
	Jc	0.056	0.014	0.303	3.945	0.000	0.028	0.084	0.857	1.167
	q	-0.041	0.006	-0.473	-6.366	0.000	-0.054	-0.028	0.916	1.092
	depth	0.001	0.000	0.258	3.114	0.002	0.000	0.002	0.734	1.363
C1c	(Constant)	2.295	0.399		5.754	0.000	1.504	3.086		
	UCS	-0.006	0.001	-0.347	-4.334	0.000	-0.009	-0.003	0.782	1.279
	Jc	0.056	0.014	0.301	3.981	0.000	0.028	0.084	0.873	1.146
	q	-0.041	0.006	-0.473	-6.413	0.000	-0.054	-0.028	0.919	1.089
	depth	0.001	0.000	0.257	3.138	0.002	0.000	0.002	0.747	1.338

Table 10.12 Results of multiple linear regression analysis, red boxes underline the no significant parameters.

C1c includes the variables that effective have affected ROP, as Sign. parameter is able to demonstrate. The geotechnical properties involved in this model are: UCS, q, Jc and depth. There are not any problems of multicollinearity. C1c model summary is reported in Table 10.13.

10.2 Application to “La Maddalena” case study

r	R²	R²_{adj}	F	Sign.
0.686	0.470	0.450	23.494	0.000

Table 10.13 C1c model summary.

The regression analysis allows to explain only the 45.00% of the total variance, in other words the model modestly represent the relationship between the geological characteristics of cluster I and ROP.

On the basis of the statistical analyses, the proposed empirical equation is as follows:

$$ROP = 2.295 - 0.006 * UCS - 0.041 * q + 0.056 * Jc + 0.001 * d \quad (10.11)$$

Cluster II

In cluster II, linear regression model about ROP and geological parameters cannot be performed, being the assumptions not satisfied.

The relation between ROP and the geomechanical parameters have been investigated by means of linear, logarithmic, quadratic, polynomial and exponential regression models. For each model statistical tests have been carried out in order to select the model better describing how dependent and independent variables are related. The results and the parameter coefficients are reported in Table 10.14.

Independent Variable	Model	R ²	F	Sign.	Constant	b1	b2
UCS	Linear	0.186	14.586	0.000	1.909	-0.006	
	Logarithmic	0.197	15.709	0.000	5.980	-1.006	
	Quadratic	0.204	8.070	0.001	3.482	-0.027	6.491E-5
	Power	0.167	12.866	0.001	116.897	-0.981	
	Exponential	0.161	12.294	0.001	2.227	-0.006	
q	Linear	0.011	0.722	0.399	1.383	-0.010	
	Logarithmic	0.011	0.722	0.399	2.349	-0.373	
	Quadratic	0.011	0.722	0.399	1.383	-0.010	0.000
	Power	0.025	1.657	0.203	8.062	-0.594	
	Exponential	0.025	1.657	0.203	1.730	-0.016	
S	Linear	0.084	5.875	0.018	1.125	-0.042	
	Logarithmic	0.067	4.638	0.035	1.149	-0.163	
	Quadratic	0.086	2.974	0.058	1.184	-0.072	0.003
	Power	0.045	2.993	0.088	1.026	-0.140	
	Exponential	0.073	5.010	0.029	1.027	0.041	
α	Linear	0.066	4.513	0.038	1.405	-0.009	
	Logarithmic	0.067	4.568	0.036	2.782	-0.468	
	Quadratic	0.069	2.348	0.104	1.842	-0.026	0.000
	Power	0.068	4.667	0.035	6.135	-0.501	
	Exponential	0.065	4.430	0.039	1.395	-0.009	
Jc	Linear	0.028	1.867	0.177	1.289	-0.018	
	Logarithmic	0.025	1.617	0.208	1.887	-0.319	
	Quadratic	0.034	1.100	0.339	0.665	0.046	-0.002
	Power	0.015	0.969	0.329	1.869	-0.263	
	Exponential	0.018	1.194	0.279	1.153	-0.015	
Depth	Linear	0.206	16.602	0.000	0.412	0.001	
	Logarithmic	0.223	18.323	0.000	-1.740	0.455	
	Quadratic	0.238	9.825	0.000	-0.152	0.005	-5.041E-6
	Power	0.300	27.396	0.000	0.032	0.559	
	Exponential	0.286	25.649	0.000	0.443	0.002	

Table 10.14 Linear and nonlinear models between geological parameters and ROP observed in cluster II. Red boxes represent the excluded variables and in bold the selected models.

Quartz content and joint conditions do not affect ROP, being the null hypothesis cannot be rejected for any regression model.

10.2 Application to “La Maddalena” case study

The mathematical functions that best describe the relation between UCS, spacing, α , tunnel depth and ROP are listed below:

$$ROP = -1.006 * \ln UCS + 5.980 \quad (10.12)$$

$$ROP = -0.042 * S + 1.125 \quad (10.13)$$

$$ROP = -0.468 * \ln \alpha + 2.782 \quad (10.14)$$

$$ROP = 0.032 * d^{0.559} \quad (10.15)$$

There are three models that can be used to describe the relation between alpha angle and ROP, they are: linear, logarithmic and power (F values are very similar: F = 4.513, 4.568 and 4.667 respectively). In this study, all of them have been considered and it was observed that logarithmic function works better than the others; in fact the regression model developed entering alpha as logarithmic related gave a higher coefficient of determination than the ones obtained considering linear or power functions.

The equations 10.12, 10.13, 10.14, 10.15 have been entered in the multiple nonlinear regression model in order to investigate the simultaneous nonlinear relationship between the geological conditions characterising cluster II and ROP.

The carried out equation is as follows (model C2a):

$$ROP = -0.650 * \ln UCS - 0.024 * S - 0.249 * \ln \alpha + 2.317E^{-5} * d^{1.540} + 9.608 \quad (10.16)$$

The coefficient of determination for this model is equal to 0.338.

Cluster III

Cluster III is defined by nine elements only. For this reason carry out a regression analysis on its data might not useful be; however, in this study linear analysis has been developed.

Quartz content, alpha angle and tunnel depth were excluded from inputs due to their p-values higher than 0.005, C3c takes in consideration only those variables determining ROP. All coefficient statistics, concerning each model, have been listed in Table 10.15.

Coefficients										
Model		Unst.ed coefficients		Std.ed coeff.	t	Sign. (p-value)	95,0% C.I. for B		Collinearity statistics	
		B	Std. error	Beta			Bottom Limit	Top limit	Tolera nce	VIF
C3a	(Constant)	-20.392	26.904		-0.758	0.504	-106.012	65.228		
	UCS	0.148	0.168	3.112	0.878	0.444	-0.387	0.682	0.002	628.979
	alpha	0.012	0.017	0.215	0.737	0.515	-0.040	0.065	0.235	4.247
	S	0.503	0.417	-5.218	1.206	0.314	-0.817	1.862	0.003	285.951
	Jc	-0.453	0.308	-5.318	-1.470	0.238	-1.434	0.528	0.002	655.688
	depth	-0.009	0.016	-1.341	-0.551	0.620	-0.059	0.041	0.003	296.840
C3b	(Constant)	-6.251	7.345		-0.851	0.443	-26.645	14.143		
	UCS	0.059	0.045	1.244	1.326	0.256	-0.065	0.183	0.019	53.444
	alpha	0.008	0.013	0.141	0.600	0.581	-0.029	0.045	0.298	3.360
	S	0.227	0.069	1.587	4.033	0.016	0.086	0.468	0.106	9.401
	Jc	-0.288	0.062	-3.374	-4.641	0.010	-0.460	-0.116	0.031	32.059
C3c	(Constant)	-9.388	4.820		-1.948	0.109	-21.778	3.003		
	UCS	0.079	0.028	1.657	2.775	0.039	0.006	0.151	0.040	24.787
	S	0.258	0.057	1.478	4.538	0.006	0.112	0.404	0.136	7.379
	Jc	-0.306	0.050	-3.593	-6.124	0.002	-0.435	-0.178	0.042	23.952

Table 10.15 Results of multiple linear regression analysis, red boxes underline the no significant parameters.

The geotechnical properties involved in C3c model are: UCS, spacing and Jc. VIF is higher than 10; this value is not due to the correlation between independent variables but to the limited number of data. The proposed empirical equation is as follow:

$$ROP = 0.079 * UCS + 0.258 * S - 0.306 * Jc - 9.388 \quad (10.17)$$

The model summary is provided in Table 10.16.

r	R ²	R ² _{adj}	F	Sign.
0.963	0.928	0.885	21.526	0.003

Table 10.16 C3c model summary.

10.2 Application to “La Maddalena” case study

10.2.4.2 Relationship between geological conditions of clusters and FPI

The same procedures of analysis described in the previous paragraph have been utilized to investigate the relationship among the geomechanical conditions of each cluster and the FPI registered in the considered tunnel portion.

Cluster I

As for cluster I, the assumptions of linearity have been satisfied, so a linear model has been carried out. At the beginning of analysis all geological variables (UCS, q, S, Jc, α and depth) have been entered then, joint condition parameter was excluded from inputs due to its p – value.

The statistical results have been provided by Table 10.17.

Coefficients										
Model		Unst.ed coefficients		Std.ed coeff.	t	Sign.	Bottom Limit		Collinearity statistics	
		B	Std. error	Beta					Toleran -ce	VIF
C1 d	(Constant)	-61.268	26.435		-2.318	0.022	-113.684	-8.852		
	UCS	0.544	0.093	0.467	5.846	0.000	0.360	0.729	0.749	1.335
	q	2.700	0.426	0.459	6.334	0.000	1.855	3.545	0.909	1.100
	S	0.110	0.035	0.227	3.156	0.002	0.041	0.179	0.927	1.079
	Jc	-0.426	0.940	-0.034	-0.453	0.651	-2.289	1.437	0.856	1.168
	depth	-0.052	0.026	-0.158	-1.960	0.053	-0.104	0.001	0.737	1.356
C1 e	(Constant)	-69.901	16.812		-4.193	0.000	-103.819	-37.157		
	UCS	0.576	0.093	0.494	6.160	0.000	0.390	0.761	0.753	1.328
	q	2.991	0.421	0.469	7.107	0.000	2.156	3.826	0.996	1.004
	S	-0.065	0.027	-0.195	-2.469	0.015	0.040	0.176	0.945	1.058
	depth	-0.049	0.026	-0.150	-1.915	0.030	-0.100	0.002	0.773	1.293

Table 10.17 Results of multiple linear regression analysis, red box underlines the no significant parameters.

C1e includes the factors that effective have influenced FPI, they are: UCS, q, S and depth. There are no problems of multicollinearity.

The regression analysis allows to carry out a new predictive equation:

$$FPI = 0.576 * UCS + 2.991 * q + 7.651 * S - 0.065 * d - 69.901 \quad (10.18)$$

C1e summary has been reported in Table 10.18.

r	R²	R²_{adj}	F	Sign.
0.703	0.494	0.475	25.624	0.000

Table 10.18 C1e model summary.

Cluster II

The model assumptions for linear regression for geology-FPI relationship in cluster II have not been verified. For this reason the same procedure previously adopted to carry out multiple nonlinear regression analyses (see section 10.2.4.1) has been applied.

Linear, logarithmic, quadratic, power and exponential regression models have been considered. About quartz content, alpha angle, Jc and tunnel depth no correlations have been recognised, on the contrary power and exponential relations have been observed for UCS and S respectively, as reported in Table 10.19.

Independent Variable	Model	R²	F	Sign.	Constant	b1	b2
UCS	Linear	0.069	4.747	0.033	77.608	0.503	
	Logarithmic	0.078	5.419	0.023	-257.537	82.189	
	Quadratic	0.098	3.429	0.039	-179.796	3.865	-0.011
	Power	0.095	6.695	0.012	4.347	0.698	
	Exponential	0.085	5.958	0.017	74.405	0.004	
S	Linear	0.094	6.608	0.012	129.166	5.703	
	Logarithmic	0.074	5.149	0.027	125.976	22.239	
	Quadratic	0.094	3.278	0.044	124.824	7.875	-0.183
	Power	0.115	8.337	0.005	41.045	0.213	
	Exponential	0.118	8.549	0.005	115.431	0.049	

Table 10.19 Linear and nonlinear models between geological parameters and FPI observed in cluster II. In bold the selected models.

10.2 Application to “La Maddalena” case study

The mathematical function that better describes the relation between UCS and FPI is the power one:

$$FPI = 4.347 * UCS^{0.698} \quad (10.19)$$

The function that better describes the relation between S and FPI are exponential one:

$$FPI = 115.431 * exp^{0.049*S} \quad (10.20)$$

The equations 10.19 and 10.20 have been entered in the multiple nonlinear regression model in order to investigate the simultaneous nonlinear relationship between UCS and spacing characterising cluster II and FPI. The obtained equation is as follows (model C2b):

$$FPI = 5.522 * UCS^{0.568} + 42.618 * exp^{0.069*S} \quad (10.21)$$

Cluster III

The results of linear regression analysis are reported in Table 10.20.

Coefficients										
Model		Unst.ed coefficients		Std.ed coeff.	t	Sign. p-value	95,0% C.I. for B		Collinearity statistics	
		B	Std. error	Beta			Bottom Limit	Top limit	Tolerance	VIF
C3d	(Const.)	-3864.774	2480.367		-1.558	0.217	-11758.40	4028.86		
	UCS	22.302	15.493	1.970	1.439	0.246	-27.004	71.607	0.002	628.979
	alpha	-5.877	1.523	-0.434	-3.859	0.031	-10.724	-1.030	0.235	4.247
	S	0.012	0.384	0.028	0.030	0.978	-1.212	1.235	0.003	285.951
	Jc	-6.204	28.425	-0.305	-0.218	0.841	-96.665	84.257	0.002	655.688
	depth	-0.797	1.451	-0.517	-0.549	0.621	-5.413	3.819	0.003	296.840
C3e	(Const.)	-3797.190	901.642		-4.211	0.014	-6300.551	-1293.8		
	UCS	21.877	5.457	1.933	4.009	0.016	6.726	37.028	0.010	104.010
	alpha	-5.901	1.123	-0.436	-5.253	0.006	-9.020	-2.782	0.325	3.080
	Jc	-5.388	7.169	-0.265	-0.752	0.494	-25.292	14.516	0.018	55.593
	depth	-0.754	0.228	-0.489	-3.311	0.030	-1.387	-1.122	0.102	9.759
C3f	(Const.)	-3144.566	231.987		-13.555	0.000	-3740.909	-2548.2		
	UCS	17.902	1.283	1.581	13.957	0.000	14.604	21.199	0.159	6.294
	alpha	-5.374	0.839	-0.397	-6.407	0.001	-7.531	-3.218	0.532	1.881
	depth	-0.643	0.165	-0.417	-3.894	0.011	-1.067	-0.218	0.178	5.607

Table 10.20 Results of multiple linear regression analysis, red boxes: no significant parameters.

10.2 Application to “La Maddalena” case study

UCS, alpha angle and tunnel depth have been influenced the FPI during cluster III excavation, the mathematical form of this relationship is given by:

$$FPI = 17.902 * UCS - 5.374 * \alpha - 0.643 * d - 3144.566 \quad (10.22)$$

The summary about this model is provided in Table 10.21.

r	R²	R²_{adj}	F	Sign.
0.995	0.990	0.984	161.731	0.000

Table 10.21 C3f model summary.

10.3 Conclusion

10.3 Conclusion

Multiple correspondence analyses and cluster analysis have been carried out on the geological, geomechanical and TBM data collected during La Maddalena excavation between the Pk. 0 + 198 m and the Pk. 2 + 010 m.

These statistical methods allow to objectively divide the rock mass into three homogeneous groups, named cluster I, II, and III respectively. Each of them can be considered as a class of excavatability at which correspond specific geological-geotechnical properties and ROP and FPI ranges. The identified clusters are comparable to the geological domains defined after rock mass surveys.

In order to obtain the mathematical representation of the relationship between the rock mass features and the TBM performances registered during its excavation multiple regression analyses have been carried out for each clusters.

When the assumptions for linear regression were satisfied, multiple linear regression method has been adopted; on the contrary, nonlinear regressions have been performed. In these cases, simple nonlinear regression analyses were considered in order to obtain the best mathematical function able to describe the nonlinear relationship between a single rock mass property and the selected TBM index. The nonlinear analyses have been obtained on the basis of this information.

The explanatory capability of the obtained empirical equations has been tested and the results are presented in Chapter 12.

11 ROCK ENGINEERING SYSTEM: FROM THE INTERACTION MATRIX TO TBM PERFORMANCE ESTIMATION

11.1 Theoretical aspects

11.1.1 General concepts

The interaction matrix, proposed by John Hudson in 1992, is defined as the tool able to identify and link all the rock mass parameters that describe rock engineering systems. The Figure 11.1 shows a simplified scheme of interaction matrix.

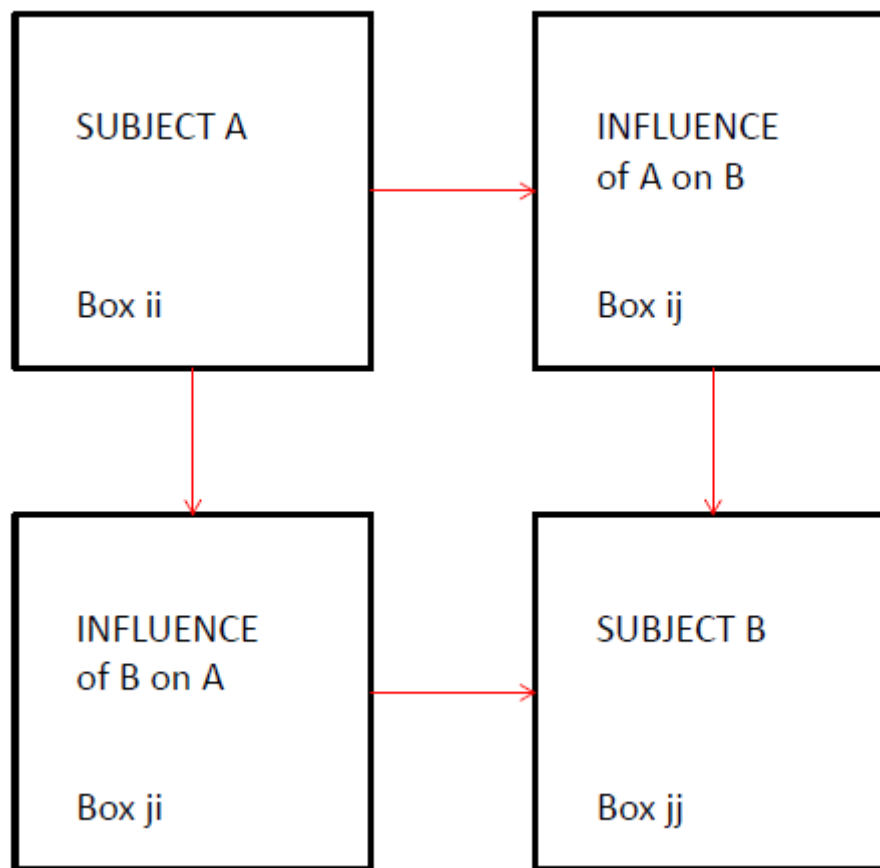


Figure 11.1 Interaction Matrix (After Hudson, 1992).

Interaction matrix was proposed by the Author with the aim of representing the total system behaviour, the relevant factors and their interactions. Even if the interaction matrix can be applied at all systems, Hudson restricted his studies to interactions both between rock/rock masses features and interactions induced by construction in natural ground and to rock slope stability problems.

11.1 Theoretical aspects

The subjects, also called parameters, have to be listed along the leading diagonal of the matrix (top left to bottom right) and we have to consider the interactions between subjects in the off-diagonal boxes, using the convention of a clockwise rotation; as it is observable in Figure 11.1 where an example of 2*2 matrix has been reported. In an $n*n$ matrix there are $n*(n-1)$ off-diagonal terms.

If the off-diagonal terms are the same (for example in a 2*2 matrix), the influence of a on b , and the influence of b on a is the same, vice versa a influences b in a different way as b influences a .

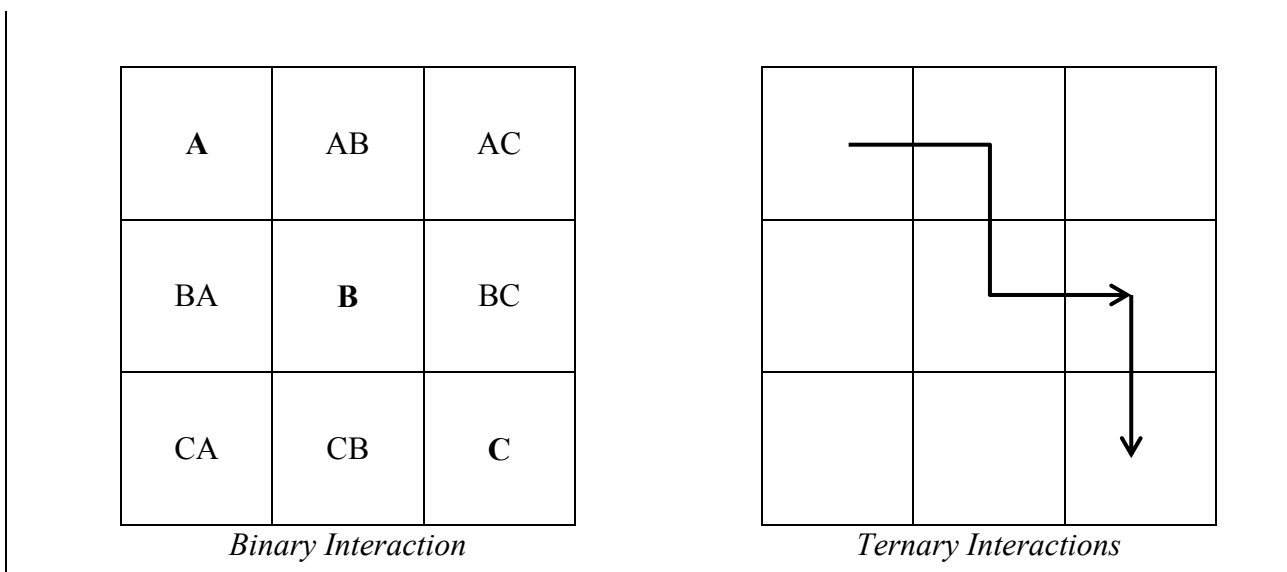
In other words:

- when the complementary off-diagonal boxes are the same the matrix is *symmetric*; it means that $Box_{ij} = Box_{ji}$. Hudson proposed the relation between stress and strain for the elastic cases as example of symmetric matrix;
- when the complementary off-diagonal boxes are not the same the matrix is *asymmetric*, the information contained in Box_{ij} is different to the one listed in Box_{ji} , an example of the relationship between stress and strain for the inelastic cases.

11.1.2 Matrix resolution

The term “matrix resolution” focuses on how many leading diagonal terms are involved in an interaction matrix; generally when the number of subjects increases the quality of resolution improves (Hudson, 1992).

Hudson introduced an algebraic method, called (AB)C concept to indicate matrix resolution when two or more subjects have been combined. To better understand this passage it might be helpful to look at Figure 11.2.



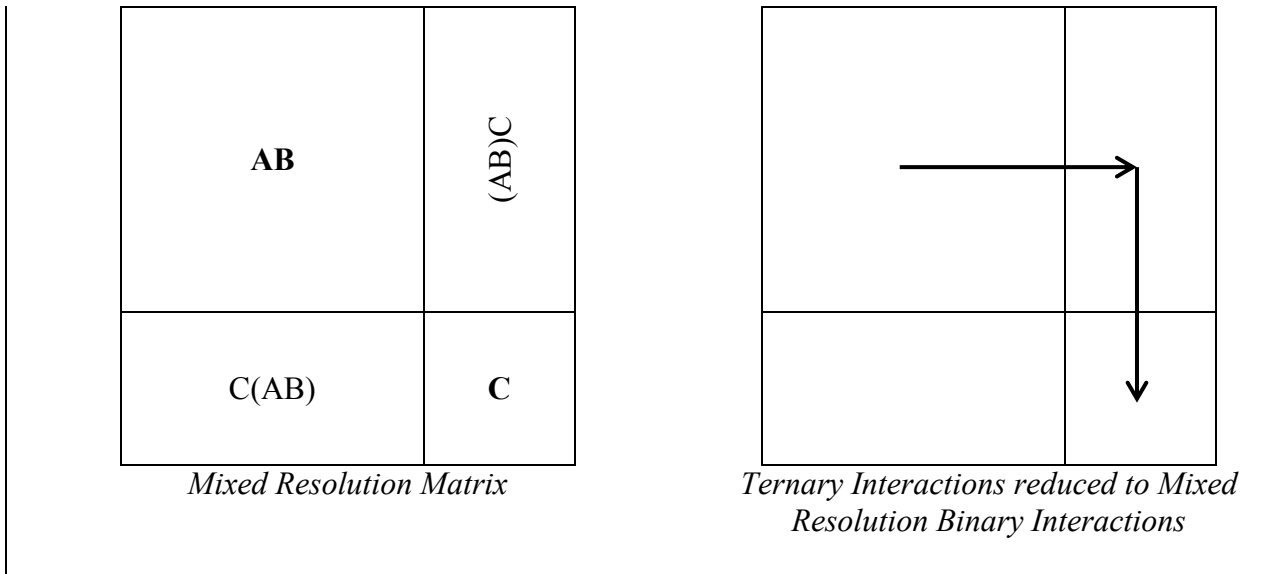


Figure 11.2 Matrix resolution methods (After Hudson, 1992).

The AB component, upper left corner, represents binary interaction (AB and BA) and each off-diagonal term is a device combining two of the subjects with the independent variable determined by the clockwise rotation (Hudson, 1992). The ternary (or higher level) interactions can be considered both as a pathway through binary interaction matrix and as an interaction where a number of parameters have been combined.

The dependent variable is inserted in the bottom right corner box of the matrix.

Figure 11.3 considers the simplest interaction matrix including rock mass properties, site features and their combined effect on a generic project engineering.

R	RS	RP
SR	S	SP
PR	PS	P

Figure 11.3 Simplest interaction matrix involving rock mass properties (R), site conditions (S) and project engineering components (P); (Modified after Hudson, 1992).

11.1 Theoretical aspects

On the basis of R-S-P matrix the resolution could be increased and coarse, medium and finest resolution, corresponding to top, intermediate and lowest level matrix respectively, are obtainable; as reported in Figure 11.4.

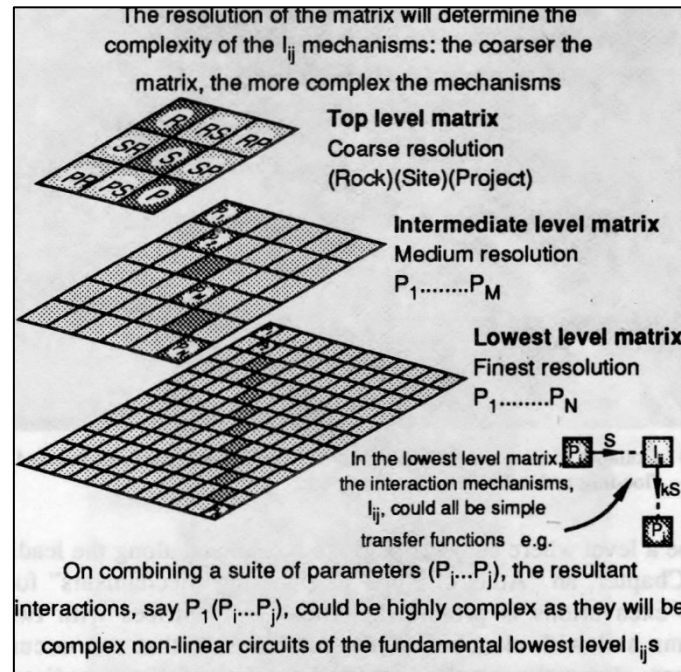


Figure 11.4 Example of coarse, medium and fine resolution matrices (Hudson, 1992).

Increasing the matrix resolution means that a sub-matrix within each element of the higher level matrix exists; furthermore a suite of cascading matrices is created and in the lowest level some measurable quantity is usually achieved.

11.1.3 Atlas of rock engineering system

Hudson proposed an atlas of rock engineering system both for slopes and underground excavation. Firstly, Author selected the appropriate leading diagonal terms; secondly, he identified the mechanism in the off-diagonal ones. The matrix has been created with the aim to provide a checklist of most important rock mechanisms and their possible interaction.

The twelve leading diagonal terms selected by Hudson for a generic underground excavation matrix have been listed below.

1. Excavation dimension;
2. Rock support;
3. Depth of excavation;
4. Excavation method;
5. Rock mass quality;

6. Discontinuity geometry;
7. Rock mass structure;
8. In situ stress;
9. Intact rock quality;
10. Rock behaviour;
11. Discontinuity aperture;
12. Hydraulic condition.

The listed leading diagonal terms generate 132 off-diagonal interactions.

The generic underground excavation matrix has been reported in Appendix IV.

11.1.4 Matrix coding

Hudson proposed five methods in order to code the interactions between matrix subjects:

- *Binary approach*: if a parameter influences another one it is necessary to assign 1 value to the corresponding off-diagonal box, vice versa code 0 will be assigned. If there is a higher number of off-diagonal boxes with a value of 1, the system can be considered interactive, contrariwise the system will not very interactive. This method is the simplest one, however it is not able to explain the intensity of interactions, and it can only say if a parameter influences another one or not.
- *The expert semi-quantitative method (ESQ)* considers five categories of interaction, ranging from 0 to 4. The rate equal to 0 means “no interaction”, 1 means “weak interaction”, rate of 2 “medium”, rate 3 means “strong interaction” and rate equal to 4 is synonym of “critical interaction”. It is an extension of binary system and it is affected by greater sensitivity than the previous approach. ESQ is the most adopted method to code matrices. The rate of each interaction parameter is usually evaluated based on the point of view of field-expert, for example Frough and Toraby, 2013; adopted this approach for estimating TBM downtimes.
- *The P_i vs. P_j slope method* consists of plotting P_i and P_j values and to evaluate the slope of the line that gives information on the rapidity by which P_j changes by function of P_i . This method requires the knowledge of parameter values and to carry out the curve P_i vs. P_j for all the off-diagonal boxes.
- The fourth method requires to represent by *partial differential equations* all the mechanisms in the boxes and to compute the constants associated with the solution. This approach could be difficult to apply, but there is potential in this method.

11.1 Theoretical aspects

- *The explicit method* is based on numerical analysis of mechanisms; it requires large knowledge of the investigated phenomena. The leading diagonal parameters have to have the same quality, for example they must be expressed in the same units. The fifth method can be linked to the ESQ and fourth ones.

11.1.5 Cause-effect plot

Once the matrix has been numerically rated, it is possible to sum the rating values of the rows and the values of the columns through each parameter to evaluate the cause and effect coordinates. In particular it is necessary to consider the sum of the row values as the “cause”: it means that it represents the way in which P_i influences the system; on the other hand, the sum of column values has to be considered as “effect”: it is the effect that P_i has on the system.

The boxes of leading diagonal parameters have no value because of they do not affect each other.

The cause and effect coordinates, calculated for each parameter, have to be plotted into a cause-effect space. The Figure 11.5 shows an example of C, E plot creation.

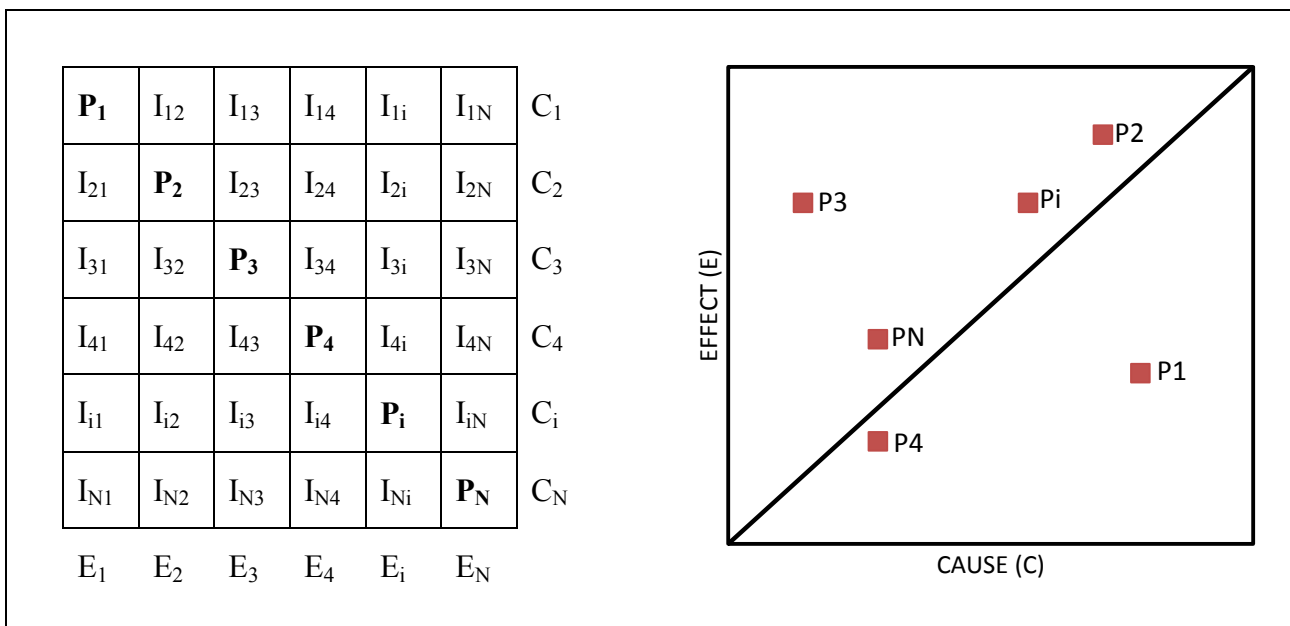


Figure 11.5 Matrix interaction for N parameter (on the left) and constellation of N parameter points (on the right).

The coordinates of causes and effects are an indicator of the interaction intensity and dominance of a parameter (Hudson, 1992). The distance along the diagonal and the perpendicular one from the diagonal to the parameter (the point in the figure) represent the parameter interaction intensity and dominance respectively, as shown in Figure 11.6.

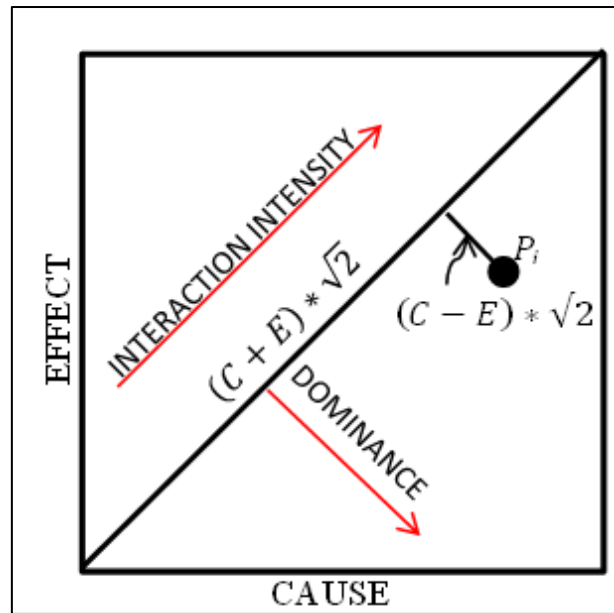


Figure 11.6 Parameter interaction intensity and dominance.

The most interactive parameter is the one characterised by the highest value of $C + E$; on the contrary, the least interactive one is the parameter affected by the least $C + E$ value.

The most dominant parameter is the one defined by the highest $C - E$ value, it means that this parameter affects the system more than the system influences itself. The least $C - E$ value is typical of the most subordinate parameter (in these evaluations it is necessary to consider the sign).

Four extremes values of $C + E$ and $C - E$ might occur, they are located at the four corner point of the C, E plot, as shown in Figure 11.7.

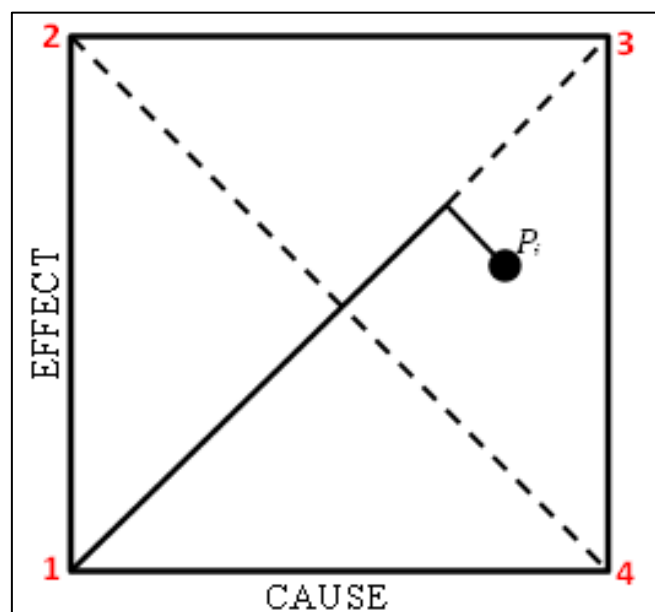


Figure 11.7 The extreme cases of parameter interaction intensity and dominance.

11.1 Theoretical aspects

Point 1 represents the extreme case of the $C + E$ and it is equal to zero. It corresponds to the “zero interaction intensity” condition and it means that the considered parameter does not affect the system and the system does not affect the parameter. On the contrary, the “maximum interaction intensity” condition is represented by point 3; it occurs when each box of the associated row and column has the maximum rate.

Point 2 represents the extreme case of dominance by the system on the parameter, row sum is zero and column is maximized. Point 4 explains the opposite situation: row is maximized and column is zero.

Generally, the four extreme cases are named as follow:

- Point 1: “Zero interaction intensity”;
- Point 2: “System dominates the parameter”;
- Point 3: “Maximal interaction intensity”;
- Point 4: “Parameter dominates system”.

11.1.6 Theorems 1 and 2

Theorem 1 establishes that the mean of C coordinates is equal to the mean of E coordinates and the mean of C and E related to all parameters lies on the $C = E$ line (the diagonal). Given that each cause coordinate is the sum of a row, the result obtained summing all the cause coordinates together is equal to all the boxes in the matrix added together; it is the same for effect coordinates.

The sum of all the causes is equal to the one of all the effects: for this reason, if it is divided by the dimension of the matrix, the resultant mean cause and the resultant mean effect are exactly the same. In conclusion, theorem 1 asserts that the gravity centre of point constellation in a C, E space lies on the $C = E$ line.

Theorem 2 asserts that parameter dominance or subordinacy is expressed by the distance of the point from the $C = E$ line and the maximum parameter dominance or subordinacy is verified when the parameter is 50% interactive.

On the basis of theorem 1 and 2, Author concluded that each constellation of points in a C, E space has the gravity centre on diagonal line ($C = E$ line); furthermore if the constellation is along this line, the parameters can be ranked in order of interactive importance; contrariwise, if the parameter are scattered on the line perpendicular to the $C = E$ line, they can be listed in order of dominance (or subordinacy) intensity.

11.2 RES application to TBM performance estimation

As it is well known, several parameters characterise ground conditions and the performance of TBM working in a given rock mass depends on them. These parameters are influencing each other, and they simultaneously affect TBM performance.

The simultaneous influence of geological site features on FPI and ROP has been evaluated by means of statistical approaches (Chapters 9 and 10) and in this chapter it is investigated using rock engineering system (RES) approach.

To establish as more as possible machine-rock mass interaction, 186 rock sections belonging to “La Maddalena” tunnel (for a total length of 2010 m) have been studied. The length investigated in this study involves the gneiss of Ambin complex (identified as domain I, DI), the micaschist of Clarea complex (domain III, DIII) and the transition zone formed by an alternation between gneiss and micaschist (domain II, DII). The detailed description of these units has been provided in Chapter 5.

11.2.1 Rock mass parameters involved in RES application

In order to apply RES at “La Maddalena” TBM performance analyses, five rock mass parameters have been selected as leading diagonal terms: UCS, quartz content (q), spacing between fractures (S), the angle between the principal set of discontinuities (α), the parameter describing joint conditions (J_c) and tunnel depth (d). Some parameters selected by Hudson for a generic excavation matrix have been excluded from the present analysis because they represent information not available in this study (for example in situ stress and rock behaviour) or because considered not relevant for this specific excavation (as excavation method and dimension or support). The quartz content and joint condition information have been added to the parameters selected by Hudson.

The indexes related to TBM performances is the field penetration index (FPI).

11.2.2 Interaction matrix

The matrix coding method adopted in this study considers both the semi-quantitative coding method developed by Hudson (Hudson, 1992; Mazzoccola and Hudson, 1996) and the method according to the slope of P_i vs. P_j relationship (instead of slope the coefficients of correlation between P_i and P_j have been used).

In this study six class of interaction have been proposed and used; in fact, in order to make the evaluation of the effect of a geological parameter on another one more objective, bivariate

correlations have been carried out and coefficients of correlation, r , have been calculated. Consequently, the parameter interaction ratings have been assigned on the basis of r value.

If between two parameters there is no relationship we will assign rating equal to 0.00, if R ranges from 0.01 to 0.20 the assigned rate is 1 (very weak interaction), if r ranges from 0.21 to 0.40 the assigned rate is 2 (weak interaction), if coefficient of regression is between 0.41 and 0.60 a rate equal to 3 has been considered (medium interaction), if r ranges from 0.61 to 0.80 the rating is 4 (strong interaction) and r between 0.81 and 1.00 involves a rate equal to 5 (very strong interaction). Ratings and classes are listed in Table 11.1.

r	Description	Rating
0.00	No interaction	0
0.01 – 0.20	Very weak	1
0.21 – 0.40	Weak	2
0.41 – 0.60	Medium	3
0.61 – 0.80	Strong	4
0.81 – 1.00	Very strong	5

Table 11.1 Rating and classes of interaction.

Bivariate correlation analyses between parameters have been carried out and r values related to each correlation between P_i and P_j are resumed in Table 11.2.

	FPI	UCS	q	S	Alpha	Jc	Depth
FPI	1.00	0.55	0.66	0.59	0.31	0.34	0.19
UCS	0.55	1.00	0.48	0.40	0.21	0.28	0.15
q	0.66	0.48	1.00	0.43	0.31	0.34	0.31
S	0.59	0.40	0.43	1.00	0.21	0.45	0.14
Alpha	0.31	0.21	0.31	0.21	1.00	0.15	0.13
Jc	0.34	0.28	0.34	0.45	0.15	1.00	0.22
Depth	0.19	0.15	0.31	0.14	0.13	0.22	1.00

Table 11.2 Coefficients of correlation between P_i vs. P_j .

The rates of each effect have been assigned based on r values reported in Table 11.2 and considering the classification proposed in this study and summarised in Table 11.1.

The interaction matrix has been completed as proposed in Figure 11.8. The seven leading diagonal terms are the Uniaxial Compressive Strength, the spacing between discontinuities, the quartz

11.2 RES application to TBM performance estimation

content, the joint condition parameter, the tunnel depth, the alpha angle and FPI. Interactions between parameters have been placed into the 42 off-diagonal boxes and 80 is the sum of ΣC_i and ΣE_i .

effects $E_i \downarrow$	causes $C_i \rightarrow$							ΣC_i
	UCS	2	0	2	0	1	3	8
0	Spacing	0	3	0	0	0	3	6
3	3	Quartz	2	0	2	3	13	
0	0	0	Jc	0	0	2	2	
1	1	2	1	Depth	1	1	7	
0	1	0	1	0	alpha	2	4	
0	0	0	0	0	0	FPI	0	
ΣE_i	4	7	2	9	0	4	14	80

Figure 11.8 “La Maddalena” interaction matrix.

It is observable that the off-diagonal terms are not symmetric to the leading diagonal, it means that the way in which a parameter influences another one is not the same as the second one influences the first one. In order to identify the “less interactive” and the “more interactive” parameters, the “most dominant” and the “most subordinate” ones, the coordinates of causes (C_i) and those of effects (E_i) have been plotted into a cause-effect space. The cause effect diagram carried out for “La Maddalena” case study is reported in Figure 11.9.

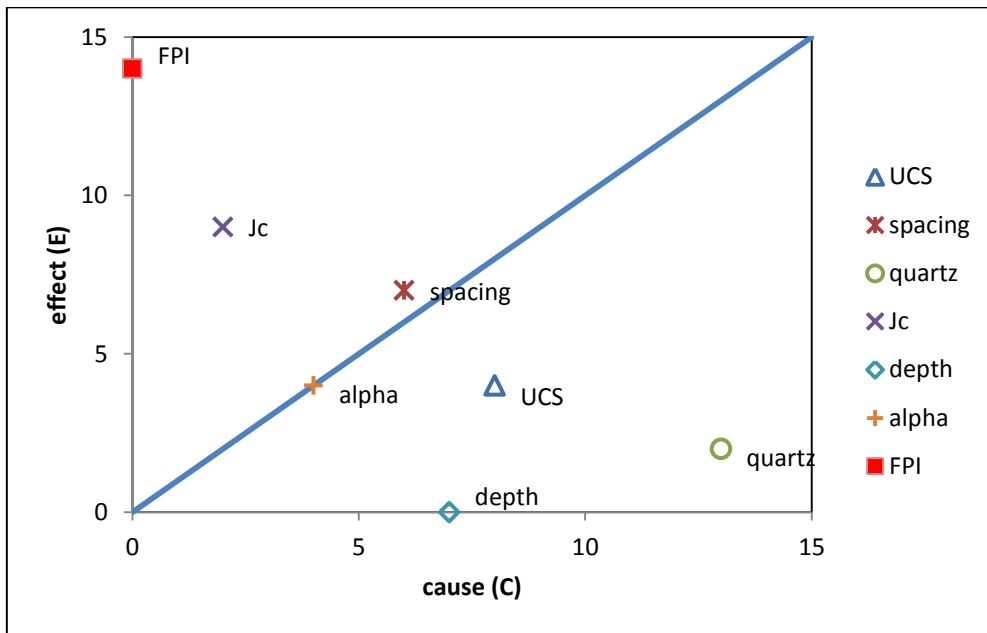


Figure 11.9 Cause-effect “La Maddalena” diagram.

The most interactive parameters fall in the upper right region, contrariwise the less interactive ones are plotted in the lower left region.

By observing cause-effect diagram, it can be observed that FPI is totally affected by the system. As we know FPI cannot influence rock mass conditions and it depends on ground features and on machine specification (not included in this RES analyses).

Tunnel depth has only effect on the system, for this reason it is located on the cause axes, because there is no one geotechnical parameter able to affect tunnel depth.

As we could expect quartz content has the maximum effect on the system followed by UCS, in particular the content of quartz results the most interactive parameter.

Spacing between fractures and alpha angle both influence the system and are influenced by it. The parameter describing joint conditions results largely affected by the system, this is in accordance with the nature of this index.

The histogram in Figure 11.10 has shown the role of system interactivity, plotting the interactive intensity obtained from the sum of causes and effects vs. the parameters.

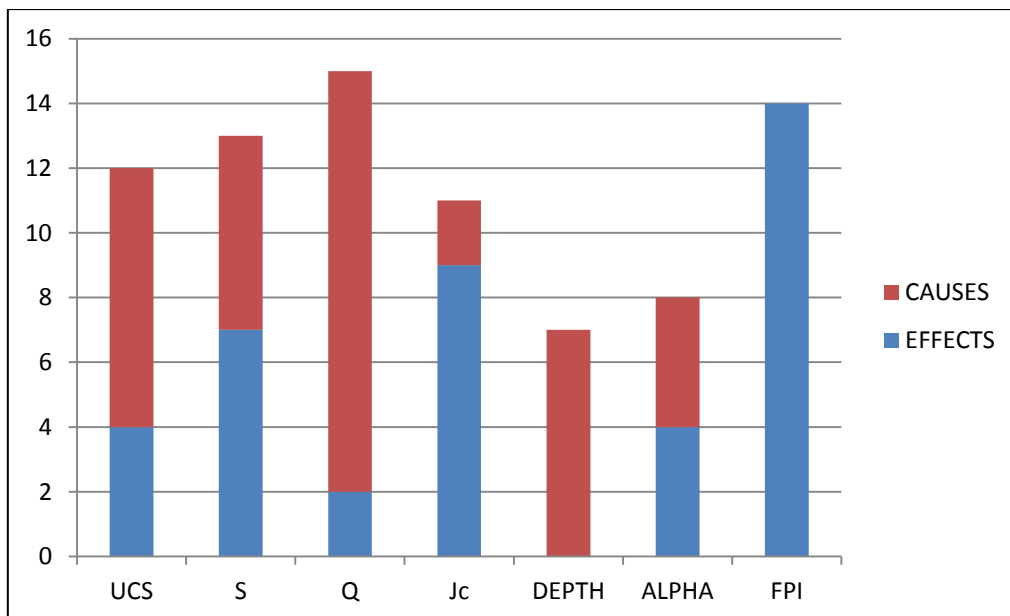


Figure 11.10 Histogram of interactive intensity.

In conclusion it is possible to assert that the most interactive parameter is quartz content ($C + E = 15$) and the least one is tunnel depth ($C + E = 7$). The most dominant element is quartz content ($C - E = 11$) and the most subordinate, excluding FPI, is Jc ($C - E = -7$).

11.2.3 Predictive model development

In order to carry out a TBM performance predictive model based on RES approach, each rock mass section (186) has been rated to calculate an index called, in this study, FPI_R (FPI-RATED). Each rock mass section is described by five geomechanical parameters and depth tunnel (UCS, q , S , α , J_c and depth); for each parameter a rating has to be assigned.

In order to assign objectiveness the rates to parameters, in a first moment ISRM recommendations, RME and Deere and Miller classifications have been involved to divide parameter values into classes; however this approach does not result effective in the following analyses. For this reason a different approach has been adopted.

The statistical distribution of collected values has been investigated for USC class determination. Rating equal to 1 has been assigned to those values ranging between the minimum value and the first quartile (68 – 105 MPa), rating equal to 2 affects the class ranging from first quartile to median value (105 – 130 MPa), rating of 3 has been assigned to the UCS values between median value and third quartile (130 – 160 MPa) and the values higher than 160 MPa have been affected by rating equal to 4.

Also quartz content classes have been defined considering first, second and third quartile of data distribution. The rating assigned to the class containing the values under first quartile ($Q_1 = 25\%$) is equal to 1, rating of 2 has been assigned to the q values ranging between first quartile and median value (25 – 30%), values between second and third quartile (30 – 45%) are affected by rating equal to 3 and rating of 4 has been assigned to quartz content values major than 45%.

The same considerations adopted for UCS and quartz content have been utilised for spacing classification. Rating equal to 1 corresponds to spacing values less than 100 cm (first quartile), rating of 2 corresponds to those values ranging between first and second quartile (100 – 150 cm), the spacing values between median and third quartile (150 – 287.5 cm) have been rated 3 and the values higher than 278.5 cm have been characterized by rating equal to 4.

The alpha angle ratings have been assigned considering the influence of discontinuity orientations on tunnel excavation. In this study the strike of the principal set of fracture is perpendicular to the tunnel axis and excavation drives against dip. For this reason the discontinuities characterized by dips less than 20° and major than 45° determine “fair” conditions of excavation and the assigned rating is equal to 1; the dips ranging between 20° and 45° result in unfavourable excavation conditions, for this reason the assigned rating is equal to 2.

About joint condition parameter (Jc) the classes proposed by RMR classification (Bieniawski, 1989) have been involved. High values of Jc coefficients mean a good global rock masses quality and it determines high values of FPI. For this reason the Jc less than 10 are characterized by rating equal to 1, Jc between 10 and 20 are affected by rating equal to 2, the rating of 3 has been assigned to Jc values ranging between 20 and 25 and values higher than 25 are related to rating equal to 4.

At the entire range of tunnel depth values has been assigned a rating equal to 0.3.

The parameter ratings have been listed in Table 11.3.

	RATING			
	1	2	3	4
UCS [MPa]	68-105	105-130	130-160	>160
q [%]	<25	25-30	30-45	>45
S [cm]	<100	100-150	150-287.5	>278.5
alpha [°]	<20; >45	20-45		
Jc	0-10	10-20	20-25	25-30
depth [m]	<1000 rating 0.3			

Table 11.3 Rating of affecting parameters in FPI.

As a result we obtained a table where in rows there are rock sections and in the columns the rated parameters describing each rock mass section (Table 11.4).

Rock mass section	UCS	alpha	S	Jc	q	depth
	[MPa]	[°]	[cm]		[%]	[m]
1	4	1	2	2	4	0.3
2	4	2	2	2	4	0.3
3	4	2	2	2	4	0.3
4	3	2	2	2	4	0.3
5	3	2	3	2	4	0.3
6	3	2	3	2	4	0.3
...	3	1	2	2	4	0.3
N	3	1	4	3	4	0.3

Table 11.4 Example of rated parameters for each rock section.

11.2 RES application to TBM performance estimation

The interactive intensity (C + E) related to each parameter and carried out by the interaction matrix has been transformed into a percentage to obtain a weighting coefficient able to express the proportional contribute of each parameter on FPI_R , according to the following equation (Hudson, 1992):

$$I_c = \frac{(C + E)}{\sum_i(C + E)} \% \quad (11.1)$$

I_c is typical for each parameter and it has been normalised by dividing it with the maximum rating assigned to that parameter. This operation gives a_i as result, in according to the following equation (Hudson, 1992):

$$a_i = \frac{1}{MP_{ij}} * \frac{(C + E)}{\sum_i(C + E)} \% \quad (11.2)$$

At this point, a_i for each parameter has been established and this allows us to compute FPI_R according to the following formulation:

$$FPI_R = \sum_{i=1}^6 a_i * P_{ij} \quad (11.3)$$

where

- i refers to the six geomechanical parameters;
- j refers to the rock mass section (1 to 186);
- a_i is the value of C + E computed for each parameter;
- P_{ij} is the rate assigned to different class parameters.

In order to better understand the calculation of FPI_R practical explanation has been reported in Figure 11.11.

Rock section	UCS	alpha	S	Jc	q	depth	FPI _R
	RATINGS						
161	1	2	1	2	1	0.3	38.13
162	3	2	1	2	1	0.3	45.63
163	2	2	2	2	1	0.3	45.94
164	3	2	1	2	1	0.3	45.63
165	1	1	2	2	1	0.3	37.19
166	3	2	2	2	1	0.3	49.69
167	2	1	1	1	1	0.3	33.44
...	2	1	1	1	1	0.3	33.44
N	3	1	1	2	1	0.3	40.63
Max. value assigned to each parameter	4	2	4	4	4	0.3	
$I_c = \frac{(C + E)}{\sum_i(C + E)} \%$	15	10	16.25	13.75	18.75	8.75	
$a_i = I_c / \max$	(15/4) 3.75	5.00	4.06	3.44	4.69	29.17	

FPI_R related to each rock section has been calculated in according to the following formula:

$$FPI_R = a_{i-UCS} * UCS_{ij} + a_{i-\alpha} * \alpha_{ij} + a_{i-S} * S_{ij} + a_{i-Jc} * Jc_{ij} + a_{i-q} * q_{ij} + a_{i-d} * d_{ij} \quad (11.4)$$

An example about FPI_R calculation, for rock section number 161, has been provided below:

$$FPI_R = 3.75 * 1 + 5.00 * 2 + 4.06 * 1 + 3.44 * 2 + 4.69 * 1 + 29.17 * 0.3 = 38.13 \quad (11.5)$$

Figure 11.11 Practical example of FPI_R calculation.

At this point the FPI value measured in each rock mass section has been related to the FPI_R computed as below described. Regression analyses have been carried out where FPI is the dependent variable and FPI_R the independent one.

Regression analyses were carried out on:

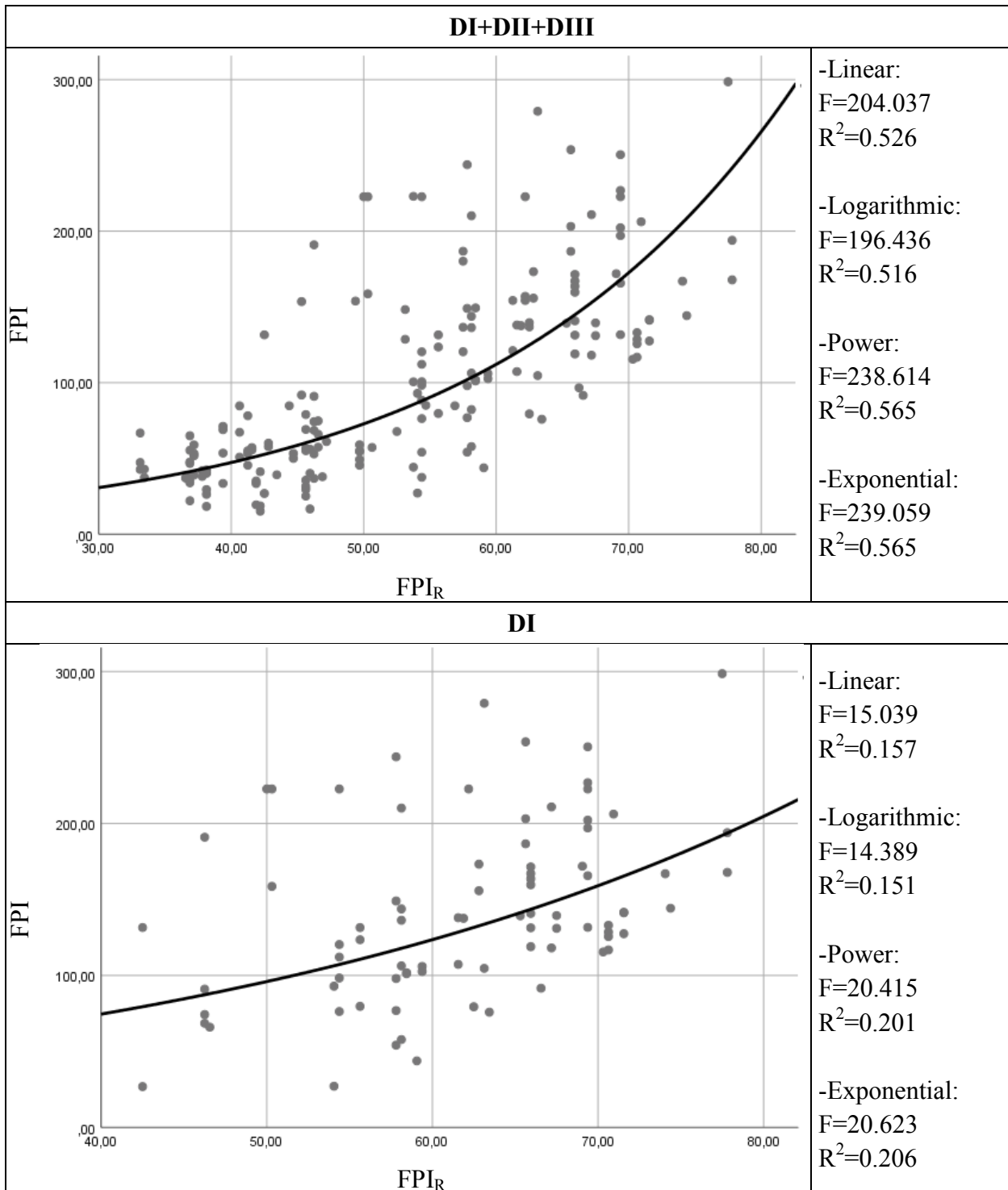
- the entire investigated tract (consisting of gneiss, domain I; gneiss and micaschist alternation, domain II; and micaschist, domain III);
- gneiss section (DI);
- gneiss and micaschist alternation (DII);
- micaschist (DIII).

For a detailed description of geological domains see Chapter 5.

11.2 RES application to TBM performance estimation

In order to select the best mathematical function able to describe the relationship between dependent and independent variables, linear, logarithmic, power, exponential relationships have been investigated by means of IBM SPSS Statistic 25.

Graphical representations of the relationship between computed FPI_R and observed FPI have been presented and statistical tests have been carried out with the purpose to individuate the best mathematical function describing the relationship (Figure 11.12).



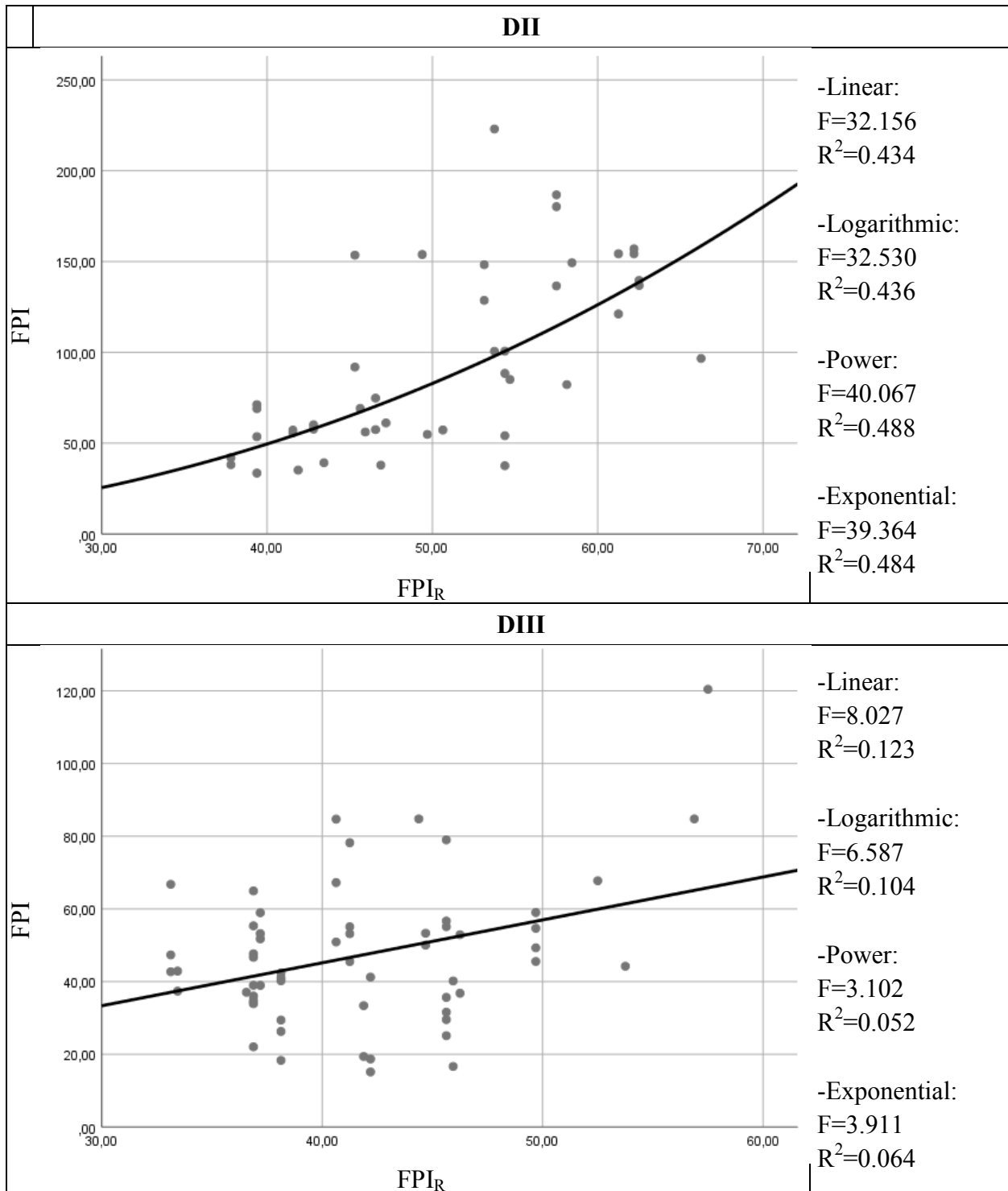


Figure 11.12 Relationships between observed FPI and FPI_R on the left and F and R² values for each tested mathematical function, on the right.

It is observable that the relationship between FPI and FPI_R are low in domain I and very low in domain III: the relationship observed in the transition zone is acceptable; however, the higher level of correlation between FPI and FPI_R has been observed involving data related to the entire tunnel tract (DI+DII+DIII). For these reasons, the subsequent analyses have been developed considering the domains all together.

11.2 RES application to TBM performance estimation

The correlation index between FPI_R and FPI measured into all domains are significantly high than the ones measured into separately considered domains. The mathematical function that best represents the relationship between FPI_R and FPI is exponential type.

At this point, we carried out an exponential regression model where FPI_R has been selected as independent variable and FPI has been considered as dependent one, in according to the following formula:

$$FPI = 8.422 * e^{0.043 * FPI_R} \quad (11.6)$$

The relationship between FPI values measured in situ and the predicted by means of RES approach is quite strong ($r = 0.706$ and $R^2 = 0.498$).

11.3 Conclusion

The purpose of this study was not to propose a new predictive formulation only, but to carry out a new approach able to reduce the subjectivity that usually affects the assignment of ratings to parameters considered in RES application.

After this study, it is possible to advise to assign ratings, for matrix interaction compilation, on the basis of Pearson correlation index (r) between the parameters. By considering the modulus of r values the operators should divide the r range into four or five classes and assign a rating to each of them. In this way, the point of views of tunnelling expert could be confirmed or rejected and parameter interactions can be objectively quantified.

Predictive models can be carried out on the basis of RES approach, as Frough and Torabi (2013) were able to demonstrate. In their research they rated parameters using classes as proposed by Bieniawski in Rock Mass Excavatability classification. In this study, it was observed that using rating proposed by common geomechanical classification (i.e. ISRM, RME, Deere and Miller) the obtained results were not appreciable. It is possible to conclude that for a given specific site the best method to identify classes of parameter is to consider their statistical distribution, then to divide them on the basis of first, second and third quartile; therefore ratings will be assigned to each class.

The proposed method is applicable to different geological and geotechnical situations and it allows to carry out a predictive model specific for a given tunnel project.

12 PREDICTIVE MODEL VALIDATION

12.1 Introduction

The utility of the models carried out in this study and presented in the previous chapters (Chapters 9, 10 and 11) has been tested, focusing on its explanatory and predictive capabilities.

Explanatory capability of models

The aim of this phase is to evaluate whether a regression equation is appropriate to represent the relationship between the geological and geotechnical features of a given rock mass and the performances of the TBM involved to bore it. In other words, being that the regression model construction implies assumptions and choices about the cause-effect relation and input parameters, it is necessary to test the reliability of the regression equation and so, the reasonableness of the assumptions and the selected inputs.

The capability of a regression model to represent the relationship between the geological and geotechnical parameters and the TBM indices is largely expressed by means of the coefficients r , R^2 and R^2_{adj} . Moreover, this capability has been evaluated comparing the ROP or FPI values got by the data recorded during the excavation phases and the ones calculated by means of the equation developed in the present work. Then the measured and the evaluated data have been plotted in a Cartesian space in order to graphically evaluate the correlation between them.

To this purpose, the dataset built with data collected from Pk. 0 + 198 m to Pk. 2 + 010 m has been used firstly to obtain the regression equations and then to compare the recorded data and the model results.

Predictive capability of models

The dataset referring to the rock mass encountered between Pk. 0 + 198 m and Pk. 2 + 010 m has been used to obtain regression models; another dataset, different from the first one, has been used to validate them. In other words, the model and the following equation are obtained by the analysis of data recorded and gathered along a specific tunnel tract (from Pk. 0 + 198 m to Pk. 2 + 010 m), and then they are validated, to verify the predictive ability of the equations, by using a dataset gathered in a different tunnel section, ranging between Pk. 2 + 0.10 m and Pk. 6 + 897 m.

12.1 Introduction

The capability of the obtained predictive models has been evaluated by comparing the TBM performances index ROP and FPI measured (by the TBM acquisition system recording data) and computed (with the regression models) gathered and obtained, respectively, along the tunnel section between Pk. 2 + 010 m to Pk. 6 + 897 m (for a total length of about 4800 m).

In this case too, the coefficient of determination and the graphical representation are adopted to evaluate the relation between measured and calculated data.

Table 12.1 reports the comparison between the main characteristics of the rock mass portion used to obtain the regression models (from Pk. 0 + 198 m to Pk. 2 + 010 m) and the one used to validate them (from Pk. 2 + 010 m to Pk. 6 + 897 m).

	Model Creation Pk. 0 + 198 m – Pk. 2 + 010 m	Model Validation Pk. 2 + 010 m – Pk. 6 + 897 m
UCS [MPa]		
range	68.00 – 251.00	60.00 – 255.00
median	129.00	143.00
Q1-Q3	104.70 – 158.00	152.00 – 168.50
Alpha [°]		
range	7.40 – 85.00	2.80 – 72.60
median	45.20	45.00
Q1-Q3	36.80 – 52.30	39.40 – 54.14
Spacing [m]		
range	0.27 – 11.80	0.20 – 4.33
median	1.50	0.83
Q1-Q3	1.00 – 2.76	0.71 – 1.00
Jc		
range	7.00 – 29.00	7.00 – 21.00
median	18.00	18.00
Q1-Q3	15.00 – 20.00	18.00 – 19.00
quartz[%]		
range	25.00 – 50.00	20.00 – 35.00
median	30.00	25.00
Q1-Q3	25.00 – 45.00	25.00 – 30.00
depth[m]		
range	79.40 – 616.70	256.80 – 1992.60
median	439.30	1083.9
Q1-Q3	285.20 – 522.10	1056.4 – 1156.00

Table 12.1 Comparison between the rock mass portion used to obtain the regression models (Pk. 0 + 198 m – Pk. 2 + 010 m) and the one use to validate them (Pk. 2 + 010 m – Pk. 6 + 897 m).

The Table 12.2 summarises the statistical description of ROP and FPI measured both in the tract of tunnel used to create models and in the one considered for their validation.

	Model Creation Pk. 0 + 198 m – Pk. 2 + 010 m	Model Validation Pk. 2 + 010 m – Pk. 6 + 897 m
ROP[m/h]		
range	0.30 – 3.74	0.62 – 3.74
median	1.40	1.47
Q1-Q3	1.00 – 2.00	1.18 – 1.97
FPI[kN/cutter/mm/rev]		
range	15.16 – 298.6	14.20 – 165.10
median	84.80	49.92
Q1-Q3	50.70 – 140.90	35.40 – 70.95

Table 12.2 Comparison between ROP and FPI measured in the rock mass portion used to obtain the regression models (Pk. 0 + 198 m – Pk. 2 + 010 m) and the one use to validate them (Pk. 2 + 010 m – Pk. 6 + 897 m).

The most reliable regression models described in Chapters 9 and 10, and validated in this Chapter, are reported in Table 12.3.

Equation	ID
$ROP = -0.004 * UCS - 0.041 * q - 0.057 * S + 0.030 * Jc + 0.001 * d + 2.889$	9.38
$ROP = 22.316e^{-2.120E-4UCS} - 1.426\ln(q) + 7.806e^{-0.0003\alpha} + 31.171S^{-0.003} - 1.412e^{-0.094Jc} + 0.001d^{1.024} - 53.952$	9.45
$ROP = 2.295 - 0.006 * UCS - 0.041 * q + 0.056 * Jc + 0.001 * d$	10.11
$ROP = -0.650 * \ln UCS - 0.024 * S - 0.249 * \ln \alpha + 2.317E^{-5} * d^{1.540} + 9.608$	10.16
$ROP = 0.079 * UCS + 0.258 * S - 0.306 * Jc - 9.388$	10.17
$FPI = 0.394 * UCS + 2.564 * q + 8.707 * S - 63.491$	9.46
$FPI = 8.408UCS^{0.509} + 7513.902q^{0.011} + 27.552\ln(S) + 0.080Jc - 7818.256$	9.51
$FPI = 0.576 * UCS + 2.991 * q + 7.651 * S - 0.065 * d - 69.901$	10.18
$FPI = 5.522 * UCS^{0.568} + 42.618 * \exp^{0.069*S}$	10.21
$FPI = 17.902 * UCS - 5.374 * \alpha - 0.643 * d - 3144.566$	10.22
$FPI = 8.422 * e^{0.043*FPI_R}$	11.6

Table 12.3 List of validated predictive models.

12.2 Validation of ROP models

12.2.1 Validation of RL2 model

This model is described in section 9.4.1.1; here the obtained empirical equation has been reported:

$$ROP = -0.004 * UCS - 0.041 * q - 0.057 * S + 0.030 * Jc + 0.001 * d + 2.889 \quad (9.38)$$

The formula is able to explain the 64.30% of the total variance of the dataset ($R^2_{adj} = 0.643$).

Firstly its explanatory capability has been verified comparing the ROP values measured between Pk. 0 + 198 m and Pk. 2 + 010 m, and the ones calculated by means of RL2 model. Then its predictive reliability has been verified comparing data registered from Pk. 2 + 0.10 m to Pk. 6 + 897 m, and the ones calculated in this tract by means of the equation.

RL2 explanatory capability

The comparison between the measured ROP values and the ones calculated by means of the equation 9.38, is reported in Figure 12.1.

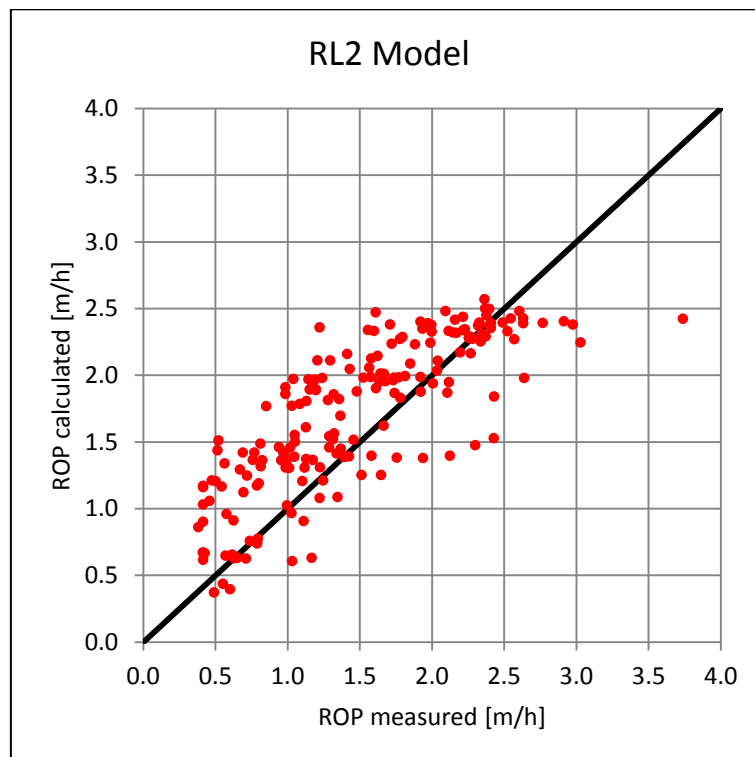


Figure 12.1 Comparison between measured and calculated ROP (RL2 model).

The correlation between the measured and calculated ROP is quite good, as it is possible to note the points are roughly aligned along the bisector. It means that the model is capable to explain the relationship between the geological parameters and the TBM one.

Use of RL2 model to predict ROP

In order to evaluate its capability to predict ROP, RL2 has been used to calculate the rate of penetration in the tract of tunnel that has not been considered during model construction. By comparing predicted and measured performance, it was noted that the model is not able to predict the rate of penetration for the whole tunnel. It can be due to the fact that the depth of tunnel sector in which model was developed is significantly lower than the one of the tract in which model has been tested. Moreover, it is necessary to consider that the depth parameter has been considered as an indicator of in situ stress conditions; however it gives a first indication of vertical stress conditions and does not provide any information about horizontal stress. In situ stress levels could be increased with depth increasing and this situation might affect the machine response.

The RL2 model could be used to predict ROP in those portions of tunnel characterised by overbunden lower than 1000 meters. The comparison between measured and predicted values is shown in Figure 12.2.

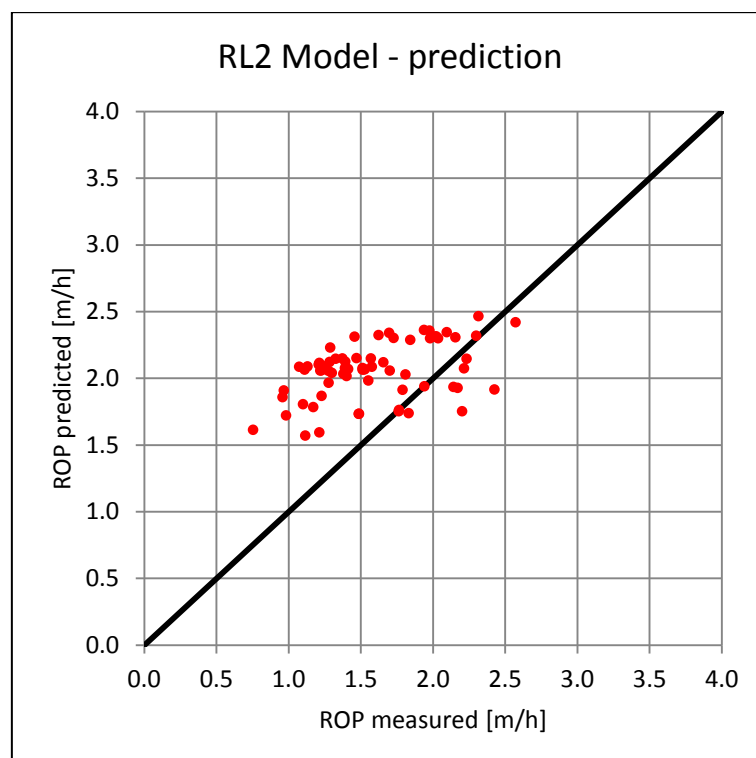


Figure 12.2 Measured vs. predicted ROP.

12.2 Validation of ROP models

The correlation coefficient, r , is equal to 0.441 and R^2 is of 0.195. It denotes a moderate correlation between the observed and evaluated data.

The model is not applicable to the entire length because of the significant increasing of depth; this remarks the fact that the empirical predictive models can be used only in site conditions similar to the ones in which the models has been built.

Moreover, the rock mass portion considered to obtain the model is characterised by spacing between fractures higher than the sector used to validate it.

12.2.2 Validation of RNL model

The nonlinear regression analyses carried out to describe the nonlinear relation between independent variables and response parameter allow the selection of the equation presented in section 9.4.1.2 and here reported:

$$ROP = 22.316e^{-2.120E-4UCS} - 1.426\ln(q) + 7.806e^{-0.0003\alpha} + 31.171S^{-0.003} - 1.412e^{-0.094Jc} + 0.001d^{1.024} - 53.952 \quad (9.45)$$

The coefficient of determination related to Equation 9.45 is equal to 0.655 so the correlation is quite good.

Also in this case the explanatory and predictive capability of the model has been tested, following the same approach described in the previous paragraphs.

RNL explanatory capability

The comparison between measured and calculated data (Figure 12.3) shows that the regression model generates an overestimation of ROP.

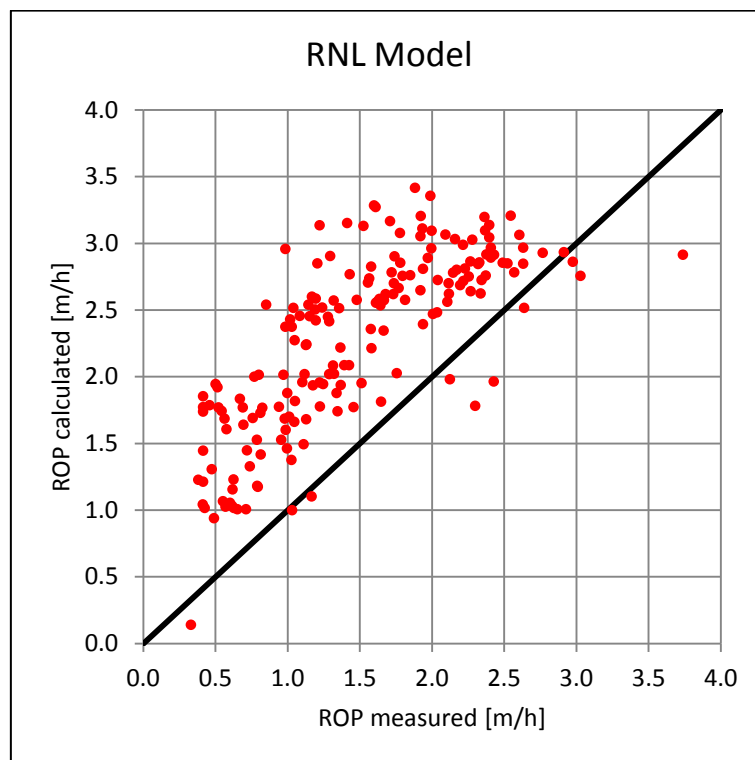


Figure 12.3 Comparison between measured and calculated ROP (nonlinear model).

12.2 Validation of ROP models

The linear model best represents the influence of geomechanical conditions on ROP. It is reasonable to consider that the input parameters have been entered with the correct mathematical nonlinear function and an overestimation of the constant value has been made.

Use of RNL model to predict ROP

The equation 9.45 has been used to predict ROP in the tract of tunnel not considered during model construction. In this case too, the formulation has been applied only in those rock mass portions where the maximum depth is of 1000 meters (for the reasons discussed about the linear model); the correlation is moderate ($R^2 = 0.114$) and the points distribution is similar to the one observed for RL2.

The comparison is graphically shown in Figure 12.4.

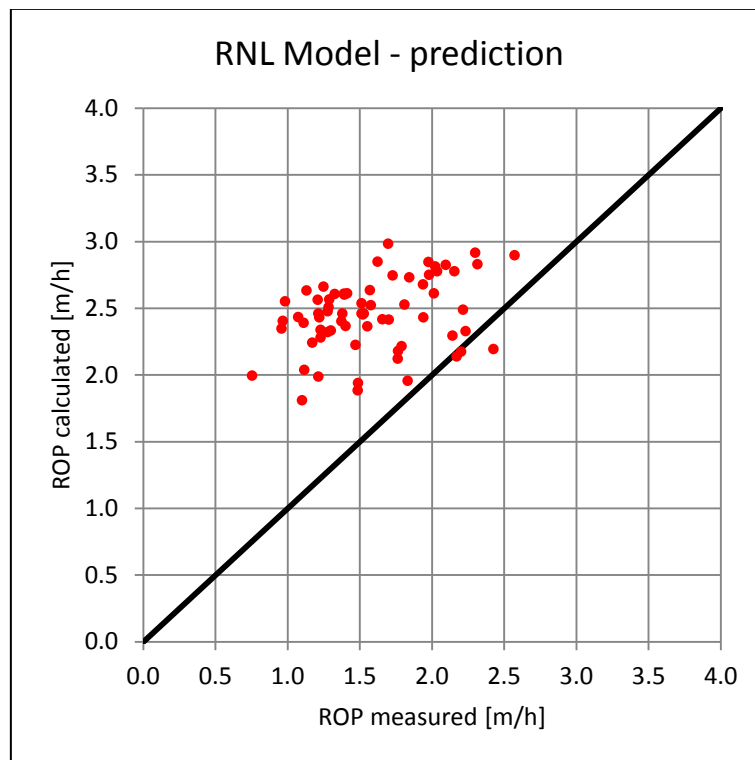


Figure 12.4 Measured vs. Predicted ROP (nonlinear model).

The overestimation of the constant of the nonlinear equation makes the predicted values overestimated with respect to the real ones.

12.2.3 Validation of ROP models carried out for each cluster

For each cluster described in Chapter 10, the relationship between the geological parameter and ROP has been investigated; this allows to carry out three empirical equations. Firstly their explanatory ability has been tested, then the equation obtained for cluster I has been considered to predict ROP. Equation 10.11 has been selected to forecast the TBM index because the cluster that best represents the Domain III (micaschist) is the cluster I.

Explanatory capability

Cluster I

Cluster I is defined by the following ranges of values: UCS = 93.0 – 135.0 MPa; $\alpha = 29.8^\circ - 49.0^\circ$; S = 0.84 – 1.56 m; q = 25 – 30 %; Jc = 15 – 19 (the detailed description is provided in Chapter 10).

The linear multiple regression analysis allows to define the geological parameters-ROP relationship; it is as follows (Model identified as C1c):

$$ROP = 2.295 - 0.006 * UCS - 0.041 * q + 0.056 * Jc + 0.001 * d \quad (10.11)$$

The comparison between the observed and the evaluated data is proposed in Figure 12.5.

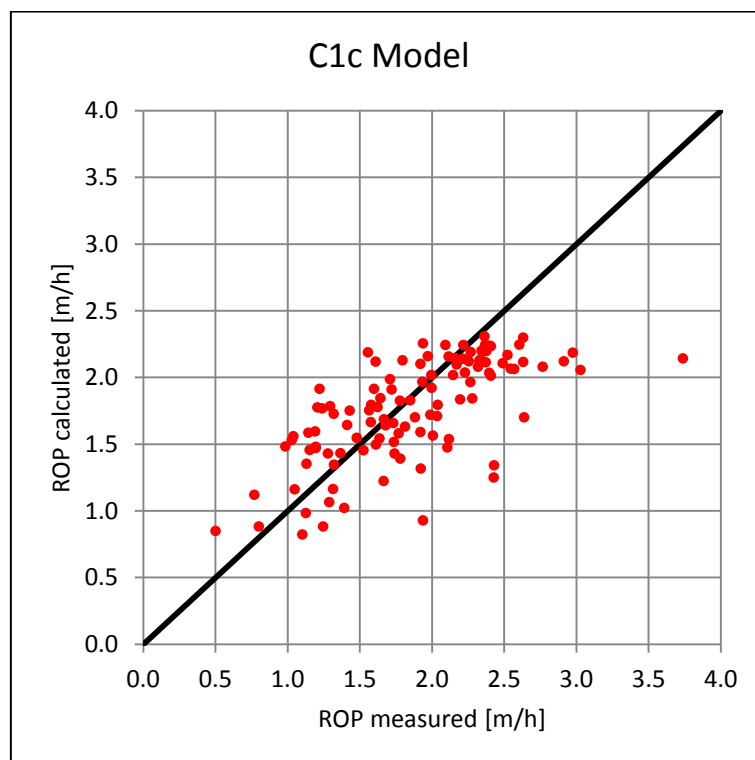


Figure 12.5 Measured vs. calculated ROP, cluster I.

12.2 Validation of ROP models

In the case of cluster I, the relationship between calculated and measured ROP is appreciable, points are plotted close to the 1:1 line. The coefficient of correlation is 0.686 and the determination one is of 0.470.

Cluster II

Cluster II, as described in Chapter 10, is defined by: UCS = 130 – 168.3 MPa; $\alpha = 44^\circ - 60^\circ$; S = 2.39 – 6.00 m; q = 45%; Jc = 17 – 23. When this situation occurs, the equation describing the relation between geomechanical properties and ROP is of nonlinear type and it is as follows:

$$ROP = -0.650 * \ln UCS - 0.024 * S - 0.249 * \ln \alpha + 2.317E^{-5} * d^{1.540} + 9.608 \quad (10.16)$$

ROP observed and the same index calculated by means on 10.16 has been compared (Figure 12.6).

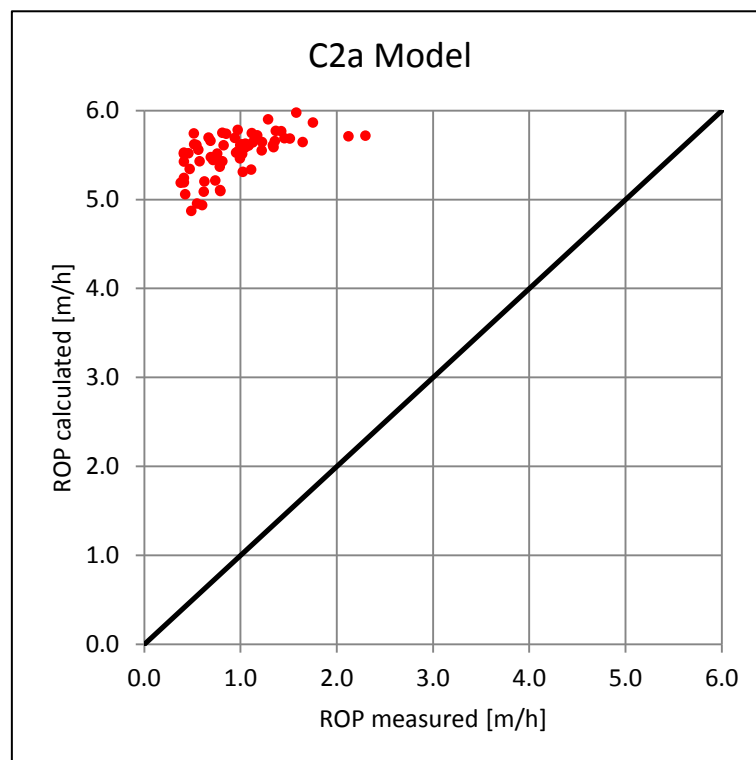


Figure 12.6 Measured vs. calculated ROP, cluster II.

As it is possible to observe, a significant overestimation of ROP has been generated. Two possible causes have been individuated. The first is related to the constant value proposed by the regression analysis; reducing it the predicted values are included in the range of the observed ones. It is possible that, by a geological point of view, the rate of penetrations might be high but technical factors, operator decisions or in general not geological conditions make ROP maintained low; although ROP values equal to 5.00 – 6.00 m/h is quite impossible to be achieved (when tunneling is performed in rock masses similar to La Maddalena one).

Cluster III

Cluster III is characterised by the following properties: UCS = 200 MPa; $\alpha = 44.75^\circ - 52.30^\circ$; S = 1.29 – 2.48 m; q = 50 %; Jc = 20. Also in this case a linear multiple regression analysis has been carried out, as result, the following empirical formulation has been obtained:

$$ROP = 0.079 * UCS + 0.258 * S - 0.306 * Jc - 9.388 \quad (10.17)$$

This equation was used to calculate the rates of penetration in cluster III then they have been compared with the measured data, a very high correlation has been noted, as it is possible to see in Figure 12.7.

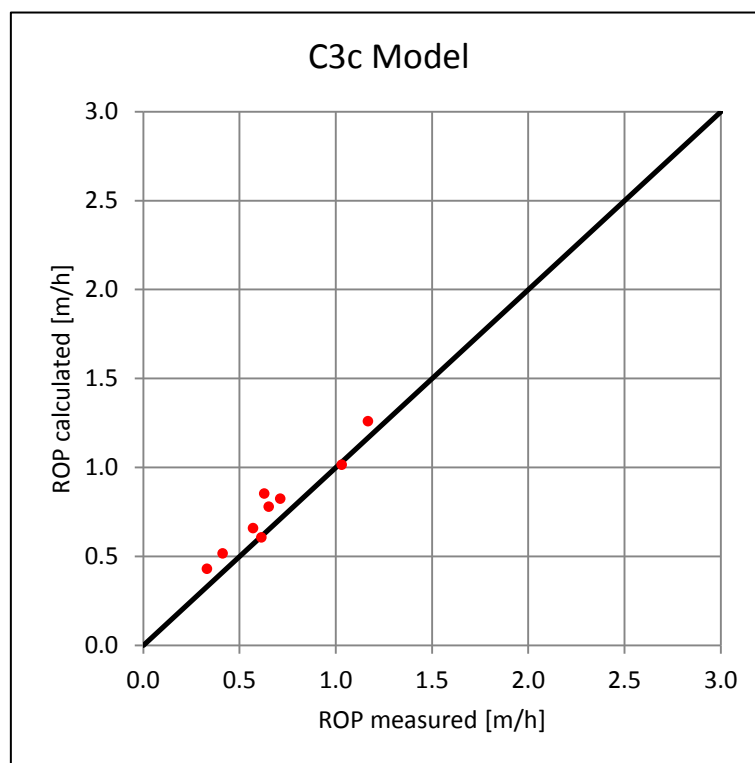


Figure 12.7 Measured vs. calculated ROP, cluster II.

In this case it is possible to conclude that the TBM performances have been determined by geological conditions only, being the R^2 equal to 0.929. It is necessary to consider that the regression analyses, in this case, were performed on nine observations only.

12.2 Validation of ROP models

Use of C1c model to predict ROP

The tract of rock mass ranging between Pk. 2 + 0.10 m and Pk. 6 + 897 is not very similar to any cluster recognised in the first tunnel sector. However the most similar one is cluster I: for this reason the model obtained for cluster I (C1c) has been used to predict ROP in the tract of tunnel from Pk. 2 + 0.10 m to Pk. 6 + 897. The depth of tunnel excavation is considered by the model: this makes it not applicable to the entire tunnel tract but only to those portions affected by maximum overbunden equal to 1000 meters.

The scatterplot of the data registered during the excavation and the ones calculated by means of the C1c model (Equation 10.11) is reported in Figure 12.8.

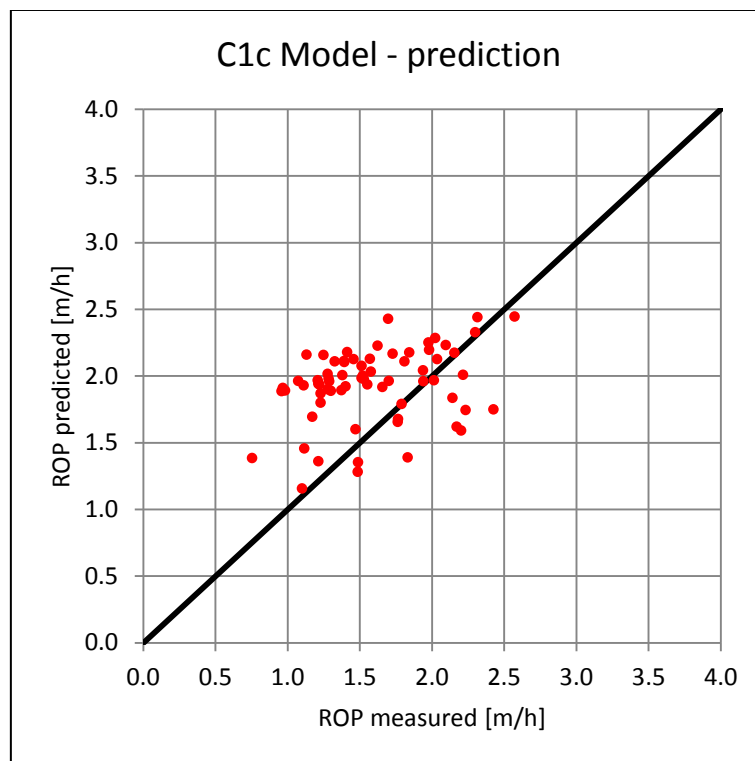


Figure 12.8 Measured vs. predicted ROP (C1c model).

The equation obtained from the analysis developed on data belonging to the cluster I is quite able to predict ROP. Points are aligned near to the bisector line; r and R^2 are equal to 0.319 and 0.102 respectively. The rock mass sections considered to develop the model are characterised by UCS ranges between 93.0 MPa and 135.0 MPa (in terms of Q1-Q3) which is very different from the UCS values measured in the validation rock mass portion (Q1 and Q2 equal to 152.00 MPa and 168.50 MPa, respectively). If the UCS values had been similar, the prediction would have been more accurate.

12.3 Validation of FPI models

The procedure adopted to validate the FPI models is the same described for ROP model validations; so the capability of the models in geology-machine relationship has been verified (comparing the FPI values measured between Pk. 0 + 198 m and Pk. 2 + 010 m, and the ones calculated by means of obtained model). Then their predictive reliability has been verified comparing data registered from Pk. 2 + 0.10 m to Pk. 6 + 897 m, and the ones calculated in this tract by means of the generated equations.

12.3.1 Validation of FL4 model

This model has been discussed in section 9.4.2.1; the obtained empirical equation is as follows:

$$FPI = 0.394 * UCS + 2.564 * q + 8.707 * S - 63.491 \quad (9.46)$$

FL4 explanatory capability

The model explains the 57.10% of the total variance of the dataset ($R^2_{adj} = 0.571$). The comparison between the FPI measured during tunnel construction and the indices calculated by means of the equation 9.46, is represented in Figure 12.9.

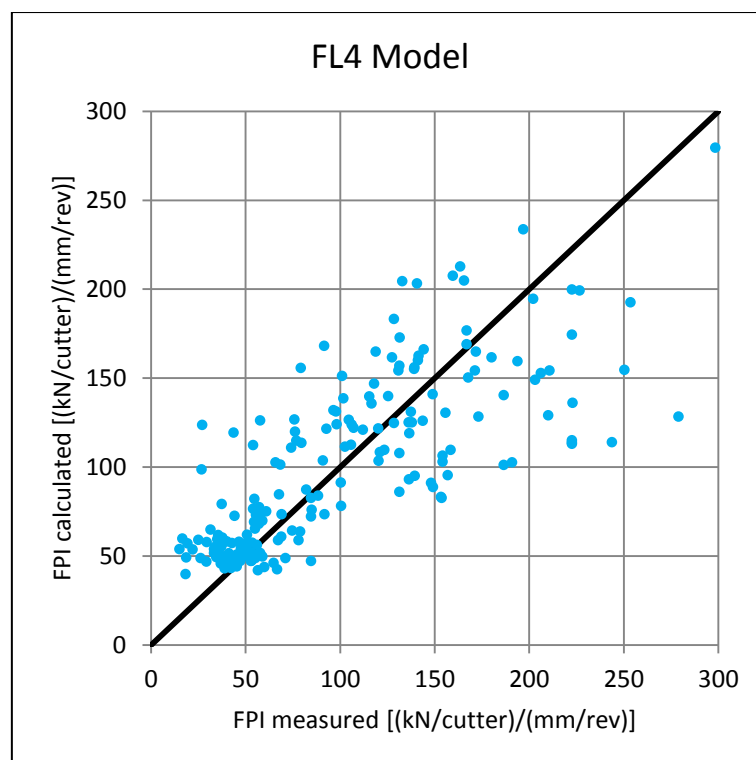


Figure 12.9 Measured vs. calculated FPI, FL4 model.

12.3 Validation of FPI models

The correlation between the registered and calculated FPI is appreciable: in fact, the points are approximately disposed along the 1:1 line and the coefficient of correlation, r , is equal to 0.761 and $R^2_{adj.}$ is 0.571. It means that the model is capable to explain the relationship between the geological parameters and the FPI.

Use of FL4 model to predict FPI

In order to evaluate the model capability to predict FPI, it has been used to calculate the field penetration index on the tract of tunnel that has not been considered during model building. By comparing predicted and observed performances it was noted that the model is not suitable to predict FPI (Figure 12.10).

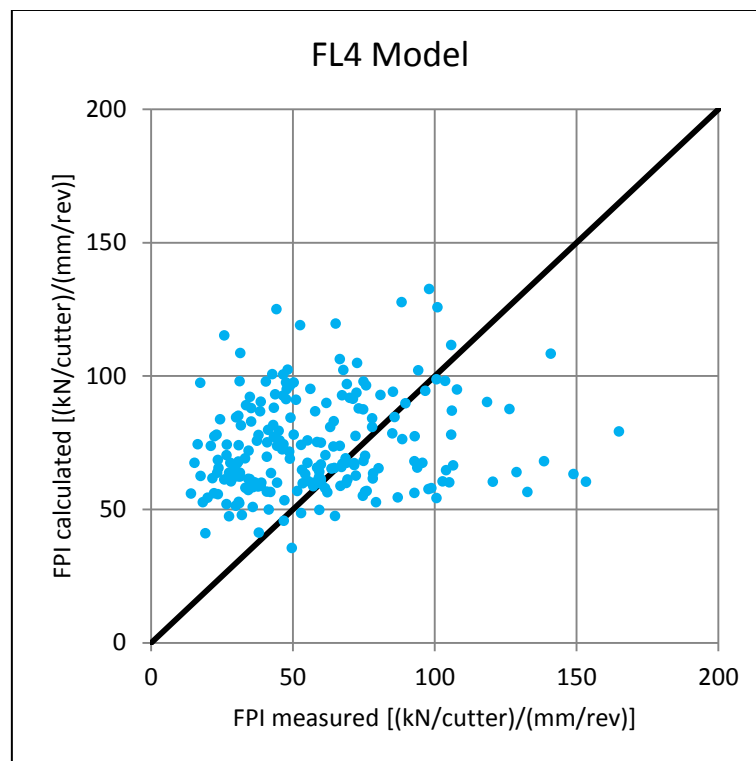


Figure 12.10 Measured vs. predicted FPI, FL4 model.

This lack may be due to the fact that only three geological factors have been entered into the regression analysis. Probably in the tract where the model has been tested, the most influencing variables have changed and one or more than one of those had not been considered by the equation.

Also this evidence underlines the situ-specificity of the empirical predictive models.

12.3.2 Validation of FNL model

The nonlinear effects of the geological parameters on FPI are represented by the model described in 9.4.2.2. The empirical equation describing this relationship is as follows:

$$FPI = 8.408UCS^{0.509} + 7513.902q^{0.011} + 27.552\ln(S) + 0.080Jc - 7818.256 \quad (9.51)$$

FNL explanatory capability

The measured data and the FPI obtained by means of equation 9.51 have been compared; the result is shown in Figure 12.11.

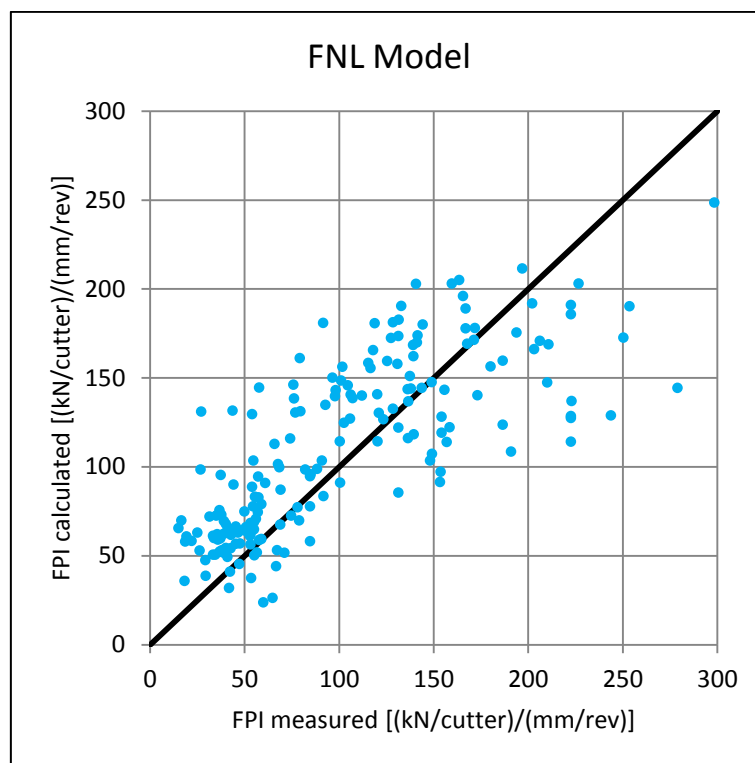


Figure 12.11 Measured vs. calculated FPI, nonlinear model (FNL).

The ability of the nonlinear model to explain the geology-FPI relation is very similar to the one observed for the linear regression model. It allows to assert that the nonlinear functions considered during nonlinear multiple regressions were correctly selected.

12.3 Validation of FPI models

Use of FNL model to predict FPI

Linear and nonlinear models are also characterised by the same difficulty to foresee FPI: as it is possible to deduct by the scatterplot interpretation (Figure 12.12), it is not possible to observe any correlations between measured and predicted FPI values.

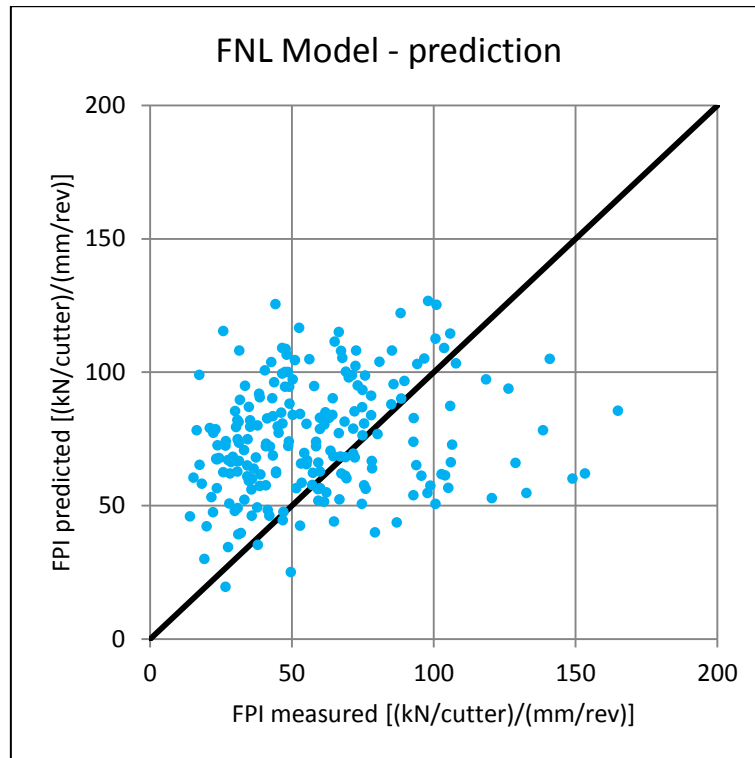


Figure 12.12 Measured vs. predicted FPI, nonlinear model (FNL).

The possible causes of this predictive inability are the same discussed for the linear model FL4.

12.3.3 Validation of FPI models carried out for each cluster

For each cluster regression analyses have been carried out to the purpose to explain the relationship between the geological framework defining the clusters and the FPI measured during their excavation. Firstly, the explanatory ability of the obtained equations has been tested, then the model obtained for cluster I has been used to forecast FPI. Equation 10.18 has been selected to predict the index because the cluster that best represents the Domain III (micaschist) is the cluster I.

Explanatory capability

Cluster I

The regression analyses carried out about data related to cluster I allow to obtain a linear equation that is as follows:

$$FPI = 0.576 * UCS + 2.991 * q + 7.651 * S - 0.065 * d - 69.901 \quad (10.18)$$

The comparison between observed and calculated data is provided by Figure 12.13.

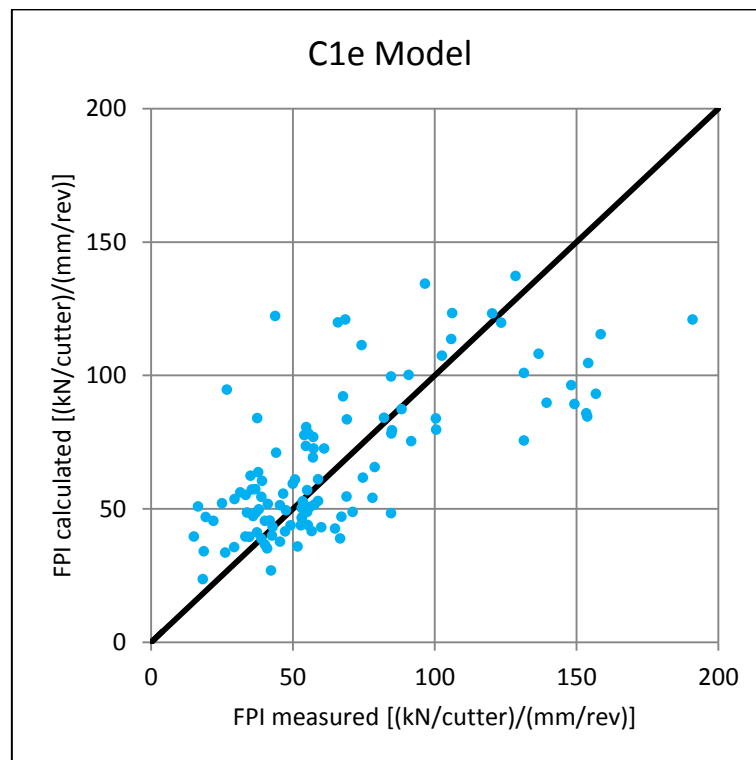


Figure 12.13 Measured vs. calculated FPI, cluster I.

The correlation between measured and calculated FPI is appreciable ($r = 0.703$; $R^2_{adj.} = 0.475$): the points are aligned close to the bisector line. The model C1e is able to represent the relationship between UCS, q , S and d and FPI. When the ground conditions described in cluster I occur, it is

12.3 Validation of FPI models

possible to use this model to predict the field penetration index; however, due to the high homogeneity of the geologic parameters related to the cluster, the model is highly situ-specific and ground feature variations make the equation inapplicable.

Cluster II

The equation that represents the relationship between the geological conditions related to the cluster II and the FPI measured during its excavation is as follows:

$$FPI = 5.522 * UCS^{0.568} + 42.618 * exp^{0.069*S} \quad (10.21)$$

FPI has been calculated by means of this equation, then the observed and the evaluated data have been compared (Figure 12.14).

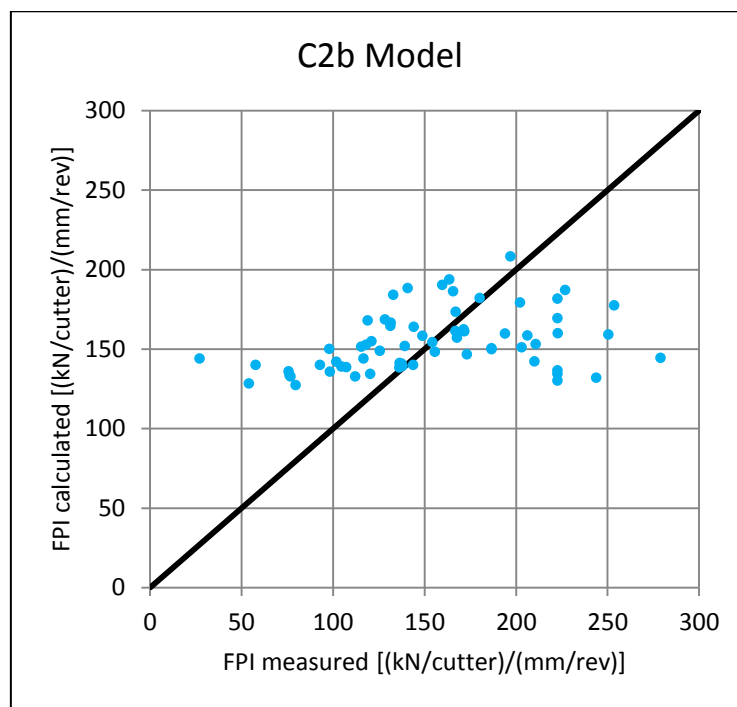


Figure 12.14 Comparison between measured and calculated FPI, nonlinear model cluster II.

The model is not able to represent the relationship between geological variables and the response variable; it is probably due both to the exclusion of some geological variables and to the selection of a wrong nonlinear mathematical form.

Cluster III

The empirical equation describing the relation between geological parameters and FPI is as follows:

$$FPI = 17.902 * UCS - 5.374 * \alpha - 0.643 * d - 3144.566 \quad (10.22)$$

The corrected coefficient of determination is equal to 0.984: it means that the regression represents very well the relationship between UCS- α -depth and FPI. It is also demonstrated by the graphical comparison between measured and calculated FPI (Figure 12.15).

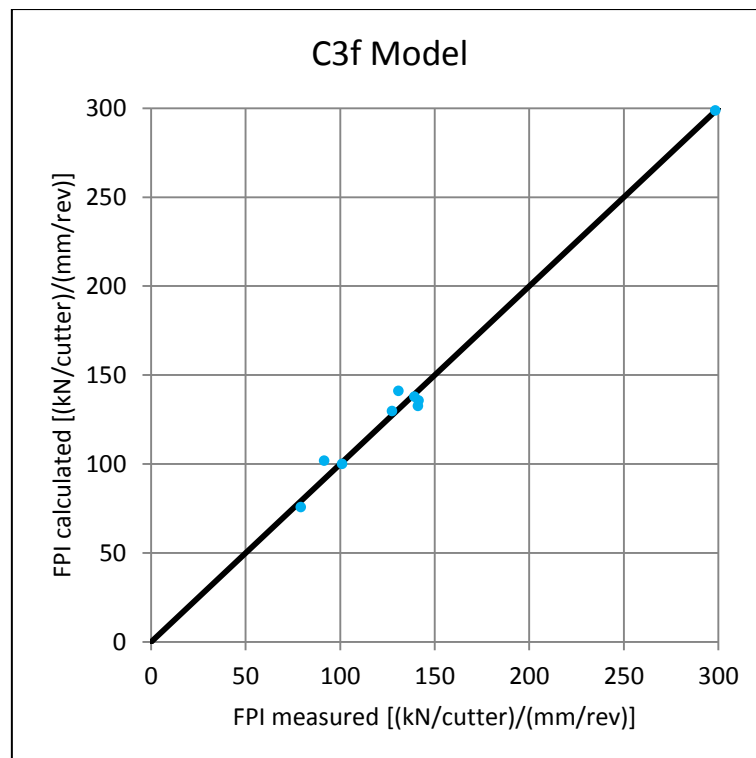


Figure 12.15 Comparison between the measured and calculated FPI, cluster III.

It is necessary to consider that C3f model reliability is affected by the low number of considered elements.

12.3 Validation of FPI models

Use of C1e model to predict FPI

The model named C1e (Equation 10.18) was developed to explain the relationship between the geological features of cluster I and the measured values of FPI. C1e was involved to predict the field penetration index in the tunnel tract ranging between Pk. 2 + 0.10 m and Pk. 6 + 897 m; also in this case only the sectors with maximum depth of 1000 meters have been considered.

The values predicted by means of C1e model and the values recorded during La Maddalena excavation have been compared. The resulting scatterplot is reported in Figure 12.16.

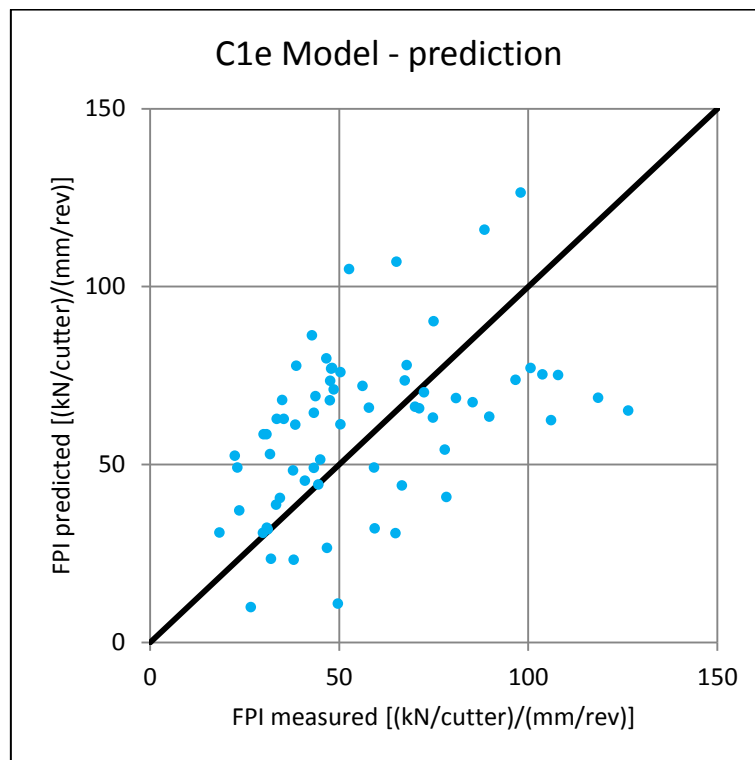


Figure 12.16 Measured vs. predicted FPI values (C1e model).

The relationship between measured and predicted FPI values is quite appreciable, as it is possible to observe in Figure 12.16. The correlation coefficient, r , is 0.461 and the determination coefficient is equal to 0.212.

C1e predictive model is the most reliable one obtained in this study; it is able to reduce the differences between the measured data and the ones calculated by means of the equation. For these reasons, it is the most useful empirical predictive model to forecast FPI.

12.3.4 Validation of FPI model obtained by means of RES approach

The Rock Engineering System (Hudson, 1992) allowed to obtain a predictive model, as presented in Chapter 11. The developed equation is as follows:

$$FPI = 8.422 * e^{0.043 * FPI_R} \quad (11.6)$$

Where FPI_R is the FPI rated.

FPI_R has been calculated in order to use the Equation 11.6 to predict FPI. The comparison between measured and predicted results is shown in Figure 12.17.

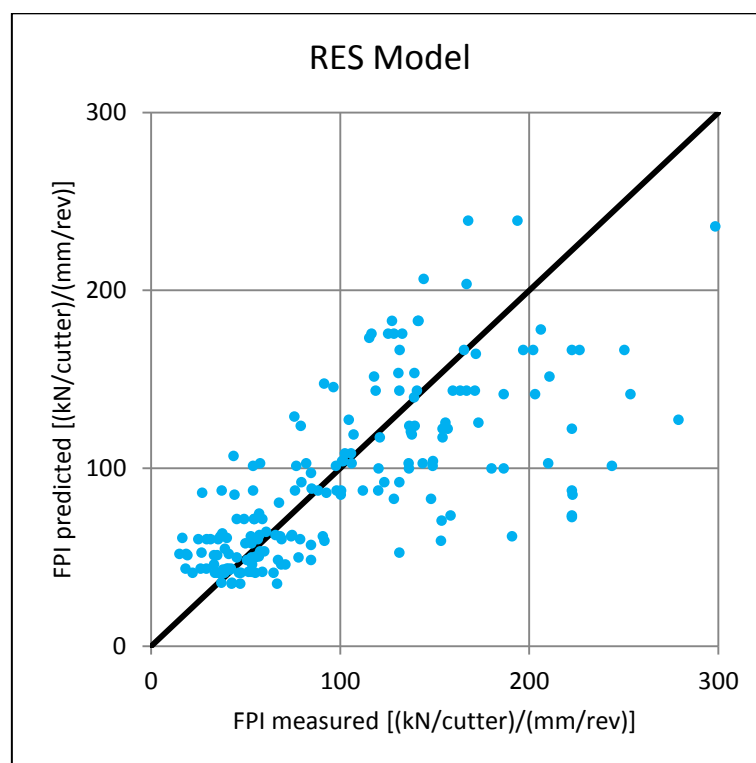


Figure 12.17 Comparison between predicted (by means of RES approach) and measured FPI.

The relationship between in situ measured FPI and predicted by means of RES approach is quite strong ($r = 0.706$), as the graphical and statistical tests have confirmed.

The approach described in Chapter 11 can be used to create regression model able to estimate the performances of a TBM.

12.4 Conclusion

Several regression analyses have been carried out with the purpose of describing the influence of rock mass properties on TBM performances; as a result, empirical equations, in which machine indices are the response variables and rock mass features are the independent ones, have been obtained. These equations can be used both as a mathematical representation of the influence of geological conditions on the machine performances and as predictive tools adopted to forecast the TBM behavior during boring phases.

In this chapter the reliability of the obtained equations has been tested, both in terms of explanatory and predictive capability.

The regression analyses conducted with a high level of detail are a reliable and useful tool to explain the relationship between the geological-geotechnical properties of ground and the machine performances observed during rock mass excavation. It was noted that the coefficients of determination, calculated for each presented model, do not exceed the value of 0.70. It means that they are able to explain the 70.0 % of the total variance, at maximum; the remaining part of variance is represented by other factors which determine the performances of a TBM which usually are not taken into account during model computing (machine specifications, cutterhead geometry, cutter features and operational factors, as reported in Chapter 2).

When linear relationship between geological and machine parameters does not occur it is necessary to consider nonlinear multiple regression models. It was noted that the best way to realise them is considering the single nonlinear forms that correlate each geological parameter to the machine index. In other words, single nonlinear regressions should be performed prior to the multiple ones in order to select the best mathematical form able to link the independent and response variables, so that the chosen ones have to be taken in consideration to construct the model. Nonlinear equations performed during this study, by following this procedure, result able to explain the relation between geological site conditions and TBM behaviour. Moreover the results of measuring-calculated comparison are not very different from the ones obtained from the linear equations related to the same dataset.

The geomechanical parameters collected in the tract of tunnel ranging between Pk. 2 + 010 m and Pk. 6 + 897 m were input as independent variables into the models carry out on the basis of the data collected in the first portion of tunnel (from Pk. 0 + 198 m to Pk. 2 + 010 m). Then, the calculated TBM performances have been compared to the measured ones: in this way the predictive capability of the previously described empirical formulations has been tested.

C1e model is the most reliable one, it was obtained on the basis of the cluster I data analysis and it is able to predict FPI with appreciable accuracy, as reported in paragraph 12.3.3.

The individuated causes able to determine some difficulty in predicting TBM performances, can be summarised as follows:

- *Problems related to the empirical equations*: the selected mathematical function could be not suitable to represent the rock mass-machine interaction and/or the constant of the equation is overestimated (or underestimated) resulting in over/under-estimated TBM indices.
- *Input data selection*: model construction implies the selection of the most influencing geological and geomechanical parameters. This selection is usually carried out on the basis of the operator experience or, in order to be more objective, according to the statistical significance of the parameters, determined by statistical significance tests. So that some variables are included and some others excluded from the final model. However, it is possible that a rock parameter is not taken into account, because in the rock mass portion considered to develop the model it is irrelevant, but it may become more important and seriously affect the machine behaviour in the context in which the model is used to forecast the TBM performances. A hypothesised solution might be to consider also the not significant parameters during model construction.
- *Geology independent factors*: there is a series of situations that not depend on geological framework which can affect the performances of a TBM. For example changes in operational and mechanical conditions or in tender contracts, which clearly cannot be predicted by geological models.
- *Machine limitations*: the excavation of hard and abrasive rock masses requires high TBM thrust, so high FPI in order to guarantee an appropriated penetration per each cutterhead revolution. Nerveless, there is a force threshold above which TBM cannot be driven, in relation to the rock hardness, because it is not possible to impart too high a force on very hard rock faces to avoid machine damages and breakage. Predictive models do not consider this limitation and evaluate FPI on the basis of geomechanical conditions, which can require values higher than the permitted ones.

The models are developed in a specific site, characterised by specific geological and geomechanical framework. When one or more than one variable ranges change the model is not perfectly able to

12.4 Conclusion

adapt itself to this variation. The situ-specificity of these models is the most important aspect that makes them hardly applicable to different contexts from the ones in which they have been achieved.

The most situ-specific models are those developed for each cluster, given that the clustering has divided the rock mass in very homogenous portions. If the geological framework of a rock mass hosting a tunnel is very similar to the one characterising the cluster, the related model (the equation carried out on the basis of cluster information) should give reliable results, as it was possible to observe about C1e model.

A possible solution to the TBM performance prediction problems may be to create a large database of rock mass clusters, considering several tunnels, with the concerning predictive equations developed for each of them. Direct or indirect geological surveys, explorative tunnels and geotechnical investigation performed prior tunnel construction, allow to recognise the cluster (or clusters) with features similar to the ones observed in the investigated ground, so it will be possible to consider the predictive equation performed for those conditions and apply it to predict the TBM performances related to the planned tunnel.

13 CONCLUSION

The general purpose of this thesis was to perform empirical models able to predict the performances of the TBM involved in tunnel excavation on the basis of the relationship between the geological features of the rock mass hosting “La Maddalena” tunnel and the machine performances measured during the excavation.

For this reason, a large database containing geological, geomechanical and structural information collected during continuous detailed survey along the tunnel wall and also the TBM performances registered was created. The database covers a total length of about 7000 meters.

The detailed direct surveys allowed to verify the reliability of the information obtained by means of seismic investigation system, such as the Tunnel Seismic Prediction system. The reliability of this system has been tested comparing the direct detected information and the indirect obtained information. TSP was able to individuate lithological variations: it resulted useful to estimate the fracturing degree and the orientation of principal discontinuity planes. It was noted that an overestimation of the angles between tunnel axis and fractures, due to TSP principles of working, occurs.

Single rock or rock mass parameters were correlated with single TBM index: it resulted of fundamental importance to understand in which way a geological parameter affects machine behaviour. The results of simple regression analyses have been considered in the further analyses; in particular, it was noted that the most influencing parameters are: UCS, quartz content and spacing, followed by joint conditions.

The information obtained by simple regressions had a primary role in the application of Rock Engineering System to this case of study; in particular the level of correlation among variables has been used to compile the rock interaction matrix. A predictive model was developed on the basis of RES approach; it implied a rating of the geological parameters. It was noted that assigning ratings on the basis of the common rock mass classification system is not suitable and the best way to assign ratings is considering the statistical distribution of the parameters. This study allowed to propose an approach applicable to different geological context in order to forecast the performances of TBMs.

Several multiple regression analyses have been carried out with the aim of describing the combined effects of geological features on machine performances: as a result empirical equations have been obtained. These equations can be used both as a mathematical representation of the geology-machine performances and as predictive tools adopted to forecast the TBM behavior during boring phases.

The regression analyses are able to explain the relationship between the geological-geotechnical properties of ground and the machine performances observed during rock mass excavation. It is reasonable that the coefficients of determination of each presented model do not exceed the value of 0.70. It means that geological conditions explain the 70.0 % of the total variance, at maximum; the remaining part is represented by other factors acting on the machine behaviour which generally are not considering during model building.

Linear and nonlinear multiple regression models have been performed. It was noted that the best way to realise them is considering the simple nonlinear regressions previously carried out.

The predictive capability of the achieved empirical models has been tested on a tract of tunnel of about 5000 meters comparing the measured and predicted TBM indices. The models present some difficulties in forecasting machine performances, some causes have been individuated.

Some problems of over/under-estimation are imputable to the constant value calculated for each equation.

One of the most relevant difficulties consists in the selection of input data. After this study, it is possible to advise to include a large number of independent variables even if they do not seem to affect the machine response, because in the context in which the model is used to forecast the TBM performances the excluded parameter may become more important and seriously affect the machine behaviour. Moreover, there are a series of situations that do not depend on geological framework which can affect the performances of a TBM, such as changes in operational and mechanical conditions or in tender contracts which clearly cannot be predicted by geological models.

Machine limitations seriously affect the machine response, in particular for FPI. In fact, there is a force threshold above which TBM cannot be driven, in relation to the rock hardness, because it is not possible to impart a too high force on a very hard rock tunnel face to avoid machine breakage. Predictive models do not consider this limitation and evaluate field penetration index on the basis of geomechanical conditions, which may require values higher than the allowed ones.

The models are performed in a specific site so when one or more than one geological variable ranges change the model is not able to adapt itself to this variation. The situ-specificity of these models makes them hardly applicable to different contexts from the ones in which they have been obtained.

The most situ-specific models are those achieved for each cluster, given that they are very homogenous portions of rock mass. The empirical equations developed for each of them are very reliable, so a possible solution to overcome the TBM performance prediction problems may be to build a large database of rock mass clusters with the concerning predictive equations developed for each of them.

Geological and geotechnical data collection performed prior tunnel construction allows the experts to ascribe the features observed to the cluster with similar characteristics and adopt the predictive equation typical of the recognised cluster to predict the TBM performances related to the planned tunnel.

14 REFERENCES

- Abdi, H., & Valentin, D. (2007). Multiple correspondence analysis. *Encyclopedia of measurement and statistics*, 651-657.
- Abdi, H., & Williams, L. J. (2010). Principal component analysis. *Wiley interdisciplinary reviews: computational statistics*, 2(4), 433-459.
- Adoko, A. C., Gokceoglu, C., & Yagiz, S. (2017). Bayesian prediction of TBM penetration rate in rock mass. *Engineering Geology*, 226, 245-256.
- Alber, M. (1996). Prediction of penetration and utilization for hard rock TBMs. In *ISRM International Symposium-EUROCK 96*. International Society for Rock Mechanics.
- Alber, M. (1998). Design of high speed TBM-drives. *Proc. 8th Int. IAEG Congress*, 3537-3543. Rotterdam: A. A. Balkema.
- Alber, M. (2000). Advance rates of hard rock TBMs and their effects on project economics. *Tunnelling and underground space technology*, 15(1), 55-64.
- Alber, M. (2008). An integrated approach to penetration, advance rates and disc cutter wear for hard rock TBM drives. *Geomechanik und Tunnelbau: Geomechanik und Tunnelbau*, 1(1), 29-37.
- Alber, M., Yaralı, O., Dahl, F., Bruland, A., Käsling, H., Michalakopoulos, T. N. & Özarslan, A. (2013). ISRM suggested method for determining the abrasivity of rock by the CERCHAR abrasivity test. In *The ISRM Suggested Methods for Rock Characterization, Testing and Monitoring: 2007-2014*(pp. 101-106). Springer, Cham.
- Grima, M. A., Bruines, P. A., & Verhoef, P. N. W. (2000). Modeling tunnel boring machine performance by neuro-fuzzy methods. *Tunnelling and underground space technology*, 15(3), 259-269.
- Argand E, Blösch E, Heim A, Heim A (1911) Les nappes de recouvrement des Alpes pennines et leurs prolongements structuraux, 31-33, In *Kommission bei A. Francke* (vorm. Schmid & Francke)
- Armaghani, D. J., Hajihassani, M., Mohamad, E. T., Marto, A., & Noorani, S. A. (2014). Blasting-induced flyrock and ground vibration prediction through an expert artificial neural network based on particle swarm optimization. *Arabian Journal of Geosciences*, 7(12), 5383-5396.
- Armaghani, D. J., Mohamad, E. T., Momeni, E., & Narayanasamy, M. S. (2015). An adaptive neuro-fuzzy inference system for predicting unconfined compressive strength and Young's modulus: a study on Main Range granite. *Bulletin of engineering geology and the environment*, 74(4), 1301-1319.
- Armaghani, D. J., Mohamad, E. T., Narayanasamy, M. S., Narita, N., & Yagiz, S. (2017). Development of hybrid intelligent models for predicting TBM penetration rate in hard rock condition. *Tunnelling and Underground Space Technology*, 63, 29-43.
- Armetti, G., Migliazza, M. R., Ferrari, F., Berti, A., & Padovese, P. (2018). Geological and mechanical rock mass conditions for TBM performance prediction. The case of "La Maddalena" exploratory tunnel, Chiomonte (Italy). *Tunnelling and Underground Space Technology*, 77, 115-126.
- Armetti, G., Migliazza, M., Comina, C., Padovese, P., Berti, A. (2017) Direct geostructural survey and seismic methods: comparison for predicting geological framework of rock mass of "La Maddalena"

tunnel - Chiomonte, Italy. *International conference AFTES 2017. Assoc. Francaise des tunnels et de l'espace souterrain.*

- Atashpaz Gargari, E., Hashemzadeh, F., Rajabioun, R., & Lucas, C. (2008). Colonial competitive algorithm: a novel approach for PID controller design in MIMO distillation column process. *International Journal of Intelligent Computing and Cybernetics*, 1(3), 337-355.
- Atashpaz-Gargari, E., & Lucas, C. (2007). Imperialist competitive algorithm: an algorithm for optimization inspired by imperialistic competition. In *Evolutionary computation, 2007. CEC 2007. IEEE Congress on* (pp. 4661-4667). IEEE.
- Balci, C. (2009). Correlation of rock cutting tests with field performance of a TBM in a highly fractured rock formation: A case study in Kozyatagi-Kadikoy metro tunnel, Turkey. *Tunnelling and Underground Space Technology*, 24(4), 423-435.
- Bamford, W. F (1984). Rock test indices are being successfully correlated with tunnel boring machine performance. In *Proceedings of the 5th Australian Tunnelling Conference*, Melbourne, 2:9-22.
- Barla, G., & Pelizza, S. (2000). TBM tunnelling in difficult ground conditions. In *ISRM International Symposium*. International Society for Rock Mechanics.
- Barton N (2000). TBM tunnelling in jointed and faulted rock. *CRC Press*.
- Barton N, Lien R, Lunde J (1974) Engineering classification of rock masses for the design of tunnel support. *Rock Mechanics* 6 (4):189-239
- Barton, N. (1978). Suggested methods for the quantitative description of discontinuities in rock masses. *ISRM, International Journal of Rock Mechanics and Mining Sciences & Geomechanics Abstracts*, 15(6).
- Bashir, Z. A., & El-Hawary, M. E. (2009). Applying wavelets to short-term load forecasting using PSO-based neural networks. *IEEE transactions on power systems*, 24(1), 20-27.
- Benardos, A. G., & Kaliampakos, D. C. (2004). Modelling TBM performance with artificial neural networks. *Tunnelling and Underground Space Technology*, 19(6), 597-605.
- Benzecri, J. P. (1979). Sur le calcul des taux d'inertie dans l'analyse d'un questionnaire, addendum et erratum à [BIN. MULT.]. *Cahiers de l'Analyse des Données*, 4(3), 377-378.
- Bieniawski, Z. T. (1989). Engineering rock mass classifications: a complete manual for engineers and geologists in mining, civil, and petroleum engineering. *John Wiley & Sons*.
- Bieniawski, Z. T., & Grandori, R. (2007). Predicting TBM excavability-part II. *Tunnels & Tunnelling International*.
- Bieniawski, Z. T., Celada, B., & Galera, J. M. (2007, June). TBM excavability: prediction and machine-rock interaction. In *Proceedings, Rapid Excavation and Tunneling Conference* (pp. 1118-1130).
- Bieniawski, Z. T., Tamames, B. C., Fernandez, J. M. G., & Hernandez, M. A. (2006). Rock Mass Excavability (RME) Indicator. In *Proceedings of ITA-AITES World Tunnel Congress and 32nd ITA General Assembly*.

- Birant, D., & Kut, A. (2007). St-dbscan: An algorithm for clustering spatial–temporal data. *Data & Knowledge Engineering*, 60(1), 208-221.
- Blindheim, O.T. (1979) Boreability predictions for tunneling. *The Norwegian Institute of Technology, Trondheim*, Norway.
- Bocquet, J. (1974). Il metamorfismo prealpino nella Vanoise (Savoia) e in altri settori dello zoccolo Brianzese. *Mem. Soc. Geol Ital*, 13, 271-284.
- Boniface, A. (2000). Tunnel Boring Machine performance in basalts of the Lesotho formation. *Tunnelling and Underground Space Technology*, 15(1), 49-54.
- Bordet, C., & Comes, G. (1975). Forecasting study of the drilling properties of rocks for tunnel construction. Example of the main arc-isere gallery. *Tunnels et ouvrages souterrains*, (7).
- Borghini, A., & Gattiglio, M. (1997). Osservazioni geologico-petrografiche nel settore meridionale del massiccio d'Ambin. *Atti Ticinensi Sci. Terra*, 5, 65-84.
- Broch E, Franklin JA (1972) The point-load strength test. *International Journal of Rock Mechanics and Mining Sciences & Geomechanics Abstracts*, 9 (6):669-676.
- Brownlee, J. (2011). Clever algorithms: nature-inspired programming recipes. *Jason Brownlee*.
- Bruland A (1998). Hard rock tunnel boring. Doctoral thesis, *Norwegian University of Science and Technology*, Trondheim, Norway.
- Callegari, E., Sacchi, R., Bovo, S., & Torassa, G. (1980). Osservazioni strutturali sul versante italiano del massiccio di Ambin (Alpi Graie). *Bollettino della Societa Geologica Italiana*, 99(4), 395-404.
- Casati C, Giovacchini A (1977) L'utilizzo delle immagini Landsat per indagini di neotettonica. *Boll. Geod. Sc. Affini*, 36:399-410
- Cassinelli, F., Cina, S., & Innaurato, N. (1983). Power consumption and metal wear in tunnel-boring machines: analysis of tunnel-boring operation in hard rock: In: Tunneling 82, Proceedings of the 3rd International Symposium, P73–81. Publ London: IMM, 1982. In *International Journal of Rock Mechanics and Mining Sciences & Geomechanics Abstracts* (Vol. 20, No. 1, p. A25). Pergamon.
- Chiaia, B. (2001). Fracture mechanisms induced in a brittle material by a hard cutting indenter. *International Journal of Solids and structures*, 38(44-45), 7747-7768.
- Christopher, D. M., Prabhakar, R., & Hinrich, S. C. H. Ü. T. Z. E. (2008). Introduction to information retrieval. *An Introduction To Information Retrieval*, 151, 177.
- Cook, N. G. W., Hood, M., & Tsai, F. (1984). Observations of crack growth in hard rock loaded by an indenter. In *International Journal of Rock Mechanics and Mining Sciences & Geomechanics Abstracts* (Vol. 21, No. 2, pp. 97-107). Pergamon.
- Crow SC (1975) Jet tunnelling machines. A guide for design. *Tunnels & Tunnelling International*, 7(2)
- Deere, D. U., & Miller, R. P. (1966). Engineering classification and index properties for intact rock. *Illinois Univ At Urbana Dept Of Civil Engineering*.
- Delisio, A., & Zhao, J. (2014). A new model for TBM performance prediction in blocky rock conditions. *Tunnelling and Underground Space Technology*, 43, 440-452.

- Delisio, A., Zhao, J., & Einstein, H. H. (2013). Analysis and prediction of TBM performance in blocky rock conditions at the Lötschberg Base Tunnel. *Tunnelling and Underground Space Technology*, 33, 131-142.
- Desmons J, Mercier D (1993) Passing through the Briançon zone. In Pre-Mesozoic Geology in the Alps, *Springer Berlin Heidelberg*, pp. 279-295
- Desmons, J. (1992). The Briançon basement (Pennine Western Alps): mineral composition and polymetamorphic evolution. *Schweizerische Mineralogische und Petrographische Mitteilungen*, 72(1), 37-55.
- Desmons, J., & Fabre, J. (1988). Contribution à la connaissance pétrographique du Mont Pourri (Savoie, France); conséquences structurales. *Géologie Alpine*, 64, 13-26.
- Dickmann, T. (2012). Predicting rock conditions ahead of the face. *TunnelTalk*.
- Dickmann, T. and Krueger, D. (2013). Is geological uncertainty ahead of the face controllable? *World Tunnel Congress 2013 Geneva*, Underground-the way to the future! G. Anagnostou & H. Ehrbar (eds), CRC Press.
- Dickmann, T., Tang, S. K. (2006) Application and research of seismic investigation methods to predict rock mass conditions ahead of the face.
- Dollinger GL, Handewith HJ, Breeds CD (1998) Use of the punch test for estimating TBM performance. *Tunnelling and underground space technology*, 13(4):403-408
- Eberhart, R., & Kennedy, J. (1995, October). A new optimizer using particle swarm theory. In *Micro Machine and Human Science, 1995. MHS'95., Proceedings of the Sixth International Symposium on* (pp. 39-43). IEEE.
- Ellenberger, F. (1958). Etude géologique du pays de Vanoise. *Impr. nationale*.
- Farmer IW, Glossop NH (1980) Mechanics of disc cutter penetration. *Tunnels and Tunnelling*, 12(6):22-25
- Farrokh, E., Rostami, J., & Laughton, C. (2012). Study of various models for estimation of penetration rate of hard rock TBMs. *Tunnelling and Underground Space Technology*, 30, 110-123.
- Feng, X., & Jimenez, R. (2015). Estimation of deformation modulus of rock masses based on Bayesian model selection and Bayesian updating approach. *Engineering Geology*, 199, 19-27.
- Franklin, J. A. (1985). Suggested method for determining point load strength. In *International Journal of Rock Mechanics and Mining Sciences & Geomechanics Abstracts* (Vol. 22, No. 2, pp. 51-60). Pergamon.
- Fudral S (1998) Etude géologique de la suture téthysienne dans les Alpes franco-italiennes nord-occidentales de la Doire Ripaire (Italie) à la région de Bourg-Saint-Maurice(France). Doctoral dissertation.
- Gay, M., Mégnien, F., & Mégnien, C. (1970). Le massif d'Ambin et son cadre de schistes lustrés (Alpes franco-italiennes): évolution paléogéographiques antéalpine. *BRGM*.
- Gehring, K., 1995. Leistungs-und Verschleissprognosen in maschinellen Tunnelbau. *Felsbau* 13 (6)
- Ghasemi, E., Yagiz, S., & Ataei, M. (2014). Predicting penetration rate of hard rock tunnel boring machine using fuzzy logic. *Bulletin of Engineering Geology and the Environment*, 73(1), 23-35.

- Giardino M, Polino R (1997) Le deformazioni di versante dell'alta valle di Susa: risposta pellicolare dell'evoluzione tettonica recente. *Il Quaternario*, 10 (2):293-298.
- Goguel, J. (1958). Présence des conglomérats à la base du “groupe d’Ambin” dans les schistes cristallins du massif d’Ambin (Savoie). *CR somm. Soc. géol. Fr*, 11, 229-231.
- Gong Q, Zhao J (2009) Development of a rock mass characteristics model for TBM penetration rate prediction. *International journal of Rock mechanics and mining sciences*, 46(1):8-18.
- Gong, Q. M., Jiao, Y. Y., & Zhao, J. (2006). Numerical modelling of the effects of joint spacing on rock fragmentation by TBM cutters. *Tunnelling and Underground Space Technology*, 21(1), 46-55.
- Gordan, B., Armaghani, D. J., Hajihassani, M., & Monjezi, M. (2016). Prediction of seismic slope stability through combination of particle swarm optimization and neural network. *Engineering with Computers*, 32(1), 85-97.
- Graham PC (1976) Rock exploration for machine manufacturers. In: *Proceedings of the Symposium on Exploration for Rock Engineering*, Johannesburg, Balkema, 1:173-180.
- Greenacre, M., & Blasius, J. (Eds.). (2006). *Multiple correspondence analysis and related methods*. CRC press.
- Guillot, F., & Raoult, J. F. (1984). Permien et base du Trias en Vanoise septentrionale: données nouvelles et hypothèses (zone briançonnaise interne, Alpes françaises). *Ann. Soc. géol. Nord*, 104(4), 183-192.
- Hamidi JK, Shahriar K, Rezai B, Rostami J (2010) Performance prediction of hard rock TBM using Rock Mass Rating (RMR) system. *Tunnelling and Underground Space Technology*, 25(4):333-345.
- Hamilton, W. H., & Dollinger, G. L. (1979). Optimizing tunnel boring machine and cutter design for greater boreability. *RETIC Proceedings, Atlanta, 1*, 280-296.
- Hassanpour J, Rostami J, Khamehchiyan M, Bruland A (2009) Developing new equations for TBM performance prediction in carbonate-argillaceous rocks: a case history of Nowsood water conveyance tunnel. *Geomechanics and Geoengineering: an International Journal*, 4(4):287-297.
- Hassanpour J, Rostami J, Zhao J (2011) A new hard rock TBM performance prediction model for project planning. *Tunnelling and underground space technology*, 26(5):595-603.
- Hassanpour, J., Vanani, A. G., Rostami, J., & Cheshomi, A. (2016). Evaluation of common TBM performance prediction models based on field data from the second lot of Zagros water conveyance tunnel (ZWCT2). *Tunnelling and Underground Space Technology*, 52, 147-156.
- Hoek E (1994) Strength of rock and rock masses. *ISRM News Journal*, 2(2):4-16.
- Hoek E, Marinos P, Benissi M (1998) Applicability of the Geological Strength Index (GSI) classification for very weak and sheared rock masses. The case of the Athens Schist Formation. *Bulletin of Engineering Geology and Environment*, 57(2): 151-160
- Hoek, E. (1988). The Hoek-Brown failure criterion-a 1988 update. In *Proc. 15th Canadian Rock Mech. Symposium* (pp. 31-38). Toronto, Dept. Civil Engineering, University of Toronto.
- Hoek, E., Carter, T.G., Diederichs, M.S. (2013). Quantification of the Geological Strength Index Chart. *47th US Rock Mechanics/Geomechanics Symposium*, San Francisco, CA, USA.

- Hudson, J. (1992). Rock engineering systems. Theory and practice. *Pergamon*.
- Hudson, J. A., & Priest, S. D. (1983). Discontinuity frequency in rock masses. In *International Journal of Rock Mechanics and Mining Sciences & Geomechanics Abstracts*(Vol. 20, No. 2, pp. 73-89). Pergamon.
- Hughes HM (1986). The relative cuttability of coal-measures stone. *Mining Science and Technology*, 3(2):95-109
- Husson, F., Josse, J., & Pages, J. (2010). Principal component methods-hierarchical clustering-partitional clustering: why would we need to choose for visualizing data. *Applied Mathematics Department*.
- Husson, F., Lê, S., & Pagès, J. (2017). Exploratory multivariate analysis by example using R. *CRC press*.
- Innaurato N., Mancini A., Rondena E., Zaninetti A. (1991). Forecasting and effective TBM performances in a rapid excavation of a tunnel in Italy. In *Proceedings of seventh ISRM Congress*, International Society for Rock Mechanics
- Innaurato, N., Oggeri, C., Oreste, P. P., & Vinai, R. (2007). Experimental and numerical studies on rock breaking with TBM tools under high stress confinement. *Rock Mechanics and Rock Engineering*, 40(5), 429.
- ISRM (1985) Suggested method for determining point load strength. *International journal of rock mechanics,mining sciences & geomechanics*; abstract Vol 22, No 2, pp 51-60.
- Jang, J. S. R., Sun, C. T., & Mizutani, E. (1997). Neuro-fuzzy and soft computing; a computational approach to learning and machine intelligence.
- Johnson, J. B., & Omland, K. S. (2004). Model selection in ecology and evolution. *Trends in ecology & evolution*, 19(2), 101-108.
- Jolliffe, I. T. (2002). Principal component analysis for special types of data. *Principal component analysis*, 338-372
- Klein, S., Schmoll, M., & Avery, T. (1995, June). TBM performance at four hard rock tunnels in California. In *Proceedings of the rapid excavation and tunneling conference* (pp. 61-76). Society for mining, metallurgy & exploration, Inc.
- Koenker, R., & Portnoy, S. (1996). Quantile regression. *University of Illinois at Urbana-Champaign, College of Commerce and Business Administration*. Office of Research Working Paper 97-100.
- Koenker, R. (2017). Quantile regression: 40 years on. *Annual Review of Economics*, 9, 155-176.
- Kretz, R. (1983). Symbols for rock-forming mineralsl. *American mineralogist*, 68, 277-279.
- Latham, J. P., Van Meulen, J., & Dupray, S. (2006). Prediction of in-situ block size distributions with reference to armourstone for breakwaters. *Engineering Geology*, 86(1), 18-36.
- Laughton, E., & Eng, P. (2011). Value engineering the construction of bored tunnels in competent rock. *Pre-Print Society of American Value Engineers*.
- Liao, Z. Y., Liang, Z. Z., Yang, Y. F., Wang, Y., & Tang, C. A. (2013). Numerical simulation of fragmentation process of jointed rock mass induced by a drill bit under dynamic loading. *Chin J Geotech Eng*, 35(6), 1147-1155.

- Liu, H. Y., Kou, S. Q., Lindqvist, P. A., & Tang, C. A. (2002). Numerical simulation of the rock fragmentation process induced by indenters. *International Journal of Rock Mechanics and Mining Sciences*, 39(4), 491-505.
- Lunn, D., Jackson, C., Best, N., Spiegelhalter, D., & Thomas, A. (2012). *The BUGS book: A practical introduction to Bayesian analysis*. Chapman and Hall/CRC.
- Macias, F. J., Jakobsen, P. D., Seo, Y., & Bruland, A. (2014). Influence of rock mass fracturing on the net penetration rates of hard rock TBMs. *Tunnelling and Underground Space Technology*, 44, 108-120.
- Mahdevari, S., Shahriar, K., Yagiz, S., & Shirazi, M. A. (2014). A support vector regression model for predicting tunnel boring machine penetration rates. *International Journal of Rock Mechanics and Mining Sciences*, 72, 214-229.
- Maidl, B., Schmid, L., Ritz, W., & Herrenknecht, M. (2008). *Hardrock tunnel boring machines*. John Wiley & Sons.
- Malusa, M. G. (2004). Post-metamorphic evolution of the Western Alps: kinematic constraints from a multidisciplinary approach (geological mapping, mesostructural analysis, fission-track dating, fluid inclusion analysis).
- Marinos P, Hoek E (2000) GSI: a geologically friendly tool for rock mass strength estimation. In *Proceedings of ISRM International Symposium*, International Society for Rock Mechanics.
- Marinos, P., & Hoek, E. (2001). Estimating the geotechnical properties of heterogeneous rock masses such as flysch. *Bulletin of engineering geology and the environment*, 60(2), 85-92.
- Marto, A., Hajihassani, M., Jahed Armaghani, D., Tonnizam Mohamad, E., & Makhtar, A. M. (2014). A novel approach for blast-induced flyrock prediction based on imperialist competitive algorithm and artificial neural network. *The Scientific World Journal*, 2014.
- Mazzoccola, D. F., & Hudson, J. A. (1996). A comprehensive method of rock mass characterization for indicating natural slope instability. *Quarterly Journal of Engineering Geology and Hydrogeology*, 29(1), 37-56.
- McFeat-Smith I (1999) Mechanised tunnelling for Asia. In *Workshop Manual*, Organized by IMS Tunnel Consultancy Ltd.
- Momeni, E., Nazir, R., Armaghani, D. J., & Maizir, H. (2014). Prediction of pile bearing capacity using a hybrid genetic algorithm-based ANN. *Measurement*, 57, 122-131.
- Monie, P. (1990). Preservation of Hercynian $^{40}\text{Ar}/^{39}\text{Ar}$ ages through high-pressure low-temperature Alpine metamorphism in the Western Alps. *European Journal of Mineralogy*, 343-361.
- Montgomery, D. C., & Peck, E. A. (1982). *Introduction to linear regression analysis*, 1992.
- Mooney, M. A., Grasmick, J., Kenneally, B., & Fang, Y. (2016). The role of slurry TBM parameters on ground deformation: Field results and computational modelling. *Tunnelling and Underground Space Technology*, 57, 257-264.
- Nash, J. C., & Walker-Smith, M. (1987). *Nonlinear parameter estimation*. New York: Marcel Decker.

- Nelson PP, Al-Jalil YA, Laughton C (1999) Improved strategies for TBM performance prediction and project management. In *Proceedings of the Rapid Excavation and Tunneling Conference*, pp. 963-980
- Nelson PP, O'Rourke TD (1983) Tunnel boring machine performance in sedimentary rocks. Report to Goldberg-Zoino Associates of New York, P.C., *School of Civil and Environmental of Civil Engineering. Cornell University, Ithaca, NY*, pp. 438
- Nelson, P. P., Ingraffea, A. R., & O'Rourke, T. D. (1985). TBM performance prediction using rock fracture parameters. In *International Journal of Rock Mechanics and Mining Sciences & Geomechanics Abstracts*, vol 22(3); 189-192.
- Nielsen B, Ozdemir L.(1993) Hard rock tunnel boring prediction and field performance. In: *Proceedings of the RECT*. Boston, Littleton, Society for Mining, Metallurgy, and Exploration, p. 833–52.
- Ozdemir L, Miller RJ, Wang FD (1978) Mechanical Tunnel Boring Prediction and Machine Design. NSF APR7307776-A03. *Colorado School of Mines*. Golden, Colorado, USA
- Ozdemir, L. (1977). Development of theoretical equations for predicting tunnel boreability (Doctoral dissertation, *Colorado School of Mines*).
- Ozdemir, L., (1992). Mechanical excavation techniques in underground construction. Short course notebook, vol 1. Istanbul Technical University, Istanbul, pp 1-49.
- Padovese, P., Berti, A., Baldovin, E., De Paola, A., Morelli, G.L., Buraschi, L., Ascari, G., (2017). Innovazioni delle tecnologie di scavo meccanizzato in ammassi rocciosi caratterizzati da roccia dura con distacchi in calotta e alte coperture. In: *Proceedings of MIR 2017 - 16°Ciclo di conferenze di Meccanica ed Ingegneria delle Rocce ‘Innovazione nella progettazione, realizzazione e gestione delle opere in sotterraneo’*. Celid, Torino, pp 33-53.
- Palmström, A. (1982). The volumetric joint count-a useful and simple measure of the degree of rock jointing. *Proc. 4th Int. Cong. Int. Assoc. Eng. Geol*, 5, 221-228.
- Palmstrom, A. (1995). RMI-a rock mass characterization system for rock engineering purposes.
- Phillips, H. R., & Bilgin, N. (1977). Correlation of rock properties with the measured performance of disc cutters. In *Proceedings of a Conference on Rock Engineering, University of Newcastle Upon Tyne, UK* (pp. 181-196).
- Pognante, U. (1984). Eclogitic versus blueschist metamorphism in the internal Western Alps along the Susa valley traverse. *Sciences Géologiques, bulletins et mémoires*, 37(1), 29-36.
- Polino, R., Dela Pierre, F., Fioraso, G., Giardino, M., & Gattiglio, M. (2002). Foglio 132-152-153 “Bardonecchia” Carta Geologica d’Italia, scala 1: 50,000. *Servizio Geologico d’Italia*.
- Price, N. J., & Cosgrove, J. W. (1990). *Analysis of geological structures*. Cambridge University Press.
- Ramezanzadeh A, Rostami J, Tadic D (2008) Impact of rock mass characteristics on hard rock TBM performance. *13th Australian tunneling conference*, Melbourne, Australia, pp 213–222.
- Ribacchi R, Lembo-Fazio A (2005) Influence of rock mass parameters on the performance of a TBM in a Gneissic formation (Varzo tunnel). *Rock Mech Rock Eng* 38(2):105–127.

- Rispoli, A., Ferrero, A. M., Cardu, M., Brino, L., & Farinetti, A. (2016). Hard rock TBM performance: preliminary study based on an exploratory tunnel in the Alps. *Rock mechanics and rock engineering: from the past to the future*. Taylor & Francis Group, London, 469-474.
- Rispoli A. (2018). Hard rock TBM excavation: performance analysis and prediction. Thesis for the degree of Doctor of Philosophy. *University of Study of Turin*.
- Roby, J., Sandell, T., Kocab, J., & Lindbergh, L. (2008). The current state of disc cutter design and development directions. In *Proceeding of 2008 North American Tunneling Conference, SME C* (Vol. 4, pp. 36-45).
- Rostami J (1997) Development of a force estimation model for rock fragmentation with disc cutters through theoretical modeling and physical measurement of crushed zone pressure. Doctoral dissertation, *Colorado School of Mines*.
- Rostami J, Ozdemir L (1993) A new model for performance prediction of hard rock TBMs. In *Proceedings of the Rapid Excavation and Tunneling Conference*, pp. 793-793
- Rostami, J. (2008). Hard rock TBM cutterhead modeling for design and performance prediction. *Geomechanik und Tunnelbau: Geomechanik und Tunnelbau*, 1(1), 18-28.
- Rostami, J. (2016). Performance prediction of hard rock Tunnel Boring Machines (TBMs) in difficult ground. *Tunnelling and Underground Space Technology*, 57, 173-182.
- Roxborough F.F., Phillips H.R. (1975). Rock excavation by disc cutter. *International Journal of Rock Mechanics and Mining Sciences & Geomechanics Abstracts*, 12 (12): 361-366.
- Salimi, A., Rostami, J., & Moormann, C. (2016). TBM performance prediction in Basalt and Pyroclastic rocks of Deacon traps, A case study of Maroshi-Ruparel water supply tunnel. *Rock Mechanics and Rock Engineering: From the Past to the Future*, Taylor & Francis Group, London, 975-980.
- Sanio HP (1985). Prediction of the performance of disc cutters in anisotropic rock. *International Journal of Rock Mechanics and Mining Sciences & Geomechanics Abstracts*, 22(3):153-161
- Sapigni M, Berti M, Bethaz E, Busillo A, Cardone G (2002). TBM performance estimation using rock mass classifications. *International Journal of Rock Mechanics and Mining Sciences*, 39(6):771-788
- Sato, K., Gong, F., & Itakura, K. (1991). Prediction of disc cutter performance using a circular rock cutting ring. In *Proceedings 1st international mine mechanization and automation symposium*.
- Snowdon RA, Ryley MD, Temporal J (1982) A study of disc cutting in selected British rocks. *International Journal of Rock Mechanics and Mining Sciences & Geomechanics Abstracts*, 19(3):107-121.
- Spalla, M. I., Zanoni, D., Marotta, A. M., Rebay, G., Roda, M., Zucali, M., & Gosso, G. (2014). The transition from Variscan collision to continental break-up in the Alps: insights from the comparison between natural data and numerical model predictions. *Geological Society, London, Special Publications*, 405, SP405. 11.
- Spiegelhalter, D. J., Best, N. G., Carlin, B. P., & Van Der Linde, A. (2002). Bayesian measures of model complexity and fit. *Journal of the Royal Statistical Society: Series B (Statistical Methodology)*, 64(4), 583-639.

- Stampfli, G. M., & Marthaler, M. (1990). Divergent and convergent margins in the North-Western Alps confrontation to actualistic models. *Geodinamica Acta*, 4(3), 159-184.
- Staub R (1937) Gedanken zum bau den Westalpen Zwischen Bernina und Mittelmeer. *Buchdruckerei Gebr. Fretz*.
- Stevenson, G. W. (1999). Empirical estimates of TBM performance in hard rock. In *Proceedings of the rapid excavation and tunneling conference* (pp. 993-1010).
- Sue C, Delacou B, Champagnac JD, Allanic C, Tricart P, Burkhard M (2007). Extensional neotectonics around the bend of the Western/Central Alps: an overview. *International Journal of Earth Sciences* 96(6):1101-1129.
- Sun, J. S., Chen, M., Chen, B. G., Lu, W. B., & Zhou, C. B. (2011). Numerical simulation of influence factors for rock fragmentation by TBM cutters. *Rock and Soil Mechanics*, 32(6), 1891-1897.
- Sundaram NM, Rafek AG, Komoo I (1998). The influence of rock mass properties in the assessment of TBM performance. In *Proceedings of the 8th IAEG Congress*, Vancouver, British Columbia, Canada, pp. 3553-3559.
- Sundin NO, Wänstedt S (1994) A boreability model for TBM's. In *Proceedings of first North American Rock Mechanics Symposium*, American Rock Mechanics Association.
- Tarkoy PJ (1973). Predicting TBM penetration rates in selected rock types. In *Proceedings of Ninth Canadian Rock Mechanics Symposium*, Montreal.
- Tarkoy, P. J. (1975). Rock Hardness Index Properties and Geotechnical Parameters for Predicting Tunnel Boring Machine Performance (Doctoral dissertation, *University of Illinois at Urbana-Champaign*).
- Tarkoy, P. J., & Marconi, M. (1991). Difficult rock comminution and associated geological conditions. In *Proceedings of the 6th international symposium: Tunnelling* (Vol. 91, pp. 195-207).
- Thélin P, Sartori M, Lengeler R, Schaerer JP (1990). Eclogites of Paleozoic or early Alpine age in the basement of the Penninic Siviez-Mischabel nappe, Wallis, Switzerland. *Lithos*, 25(1):71-88
- Torabi, S. A., Sahebjamnia, N., Mansouri, S. A., & Bajestani, M. A. (2013). A particle swarm optimization for a fuzzy multi-objective unrelated parallel machines scheduling problem. *Applied Soft Computing*, 13(12), 4750-4762.
- Tuncdemir, H., Bilgin, N., Copur, H., & Balci, C. (2008). Control of rock cutting efficiency by muck size. *International Journal of Rock Mechanics and Mining Sciences*, 2(45), 278-288.
- Valantin A. (1973). Examen des diffe´rents proce´de´s classiques de´termination de la nocivite´ des roches vis-a`-vis de l'abattage me´canique. Expose Presente´ Aux *Journe´es d'information Techniques de Creusement*, Luxemburg, pp 133–140.
- Wang, L., Kang, Y., Zhao, X., & Zhang, Q. (2015). Disc cutter wear prediction for a hard rock TBM cutterhead based on energy analysis. *Tunnelling and Underground Space Technology*, 50, 324-333.
- Wickham GE, Tiedemann HR, Skinner EH (1972). Support determinations based on geologic predictions. In *Proceedings of North America Rapid Excavation & Tunnelling*, 1.
- Wijk G (1992) A model of tunnel boring machine performance. *Geotechnical and Geological Engineering*, 10(1):19-40.

- Wyllie, D. C. (1999) Foundations on Rock, 2nd Edition, *Taylor and Francis*, London, UK, 401.
- Wyllie, D. C., & Mah, C. (2014). Rock slope engineering. *CRC Press*.
- Xia, Y., Zhang, K., & Liu, J. (2015). Design Optimization of TBM Disc Cutters for Different Geological Conditions.
- Yagiz S (2002) Development of rock fracture and brittleness indices to quantify the effects of rock mass features and toughness in the CSM Model basic penetration for hard rock tunneling machines. Doctoral dissertation, *Colorado School of Mines*.
- Yagiz, S (2006). TBM performance prediction based on rock properties. *Proceedings of Multiphysics Coupling and Long Term Behaviour in Rock Mechanics*, EUROCK, 6, 663-670.
- Yagiz S (2008). Utilizing rock mass properties for predicting TBM performance in hard rock condition. *Tunnelling and Underground Space Technology*, 23(3):326-339
- Yagiz, S., & Karahan, H. (2011). Prediction of hard rock TBM penetration rate using particle swarm optimization. *International Journal of Rock Mechanics and Mining Sciences*, 48(3), 427-433.
- Yagiz, S., Gokceoglu, C., Sezer, E., & Iplikci, S. (2009). Application of two non-linear prediction tools to the estimation of tunnel boring machine performance. *Engineering Applications of Artificial Intelligence*, 22(4-5), 808-814.
- Yang, X. S., & Deb, S. (2010). Engineering optimisation by cuckoo search. *arXiv preprint arXiv:1005.2908*.
- Yavari, M., & Mahdavi, S. (2005). Prediction of penetration rate of TBM using ANN. In *National mining conference* (pp. 1-3).
- Yin, L., Miao, C., He, G., Dai, F., & Gong, Q. (2016). Study on the influence of joint spacing on rock fragmentation under TBM cutter by linear cutting test. *Tunnelling and Underground Space Technology*, 57, 137-144.
- Zhang, L., & Einstein, H. H. (2000). Estimating the intensity of rock discontinuities. *International Journal of Rock Mechanics and Mining Sciences*, 37(5), 819-837.
- Zhao Z, Gong Q, Zhang Y, Zhao J (2007) Prediction model of tunnel boring machine performance by ensemble neural networks. *Geomechanics and Geoengineering: An International Journal*, 2(2):123-128
- Zou, D. (2017). Mechanical Underground Excavation in Rock. In *Theory and Technology of Rock Excavation for Civil Engineering* (pp. 435-472). Springer, Singapore.
- Zurada, J. M. (1992). *Introduction to artificial neural systems*(Vol. 8). St. Paul: West publishing company.

www.googlemaps

www.europeancommission.com

www.herrenknecht.com

www.igm.org.my

www.ltf

www.palmierigroup.com

www.R-project.org

www.robbscompany

www.telt-sas.com

www.therobbscompany.com

www.tunneltalk.com

APPENDIX I

Schemes used during geological surveys

GENERAL INFORMATION

Date:.....

Survey N°:.....

Pk. Initial:m;

Pk. Final:.....m

Tunnel axis direction:.....

Tunnel depth:.....m

GEOLOGICAL DESCRIPTION OF INTACT ROCK

(global aspect, colour, forming minerals, texture, weathering, lithologies, evidences of instability etc)

.....
.....
.....
.....

GRAPHICAL REPRESENTATION OF ROOF AND WALL STRUCTURES

<i>Sinistral wall</i>	→
<i>Dextral wall</i>	←
<i>Roof</i>	

SCHEME FOR PRINCIPAL SET DESCRIPTION

ID set:

Type of discontinuity:

Estimation of mean orientation:.....Dip Direction;.....Dip. β:

SPACING [cm]

PERSISTENCE [m]

< 1

1 – 3

3 – 10

10 – 20

>20

APERTURE [mm]

< 0.5

0.5 – 10.0

> 10.5

FILLING [mm]

Absent

Hard, width < 5

Hard, width > 5

soft width < 5

soft width > 5

ROUGHNESS

Very rough

Rough

Slightly rough

Smooth

Slickenside

WEATHERING DEGREE

Unweathered

Slightly w.

Moderately w.

Highly w.

Decomposed

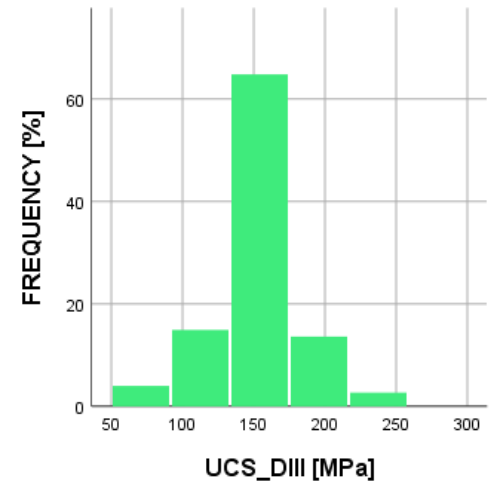
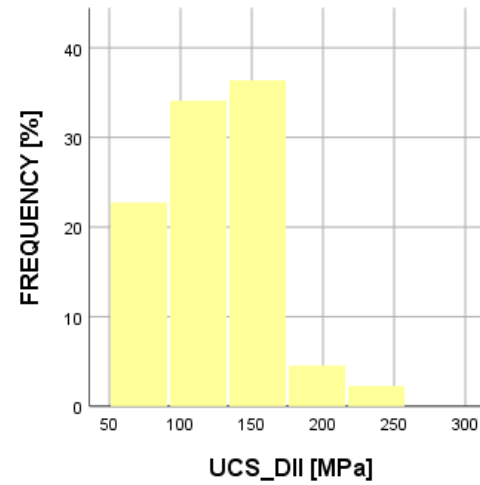
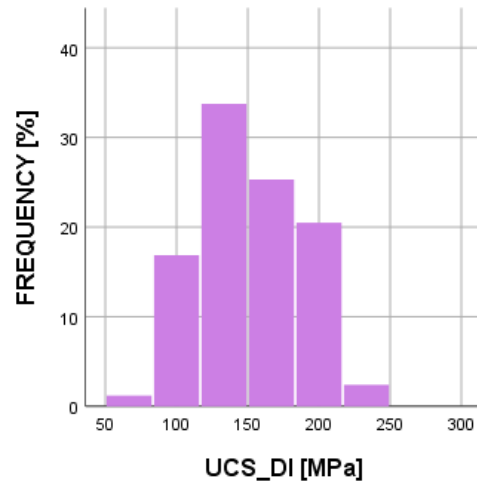
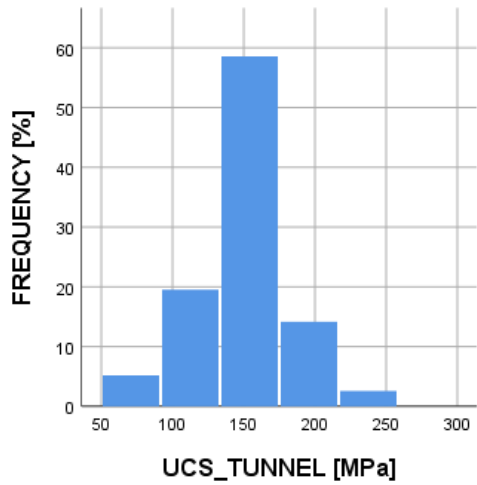
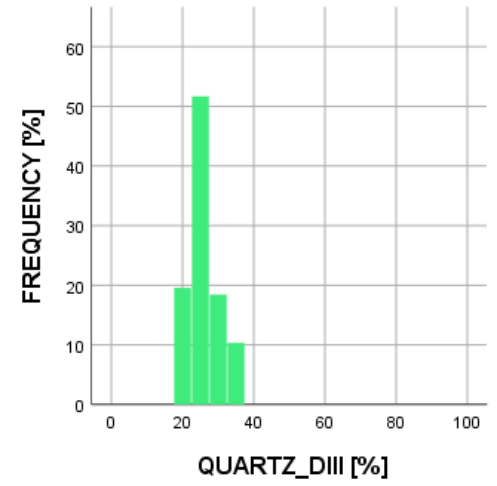
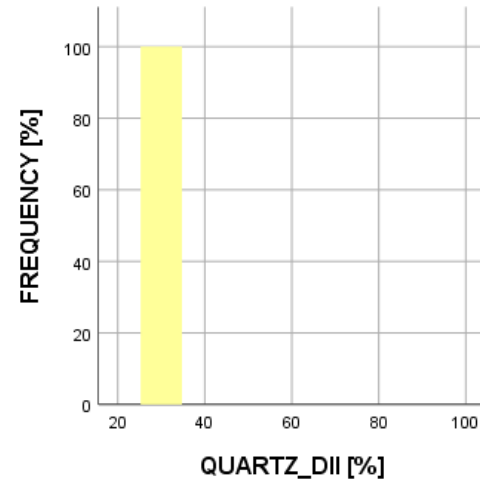
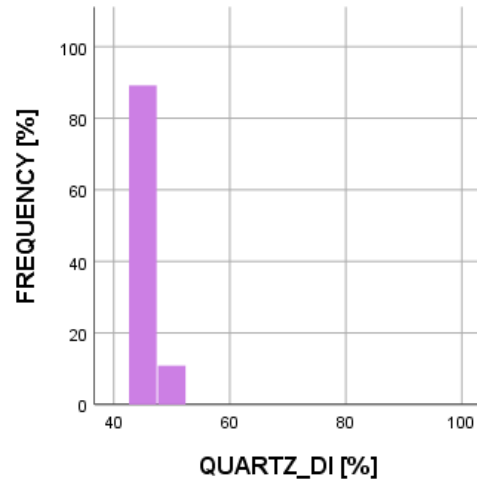
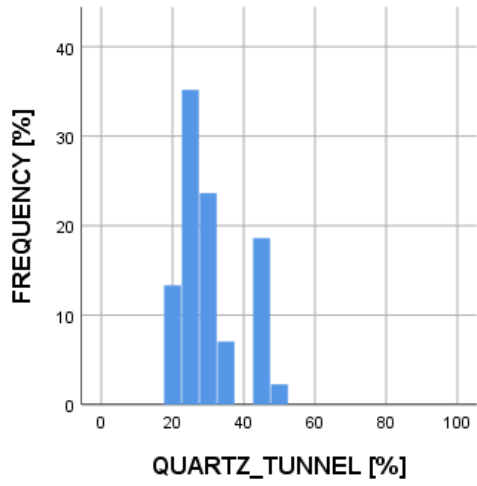
GSI:.....

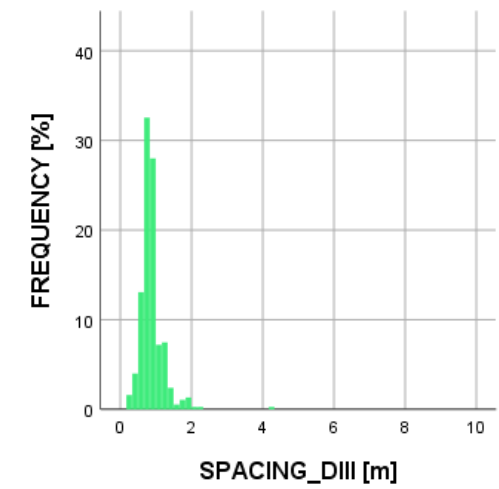
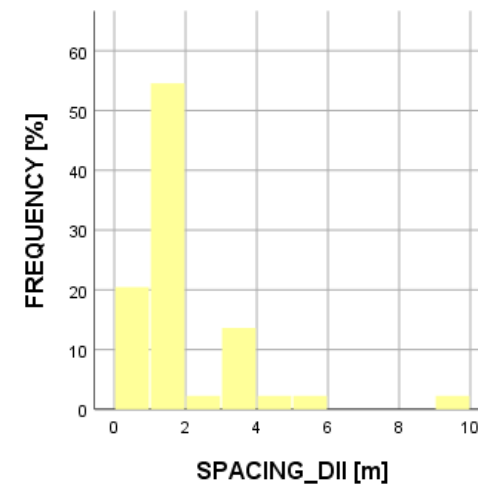
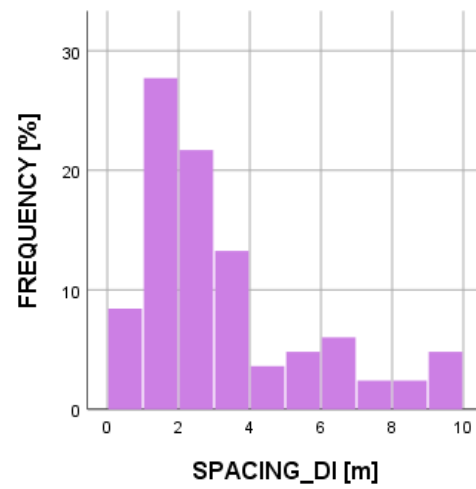
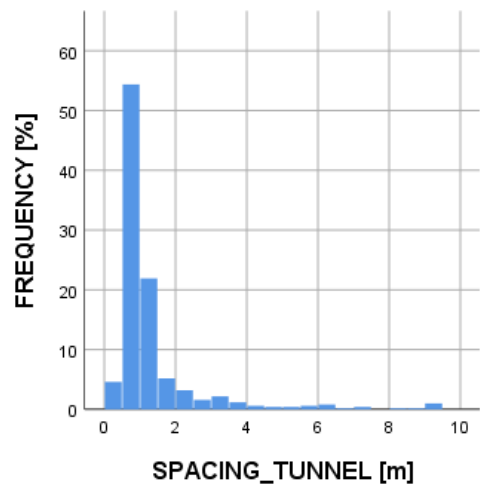
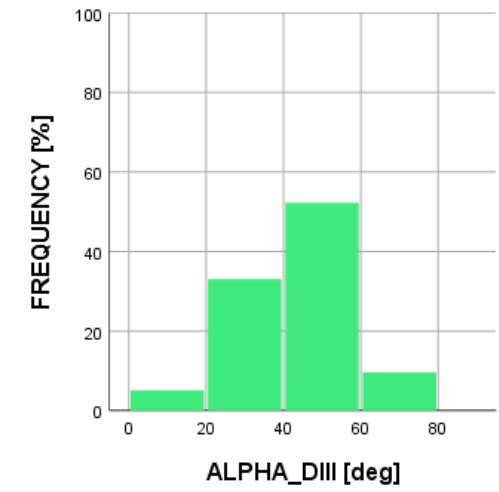
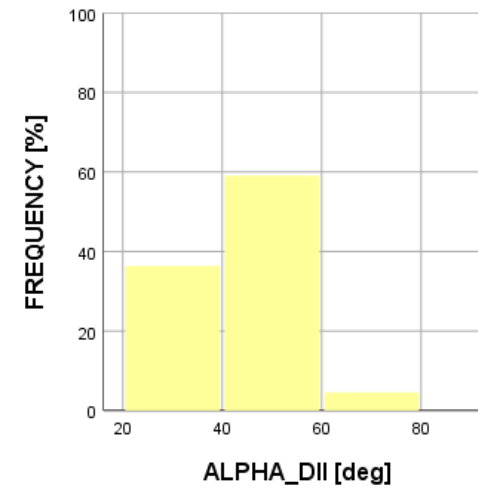
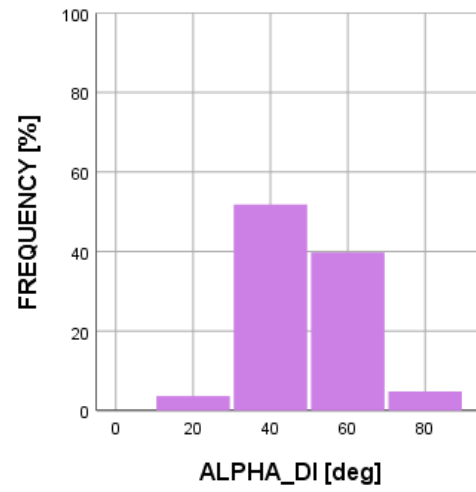
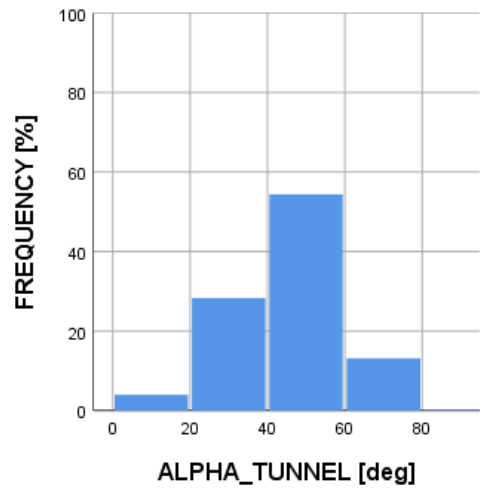
OBSERVATIONS:

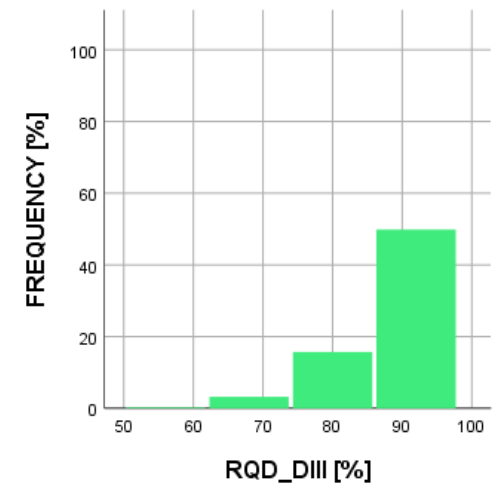
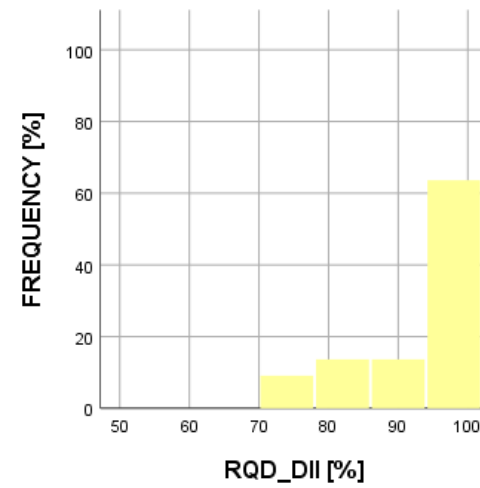
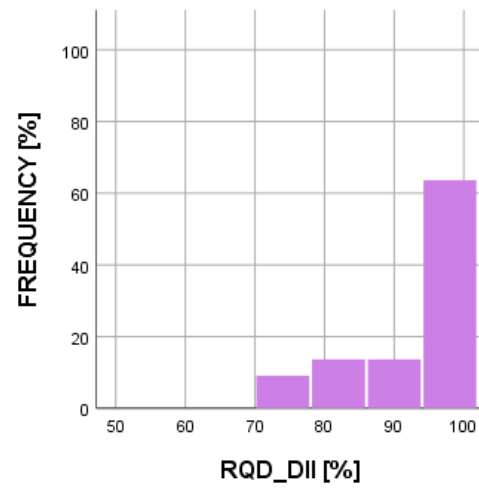
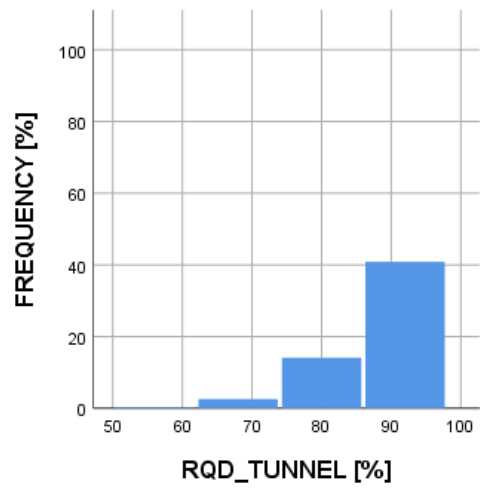
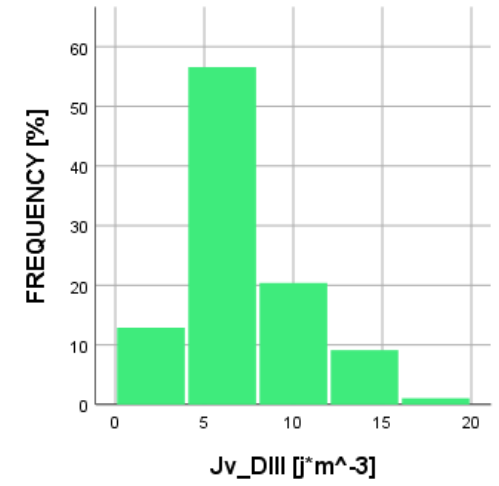
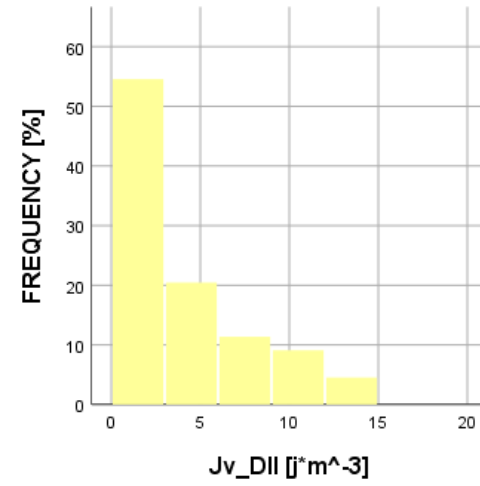
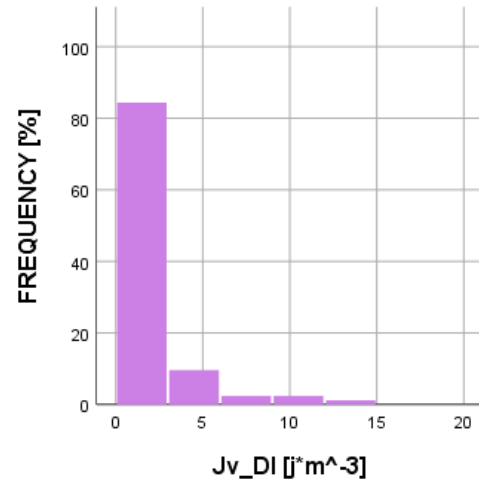
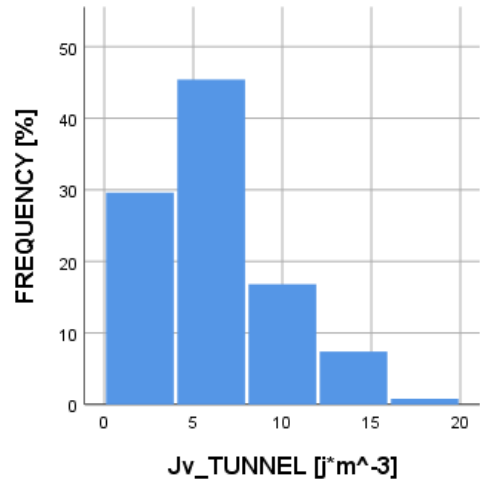
.....

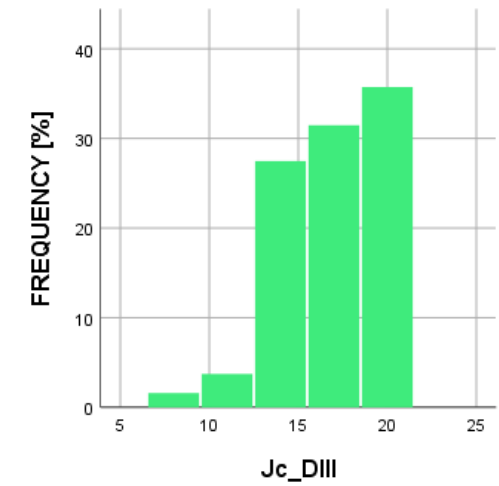
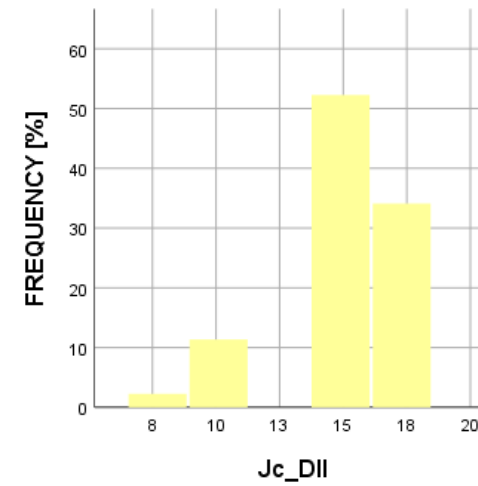
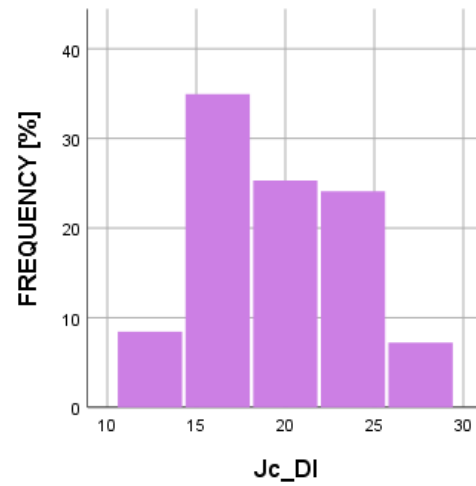
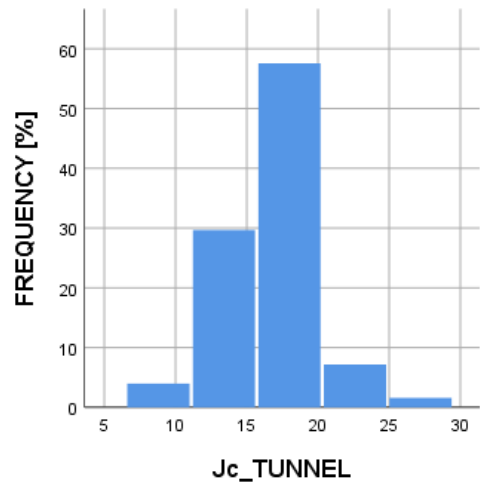
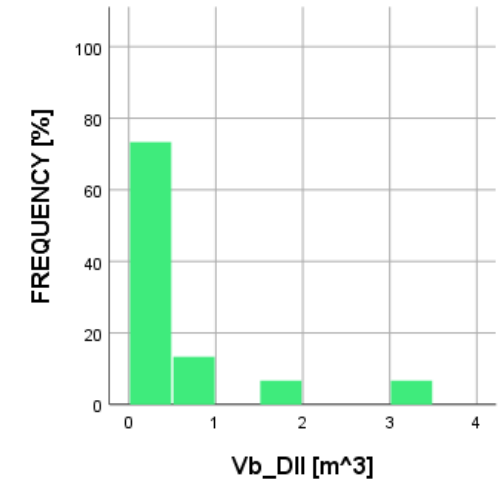
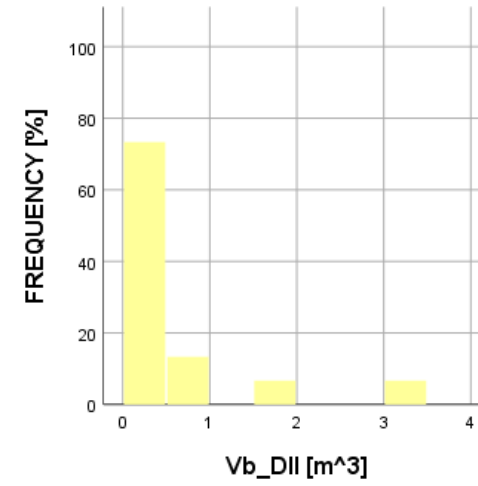
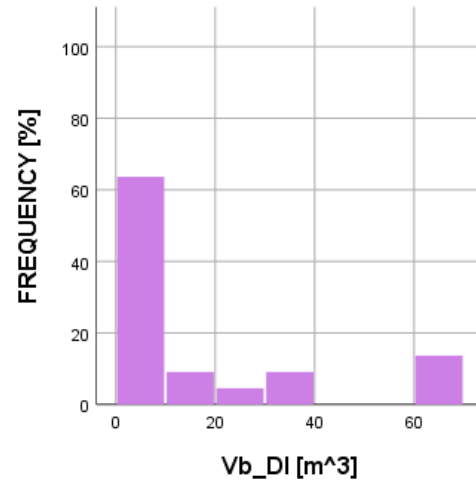
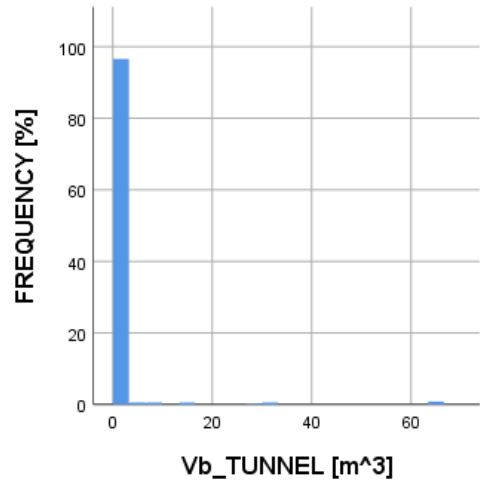
APPENDIX II

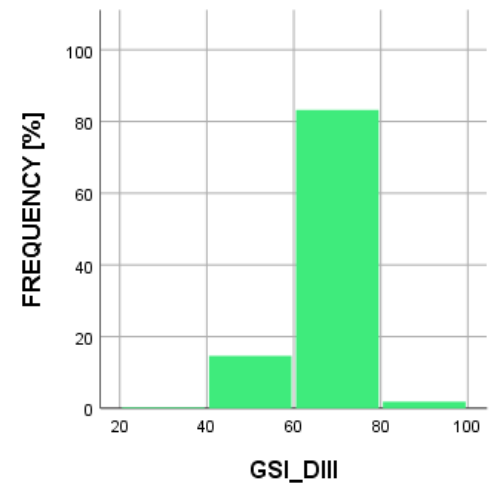
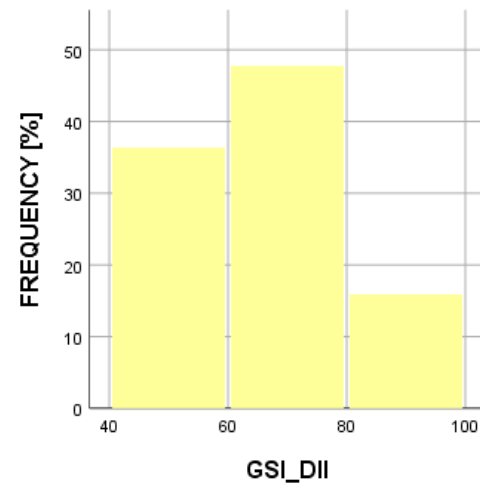
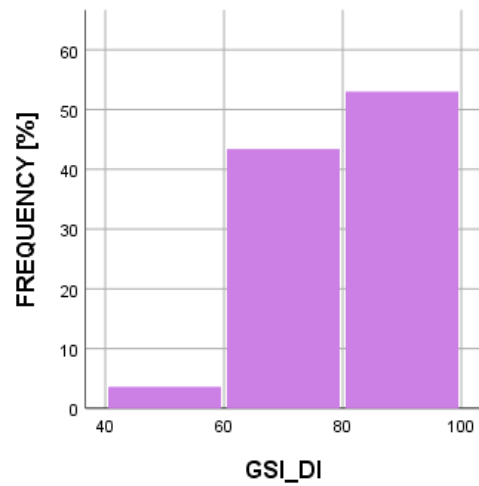
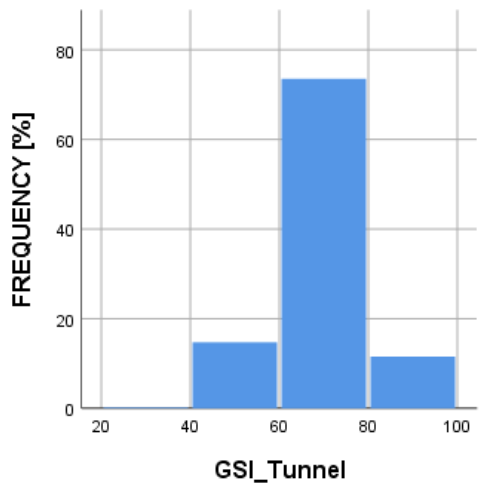
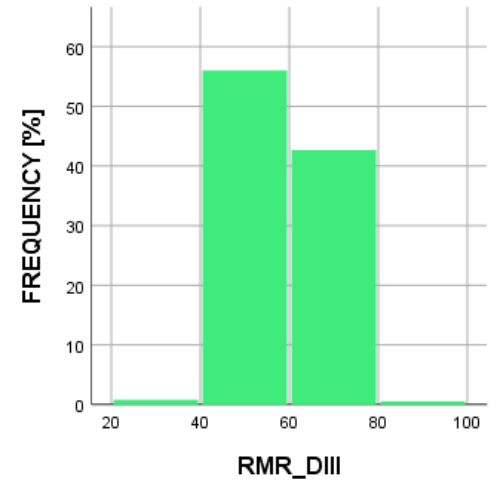
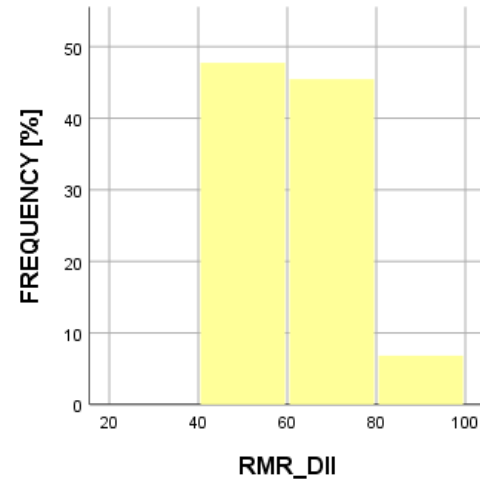
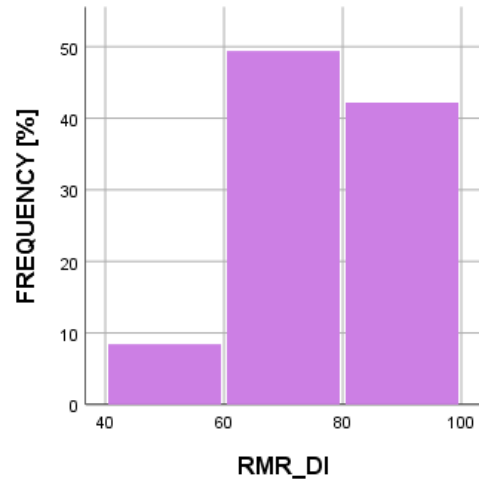
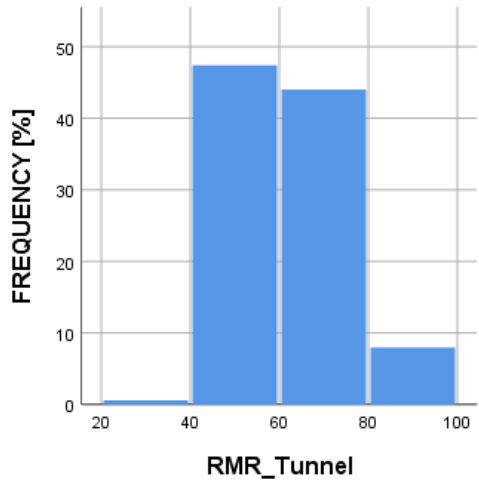
Histograms of frequency of the principal geological and geotechnical variables

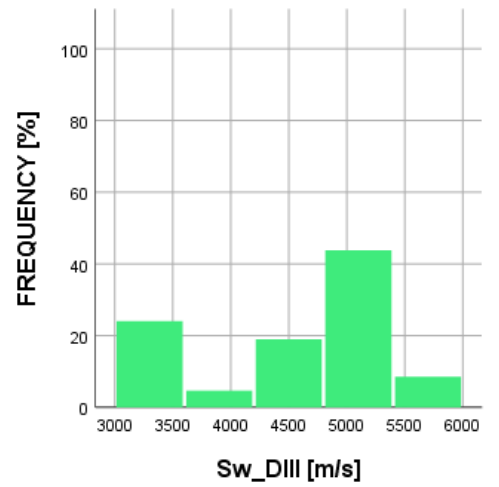
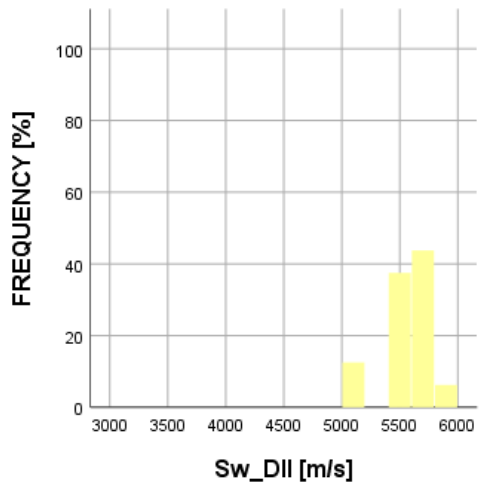
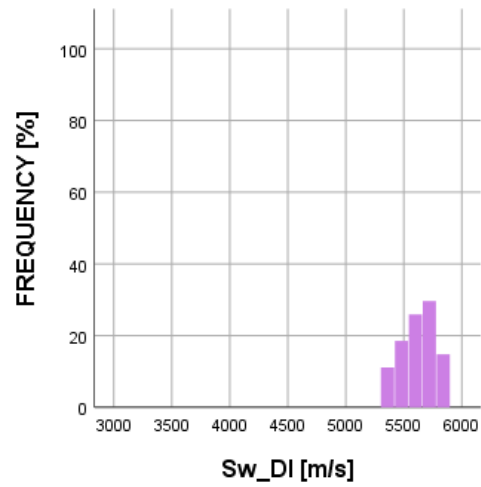
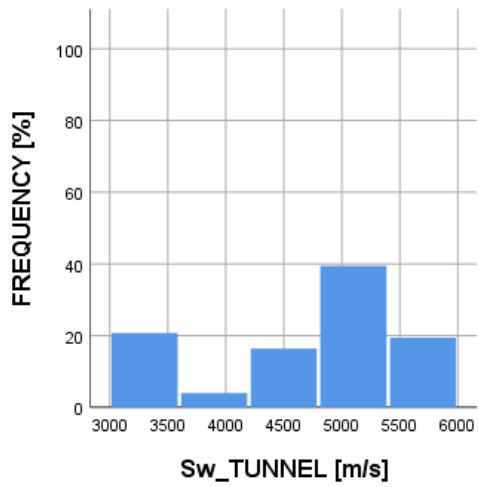
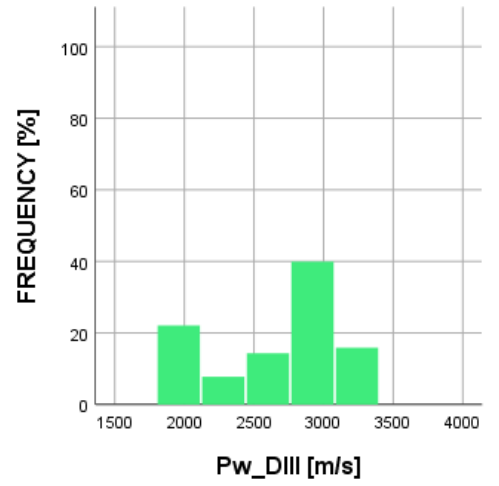
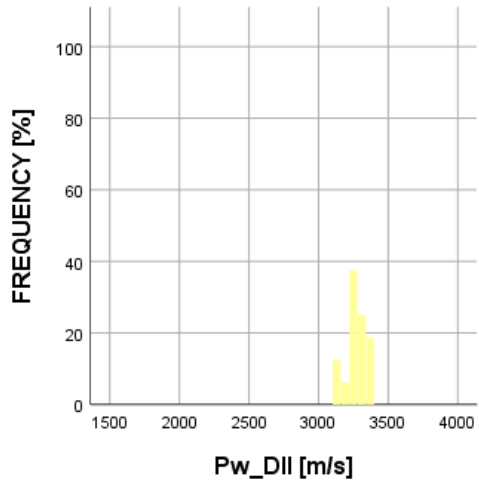
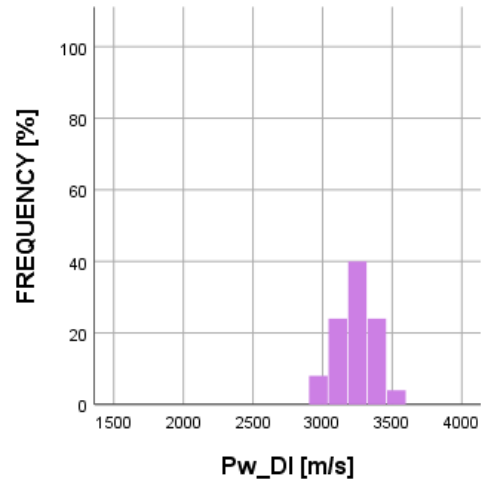
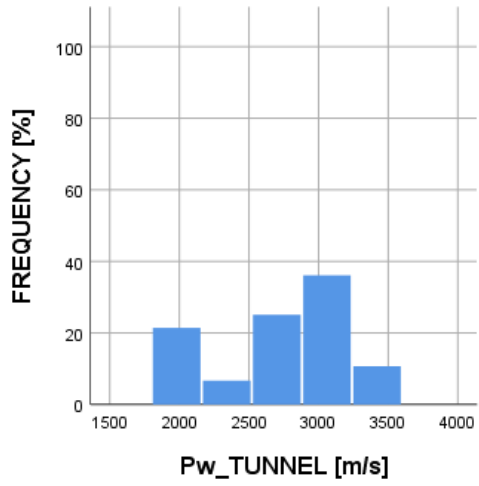


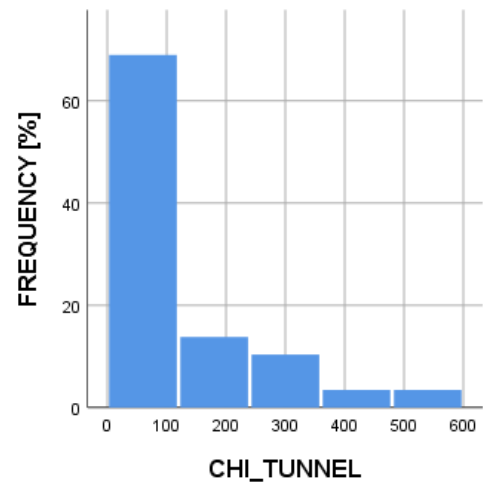
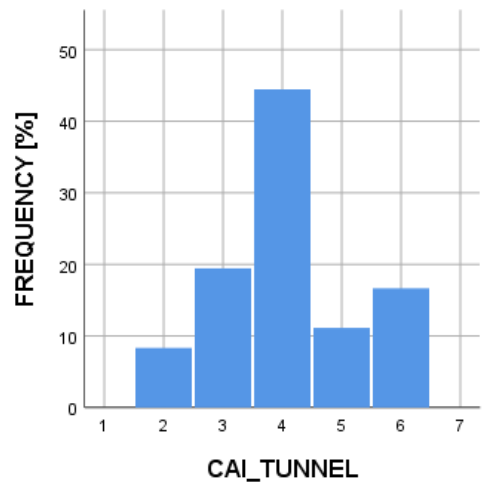
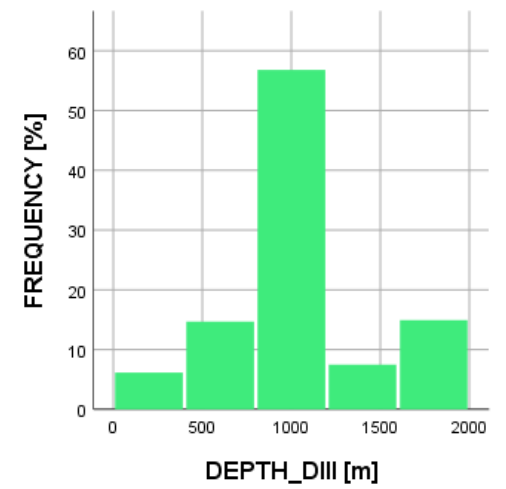
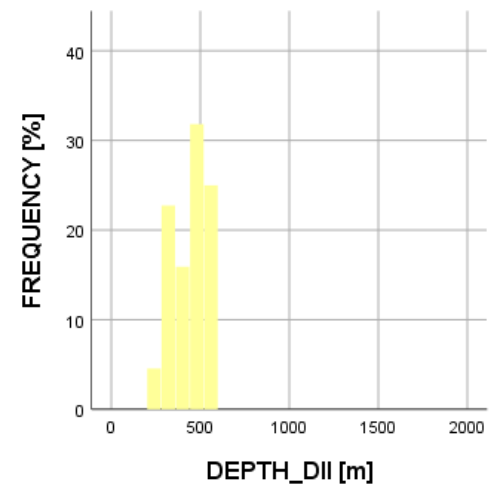
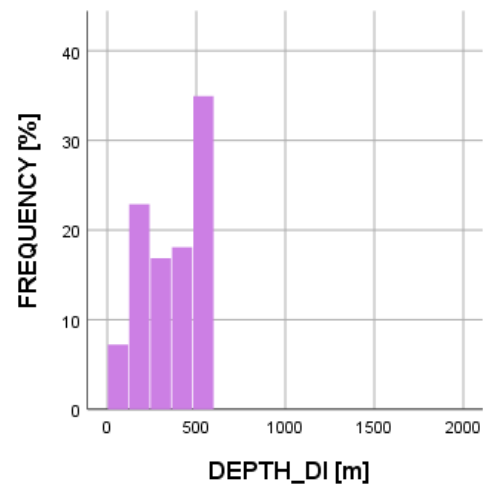
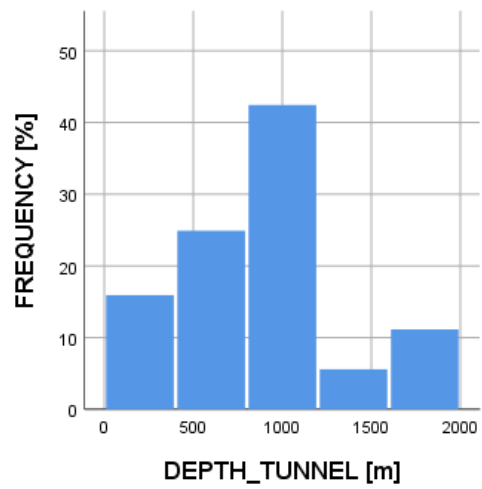








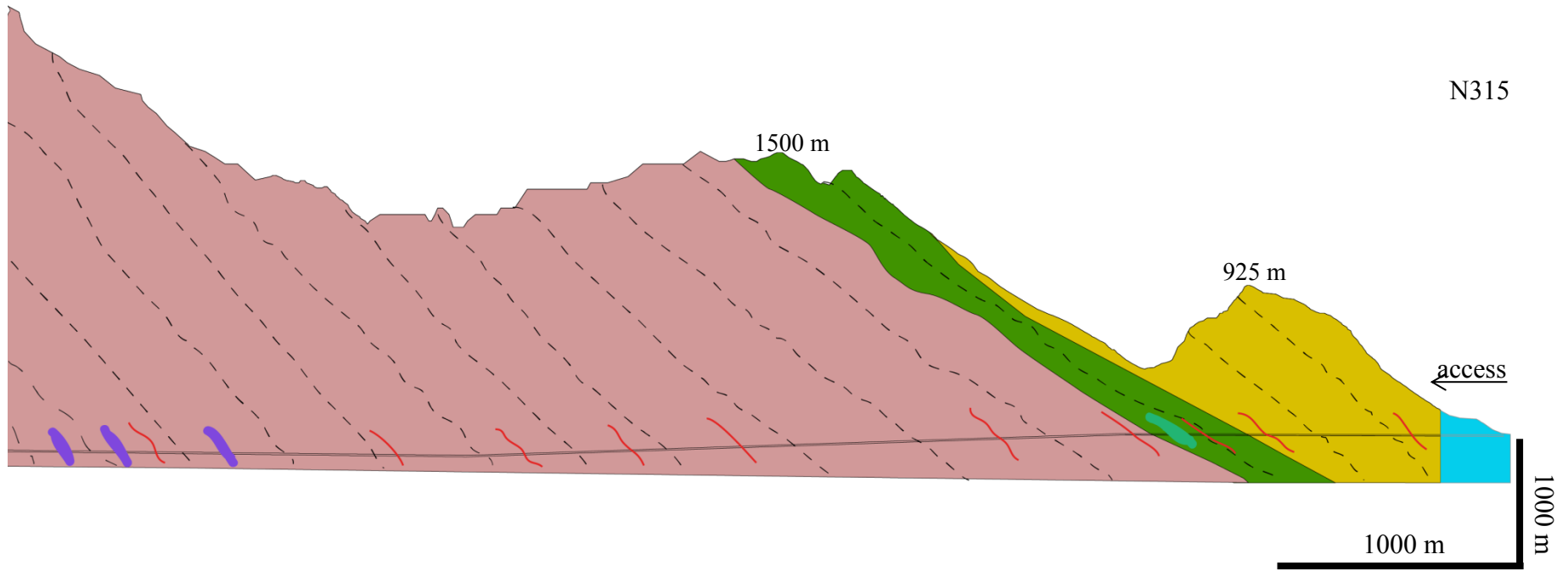










APPENDIX III

Longitudinal geological section of “La Maddalena” tunnel

LONGITUDINAL GEOLOGICAL SECTION OF "LA MADDALENA" TUNNEL



LEGEND

- | | |
|---|--|
|  Micaschist – Clarea complex |  Minuti Gneiss |
|  Gneiss Micaschist alternation – Ambin complex |  Drill and Blast Tunnelling |
|  Aplitic Gneiss – Ambin complex | ----- Schistosity |
|  Albitic Gneiss | — Principal fracture |
| | ==== Tunnel |

APPENDIX IV

The generic underground excavation matrix; Hudson, 1992

